Developing *in vitro* and *in vivo* Models of Retinal Degeneration

Thesis submitted for the degree of

DOCTOR OF PHILOSOPHY

To

THE DEPARTMENT OF ANIMAL BIOLOGY
SCHOOL OF LIFE SCIENCES
UNIVERSITY OF HYDERABAD
HYDERABAD – 500 046
INDIA

By

Praveen Joseph S.

Under the supervision of
Dr. Indumathi Mariappan

Sudhakar and Sreekanth Ravi Stem Cell Biology Laboratory
Prof. Brien Holden Eye Research Centre
L V Prasad Eye Institute
Hyderabad- 500 034

June 2019
Enrolment No: **13LAPH12**

University of Hyderabad
Hyderabad-500 046, India

CERTIFICATE

This is to certify that this thesis entitled "***Developing in vitro and in vivo models of retinal degeneration***" submitted by **Mr. Praveen Joseph S** bearing registration number **13LAPH12** in partial fulfillment of the requirements for the award of Doctor of Philosophy in the Department of Animal Biology, School of Life Sciences, is a bonafide work carried out by him under my supervision and guidance. This thesis is free from plagiarism and has not been submitted previously in full or parts, have not been submitted to any other University or Institution for the award of any degree or diploma. Parts of this thesis have been:

A. Published/Under review

1. **Susaimanickam PJ**, Maddileti S, Pulimamidi VK, Boyinpally SR, Naik RR, Naik MN, Reddy BG, Sangwan VS and Mariappan I. Generating minicorneal organoids from human induced pluripotent stem cells. *Development*. 2017 Jul 1;144(13):2338–51.
2. Mariappan I, Maddileti S, **Joseph P**, Siamwala JH, Vauhini V. Enriched cultures of retinal cells from BJNhem20 human embryonic stem cell line of Indian origin. *Investig Ophthalmol Vis Sci*. 2015;56(11):6714–23.
3. Dave VP, Maddileti S, **Susaimanickam PJ**, Pulimamidi VK, Boyinpally SR, Mishra DK, Naik RR, Jalali S, Das TP and Mariappan I. Validation of pluripotency of a newly generated human induced pluripotent stem cell line by teratoma assay. *Indian J Ophthalmol* 2019; (Manuscript under review)

B. Presented in the following conferences

1. Oral presentation of a paper titled "**Eye Field Differentiation and Generation of Corneal Organoids from Human Induced Pluripotent Stem Cells**" at the ARVO 2017-Baltimore, USA.
2. Poster presentation of a paper titled "**Retinal and corneal organoids generated from human induced pluripotent stem cells**" at the IERG-ARVO 2016-Hyderabad.
3. Oral presentation of a paper titled "**Characterization of human RD3 promoter for the construction of retina-specific gene expression cassette**" at the IERG-ARVO 2014-Hyderabad.

Further, the student has passed the following courses towards fulfillment of coursework requirement for Ph.D.

Name	Credits	Pass/Fail
Molecular Genetics	4	Pass
Research Ethics	2	Pass
Biostatistics	2	Pass
Cell Biology	4	Pass

Dr. Indumathi Mariappan
Supervisor

Head, Department of Animal Biology

Dean, School of Life Sciences

University of Hyderabad
School of Life Sciences
Department of Animal Biology
Hyderabad-500 046, India

CERTIFICATE

This is to certify that this thesis entitled **"*Developing in vitro and in vivo models of retinal degeneration*"** submitted by **Mr. Praveen Joseph S** bearing registration number 13LAPH12 for the degree of Doctor of Philosophy to the University of Hyderabad is a bonafide record of research work carried out by him at the L.V. Prasad Eye Institute, Hyderabad under my supervision. The contents of this thesis, in full or parts have not been submitted to any other University or Institution for the award of any degree or diploma. I hereby, recommend his thesis for submission, for the award of the degree of Doctor of Philosophy from the University.

Dr. Indumathi Mariappan	**Head, Department of**	**Dean, School of**
Supervisor	**Animal Biology**	**Life Sciences**

University of Hyderabad
School of Life Sciences
Department of Animal Biology
Hyderabad-500 046, India

DECLARATION

I, **Praveen Joseph S** hereby declare that this thesis entitled **"*Developing in vitro and in vivo models of retinal degeneration*"** submitted by me under the guidance and supervision of **Dr. Indumathi Mariappan**, is an original and independent research work. I also declare that it has not been submitted to any other University or Institution for the award of any degree or diploma.

Date: 28th June 2019

Praveen Joseph S
13LAPH12

DEDICATED TO

ALL THE VISUALLY IMPAIRED

AND

MY LOVING PARENTS

ACKNOWLEDGEMENTS

This doctoral thesis work has been an amazing and fulfilling learning process that helped me to become a better version of myself both academically and personally. A lot of people were involved directly or indirectly in the successful completion of this doctoral thesis work, which would have been impossible for me, without the help and continuous support of the wonderful people around me. I could not possibly leave the institute without expressing my sincere gratitude.

First of all, I would like to thank my supervisor and mentor, **Dr. Indumathi Mariappan** for offering me this excellent opportunity of pursuing doctoral thesis work under her supervision. I have been fortunate to have such a supervisor with deep knowledge in the field of stem cell biology. She had been available all the time providing guidance and support throughout my career. Her dedication and passion for research fills the room and is contagious. When there is a hurdle, or one is stuck, she makes these two simple statements "If others can do it why can't we do it!?, If others can't do it, then we must do it". I am thankful for her demand for high quality work; and an excellent example of a successful scientist she set for me. I could not have asked for more and I am extremely proud that I am her first Ph.D. student and will carry it like a badge of honor throughout my scientific career. Thank you Madam!

I would like to thank all HoDs of the Department of Animal Biology, University of Hyderabad (UoH) during the Ph.D. tenure: **Prof. B. Senthil Kumaran**, **Prof. Jagan Pongubala** and **Dr. Anita Jagota**; The Deans, School of Life Sciences, UoH during the Ph.D. tenure: **Prof. A.S. Raghavendra**, **Prof. P. Redanna**, **Prof. K.V.A. Ramaiah**, **Prof. S. Dayananda**; the Controller of Examinations and the School Board for all the administrative help and access to the University infrastructures. I also specially thank **Prof. Jagan Pongubala** and all the faculty at the Department of Animal Biology, UoH for their academic and logistics support.

I have been blessed to have two eminent scientists as members of my doctoral research committee: **Prof. Dorairajan Balasubramanian** and **Dr. Chitra Kannabiran.** Prof. Balu (as we all fondly call him) keeps himself updated with current trends in science and makes sure that the students are updated too. His way of explaining complicated concepts to a layman is something every scientist aspires to master. Dr. Kannabiran on the other hand has provided insightful comments and questions from a different perspective that helped me widen my knowledge and bring the thesis to where it is today. I am extremely thankful to both of them.

I would like to thank **Dr. Gullapalli Nageshwara Rao**, chairman of LV Prasad Eye Institute (LVPEI), **Dr. G Chandrasekhar**, vice-chair, LVPEI and **Dr. S Shivaji**, director of

research, LVPEI for providing world-class infrastructure and laboratory facilities and for granting me an opportunity to carry out my doctoral research work. I thank LVPEI for arranging informative lectures and seminars and occasions to meet eminent scholars from various fields.

I specially thank **Dr. Chitra Kannabiran** and **Dr. Subhadra Jalali** for their genetic studies on inherited retinal degeneration conditions that laid a foundation for my thesis work.

I am delighted to have had a wonderful lab family – **Ms. Savitri Maddileti**, **Mr. Vinay Kumar Pulimamidi**, **Ms. Puja Sarkar**, **Ms. Divya Pidishetty**, **Ms. Sudipta Mahato** and **Ms. Trupti Agrawal**. Ms. Maddileti has been there since the beginning of my Ph.D. career and has been a continuous source of help and support in the lab and in my personal welfare. I have learnt a great deal on determination and taking a stand for what is right, from her. My heartfelt thanks to her, for all her contributions in this thesis work. Vinay is the "go-to-person" and a great friend of mine. He had been extensively helpful throughout and I have learnt how to be calm and composed from him. Puja helped in the initial set up of zebrafish facility at our institute. Divya was of great help in zebrafish knockouts screening which is laborious and I am greatly thankful to her. Sudipta and Trupti have always been around, when in need, and gladly helped with smile on their faces. I could not have asked for a better lab family and will greatly miss you all when I leave the institute. Thank you all so much!

I am thankful to all the patient volunteers and their family for participating in the study. I thank **Dr. Milind Naik** for helping in obtaining the skin punch biopsies from the patients. I thank **Dr. Vivek Dave** for helping with sub-retinal injections in rat models. I thank Ramayamma International Eye Bank (RIEB), for providing cadaveric eye balls that was carefully and efficiently used in my research.

I thank **Dr. Dilip. K. Mishra**, Pathology, LVPEI and his team **Mr. Chinchi Naidu**, **Mr. Sreedhar Rao Boyinpally** and **Mr. Balaji** for their help in IHC analysis. A special thanks to Sreedhar for taking an extra step and being always available whenever in need of help.

I am grateful to **Dr. Kapil Bharti,** NEI, NIH, USA for providing me space in his lab for 9 months, for carrying out functional characterizations of patient-specific RPE cells. I thank **USIEF** for the Fulbright Nehru Doctoral Research fellowship for these 9 months. My heartfelt thanks to Dr. Bharti's crew: **Dr. Ruchi Sharma**, **Mr. Davide Ortolan**, **Dr. Mitra Farnoodian**, **Dr. Karla Barbosa**, **Dr. Qin Wan**, **Mr. Justin Chang**, **Mr. Vladimir Khristov**, **Mr. Balendu Shekhar Jha**, **Mr. Roba Dejene**, **Dr. Nathan Hotaling** and **Dr. Arvydas Maminishkis** for providing all sorts of help in the lab and also for making my stay

in US at home. I thank **Dr. Mones AbuAsab**, NEI for his help in electron microscopy and **Dr. Elangovan Boobalan**, NEI for his help in molecular biology work at NEI.

I thank **Dr. Rakesh Mishra**, Director, CCMB for letting me work at the pisciculture lab, CCMB to learn zebrafish maintenance and microinjections. I am greatly thankful to **Dr. Gopal Kushwah** who patiently taught the microinjection technique to me until I was comfortable on my own. I also thank **Dr. Ravinder**, previous technical officer, zebrafish facility, CCMB and the current technical officer, **Mr. Arvinda Swamy** for their continuous support. I also thank **Raju anna** for his help in maintaining the fish at CCMB.

I thank **Mr. Jai Ganesh**, **Ms. Elena Roopchandra** and **Mr. Poornachandra Rao** for providing me administrative support. The support and co-operation from the Institute's communications department, ISD, purchase (**Mr. S. Jagadeesh**), accounts (**Mr. A. Srinivas**), stores, maintenance (**Mr. Ravi, Mr. Suneel Birusanti**), biomedical and house-keeping departments were immense and I would like to thank all of them. I sincerely thank **Ms. Sabera Banu**, **Mr. Sudhakar Kothapalli** and **Mr. Quddus** from Library for helping me get all the books, journal and photocopies needed for my research work.

I made few 'friends for life' during this amazing journey. **Dr. Meha Kabra**, my most awesome friend of all time. She is kind, extremely helpful and enjoys planning trips that never happened. The moral support I continue to receive from her is invaluable. I wish we would complete all the planned trips. **Mr. Syed Hameed** is like a brother to me. As a proud hyderabadi, he showed us around all the important landmarks of Hyderabad and introduced the hyderabadi cuisines which are a delight. He is starting an amazing career in Saudi Arabia, as I write this, and I wish him great success. **Mr. Praveen Edwin Paul**, AKA Kili is extremely generous and is the man of our sports and fun activities. **Ms. Shahna Shahul Hameed** has been a caring friend and has been helpful throughout and especially in the final stages of my thesis writing. **Mr. Baggam Satish Patnaik,** a loving and understanding friend and an awesome roommate. He along with another roommate, **Mr. Aniket Wakure,** are the best and I will miss them greatly when I vacate. **Dr. Sonika Rathi** has been an amazing friend and is fun to be around. I thank **Mr. Tahavar Khan** for being a true and caring friend. I would like to thank all of you for making my stay in Hyderabad the most memorable one. I know I have acted cranky at times but none of you forsook me. I thank each one you for being there as friends and family.

I thank all the faculty of LVPEI. I specially thank **Dr. Subhabrata Chakrabarti** and **Dr. Inderjeet Kaur** for considering me a part of their group and hosting numerous parties.

I feel obliged to thank my friends from other departments of LVPEI. First and foremost, my special thanks to **Ms. Aishwarya Pillai** and **Ms. Priya Varghese**. You both have been a great inspiration and I admire you. I thank **Dr. Beulah Christy, Ms. Lakshmi, Ms. Malathi, Mr. Vinay** and their team for their immense rehabilitation work and letting me volunteer in their department. I am thankful to my good friends **Ms. Mansha Palo** from Oculoplasty, **Mr. Sunil Kumar** from ISD and **Mr. Giridhar Velluri** from Biomedical department.

I would like to thank my friends and colleagues at LVPEI: Mr. **Cyril Jones**, Mr. **Daniel Nisakar**, Mr. **Abubakar Siddiqui**, Ms. **Chitra Joseph**, Ms. **Stanley Ancy**, Dr. **Nageshwar Rao**, Dr. **Pulla Rao Vendra**, Dr. **Ganeswara Rao Musada**, Dr. **Rachna Shukla**, Dr. **Praveen K Balne**, Mr. **Ranjith Konduri**, Mr. **Srinivasu K**, Ms. **Mangalangi Praveen**, Mr. **Abhinav Kethri**, Mr. **Nanda Shivshankar**, Dr. **Nagaveni Shivshetty**, Dr. **Kalyan Chakravarthy**, Mr. **Rishikesh Gupta**, Mr. **Mukesh Damala**, Ms. **Swatilekha Hazra**, Dr. **Jayasudha R**, Dr. **Khatija Tabassum**, Ms. **Natalia Sharma**, Mr. **Enoch Raju**, Mr. **Gaurav Naik**, Ms. **Dhanashree Deshmukh,** Ms. **Priyanka Jayabhaskar**, Ms. **Meenakshi Rai**, Ms. **Shannon Shetty**, Ms. **Sneha Kumari**, Mr. **Samir Bera**, Mr. **Fatin Khan**, Ms. **Jaishree Gandhi**, Ms. **Ravali Pulipaka**, Ms. **Supriya Krishna** and Dr. **Derin Thomas**.

I thank the funding agencies, **Department of Biotechnology**, **Hyderabad Eye Research Foundation**, **Champalimaud Translational Centre for Eye Research** and **Prof. Brien Holden Eye Research Centre** for all their financial and infrastructure support.

Lastly, I would like to thank my family for all their love and encouragement. Words cannot express how grateful I am. **Mom** and **Dad**, this is for you!! Without your faith and support this would not have been possible. I am lucky to have you two in my life. Thank you both for raising and supporting me in all my pursuits, for all of the sacrifices that you have made and for all your prayers that have sustained me thus far. I wish God provides me with the strength and ability to make you proud and bring every possible reason of happiness to you. I also thank my sister **Flora**, my brother **Jerin** for supporting me throughout my life. My brother-in-law, **Elaa** and my sister-in-law, **Remy**. Thank you all for understanding me, for thinking of my welfare and my happiness. I am privileged to have you all as my family. I would also like to mention the kids at home (**Grace**, **Levin**, **Shara** and **Jheel**), whose charming smiles work like an anti-depressant during the hard times. Love you all!!

Lastly I thank the Almighty for everything!

Praveen Joseph Susaimanickam

LVPEI, Hyderabad

ABSTRACT

Retinal degeneration (RD) is a progressive disorder wherein, there is a gradual loss of rod and cone cells leading to disease manifestations like night blindness, which progresses to peripheral vision loss and finally leading to loss of central vision and complete blindness. Pathogenic mutations in over 260 genes associated with retinal development, maintenance and function are linked to the disease. However, the underlying molecular mechanisms that result in retinal cell loss remain elusive for most of the reported gene mutations. Studies based on limited patient samples, retinal cell lines and knock out animal models has led to our current understanding of the disease. However, the diverse disease phenotypes and severities observed among patients are attributed to hundreds of different mutations reported within the same gene involved. Whole gene knockout animal models are therefore insufficient to understand such diverse retinal phenotypes. This study is aimed to establish relevant developmental model systems to evaluate the effect of patient-specific mutations in two of the RD conditions – Autosomal recessive retinal degeneration, ARRD and Leber congenital amaurosis, LCA12. The ARRD patient-specific iPSC line (KR) carrying mutation in *ABCA4*, showed abnormal eye field commitment with defective optic cup formation and the retinal progenitors exhibited preferential fate commitment towards RPE lineage. Also, the RPE cells derived from KR, displayed abnormal tight junctions and microvilli projections that resulted in severely altered epithelial barrier functions and ion transport functions. The LCA12 patient-specific iPSC line (VS) carrying a mutation in *RD3*, showed normal eye field commitment and gave rise to three-dimensional retinal organoids and RPE, upon retinal differentiation. While the RPE cells derived from VS showed no significant difference in their morphology and function when compared to the healthy control cells (F2), the retinal organoids indicated possible lamination defects. Similar lamination defects was also observed in the homozygous zebrafish mutant model of *rd3 (rd3*$^{-/-}$*)*, created in this study. The patient specific iPSC models thus generated can serve as useful tools, to understand the molecular mechanisms behind inherited retinal degenerative conditions; for potential drug screening applications and to carry out proof-of-concept studies on mutation correction. The zebrafish mutant models are ideal to understand disease manifestations at various time points, right from early stages of retinal degeneration to its progression into late and severe form of the disease, leading to complete blindness. Finally, a lentivirus-based vector system, encoding the RD3 promoter driven *RD3* transgene cassette with a GFP reporter, was designed and constructed to evaluate its applications in future gene supplementation studies.

Contents **Page No**

15. **Published papers**

16. **Plagiarism report**

List of Tables

List of Figures

List of Abbreviations

Abbreviations	Full forms
A2E	N-retinylidene-N-retinyl-ethanolamine
A2PE	di-retinoid-pyridinium-PE
ABCA4	ATP Binding Casette subfamily A member 4, gene
ABCA4	ATP Binding Cassette subfamily A
ABCR	retina specific ABC transporter
AEC	Animal Ethics Committee
AGE	Agarose gel electrophoresis
ALP	Alkaline phosphatase
AMD	Age-related macular degeneration
A-P	Anterior-Posterior
ARR1	Arrestin
ARRD	Autosomal recessive retinal dystrophy
ARRP	Autosomal recessive retinitis pigmentosa
ARVO	Association for Research in Vision and Ophthalmology
ATP	adenosine triphosphate
atRDH	all-trans retinal dehydrogenase
BEST1	Bestrophin1
bFGF	basic Fibroblast growth factor
BMP4	Bone morphogenetic protein 4
bp	base pair
BSA	Bovine serum albumin
C1orf36	chromosome1 open reading frame 36
$CaCl_2$	calcium chloride
Cas9	CRISPR-associated endonuclease 9
CBA	chicken β actin promoter
CDM	corneal differentiation medium
cDMEM	complete Dulbecco's Modified Eagle medium
cDNA	complementary DNA
CDS	cell dissociation solution
cGMP	cyclic guanosine monophosphate
CMV	cytomegalovirus
CP	corneal primordia
CRALBP	cellular retinaldehyde binding protein
CRBP	cellular retinoid binding protein

CRD	cone rod dystrophy
CRISPR	clustered regularly interspaced Short Palindromic Repeats
crRNA	CRISPR-RNA
DAB	3,3'-diaminobenzidine
DAPI	4',6-diamidino-2-phenylindole
ddATP	dideoxyadenosine triphosphate
ddCTP	dideoxycytosine triphosphate
ddGTP	dideoxyguanosine triphosphate
ddNTPs	dideoxynucleotides triphosphates
ddTTP	dideoxythiamidine triphosphate
DKK1	Dickkopf protein
DM	differentiation medium
DNA	deoxyribonucleic acid
dNTP	deoxyribonucleotide triphosphate
dpf	days post fertilization
DPX	distyrene plasticizer xylene
DSBs	double strand breaks
DTT	dithiothreitol
D-V	Dorsal-Ventral
EB	embryoid body
EC	Ethics Committee
ECD	extracellular domain
ECM	extracellular matrix
EDTA	ethylenediaminetetraacetic acid
EF	eye field
eEF1α	eukaryotic elongation factor 1α promoter
EFP	eye field primordium
EFTFs	eye field transcription factors
EGF	epidermal growth factor
EGFP	enhanced green fluorescent protein
EHS	Engelbreth-Holm-Swarm
ELISA	enzyme-linked immune sorbent assay
ELU	elution buffer
EMT	epithelial to mesenchymal transition
EQU	equilibration buffer
ERG	electroretinogram
ESC	embryonic stem cell
EtBr	ethidium bromide

F2	healthy human control
FBS	fetal bovine serum
FGF	Fibroblast growth factor
G*	Gα-GTP
GAP	GTPase activating protein
GC	guanylate cyclase protein
GCAPs	guanylate cyclase activating proteins
GDP	guanosine diphosphate
GMP	guanosine monophosphate
cGMP	current good manufacturing practice
GRK1	Rhodopsin kinase
GTP	guanosine triphosphate
GUK	guanylate kinase
H&E	hematoxylin and eosin
hAM	human amniotic membrane
HDAC	histone deacetylase
HDFs	human dermal fibroblasts
HDR	homology directed repair
hESC	human embryonic stem cell
hiPSC	human induced pluripotent stem cell
HRP	horseradish peroxidase
ICC	immunocytochemistry
ICF	informed consent form
ICM	inner cell mass
IC-SCR	Institutional Committee for Stem Cell Research
IHC	immunohistochemistry
indels	insertions-deletions
iPSCs	induced pluripotent stem cells
IRB	Institutional Review Board
IRBP	inter-photoreceptor retinoid binding protein
IRDs	inherited retinal diseases
IRES	internal ribosomal entry site
IS	inner segment
IVC	in vitro cleavage
IVT	in vitro transcription
KCl	potassium chloride
KR	patient with mutation in *ABCA4* gene
LB	Luria-Bertani

LCA	Leber congenital amaurosis
Lhx2	LIM homeodomain transcription factor
LRAT	lecithin retinol acyl transferase
LSCD	limbal stem cell deficiency
LYS	lysis buffer
MERTK	membrane-bound receptor tyrosine kinase
MET	mesenchymal to epithelial transition
MG	Müller glia
$MgCl_2$	magnesium chloride
MITF	microphthalmia-associated transcription factor
NaB	sodium butyrate
NaCl	sodium chloride
NaH_2PO_4	sodium dihydrogen phosphate
$NaHCO_3$	sodium bicarbonate
NaOH	sodium hydroxide
NBD	nucleotide binding domain
NBD2	second nucleotide binding domain
NCBI	National Centre for Biotechnology Information
NCLAS	National Center for Laboratory Animal Sciences
NEU	neutralization buffer
NGS	next generation sequencing
NHEJ	non-homologous end joining
NIM	neural induction medium
NIN	National Institute of Nutrition
NMD	nonsense mediated decay
NR	neuro-retina
NRM	neuro-retinal medium
NR-PE	N-retinylidene-phosphotidylethanolamine
OCT	optical coherence tomography
OD	optical density
OLM	outer limiting membrane
ONL	outer nuclear layer
OPL	outer plexiform layer
OPN1MW	middle wavelength opsin1 or green opsin
OPN1MW	medium wavelength opsin 1 or green opsin
OS	outer segment
OSKM	OCT4, SOX2, KLF4 and cMYC / Yamanaka factors
OVs	optic vesicles

PBS	phosphate buffered saline
PCR	polymerase chain reaction
P-D	Proximal-Distal
PDE	phosphodiesterase
PDE*	activated phosphodiesterase
PDE6C	phosphodiesterase 6C
PE	phosphatidylethanolamine
PEDF	pigment epithelium derived factor
PI	propidium iodide
PKC-β	protein kinase C beta
PKC-β	protein kinase C beta
Plat-A	Platinum-A
pNR	prospective neuro-retinal
pOS	prospective Optic stalk
POS	photoreceptor outer segment
PRC	photoreceptor cell
pre-crRNA	precursor CRISPR-RNA
pRPE	prospective retinal pigmented epithelium
PSCs	pluripotent Stem cells
R*	metarhodopsin
RA	retinoic acid
RD	retinal degeneration
RD3	retinal degeneration 3 protein
RD3PFL	full length RD3 promoter
RD3P-FL	full length RD3 promoter
RD3PM	minimal RD3 promoter
RD3P-M	minimal RD3 promoter
RDH	retinal dehydrogenase
RDM	retinal differentiation medium
REC	Recoverin
RES	resuspension buffer
RetGC	retinal guanylyl cyclase
RGCs	retinal ganglion cells
RHOK	rhodopsin kinase
RIEB	Ramayamma International Eye Bank
RLBP1	retinaldehyde binding protein 1
RNA	ribonucleic acid
RNP	ribonucleoprotein
ROCK	Rho-associated protein kinase
RP	Retinitis Pigmentosa

RPCs	retinal progenitor cells
RPE	retinal pigment epithelium
RPE65	retinoid isomerohydrolase 65
RPEM	RPE maturation medium
rpm	revolutions per minute
RT	room temperature
RT-PCR	Reverse Transcriptase PCR
RX	retinal homeobox 1
SDS	sodium dodecyl sulphate
SEAM	self-formed ectodermal autonomous multi-zones
SEM	scanning electron microscope/microscopy
SER	smooth endoplasmic reticulum
SFEB	serum-free floating culture of embryoid-body-like aggregates
sgRNA	single guide RNA
SNP	single nucleotide polymorphism
STR	short tandem repeats
TAE	Tris, Acetic acid and EDTA
TALEN	Transcription Activator Like Effector Nuclease
TEM	transmission electron microscope/microscopy
TEP	trans-epithelial potential
TER	trans-epithelial resistance
TGFß	Transforming growth factor beta
TMD	trans-membrane domain
tracrRNA	trans-activating crRNA
TSS	transcription start site
TYR	Tyrosinase
UCSC	University of California, Santa Cruz
UV	ultraviolet
VEGF	vascular endothelial growth factor
VS	patient with mutation in *RD3* gene
VSX2	visual homeobox2
WASH	wash buffer
ZFIN	Zebrafish Information Network
ZFNs	zinc finger nucleases

CHAPTER 1

INTRODUCTION

1. Introduction

Retina is the light sensitive tissue at the back of a vertebrate eye that converts the light signals into nerve impulses by a biochemical phenomenon known as photo-transduction. The light sensitive cells of the retina are called the photoreceptors and are of two types namely, the rods and the cones. The initial nerve impulse generated in the photoreceptors travel through other cells of the retina, like the bipolar cells and ganglion cells and finally reaches the visual cortex of the brain. The neurons in the brain decodes this message and help in image perception and visual response (Hurley 2009).

Retinal degeneration (RD) is a progressive disorder wherein, there is a gradual loss of rod and cone cells leading to disease manifestations like night blindness, which progresses to peripheral vision loss and finally leading to loss of central vision and complete blindness. Such degenerative changes occur as a result of aging (E.g. Age-related macular degeneration (AMD)) or due to inherited genetic abnormalities (E.g. Retinitis Pigmentosa (RP), Leber congenital amaurosis (LCA), Stargardt disease etc.).

Pathogenic mutations in over 260 genes associated with retinal development, photoreceptor and retinal pigment epithelial cell functions such as photo-transduction, retina-specific intracellular transport, vitamin A metabolism, energy metabolism, phagocytosis, pigment biogenesis, retina-specific gene regulation etc., are linked to inherited retinal degeneration (Daiger *et al.* 1998). However, the underlying molecular mechanisms that result in retinal cell loss remain elusive in case of most mutations reported so far. Studies based on limited patient samples, retinal cell lines and on knock out animal models had led to our current understanding of the disease. However, the diverse disease phenotypes and severities observed among patients can be attributed to hundreds of different mutations reported within the same gene involved. Whole gene knockdown animal models are therefore insufficient to understand such diverse retinal phenotypes. Therefore, it is important to establish relevant *in vitro* and *in vivo* developmental model system to evaluate a multitude of patient-specific mutations that result in various disease phenotypes.

A landmark report in 2007 showed that an adult human somatic cell can be reprogrammed to an embryonic stem cell (ESC)-like state by ectopic expression of transcription factors such as OCT4, SOX2, KLF4 and cMYC (OSKM) or collectively called as Yamanaka factors (Takahashi *et al.* 2007). Like ESCs, these reprogrammed stem cells can differentiate into tissue-specific cell types of all three lineages and are therefore termed as 'induced pluripotent

stem cells' or shortly 'iPSCs'. Human iPSCs have been shown to differentiate efficiently into retinal cells and are currently being evaluated for their applications in basic research, disease modeling, drug screening and for regenerative applications (Link and Collery 2015).

Human iPSCs can be differentiated into retinal cells *in vitro,* in a step-wise lineage commitment strategy and can recapitulate most of the early developmental steps in a dish. This is achieved by the addition of various growth factors, small molecules and other supplements in culture medium, either to stimulate or to suppress the activities of various signaling cascades, at different stages of differentiation. It is thus possible to direct the differentiation of iPSCs, first towards an anterior, neuro-ectoderm fate and then towards eye field specification; followed by RPE and neuro-retinal cup development (Bertacchi *et al.* 2015; Ikeda *et al.* 2005; Lupo *et al.* 2013; Mellough *et al.* 2015; Osakada *et al.* 2009). Retinal dystrophic patient-specific iPSC-derived retinal tissues would then serve as ideal *in vitro* models to study the effects of patient-specific mutations during early stages of retinal development, resulting in disease phenotypes.

Recent reports have also shown that iPSC-derived retinal cells could be maintained in culture for longer durations to achieve morphological and functional maturation (Zhu *et al.* 2018). However, their gene expression signature mostly matches that of fetal stage retinal cells. Incomplete maturation of iPSC-derived tissues *in vitro* is therefore a bottle neck in considering them as disease models to understand mature cell-specific functions and disease phenotypes. This requires a simpler *in vivo* animal model that will allow us to carryout quick validations of several disease-specific mutations, in fully developed adult retinal tissues.

Zebrafish models have various advantages owing to their small size, which enables easy maintenance, short generation time, high breeding ability and relatively large clutch size, external fertilization, rapid development, transparent embryos, efficient genetic manipulations with simpler tools and easily testable developmental behaviors. With the advent of CRISPR-Cas9 based genome editing systems (Doudna and Charpentier 2014; Jinek *et al.* 2012; Mali *et al.* 2013; Wiedenheft, Sternberg, and Doudna 2012), zebrafishes have proven to be useful models in forward genetic studies to understand the functions of various genes and to elucidate the mechanisms behind inherited disease pathogenesis (Link and Collery 2015). Further, the visual system of zebrafish is strikingly similar to that of humans and 72% of the human genes have at least one ortholog in zebrafish. Few reports have shown them to be useful models to study various ocular disease conditions such as, retinoblastoma, glaucoma, retinitis pigmentosa (RP), ciliopathies and albinism (Link and

Collery 2015). Therefore, mutant fishes with retinal dystrophy related gene-specific edits would serve as valuable *in vivo* models to understand the development of disease.

Long-term genetic studies on hundreds of retinal dystrophic patients treated at our clinic have identified novel and reported mutations in several genes linked to autosomal recessive retinitis pigmentosa (ARRP), Leber congenital amaurosis (LCA) and age-related macular degeneration (AMD) (Biswas *et al.* 2016; Falk *et al.* 2012; James S. Friedman *et al.* 2006; Kannabiran, H. Singh, *et al.* 2012; Kannabiran, Palavalli, and Jalali 2012; Kannabiran, H. P. Singh, and Jalali 2012; Lalitha *et al.* 2002; Singh *et al.* 2006, 2009). Based on the available patient-data and genetic information, two affected probands and a healthy individual were chosen as candidates to generate patient-specific iPSCs as *in vitro* disease models. The first one with autosomal recessive retinal dystrophy (ARRD) (coded as KR), carried a homozygous c.6088C>T variation in *ABCA4* (Singh *et al.* 2006) and the second one with Leber congenital amaurosis 12 (LCA12) (coded as VS), carried a homozygous c.296+1G>A variation in *RD3* (Friedman *et al.* 2006) and the healthy human control is coded as F2. Both *ABCA4* and *RD3* play a very important role in mediating visual transduction cycles within photoreceptor cells (S. Azadi, Molday, and Molday 2010; Quazi, Lenevich, and Molday 2012). RD3 being a small transcript encoded by 2 exons, a whole gene supplementation strategy would be feasible in patient-specific iPSCs to enable mutation correction *in vitro*. ABCA4 being a large transcript with 50 exons, an *in situ* genome editing of patient-specific mutations in iPSCs would be an ideal strategy to achieve disease reversal. Such patient-specific iPSCs would therefore serve as ideal *in vitro* models to understand the disease and also evaluate the proof-of-concept of different disease reversal strategies in future.

Based on the above rationale, this study was carried out to establish and characterize suitable model systems for two of the inherited retinal degenerative disease conditions namely, ARRD and LCA12, with the following aims.

1. To develop patient specific iPSC-derived retinal cultures as *in vitro* models of retinal degeneration.
2. To develop zebrafish null mutants as *in vivo* models of retinal degeneration.

CHAPTER 2

REVIEW OF LITERATURE

2. Review of literature

2.1. Human eye and visual perception

An eye is a major sensory organ that enables light perception and empowers us to see the outside world and respond to visual cues (**Fig 2.1.A**). It functions like a camera, with a transparent cornea in the front that allows light entry into the eye. The lens on the inside helps to focus the light on to the retina, which is the sensory screen at the back of the eye. The light sensing photoreceptor cells of the retina captures the photons and activates a series of biochemical reactions that results in the generation of action potentials across membranes. The electrical signals from both the eyes are then transmitted via the optic stalk to the visual cortex of the brain, which decodes the signals and help in binocular vision, depth perception, color perception and visual response. Abnormalities affecting any parts of the eye or the visual cortex can lead to visual impairment.

2.2. Development of the eye

The human eye, like any vertebrate eye is derived from the tissues of ectodermal and mesodermal origin in the head region of a developing embryo. The ocular surface ectoderm develops into conjunctival and corneal epithelia, eye lids, the lens and the lachrymal apparatus. The neural ectoderm develops into the optic cup, which develops into the neuronal retina and RPE, epithelial linings of the ciliary body and iris, the optic nerve and a portion of the vitreous humor. The rest of the eye tissues such as the orbital muscles, the iris and eye lid sphincter muscles, choroidal and corneal stromal cells and the entire vasculatures are derived from the mesenchyme and head surface neural crest cells.

2.2.1. Bilateral optic cups and lens vesicle

The initiation of eye development is marked by the appearance of shallow grooves, called optic grooves or optic sulci, on each side of the invaginated forebrain at day 22 of embryonic development (Warwick 1977). The neural tube is open at the anterior side. With the closing of the neural tube, the optic grooves out pocket towards the surface ectoderm, through the adjacent mesenchymal cells, to form the optic vesicles. During this process, the connection of the optic vesicles with the forebrain forms the optic stalks, which further develop into optic nerves. When the optic vesicles come in contact with the surface ectoderm, they induce the surface ectoderm cells to proliferate and form the lens placodes (precursor of the lens). The thickening lens placode further invaginates and in turn pushes the distal margins of the optic vesicles simultaneously. The invaginated lens placode is now called the lens pit, which soon becomes circular and detaches from the surface ectoderm and form the lens vesicle.

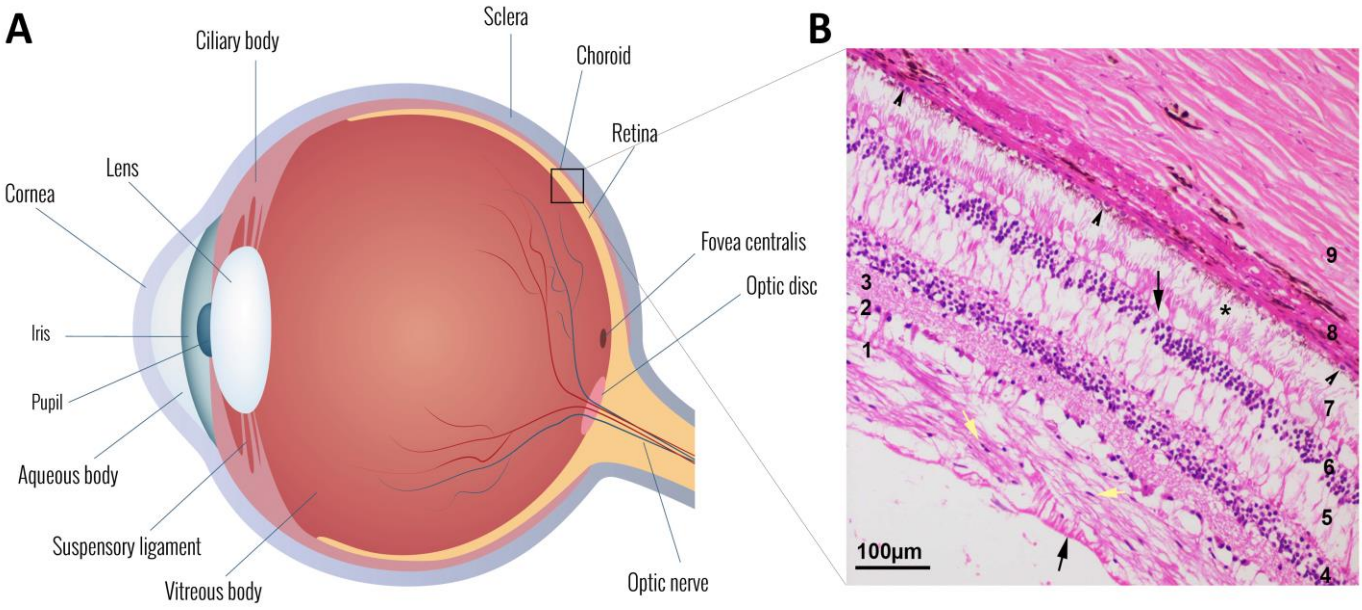

Figure 2.1: Cross sectional view of an adult human eye and the retina. ***A***. *Cross sectional view of a human eye, showing the presence of a transparent cornea on the front, the crystalline lens in the middle and the light sensitive retina on the posterior side (image designed by Freepik).* ***B***. *Hematoxylin and eosin (H&E) stained section of the posterior segment of a human eye ball. An adult retina comprises of ten distinct layers namely the inner limiting membrane (**ILM**) (bottom upright arrow), which acts as the boundary between the retina and the vitreous body and formed by the end feet of Müller glial cells. The neurofilament layer (**NFL**) (**1**) is made of ascending axons from retinal ganglion cell layer (**GCL**) (**2**). Astrocytes can be seen populating the NFL layer (yellow arrow heads). The inner plexiform layer (**IPL**) (**3**) is made of inter connecting dendritic networks of inter neurons (horizontal cells, bipolars and amacrine cells) in the inner nuclear layer (**INL**) (**4**). The outer plexiform layer (**OPL**) (**5**) is made of inter connecting dendritic networks of photoreceptor (PR) cells (rods and cones) in the outer nuclear layer (**ONL**) (**6**). The outer limiting membrane (**OLM**) (top inverted arrow) is made of tight junction complexes between the plasma membranes of photoreceptor inner segments and the apical processes of Müller glial cells, thus establishing a natural barrier between the sub-retinal space and the ONL. The photoreceptor outer segment (**OSL**) layer (**7**), carry photo pigments (opsins) in their specialized disc like membrane structures, for capturing the incoming photons. The retinal pigmented epithelial (**RPE**) cell layer (black arrow head) provides paracrine support to PR cells, clear away the routinely shed PR outer segments in the sub-retinal space, participate in visual cycle and establishes the blood-retinal barrier by way of tight intercellular junctions and Bruch's membrane (basement membrane) adhesions. The choroid layer (**8**) beneath the RPE layer is richly supplied with blood vessels for gas exchange and to nourish the retinal cells. The thick and acellular sclera (**9**) forms the outermost covering of the eye.*

The invaginated optic vesicle forms a bi-layered structure termed as the optic cup. This further takes up a shape of a goblet and the lens vesicle is found hanging in the mesenchymal mass of cells at this point. The developing optic cup and the optic stalk have an opening, called the choroidal fissure, throughout their inferior side for the hyaloid vessels to reach the optic cup and also the lens vesicle. At the end of the 7th week, the lips of the choroidal fissure fuse and the mouth of the optic cup narrows into a circular opening that becomes the future pupil. This process also leads to the formation of a canal in the optic stalk (lumen),

within which the hyaloid vessels are enclosed. When the fetal lens matures, the hyaloid vessels disintegrate on the distal end and the hyaloid vessels on the proximal end persist to form the central retinal artery.

2.2.2. Retina

The outer layer of the optic cup is thin compared to the inner layer. The outer and inner layer of the optic cup is separated by the intra-retinal space which becomes the sub-retinal space in the developed eyeball. The cells of the outer layer start accumulating melanin granules and become the future retinal pigment epithelium. Around 5 weeks of development, the inner layer of the optic cup can be defined into two parts. The anterior $1/4^{th}$ portion including the rim is called the Caeca retinae and the posterior $4/5^{th}$ portion called the Optica retinae (containing photoreceptors and the other retinal neurons).

While the development of RPE is simple, the development of the neuronal retina is a bit complicated. The cells of the optica retinae next to the intra-retinal space begin to develop into external neuroblastic layer which then matures to rod and cone photoreceptors. The internal neuroblastic layer gives rise to the Müller glia (MG), bipolar neurons, amacrine and horizontal cells. The ganglion cell layer (GCL) present at the inner side of the retina begins to appear by day 120. The axons of the GCL group together and fill the lumen of the optic stalk to form the optic nerve, thus linking the retina to the brain's visual cortex. The intra-retinal space diminishes in volume as the RPE and neural retinal layer comes close to each other and is now called the sub-retinal space. Although all the layers of the retina develop by 8 months, the photoreceptors attain complete maturity only few months after birth. This is why the visual acuity of newborns is poor and becomes better as they grow. The mature retina has ten layers and is almost transparent (except the RPE layer), so that light can pass through all the layers until the photoreceptor layer at the distal end, without undergoing much loss due to absorption or refraction (**Fig 2.1.B**).

2.2.3. Lens

At about six weeks, after the lens vesicle's formation, the epithelial cells at the posterior region of the vesicle elongate towards the anterior side, give rise to the primary lens fibers and fill the lumen of the vesicle. By the end of seven weeks, the primary lens fibers reach the anterior epithelium, completely replacing the lumen, forming the lens nucleus. The lens keeps on developing as the epithelial cells in the equatorial zone continuously adds secondary lens fibers around the primary lens fibers. The lens fiber cells at the center lose their nucleus and arrange themselves in a compact manner so that, the lens is almost transparent.

2.2.4. Ciliary body

At seven weeks, the eye primordium is completely embedded in the mesenchyme. The caeca retina, the 1/5th anterior portion of the optic cup, undergoes few folds to form the ciliaris retinae, which in turn contributes to ciliary body formation. The portion anterior to ciliaris retinae becomes iridica retinae, which forms the inner layer of the iris. The inner and outer layer of the iridica retinae and ciliaris retinae, forms the non-pigmented and the pigmented epithelium of the ciliary body and the iris respectively. The ciliary body and stroma of the iris are made up of the neural crest cells that migrate into that area. The sphincter pupillae and the dilator pupillae muscles of the iris, develop from the neuroectoderm-derived neural crest cells at the tip of the optic cup. The ciliary muscles develop from the mesenchymal cells in the surrounding. The melanin pigmentation of the iris varies resulting in different eye color.

2.2.5. Cornea, sclera and the choroid

During the 6th and the 7th week, the mesenchyme surrounding the eye primordium differentiates into a bi-layered structure around the optic cup including the region anterior to the iris. The outer layer, comparable to the dura mater of the brain, develops into the fibrous sclera and is continuous with the optic nerve's dura mater. The inner layer, comparable to the pia mater of the brain, develops into a highly vascularized pigmented layer called the choroid. In the anterior region of the iris, the two layers differentially arrange themselves with a gap in between, called the anterior chamber. The thin inner layer, now called the iridopupillary membrane separates the anterior chamber from the posterior side of the eye primordium. The outer layer becomes thick and runs continuous with the sclera. The mesenchymal cells of the outer layer later flatten to form the corneal stroma. The anterior side of the stroma is lined by neatly arranged epithelial cells from the surface ectoderm and the posterior side is line by a monolayer of hexagonal endothelial cells derived from the neural crest cells that moves from the optic cup rim. The epithelium, the stroma and the endothelium together form the cornea on the anterior side. Eventually, the iridopupillary membrane disintegrates completely, allowing the interaction between the anterior and the posterior chamber of the eye.

2.2.6 Vitreous body

The mesenchyme, in which the eye primordium is suspended, invades the inside of the optic cup through the choroidal fissure, prior to its closure. Inside the optic cup, the mesenchymal cells form a delicate network of fibers connecting the retina and the lens along with the hyaloid vessels-to enrich the lens and the retina. The interstitial space, between the retina and the lens, is later filled with the vitreous body, which is a gelatinous substance that develops

from the neural crest mesenchymal cells. Later, the hyaloid artery disintegrates leaving a canal like structure in the vitreous known as the hyaloid canal.

2.2.7. Optic nerve

The closure of choroid fissure encloses the hyaloid artery in the middle and the nerve fibers around them, thus forming the optic stalk. The inner layer of the optic stalk thickens, with an increasing number of nerve fibers projecting from the ganglion cells to the brain. The outer layer (dura mater) of the optic stalk merges with the sclera and the inner layer (pia mater) merges with the choroid. The outer layer and the inner layer of the optic stalk fuse to form the optic nerve.

2.2.8. Eyelid, conjunctiva and the lachrymal gland

During the sixth week, the neural crest cells and the surface ectoderm assembles itself in front of the cornea to form the eyelids. The eyelids are like small folds of surface ectoderm filled with the neural crest cells both the in superior and inferior region of the eye. Until 7 months of gestation the eyelids are fused creating a space between the cornea and the eyelids called the conjunctival sac. After 7 months the eyelids separate, with well-developed orbicularis oculi (eyelid muscle), eyelashes and Meibomian glands. As the eyelids separate, the conjunctival sac develops a continuous epithelial lining on the inner sides of both the eyelids, which also runs continuously on the sclera and cornea. The lachrymal gland arises from the ectodermal cells in the conjunctival sac. The lachrymal gland undergoes 3 stages of development – the presumptive glandular stage, epithelial bud stage and the glandular maturity stage. By the end of 16 weeks, mature lachrymal gland is fully developed.

2.2.9. Extraocular muscles

The development of extraocular muscles requires the interaction between the mesenchymal cells and the neural crest cells around the eyeball. Three cranial innervated somites are required for the development of extraocular muscles. The cranial nerve III innervated somite forms five of the seven extraocular muscles. The remaining two somites form the other two extraocular muscles.

2.3. Genetic regulation of eye development

The molecular mechanism behind eye development has been extensively studied in the past few decades. We have understood the roles of only a fraction of molecules identified to be involved in eye development so far (Jean, Ewan, and Gruss 1998). Large scale mutation screens in mouse and zebrafish have led to the development of a number of eye mutants (Graw 1996; Heisenberg *et al.* 1996; Karlstrom *et al.* 1996; Malicki *et al.* 1996). Few genes are

well characterized and their mutation phenotypes are correlated to the human disease. However, the roles of a majority of mutated genes in eye development and function are not fully understood. Studying inherited human eye diseases and the disease pathology have enabled the identification of several regulatory molecules in eye development and function (J.L. Zagozewski, Zhang, and Eisenstat 2014a). Such regulatory molecules can be classified based on their involvement in different stages of eye development

- Eye field specification
- Splitting/bifurcation of the eye field
- Optic vesicle development
- Optic cup formation
- Maturation of eye structures

2.3.1. Eye field specification

As the forebrain develops, after the neural induction and patterning, its anterior region is specified to form the eye field. This is achieved by graded Wnt signaling which establishes the anterior-posterior (A-P) polarity in the developing forebrain (Erter *et al.* 2001; Lekven *et al.* 2001). Increased Wnt signaling promotes posterior neural fates and decreased Wnt signaling promotes anterior neural fates (Kiecker and Niehrs 2001). In the anterior neural plate, the eye field is specified by the co-ordinated expression of the eye field transcription factors (EFTFs) (Zuber *et al.* 2003). Most of the studies on EFTFs have been done on *Xenopus laevis* and it includes Pax6, Tbx3/ET, Lhx2, tll/Tlx, Six3, Rx1/Rax and Six6/Optx2. Loss of function studies of one of these EFTFs in animal models lead to abnormal or absent eyes, implying the importance of these gene in early eye development (Carl, Loosli, and Wittbrodt 2002; Mathers *et al.* 1997; Porter *et al.* 1997). *PAX6* and *RAX* mutation in humans cause aniridia (absence of iris) and anophthalmia (absence of eye) respectively (Brown *et al.* 1998; Voronina *et al.* 2004). Also, overexpression of an individual EFTF or a 'cocktail' of EFTFs can induce ectopic eye formation in vertebrate models (Chow *et al.* 1999; Loosli, Winkler, and Wittbrodt 1999; Oliver *et al.* 1996). Thus, the EFTFs and more specifically the *PAX6*, is considered the "Master regulator of eye development".

2.3.2. Splitting of eye field

Splitting of the EF (Bilitou and Ohnuma 2010; Zuber *et al.* 2003), is crucial to form two distinct eyes, failure of which results in cyclopia (single eye) (Chiang *et al.* 1996). Shh signaling is crucial for midline establishment and for the bifurcation of the anterior eye field. The EF splitting fails in *Shh* mutant mice, thus producing a single midline EF and holoprosencephaly

(failure of forebrain to develop into two hemispheres) (Chiang *et al.* 1996). Also, *Shh* is regulated by *Six3* and any deregulation here leads to holoprosencephaly (Geng *et al.* 2008). In addition to regulating the splitting of EF, Shh upregulates *Pax2*, which in turn establishes the boundary between the optic stalk and the optic vesicle (Keller *et al.* 1994).

2.3.3. Optic vesicle development

Following the eye field specification and splitting, the EFTF, *Rx* starts expressing in the lateral walls of the forebrain-the anterior neural plate and subsequently in the optic vesicles. Mouse embryos that lack Rx fail to form the optic groove and the vesicle (Mathers *et al.* 1997), suggesting that Rx is the key regulator in the induction of the anterior neural plate to form the optic groove and then the vesicle. In zebrafish, lateral evagination and expansion of the optic vesicles (OVs) from the forebrain are driven by the migration of $rx3^{+}$ retinal progenitor cells (RPCs) (Rembold *et al.* 2006).

While the OV evaginates, Dorsal-Ventral (D-V) and Proximal-Distal (P-D) patterning occurs simultaneously. Shh plays a vital role in providing ventral identity to the optic vesicles by driving the expression of *Vax1* and *Vax2,* the ventralizing homeodomain transcription factors (Bertuzzi *et al.* 1999; Mui *et al.* 2005; Ohsaki *et al.* 1999; Sasagawa *et al.* 2002; Take-uchi 2003). The dorsal OV patterning is mediated by bone morphogenetic protein-4 (*BMP4*), that belongs to the transforming growth factor -beta (TGF-ß) family by inducing *Tbx5* expression (Behesti, Holt, and Sowden 2006; Koshiba-Takeuchi 2000; Sasagawa *et al.* 2002). Dorsalization fails then Tbx5 is misexpressed (Koshiba-Takeuchi 2000). Another transcription factor involved in D-V patterning of the OV is *Lhx2*, a LIM homeodomain transcription factor (Hägglund, Dahl, and Carlsson 2011; Porter *et al.* 1997; Yun *et al.* 2009). Absence of *Lhx2,* completely arrests the development of the eye at the optic vesicle stage. Further the dorsal-ventral determinants, Bmp4, Tbx5 and Vsx2 are completely misregulated in the arrested OVs leading to D-V patterning defects (Yun *et al.* 2009).

Adding to D-V patterning, Shh also plays a role in P-D patterning by regulating the specific expression of Pax2 in the proximal side (which later develops into optic stalk) and Pax6 in the distal side (which later develops into optic cup) (Ekker *et al.* 1995; Macdonald *et al.* 1995). Also, the Pax2 and Pax6 suppress each other to maintain the optic stalk and optic cup boundary (Schwarz *et al.* 2000). Similarly, the ventral identifiers *Vax1* and *Vax2* restrict their expression to optic stalk and the ventral-neural retina respectively. Misexpression of Vax1, Vax2, Pax2 and Pax6 leads to defective boundaries between the optic stalk and the optic cup (Barbieri *et al.* 1999; Bertuzzi *et al.* 1999; Ekker *et al.* 1995; Hallonet *et al.* 1999; Macdonald *et al.* 1995; Mui *et al.* 2002; Ohsaki *et al.* 1999; Schwarz *et al.* 2000).

Initiation of optic cup formation and the lens placode invagination happens when the OV comes in contact with the surface ectoderm. TGFß signaling from the surrounding mesenchyme is important for the specification of the prospective retinal pigmented epithelium (pRPE), by inducing MITF and OTX2 in the proximal-dorsal OV (Hägglund, Berghard, and Carlsson 2013; Heisenberg *et al.* 1996; Jean *et al.* 1998; Westenskow, Piccolo, and Fuhrmann 2009). FGF signaling from the surface ectoderm to the adjacent OV is crucial for the specification of neuro-retina (NR) (Nguyen and Arnheiter 2000; Pittack, Grunwald, and Reh 1997). The first transcription factor to appear in the prospective neuro-retinal (pNR) region is VSX2 (visual homeobox2), formerly known as CHX10 (Liu *et al.* 1994). VSX2 and MITF negatively regulate each other to maintain the NR and RPE identities respectively (Fuhrmann 2010; Horsford *et al.* 2004). Loss of expression of VSX2 in the NR changes its fate into RPE cells. SIX3 is another transcription factor which is known to be involved in the specification of NR (Liu *et al.* 2010). Upon conditional loss of SIX3, the NR specification is distorted. However, SIX3 loss does not affect RPE commitment. PAX6 is expressed in the pNR, but its absence does not change the fate of pNR at the OV stage (Brown 1998; Grindley, Davidson, and Hill 1995; Hill *et al.* 1991; Tzoulaki, White, and Hanson 2005). However, PAX6 is indispensable for sustaining the multipotency of retinal progenitor cells (RPCs) of pNR. Once the pNR, pRPE and the optic stalk are specified, the OV invaginates to form the bi-layered optic cup.

2.3.4. Gene regulation in the development of the retina

The vertebrate retina consists of glial cell types and six different neural cell types that arise from the RPCs (Turner and Cepko 1987). The retinal cells develop in a highly conserved, temporal and an overlapping manner in the order: retinal ganglion cells (RGCs), horizontal cells, cone cells, amacrine cells, bipolar cells, rod cells and Müller glia (MG) (Young 1985). The retinal cells are arranged in a trilaminar fashion in a mature retina that consists of the GCL, inner nuclear layer (INL) and the outer nuclear layer (ONL). The synaptic connections between these cells form two more layers called the inner plexiform layer (IPL) and the outer plexiform layer (OPL). The RPE cells that arise from the outer layer of the optic cup form an additional layer in the retina. In total, an adult human retina consists of ten layers. Numerous transcription factors and their families are involved in maintaining the multipotency of RPCs, retinal cell fate specification and retinal cells differentiation. **Table 2.1** lists the transcription factors that are expressed in different retinal cell types and are required for their development and maintenance.

Table2.1: Transcription factors that regulate different retinal cell fates

Retinal Cell type	Transcription factors expressed
Retinal progenitor	VSX2, PAX6
Retinal ganglion cell	ATOH7, BRN3B, DLX1/DLX2
Horizontal cell	FOXN4, PTF1A, ONECUT1
Cone photoreceptor	OTX2, CRX, RORB, TRB2, BLIMP1
Amacrine cell	FOXN4, PTF1A, MATH3, NEUROD
Rod photoreceptor	OTX2, CRX, NRL, BLIMP1
Bipolar cell	VSX2, MASH1, MATH3
Müller glia	NOTCH1, HES1, HES5, SOX2, SOX8, SOX9

2.4. Retinal photo-transduction

Retinal photo-transduction is one of the best characterized vertebrate signaling cascades (Fu 1995). Retina is the light sensitive tissue of about 100-300 μm thickness, located at the posterior part of the eye. External light passes through the cornea, lens and the vitreous and falls onto the retina, which converts the light photons into nerve impulses, which are then relayed to the brain through the optic nerve, resulting in vision. Basically, retina acts like a film or a photosensitive chip of a camera. A cross section of the retinal tissue reveals 10 different layers. They are:

- Retinal Pigment Epithelium, **RPE** – a monolayer of hexagonal-shaped, pigmented epithelium of the retina
- Photoreceptor layer – consists of outer segments of rod and cone cells
- Outer limiting membrane, **OLM**
- Outer nuclear layer, **ONL**- consists of the rod and cone cells
- Outer plexiform layer, **OPL**
- Inner nuclear layer, **INL**- consists of horizontal, bipolar, amacrine cells and the Müller glia
- Inner plexiform layer, **IPL**
- Ganglion cell layer, **GCL**- contains the retinal ganglion cells, **RGC**s
- Retinal nerve fiber layer, **RNFL** - contains the neural axons and astrocytes
- Internal limiting membrane, **ILM**

The photoreceptors, as their name suggests are the cells that converts the light into nerve impulses. They are morphologically distinct with four discrete regions – the outer segment (OS), the inner segment (IS), the cell body comprising the nucleus and the nerve fiber extension with synaptic ending. The outer segment consists of lipid bilayer discs stacked one above the other. Each photoreceptor contains around 1000 discs. Most of the molecules

playing a role in the signal transduction cascade are embedded in the disc membranes of the OS. One such molecule found in a rod photoreceptor outer segment disc is the Rhodopsin, also known as the visual purple. Rhodopsin is made up of the protein opsin, which is covalently linked to a photosensitive pigment called 11-cis retinal (a derivative of vitamin A). Like Rhodopsin in rod photoreceptors, there are different kinds of iodopsins in cone photoreceptors, namely erythrolabe (sensitive to red light), chlorolabe (sensitive to green light) and cyanolabe (sensitive to blue light) in L-cones, M-cones and S-cones respectively.

In the dark state, the 11-cis retinal is bound to Rhodopsin, the G-protein, transducin and the enzyme phosphodiesterase (PDE), suspended in the disc lipid bilayer are in an inactive state. Guanylate cyclase (GC) which is also suspended in the disc lipid bilayer is active and is continuously converting the GTP molecules to cyclic GMP. So, during the dark phase, there are sufficient amounts of cGMP molecules in the cytoplasm and the cGMP gated channels remain open. Sodium and calcium ions keep flowing inside the photoreceptor outer segments through the cGMP gated channels. Equilibrium in the charge of the cell is maintained by an outward movement of potassium ions through the potassium transmembrane transporter protein in the inner segment of the photoreceptors. As a result of this balanced flow of ions, a photoreceptor cell in dark phase is in a depolarized state and constantly releasing glutamate (neurotransmitter) to the bipolar cells.

When a light photon enters the eye, it passes through the retinal layers and hits the 11-cis retinal in the disc membranes of photoreceptors causing a conformational change to all-trans retinal or a-t retinal. The a-t retinal does not have affinity towards opsins, unlike the 11-cis retinal and thus dissociates to form an excited rhodopsin. After excitation, rapid isomerization of rhodopsin leads to the formation of various intermediates. During this process, the rhodopsin molecule loses its color and this process is called photo-bleaching. Metarhodopsin (R*), a rhodopsin intermediate, is the actual activator of the G-protein, transducin. It is estimated that a single R* can activate about 120 transducin proteins per second (Leskov *et al.* 2000).

The number of transducin proteins in a photoreceptor cell is 10% of the total number of rhodopsin molecule in a cell (Lerea *et al.* 1986). Like any other G proteins, the transducin has the alpha, beta and gamma subunits. R* activates transducin by promoting the exchange of GDP in the alpha (α) subunit of transducin for GTP. Gα-GTP (G*) as an activated form dissociates from the Gβγ subunit and activates phosphodiesterase (PDE*) and induces the signaling cascade (Fu 1995).

The number of PDE proteins in a photoreceptor cell is ~1-2% of the total rhodopsin molecules. Thus the protein molecules involved in the initial photo-transduction are present in the ratio of 100R:10G:1PDE (Fu 1995). The PDE is a tetrameric protein containing an highly catalytic α and β subunits and a γ subunit on either side (Baehr, Devlin, and Applebury 1979; Deterre *et al.* 1988; Hurley and Stryer 1982). In dark phase, The PDE γ subunit is closely associated with the α and β subunits and inhibits their catalytic activity. In light phase, the G* displaces the γ subunit on either side, enabling the α and β subunits to hydrolyze cyclic GMPs to GMPs. The PDE α and β subunits are so highly active that they can convert 2200 cGMPs to GMPs in a second (Kcat 2200 s^{-1}) (Baehr *et al.* 1979; Leskov *et al.* 2000). The sudden drop in cGMP levels in the cytoplasm makes the cGMP gated ion channels close, thus stopping the inflow of sodium and calcium ions (Fesenko, Kolesnikov, and Lyubarsky 1985; Yau and Nakatani 1985). Potassium ions are continuously sent out of the cell as the potassium transmembrane transporter protein is independent of cGMP levels inside the cell. Resulting to that, the photoreceptor cells get hyperpolarized, ceases the release of glutamate, thus activate the bipolar cells, which in turn triggers a nerve impulse through the RGC, optic nerve fiber and finally to the visual cortex.

Visual impulse from a series of static images, when triggered at enough rates, helps the brain to see the outside world in real time. However, it is crucial, for the activated visual transduction proteins (R*, G*, PDE*) to recover, for subsequent response to incoming photons.

The first step in the recovery process is the inactivation of R*. Rhodopsin kinase (GRK1) phosphorylates R* lowering its activity, followed by the binding of arrestin (ARR1) which completely blocks the residual activity of R* (Kühn and Wilden 1987; Wilden, Hall, and Kuhn 1986). Photoreceptors have a specialized calcium dependent protein called Recoverin (REC). In the dark, REC-Ca^{2+} is bound to GRK1, thus inhibiting its activity on R*. When intracellular Ca^{2+} levels go down as a response to light trigger, Ca^{2+} dissociates from REC-Ca^{2+}, reducing the affinity between Recoverin and GRK1 and thereby activates GRK1, leading to the inactivation of R* (Chen *et al.* 1995; Kawamura 1992, 1993).

Inactivation of R* must be followed by the inactivation of G*-PDE* to complete the termination process. The hydrolysis of G* bound GTP to GDP, is required for the inactivation of G*. This hydrolysis is mediated by the GTPase activating protein (GAP) complex (He W, Cowan CW 1998). Once hydrolyzed, The Gα-GDP dissociates from PDEγ, which in turn associates strongly to the catalytic PDEαβ (PDE*) subunits and inactivates it.

At this point, the guanylate cyclase (GC) is in an inhibited state mediated by Ca^{2+}-bound guanylate cyclase activating proteins (GCAPs). In the presence of light, just like Recoverin activating GRK1, the GCAPs free of Ca^{2+}, activates guanylate cyclase, ultimately restoring cGMP levels in the cytoplasm of the photoreceptors. Once the cGMP levels are stabilized, there are enough cGMP in the vicinity of cGMP gates channels to open restoring the influx of sodium and calcium ions, bringing the photoreceptor cells to a depolarized state once again.

This light mediated, swift and continuous, activation and deactivation of visual cascade proteins leading to hyperpolarization and depolarization trigger continuous nerve impulses to the brain. These are then interpreted by the brain as a visual sequence called the visual transduction or photo-transduction. The whole process of visual transduction happens in milliseconds, and that is why photoreceptors are the most metabolically active cells in the human body. Hence, the outer segments of the photoreceptors and its components must be constantly replenished. This is made possible by the RPE adjacent to the photoreceptors in the retina.

2.4.1. Classical visual cycle

After photo-isomerization of 11-cis retinal to a-t retinal, it is essential for the a-t retinal to be reverted into 11-cis retinal (Travis *et al.* 2007). Rods undergo the classical visual cycle, involving RPE in a-t retinal conversion to 11-cis retinal, whereas the cones undergo a different visual cycle, involving the Müller glia (Wolf 2004). The variation is due to the high demand of 11-cis retinal in cone cells that are active in the bright day light, when compared to the rod cells that are active at night in dim light.

In the classical pathway of visual cycle, the a-t retinal is released in the inner leaflet of the discs of the rod photoreceptors after isomerization. This released a-t retinal then complexes with phosphatidylethanolamine (PE) and form N-retinylidene-phosphotidylethanolamine (NR-PE) (Liu *et al.* 2000). A disc membrane protein called ATP binding cassette transporter (ABCA4) binds to the NR-PE and flips the a-t retinal from the inside of the disc to the outside and recycles the phosphatidylethanolamine back to the disc lipid bilayer (Quazi *et al.* 2012) (**Fig 2.3.B**). Thus, ABCA4 is also commonly known as the retinal flippase. Once the a-t retinal is in the cytoplasm, it is reduced to a-t retinol, commonly known as vitamin A, by a-t retinal dehydrogenase (atRDH) (Haeseleer *et al.* 1998). The a-t retinol then exits the cytoplasm of the photoreceptors and is carried, through the interstitial space between the photoreceptors and RPE with the help of the inter-photoreceptor retinoid binding protein (IRBP), entering the RPE (Wu *et al.* 2007).

Once inside the RPE, the a-t retinol is carried by cellular retinoid binding protein (CRBP) to the enzymes of the smooth endoplasmic reticulum (SER) (Saari, Bredberg, and Garwin 1982). There are three important enzymes present in the SER of RPE that are involved in converting the newly entered a-t retinol to 11-cis retinal, which should be sent back to the photoreceptors for further visual transduction. The first one is the lecithin retinol acyl transferase (LRAT) which links a-t retinol to phosphatidylcholine in the ER membrane forming a-t retinyl esters (Saari and Bredberg 1989). The a-t retinol (vitamin A) being a component of the diet, also enters the visual cycle from systemic circulation through the basal side of the RPE, and gets esterified by LRAT. The a-t retinyl esters, thus formed, are the major storage forms of retinoids and their accumulation is crucial for proper functioning of the visual cycle. The second enzyme is RPE65, commonly called as isomerohydrolase. As its name suggests, it catalyzes the simultaneous isomerization and hydrolyzation of a-t retinol to 11-cis retinol (Jin *et al.* 2005). 11-cis retinol then binds with cellular retinaldehyde binding protein (CRALBP) (Saari *et al.* 2001), which delivers it to the last and final enzyme of the visual cycle, 11-cis RDH, which oxidizes 11-cis retinol to 11-cis retinal (Driessen *et al.* 1995; Simon *et al.* 1995). The newly formed 11-cis retinal then crosses the interstitial space and enters the photoreceptors with the help of IRBP (Wu *et al.* 2007). It is proposed that IRBP protects the 11-cis retinal from isomerization during the intercellular transport (Crouch *et al.* 1992). The 11-cis retinal is now ready to bind to opsins, to form the visual pigment rhodopsin and thus completes the visual cycle.

2.4.2. Cone visual cycle

It is proposed that the cones may have a unique visual cycle, other than the classical ones of rods, justifying their ability to function in daytime where constant presence of light demands higher amounts of 11-cis retinal. The cone visual cycle is based on the observation of the unique ability of cone cells to convert 11-cis retinol, administered to the inner segment, to 11-cis retinal (Jones *et al.* 1989). It is believed that after photo-isomerization and reduction, the a-t retinol leaves the cone outer segment and enters the Müller glial cells, where it gets converted into 11-cis retinol by an unknown isomerase or a group of enzymes in the Müller cells. Moreover, inner segment of the cone cells is present in close proximity to the apical microvilli of Müller cells. This 11-cis retinol is then transported to photoreceptors inner segment where it gets oxidized to 11-cis retinal, thus completing the visual cycle. The presence of CRALBP in the Müller cell microvilli and IRBP in both the Müller cell microvilli and around the cone photoreceptors in high concentration further adds weightage to the proposed theory (Bunt-Milam and Saari 1983). Recent reports have shown that RPE65 is

also present in the cones apart from RPE cells and could be functioning as the unknown isomerase enzyme that enables the conversion of a-t retinol to 11-cis retinol in cone cells (Kolesnikov, Tang, and Kefalov 2018; Tang *et al.* 2011; Wenzel *et al.* 2007; Znoiko *et al.* 2002).

2.5 Retinal dystrophy

Retinal dystrophy is a hereditary condition in which the retinal cells, especially the rods and cones die, leading to irreversible vision loss and blindness. It affects 1 in 2000-3000 individuals worldwide. Over 260 genes are found to be linked with monogenic retinal blindness (Daiger *et al.* 1998), where a single gene mutation can result in retinal degeneration (**Fig 2.2**). At present there is no established cure for retinal dystrophy, however, extensive research is ongoing worldwide to establish gene therapeutic and cell therapeutic possibilities or a combination of both for treating monogenic retinal disorders.

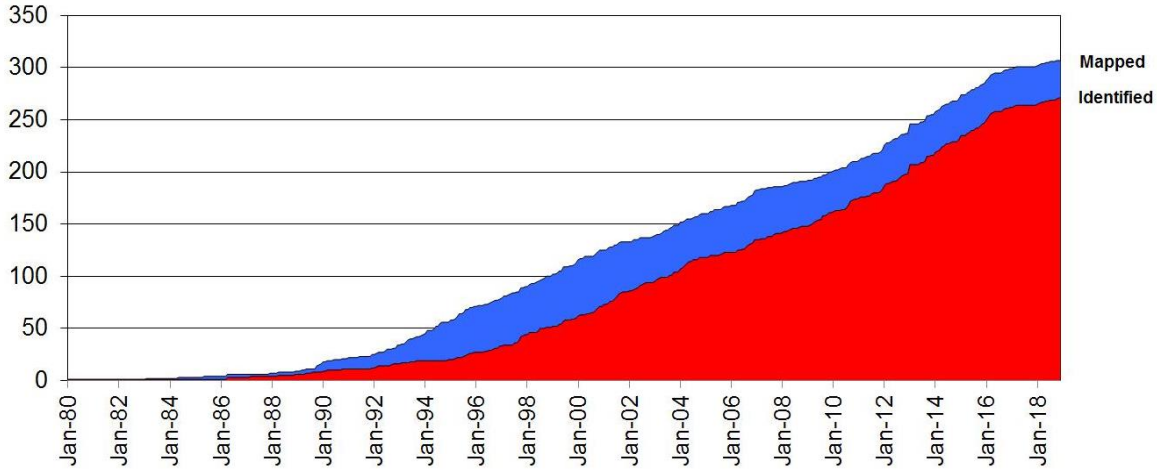

Figure 2.2: Mapped and identified retinal disease genes until April 2019

2.5.1. Autosomal recessive retinal dystrophy (ARRD)

ARRD is a condition in which both the alleles of the gene must be mutated for the disease to manifest. The prevalence of ARRD is more common in families with consanguineous marriages. ARRD includes a wide variety of retinal dystrophic conditions like Leber congenital amaurosis (LCA), retinitis pigmentosa (RP), Stargardt disease, cone rod dystrophy (CRD) and so on. Till date, mutations in 46 genes have been identified to be linked to ARRD (Nash *et al.* 2015). Some of the major genes with high frequency of ARRD association are PDE6A (Dryja *et al.* 1999; Huang *et al.* 1995), PDE6B (McLaughlin *et al.* 1993; Shen, Sujirakul, and Tsang 2014), ABCA4 (Martínez-Mir *et al.* 1998; Singh *et al.* 2006; Zhang *et al.* 2015), USH2A (Martínez-Mir *et al.* 1998; Singh *et al.* 2006; Zhang *et al.* 2015) and EYS

(Martínez-Mir *et al.* 1998; Singh *et al.* 2006; Zhang *et al.* 2015). Various kinds of mutations in each of the identified genes may give rise to similar phenotype that are categorized under one retinal dystrophic condition. Conversely, mutations at different sites of the same gene gives rise to different phenotypes that are categorized under different retinal dystrophic condition. *ABCA4* is one such gene identified to be associated with different retinal dystrophic conditions like the Stargardt macular dystrophy, autosomal recessive RP, autosomal recessive CRD and also LCA is the gene called *ABCA4*.

2.5.1.1. ABCA4

ABCA4 belongs to the family of ATP binding cassette (ABC) transporters and the subfamily A and is widely expressed in vertebrate's photoreceptors. It is also termed as retina specific ABC transporter shortly, ABCR. *ABCA4* is positioned on the short arm of chromosome 1 (1p22) and comprised of 50 exons. The gene codes for a 2273 amino acid long protein, localized to the outer membrane discs of photoreceptors with a molecular weight of 256 kDa (**Fig 2.3.A-C**). Because of its localization within the margins of the photoreceptor discs, it is also termed as the rim protein. Structurally the protein has two symmetrical halves, each half comprising of a transmembrane domain with six membrane spanning segments, a large extra cellular domain (ECD) which is glycosylated and a cytoplasmic nucleotide binding domain (NBD) that binds to ATP (the ATP binding cassette) and ending with a conserved VFVNFA motif at the C terminus (Illing, Molday, and Molday 1997) (**Fig 2.3.A**).

As mentioned earlier in the visual cycle (**section 2.3.1**), ABCA4 transports the a-t retinal from the inside of the photoreceptor outer membrane discs, i.e. from the lumen of the outer segment discs to the cytoplasmic side (**Fig 2.3.B,C**).

Initially, NR-PE (the compound formed by the binding of a-t retinal with the PE in the disc lipid bilayer) binds to the high affinity site at the ABCA4 transmembrane domain on the lumen side, causing a conformational change in the nucleotide binding domain, thus promoting the binding of ATP to NBDs. The ATP molecules hold the two NBDs close resulting in the formation of an NBD dimer, which in turn decreases its affinity for NR-PE binding at the trans-membrane domain (TMD). As a result, the NR-PE is flipped to the other side of the lipid bilayer by ABCA4 enabling the transport of NR-PE from the lumen of the outer segment discs to the cytoplasm. The ATP bound to the NBD dimer is then hydrolyzed to ADP resulting in the loss of NBD dimer. ADP then dissociates from NBD, thus allowing the TMD to attain its original conformation with high affinity to NR-PE (Quazi, Lenevich, and Molday 2012).

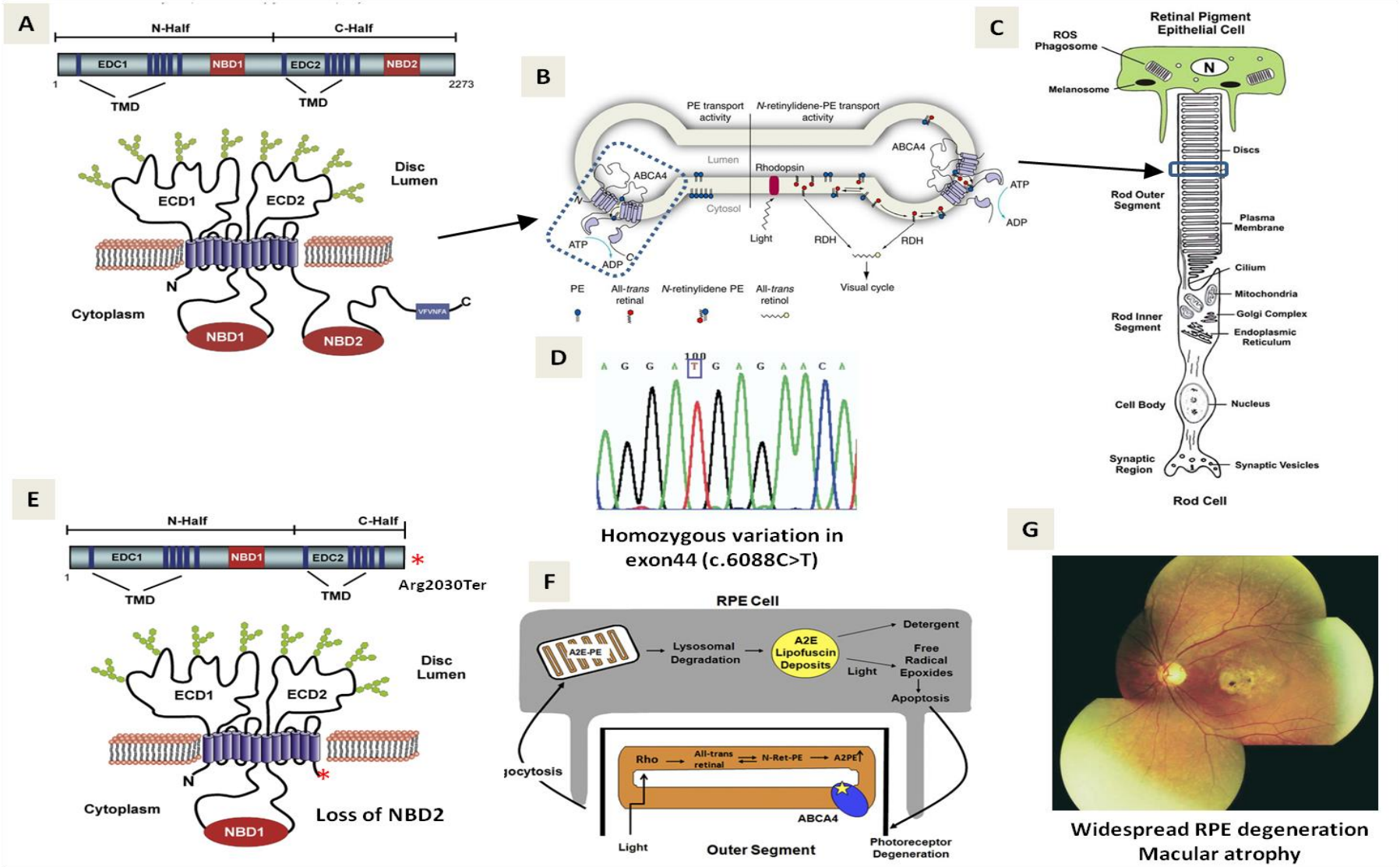

Figure 2.3: ABCA4 structure and function. A*. Structure of* ABCA4. ***B****.* ABCA4 *is localized to disc membranes of the photoreceptor outer segments and act as a retinal flippase.* ***C****. Rod photoreceptor cell morphology with cell body, inner and outer segment, which is in close proximity to RPE cells.* ***D****. c.6088C>T variation in exon44 of ABCA4 in KR.* ***E****. NBD2 loss due to c.6088C>T variation in KR.* ***F****. Mechanism of lipofuscin deposits in RPE due to loss of function of* ABCA4. ***G****. Fundus image of KR showing retinal degeneration.(image courtesy: Illing et al, 1997; Singh HP et al, 2006; Molday RS et al, 2009;Quazi F et al, 2012)*

Loss or decrease of ABCA4 flippase activity leads to the accumulation of NR-PE within the disc membranes (**Fig 2.3.F**). These NR-PE then react with a-t retinal to form the di-retinal compound, A2PE (di-retinoid-pyridinium-PE). As a part of regular maintenance, outer segments of the photoreceptors are shed every 10 days, followed by their phagocytic clearance by RPE cells, which is known as the sub-retinal space clearance mechanism. Inside the RPE cells, the phagosomes with A2PE and other retinal derivatives fuse with lysosomes to form phagolysosomes. The enzymes contained within the phagosomes degrade the outer segments and hydrolyze A2PE to a toxic cationic bis-pyridinium salt, N-retinylidene-N-retinyl-ethanolamine (A2E) that cannot be metabolized further (Liu *et al.* 2000). The non-metabolizable A2E and other retinal compounds deposit in RPE cells to form auto fluorescing deposits, which are clinically referred to as lipofuscin. These lipofuscin deposits form toxic epoxides upon exposure to blue light, leading to the death of RPE cells. Eventually the photoreceptors that are dependent on RPE cells for their maintenance and survival also undergo degeneration, resulting in vision loss.

Over 500 mutations all across the length of *ABCA4* has been identified to be linked with a range of ARRD conditions like cone-rod dystrophy, retinitis pigmentosa and Stargardt disease (Molday, Zhong, and Quazi 2009). According to a proposed model, the intensity of the disease phenotype is inversely correlated with the residual functional activity of mutated ABCA4 (van Driel *et al.* 1998; Maugeri *et al.* 1999; Shroyer *et al.* 1999). Mutations resulting in partial functional loss of ABCA4 activity, lead to Stargardt disease. Compound heterozygous individuals with only residual ABCA4 activity give rise to cone-rod dystrophy (van Driel *et al.* 1998). Complete loss of ABCA4 with homozygous mutations producing non-functional proteins results in wide spread photoreceptor cell death and retinitis pigmentosa (RP).

Mutations within the transmembrane domain seem to drastically diminish protein levels indicating that these mutations translate into highly misfolded proteins that are rapidly degraded (Sun, Smallwood, and Nathans 2000). Mutations at NBD sites do not alter the protein levels but alter the ATP binding capacity of the protein, making the protein less effective. Mutations at the C-terminus leading to the loss of VFVNFA motif showed protein misfolding defects leading to faulty trafficking, decreased protein levels and total loss of retinal and ATP binding activity (Zhong, Molday, and Molday 2009).

An in-house genetic study (Singh *et al.* 2006) has identified a non-sense mutation (c.6088C>T) wherein, the codon for arginine at 2030 position is mutated to form a stop codon, leading to pre-mature translational termination (**Fig 2.3.D**). The 2030th amino acid is

located within the second nucleotide binding domain (NBD2) and the mutation could lead to its total loss of function (**Fig 2.3.E**). Alternatively, the c.6088C>T mutation is predicted to code for an unstable mRNA, that could be degraded by nonsense mediated decay (NMD), leading to a complete loss of protein expression.

The same homozygous mutation was detected in all the three siblings of the family studied and the parents were heterozygous carriers. The mutation was not present in hundreds of ethnically matched normal control individuals. The two older siblings had an early onset retinal dystrophy while the younger had a late onset disease. By third decade of life, all the affected siblings had a best corrected Snellen visual acuity less than 20/200 or 6/60. Fundus evaluation showed diffuse RPE changes in the peripheral retina in all three siblings (**Fig 2.3.G**). The macular region had significant changes in the affected individuals. The oldest sibling had pigment migration in a whorl-like pattern at the posterior pole and also beyond. The other two siblings had pigment blotches due to widespread RPE degeneration, arterial narrowing and macular involvement.

The clinical findings and electroretinogram (ERG) were symmetrical in both the eyes. While one of the affected individuals showed nearly extinguished ERG response, the other two siblings showed cone-rod type of response. The parents who were carriers of the mutation showed normal fundus while on ERG subnormal cone response was observed.

Studies have shown that, the occurrence of heterozygous mutations in ABCA4 could lead to mild or late-onset disease. Heterozygous changes in ABCA4 have also been shown to play a significant role in macular degeneration. It is logical that prolonged deficiency in ABCA4 activity could trigger the disease development, even though there is no conclusive evidence.

2.5.2. Leber Congenital Amaurosis (LCA)

LCA is a severe form of autosomal recessive retinal dystrophy manifested in the first year of life. It accounts for 5% of the whole inherited retinal dystrophies (Schappert-Kimmijser, Henkes, and Van Den Bosch 1959) with a world-wide prevalence of about 1 in 30000 (Koenekoop 2004) to 1 in 81000 (Chung and Traboulsi 2009; Stone 2007). LCA is more frequent in consanguineous or isolated populations. Pathogenic variations in around 22 genes involved in, protein trafficking, photoreceptor morphogenesis, cell-cycle progression, transcription, photo-transduction and visual cycle have been reported to cause LCA. Pathogenic variations can lead to a total loss of protein expression or the formation of non-functional protein resulting in photoreceptor cell death.

LCA was first identified and described by Theodor Leber in the 19th century based on the following clinical findings

- Early blindness or severe visual impairment presenting at the age less than a year
- Visual acuity worse than 20/400
- Extinguished or severely reduced ERG response (both scotopic and photopic)
- Babies exhibiting oculo-digital sign (which involves poking, rubbing/pressing of the eyes
- Family history
- Deteriorated pupillary action indicating severely damage retina
- Roving eye movements or nystagmus in all positions of gaze
- Photophobia

Genetic variants of LCA do not form defined patterns of retinal lesions, which makes it difficult to categorize them base on retinal findings, without genetic testing. Moreover, the infants with LCA display normal fundus during the initial months. Fundus abnormality presents later in life. Hence molecular testing becomes inevitable for a definitive diagnosis and to understand the disease subtype.

2.5.2.1. LCA genes

Genetic screening for LCA by older methods like linkage analysis and candidate gene approach and using newer methods like SNP arrays and next generation sequencing (NGS) has revealed several mutations in 22 different genes. **Table 2.2** shows the list of genes identified so far in LCA and their genotype-phenotype correlations. However, the genetics of about 30-50% of LCA patients still remain unknown.

2.5.2.1.1. RD3

Retinal degeneration 3 (RD3) is a 22 kDa protein, present in the photoreceptors. The human *RD3* is situated in the long arm of chromosome 1 at 1q32.3 locus. Initially identified as C1orf36 (Chromosome1 open reading frame 36), the protein product was named as retinal degeneration 3 (RD3) as the patients carrying truncation mutations show a severe retinal degeneration phenotype (Friedman *et al.* 2006). This gene (NCBI Gene ID: 343035) consist of 3 exons and the disease was categorized as LCA12 as the symptoms were similar to other LCA conditions. The mRNA is 4287 bp long, with 588 bp coding sequence spanning over exon 2 and 3 and produces a protein of 195 amino acids long (**Fig 2.4.A**). The protein structure of RD3 is not known yet but is predicted to contain many alpha helices, with two coiled coil domains from 22-54 amino acids and 115-141 amino acids. The protein contains

many conserved sites for post-translational modifications such as phosphorylation by Protein kinase C and Casein kinase II and also N-myristoylation for membrane anchoring. The function of RD3 has been elucidated only in recent years. Rd3 transcripts in the mouse retina are detected at low levels at E12 (embryonic day 12) but the expression levels go up at E18, with further increase until PN6 (post natal day 6), after which the transcript levels remained stable (Friedman *et al.* 2006). An important function of RD3 is to transport the disc membrane protein, retinal guanylyl cyclase (RetGC) from the inner segment to the outer segment through the narrow connecting cilium of 0.3 μm diameter (Azadi, Molday, and Molday 2010) (**Fig 2.4.B**). RD3 is known to bind RetGC and inhibit its activity during its intracellular transport (Peshenko *et al.* 2011).

The disease phenotype of LCA12 (caused by *RD3* mutations) is reported to be more severe than LCA1 (caused by RetGC/*GUCY2D* mutations) (Perrault *et al.* 2013; Preising *et al.* 2012). Therefore, RD3 is thought to be involved in additional cellular functions other than its role in RetGC trafficking and regulation. A recent study has showed that RD3 also interacts with and upregulates the activity of guanylate kinase (GUK) which is partially involved in the conversion of 5'-GMP to 5'-GTP (Wimberg, Janssen-Bienhold, and Koch 2018). Another recent report has shown ubiquitous expression of RD3 in multiple tissues (Aravindan *et al.* 2017). *Rd3* transcript was also detected in the retinal inner nuclear layer, which suggests that RD3 may have other, unknown functions in cells other than photoreceptors (Aravindan *et al.* 2017). Over expression of RD3 protein in COS-1 cells formed sub nuclear puncta (RD3 bodies) of different sizes, both within the nucleus and in the cytoplasm.

These RD3 bodies in the nucleus were in close-proximity to PML bodies (Friedman *et al.* 2006), which are involved in DNA damage/cellular stress responses and are known to sequester and regulate many of its sumoylated protein partners. PML is regarded as a tumor suppressor, and a recent study by Khan *et al* 2015 had suggested a tumor suppressor role for RD3 in neuroblastoma (Khan *et al.* 2015). Based on these evidences, we believe that RD3 may be involved in some unknown nuclear functions and regulates various retinal functions.

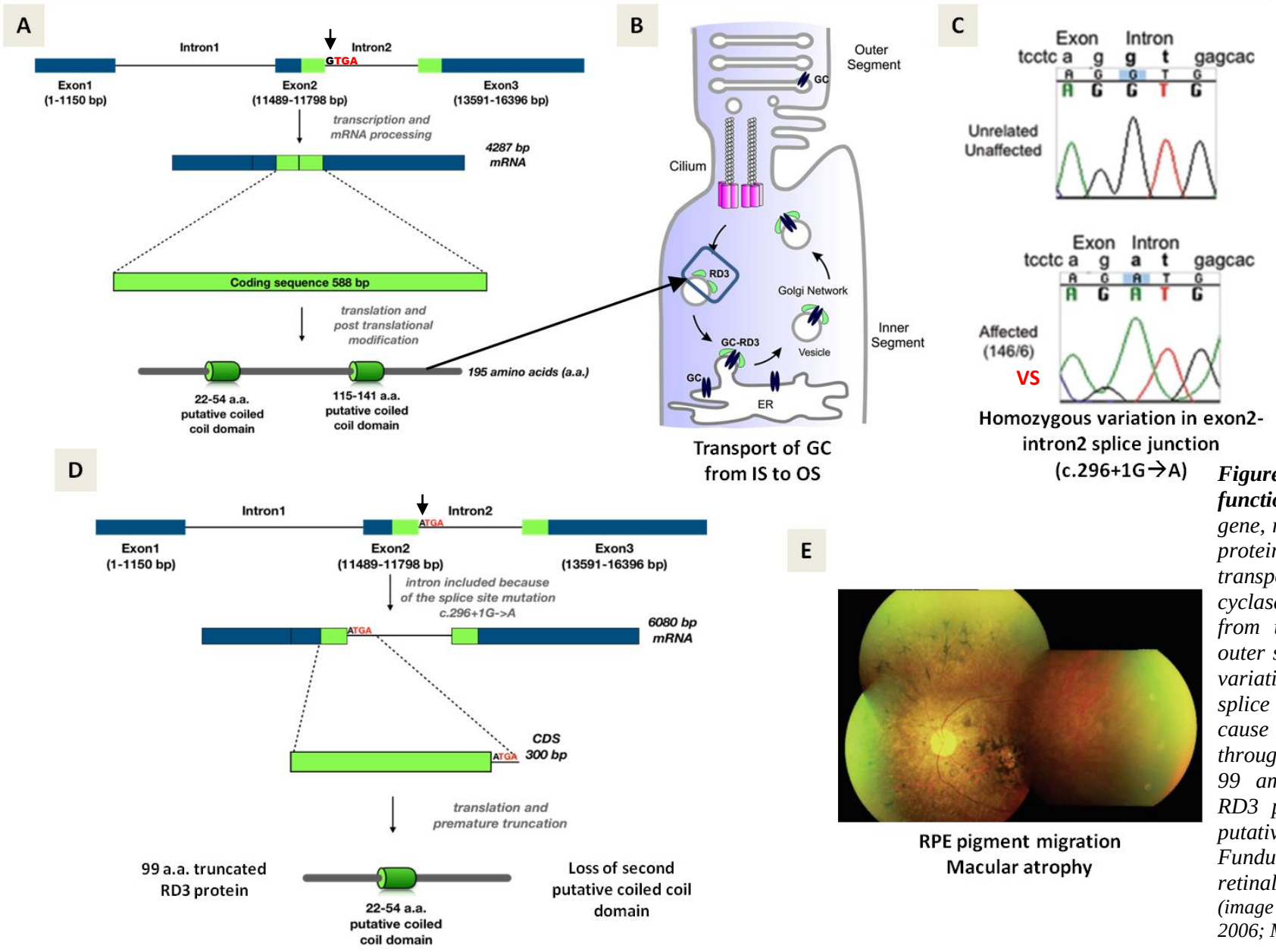

Figure 2.4: RD3 structure and function. ***A****. Structure of RD3 gene, mRNA and protein.* ***B****. RD3 protein is involved in the transport of retinal guanylyl cyclase within photoreceptors, from the inner segment to the outer segment.* ***C****. c.296+1 G→A variation in VS.* ***D****. The above splice junction mutation may cause intron 2 inclusion and read through translation, resulting in a 99 amino acid long truncated RD3 protein that lacks the 2nd putative coiled coild domain.* ***E****. Fundus image of VS showing retinal degeneration.*
(image courtesy: Friedman et al, 2006; Molday LL et al, 2014)

Table 2.2: LCA and phenotype-genotype correlations

Locus name	Gene symbol	Chromosomal locus	Protein name	Protein function	% of LCA	LCA phenotype
LCA1	*GUCY2D*	17p13.1	Retinal guanylate cyclase1	Hydrolysis of cGMP in photoreceptors during visual transduction	6-21	Poor vision, photophobia, hyperopia, nystagmus, OCT with significant perifoveal thinning (Perrault *et al.* 2005)
LCA2	*RPE65*	1p31.3-p31.2	Retinal pigment epithelium protein 65	Isomerohydrolase activity in vitamin A visual cycle	3-16	Night blindness, nystagmus, OCT shows a thinner retina (Redmond *et al.* 2005)
LCA3	*SPATA7*	14q31.3	Spermatogenesis associated protein7	Possible vesicular transport	3	Night blindness at 3 years of age. Fundus with typical appearance of RP, rapidly progressive (Wang *et al.* 2009)
LCA4	*AIPL1*	17p13.1	Aryl hydrocarbon interacting protein	Rod PDE chaperone	5-10	Keratoconus, cataract and hyperopia. Fundus with bone spicule pigmentation and variable degree of maculopathy. OCT with reduced macular thickness (Dharmaraj *et al.* 2004)
LCA5	*LCA5*	6q14	Lebercilin	Ciliary functions	1-2	Severe reduced vision at birth. Nystagmus and high hypermetropia. Fundus examination with widespread atrophy of the retina and RPE. OCT: macular atrophy, disruption of retinal lamination and presence of hyporeflective, well-circumscribed area in the outer nuclear layer with a hyper reflective borders (osettes) (Mohamed *et al.* 2003)
LCA6	*RPGRIP1*	14q11	RP GTPase regulator interacting protein1	Connecting cilium, disc morphogenesis	4-6	Severe loss of vision early in life. (Dryja *et al.* 2001)

LCA7	*CRX*	19q13.3	Cone-rod homeobox	Elongation of photoreceptor outer segment, photoreceptor development, photo transduction	1-3	Severe vision impairment in early life. OCT shows macular atrophy without junctions between the inner segments and outer segments (Freund *et al.* 1998)
LCA8	*CRB1*	1q31-32.1	Crumbs homologue	Determining and maintaining photoreceptor architecture	9-13	Nictalopia, nystagmus, keratoconus, corioretinal atrophy and nanophthalmos. Fundus with numular pigment clump, bone spicules and para-arteriolar preservation (Hollander *et al.* 2001)
LCA9	*NMNAT1*	1p36.22	Nicotinamide nucleotide adenylyl transferase1	Rate-limiting enzyme NAD (+) biosynthesis	-	Severe form of retinal hereditary degeneration, mainly atrophic macular lesion. Nystagmus and severe loss of vision (Koenekoop *et al.* 2012)
LCA10	*CEP290*	12q21.32	Centrosomal protein Cep290	Ciliary function	20	Nystagmus, hyperopia, keratoconus and cataract. Photophobia. Light perception or no vision. Perifoveal thinning by OCT. (den Hollander *et al.* 2006)
LCA11	*IMPDH1*	7q32.1	Inosine 5'-monophosphate dehydrogenase 1	De novo synthesis de guanine nucleotide	8	Nystagmus with no fixation to light. Retina showing diffuse RPE mottling. No pigmentary deposits. (Bowne *et al.* 2006)
LCA12	*RD3*	1q32.3	Retinal Degeneration 3 protein	Transcription and splicing. Suppress retinal membrane guanylate cyclase activity. Role in retinal maturation	<1	Night blindness, severe nystagmus. Initial refraction was hypermetropic and changed to myopic in the disease's course. Severe impaired visual acuity. Attenuated vessels, salt and pepper aspect, bone spicules in the fundus. Macular changes with hammer beaten appearance are notable on the third decade of life. OCT reveal disorganization of all retinal layers (Friedman *et al.* 2006)

LCA13	*RDH12*	14q23.3	Retinal dehydrogenase 12	Unusual dual specificity for a-t retinol and cis-retinol	4-5	Poor vision. Night blindness. SD-OCT: severe macular thinning and loss of the foveal laminar architecture (Perrault *et al.* 2004)
LCA14	*LRAT*	4q31.3	Lecithin retinol acyl transferase	Esterification-essential in vitamin A visual cycle	<1	Poor vision, nyctalopia and visual field constriction since childhood. Peripheral RPE atrophy with pigment migration into retina (Dev Borman *et al.* 2012)
LCA15	*TULP1*	6p21..3	Tubby-like protein	Protein transport from the photoreceptor inner segment to the outer segment	-	Night blindness, nystagmus, moderate to severely limited visual field. Severely disturbed color vision (Mataftsi *et al.* 2007)
LCA16	*KCNJ13*	2q37	Inwardly-rectifying potassium channel subfamily J member	Maintaining resting membrane potential	-	Poor night vision, nystagmus, cataract. Fundoscopy reveals considerable levels of pigments at RPE and show snowflake type degeneration (Sergouniotis *et al.* 2011)
LCA17	*GDF6*	8q22.1	Growth differentiation factor 6	Codes for a widely expressed growth factor in the TGF-b pathway specifying the dorsal-ventral retinal axis	-	Ocular and skeletal features. Limited vision to detect hand motions (Asai-Coakwell *et al.* 2013)
LCA18	*PRPH2*	6p21	Peripherin 2	Maintaining photoreceptor disc outer segment stability	-	Infantile nystagmus, decreased vision, photophilia, non-recordable ERG (Khan *et al.* 2016)

2.5.2.2. LCA12

As mentioned earlier in the **Table 2.2**. LCA12 is the severe autosomal recessive form of retinal degeneration in infants and is caused by mutations in *RD3* (Friedman *et al.* 2006). The association of this gene to retinal dystrophy was first identified in a blind mice model in 1969 and linkage analysis has mapped the mutation to chromosome 1 at 10±2.5cM distal to *Akp1* (Chang *et al.* 1993). Other linkage studies has further narrowed down the mutation loci to a 230 kb region in chromosome 1, which contained three genes *TRAF5, C1orf36* and *SLC30A* s (Kukekova *et al.* 2009).

However, Friedman *et al.* 2006 had already confirmed that LCA12 is caused by mutations in the gene *C1orf36*, which was then renamed as *RD3*. The authors further showed that the mutant gene when expressed in COS-1 cells resulted in a truncated protein. Overexpression of wild type RD3 resulted in its accumulation both in the nucleus and the cytosol as discrete punctate structures. These nuclear puncta were localized close to the PML bodies inside the nucleus. A large genetics screen involving 881 LCA patients has reported several novel mutations in *RD3*, including a homozygous, splice-site mutation in two siblings of Indian origin.

Both the siblings carried a homozygous G→A transition at the exon 2 donor splice site (c.296 + 1 G→A) (**Fig 2.4.C**) and had poor vision and nystagmus since birth. Fundus examination revealed atrophic lesions in the macular area with pigment migration (**Fig 2.4.E**). The disruption of donor splice site was predicted to affect intron 2 splicing, leading to its inclusion in the mature RNA. This aberrantly spliced transcript carried an in-frame stop codon within intron 2, immediately downstream of the splice junction. Upon translation, the mutant transcript is therefore predicted to form a truncated protein of only 99 amino acids, resulting in loss of function and an LCA phenotype (**Fig 2.4.D**).

2.6. Treatment of retinal dystrophy

As discussed earlier, retinal dystrophies are a result of gradual degeneration of RPE and/or photoreceptor cells of the retina leading to gradual vision loss and blindness. Various treatment options such as gene therapy and cell therapy are being explored worldwide (Garita-Hernandez, Goureau, and Dalkara 2016). Gene therapy strategies are mainly aimed to complement the mutant genes in retinal tissues, to regain the lost cellular functions (Takahashi *et al.* 2018). However, this requires genetic screening of all patients for mutation identification and demands gene-specific therapies to be tailored using suitable gene delivery systems. The success of gene therapy is also dictated by the health status of target cells at the

time of treatment. Therefore, gene therapy can never be an option for treating patients with an advanced disease wherein, the target cells are already lost. Therefore, only a very small sub-set of patients would ideally benefit from successful gene therapies. However, in case of cell-based therapies, the major approach is to replace the lost cells to regain normal tissue functions. This requires healthy and tissue-specific cells for transplantation purposes, irrespective of the genetic background and stage of the disease. Cell replacement therapy therefore holds a great promise in treating large number of patients with dystrophic conditions (Garita-Hernandez *et al.* 2016).

2.7. Stem cells for retinal regeneration

For genetic diseases such as retinal dystrophies, most of the ongoing clinical trials on cell therapy are aimed to deliver healthy allogeneic cells with two major objectives.

1. To provide trophic support and prevent further retinal degeneration, thereby preserving the existing vision.
2. To replace the lost cells with normal and functional cells, to regain vision and improved retinal function.

Unlike an actively regenerating tissue such as the bone marrow or the cornea or the skin, an adult retina does not harbor any stem cells that are beneficial for regenerative applications. Therefore, alternative stem cell sources such as the mesenchymal stem cells (Ding, Kumar, and Mok 2017; Park *et al.* 2015; Siqueira *et al.* 2011), fetal retinal tissue derived progenitor cells (Algvere *et al.* 1994; Little *et al.* 1996) and pluripotent stem cell (ESC and iPSC)-derived retinal cells (Lu *et al.* 2009; Mandai *et al.* 2017; Mehat *et al.* 2018; Schwartz *et al.* 2012, 2015; Sharma *et al.* 2019; Song *et al.* 2015; Sowden 2014) have been evaluated for their ability to promote retinal regeneration in a large number of pre-clinical studies and the promising ones are being currently evaluated in various clinical trials worldwide.

2.7.1. Induced Pluripotent Stem Cells (iPSCs)

Stem cells are a kind of specialized cells that can proliferate continuously to produce more cells of the same type and also have the ability to differentiate into other specialized cell types. Stem cells found in an adult body take part in regular wound healing responses and helps in the maintenance of tissue homeostasis. Different tissue-specific stem cells vary in their regenerative capacities based on their ability to proliferate and differentiate into different cell types. Adult tissue-derived stem cells have a limited capacity to expand in culture. But they are useful in generating uniform populations of tissue committed cells for

Table 2.3: Characteristics of induced pluripotent stem cells

Parameters	Characteristics
Morphology (by phase contrast imaging)	Flat and circular colonies with smooth margins; small and rounded cells with high nuclear to cytoplasmic ratio and prominent nucleoli. Ability to expand stably in culture over infinite passages. (**Fig 2.5.A**)
Expression of endogenous Yamanaka genes	OCT4, SOX2, KLF4, C-MYC (**Fig 2.5.B**)
Expression of endogenous stem cell factors	Cell surface markers: SSEA3, SSEA4 (**Fig 2.5.E**), TRA-1-60, TRA-1-81 Nuclear markers: OCT4 (**Fig 2.5.C**), SOX2, NANOG (**Fig 2.5.D**) Enzyme markers: ALP, TERT (**Fig 2.5.F**)
Genome stability	Normal karyotype and STR profiles
Epigenetic state	Hypomethylated status of OCT4 and NANOG promoters
Pluripotency	*In vitro:* Embryoid body formation *In vivo:* Teratoma formation
Ability to give rise to a whole animal	Tetraploid complementation (Kang *et al.* 2009)

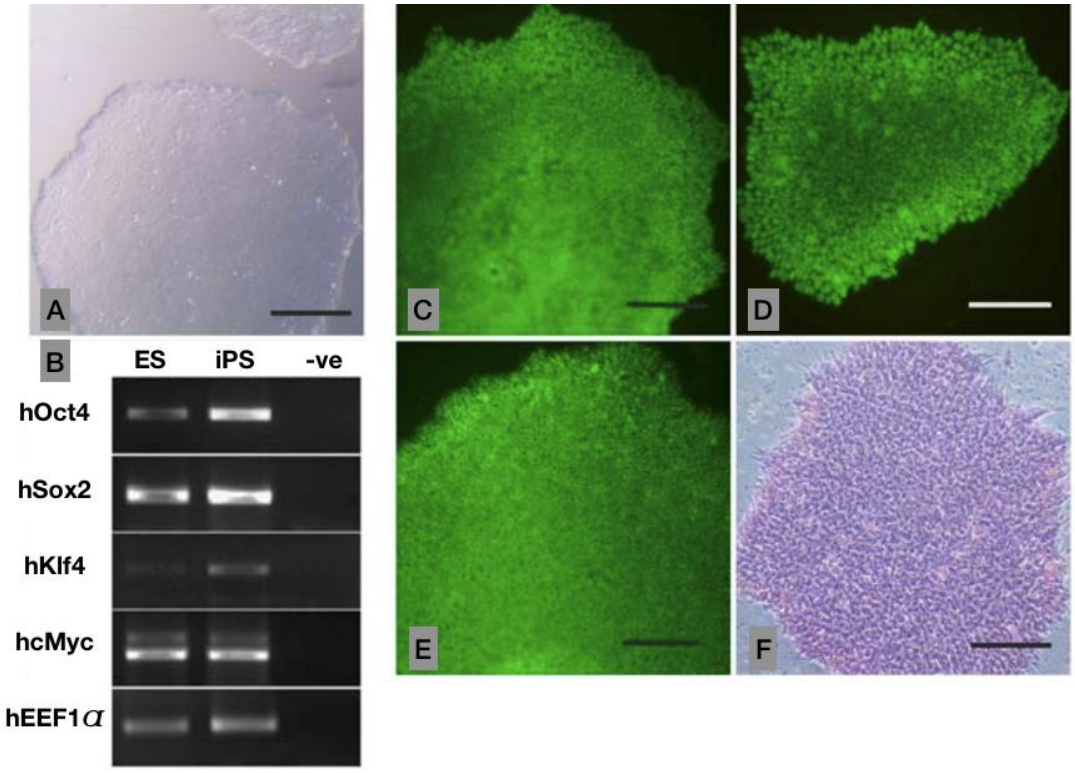

***Figure 2.5: Human iPSC characteristics. A**. Morphology of a typical iPSC colony cultured on Matrigel™ extracellular matrix (ECM). **B**. Agarose gel image of RT-PCR profiles of stemness genes, hOCT4, hSOX2, hKLF4 and hcMYC in human ES and iPS cells. **C-E**. Immunostained images of iPSC colonies expressing nuclear OCT4 and NANOG and cell surface SSEA4 respectively (in green) **F**. An enzyme assay showing alkaline phosphatase (ALP) expression in proliferating iPSCs*

various regenerative applications. E.g. Bone marrow stem cells, skin epithelial stem cells and limbal stem cells. However, since an adult retina do not have stem cells, pluripotent stem cells (PSCs) have offered a great promise for generating retinal cells meant for downstream applications in basic research, drug screening and in regenerative medicine, E.g., ESCs and iPSCs. Human ESCs are derived from the inner cell mass (ICM) of a developing embryo at the blastocyst stage that can differentiate into most cell types of the body, including the eye tissues (Thomson *et al.* 1998). They can be expanded in culture to generate billions of cells and are amenable for genetic manipulations *in vitro*, thus considered an ideal stem cell source for regenerative applications. However, the ethical issues with the need for fertilized human embryos for ESC derivation, their allogenic nature and the risk of immune rejection has been a major concern for their widespread application in cell therapies. A landmark report in 2017 by Prof. Shinya Yamanaka's group at the Kyoto University, Japan had shown that any somatic cell of our body can be reprogrammed into ES-like cells by exogenous expression of four transcription factors namely, OCT4, SOX2, c-MYC and KLF4 (Takahashi *et al.* 2007). These transcription factors are shortly called as "OSKM" or the "Yamanaka factors" and such engineered stem cells are called as "induced pluripotent stem cells" or shortly " iPS cells or iPSCs". Most properties of iPS cells are very similar to ES cells except their somatic cell of origin and therefore the parental cells dictate their genetic age and epigenetic status. Various somatic cell sources such as the skin fibroblasts, epithelium, peripheral blood cells, hair follicle stem cells, bone marrow stem cells, mesenchymal stem cells of different origins, neural stem cells, cord blood stem cells…etc. have been successfully reprogrammed into stable iPSCs so far (Zhao *et al.* 2013). A fully reprogrammed cell line is called an iPSC line when it exhibits all the characteristics listed in **Table 2.3**. Over the past decade, iPSCs have been extensively studied and explored for their applications in various avenues such as drug testing, disease modeling and cell based therapies (Ebert, Liang, and Wu 2012; Kim 2014; Shi *et al.* 2017). Also, patient specific-iPSCs have opened up newer possibilities of personalized therapies such as tailoring autologous cell therapies for the treatment of patients with or without genetic disorders. Various kinds of cells and tissue types such as, cerebral and spinal neurons, retinal and corneal cells, skin epithelium, cardiac and skeletal muscle cells, mesenchymal stem cells, blood cells, bone and cartilage cells and cells of various organs such as, the eye, kidney, heart, liver, pancreas etc., have been successfully differentiated from iPSCs for various purposes (Mahla 2016).

2.7.2. Generation of retinal cells and tissues from iPSCs

Past two decades of research on pluripotent stem cells (both ESCs and iPSCs), several groups have established and reported various protocols for differentiating them into retinal lineage cells (Lad, Cheshier, and Kalani 2009; Lamba and Reh 2011; Linker *et al.* 2004; Perea-Gomez *et al.* 2002; Shen 2007; Streit and Stern 1999). Most of the differentiation strategies in the dish have aimed to recapitulate the signaling events that occur during early eye development of a vertebrate embryo. As discussed in the earlier sections, eye development starts with eye field specification, formation of the optic groove, then the vesicle and finally the optic cups. An optic cup is a bi-layered structure, with the outer layer being specified to become the RPE cells and the inner layer being specified to become the neuro-retina. The RPE fate commitment is fairly simple and requires mainly the withdrawal of bFGF and random differentiation. However, the cells of the neuro-retina need efficient biochemical and mechanical signaling. This has been achieved by the addition of various growth factors and nutrient supplements extrinsically at different stages of differentiation and by growing them in suspension or on suitable ECM enriched scaffolds to allow differentiation and to promote simultaneous self-organization of different cell types to form complex three-dimensional tissues *in vitro*.

Recapitulation of eye development in 3D was first demonstrated by (Eiraku *et al.* 2011) with mouse ESCs and by (Nakano *et al.* 2012) with human ESCs. At day 5 of differentiation, eye field induction was visualized by the appearance of Rx^+ cells, which was in turn followed by increased proliferation, sequential evagination and invagination of Rx^+ retinal precursors, resulting in the formation of optic cups by day 9. The optic cups thus developed were bi-layered and had clear demarcation between the RPE ($Pax6^+Mitf^+$) and neuro-retinal ($Rx^+Chx10^+Pax6^+$) committed cell types.

Various groups have shown the importance of BMP inhibition (with Noggin) and canonical Wnt pathway inhibition (with DKK1) during the initial phases of iPSC differentiation to enable neuro-ectoderm and anterior fate commitments (Ikeda *et al.* 2005; Messina *et al.* 2015; Meyer *et al.* 2009; Perea-Gomez *et al.* 2002; Shen 2007). They have also demonstrated a step-wise progression of differentiation from undifferentiated iPSCs to neuro ectodermal fate to eye field specification to optic vesicle stage to RPE vs neuro-retinal fate commitments, thus recapitulating the normal developmental events *in vitro*.

(Zhong *et al.* 2014a) showed the spatiotemporal generation of different retinal cells at different time points by extrinsic addition of fetal bovine serum (FBS), retinoic acid (RA)

and taurine. It has been observed that the timelines and sequence of retinal cell type emergence *in vitro* was almost very similar to that of *in vivo* development. The reported observations confirm that the Ganglion cell (GC) and photoreceptor cell (PRC) progenitors appear by week 8. The amacrine cells and horizontal cells appear by week 9 and finally the bipolar cells and Müller glial cells by week 21.

The cells continue to develop and mature until week 27, where optic cups with proper lamination, cone-opsin and rod-opsin expressing photoreceptors are formed. Electron microscopy of the optic cups showed the presence of well-formed outer segment discs, connecting cilia and basal body indicating that mature photoreceptors can be generated from iPSCs. When these mature optic cups were transplanted into dystrophic mice retina, they formed synaptic connections demonstrating the proof-of-concept of retinal regeneration using iPSC derived retinal cells.

Our lab has generated mouse iPSC lines and reported their differentiation into RPE and neuro-retinal cells earlier (Mekala *et al.* 2013). The mature RPE cells were heavily pigmented, developed cobblestone morphology and expressed the tight junction marker, ZO1 and also other RPE-specific markers such as: PAX6, MITF, MERTK and TYR. These cells were also shown to exhibit phagocytic activity, which is a crucial function of RPE cells. Very recently, Prof. Masayo Takahashi's group at the CDB, RIKEN, Japan and Dr. Kapil Bharti's group at NEI, NIH, USA, reported the generation of autologous, clinical grade, fully functional mature RPE cell sheets under GMP culture conditions for their use in clinical trials involving AMD patients (Mandai *et al.* 2017; Sharma *et al.* 2019).

Table 2.4: Characteristics of photoreceptors and RPE cells

Parameters	Ideal characteristics of iPSC derived photoreceptors	Ideal characteristics of iPSC derived RPE
Morphology (light microscopy)	Should be lining the outer margins of optic cups similar to the outer nuclear layer positioning; Cell bodies with outer segment-like processes.	Monolayer epithelium with tightly packed, hexagonal arrangement of cells, Moderate to intense pigmentation.
Morphology (electron microscopy)	Outer segment with disc membranes, connecting cilium, basal body.	Apical microvilli, basal infoldings, tight-junction complexes, pigment granules
Cellular markers (progenitors/precursor cells)	PAX6, CHX10, CRX, OTX2, NRL	PAX6, MITF

Cellular markers (differentiated/mature cells)	**Photo-transduction markers:** Recoverin, Rhodopsin, Cone opsins, Arrestin, Transducin, RetGC, RLBP1, PDE6A, PDE6C, PKC-β, RHOK.	**Visual cycle markers:** RPE65, RLBP1, CRALBP; **Phagocytosis markers:** FAK, MERTK; **Pigmentation markers:** Tyrosinase; **Growth factors:** VEGF, PEDF, PDGF; **Membrane markers:** Na/K ATPase, ZO-1, BEST1
Functional (*in vitro*)	Patch recordings, response to light flash.	Phagocytosis assay / Photoreceptor outer segment (POS) clearance assay; **Others:** Fluid transport, Polarized secretion of growth factors (PEDF/VEGF); Trans epithelial resistance
Functional (*in vivo*)	Preservation of host retina and/or rescue of visual function post-transplantation of optic cups or isolated photoreceptor precursors.	Preservation of host retina and/or rescue of visual function post-transplantation of RPE cells in suspension or as sheets on biomaterial scaffolds.
Genome stability	Normal karyotype and absence of any oncogenic genome alterations.	Normal karyotype and absence of any oncogenic genome alterations.

2.7.3. iPSCs in retinal disease modeling

Retinal tissue derived immortal cell lines, cancer cells and retinal tissues of patients and cadavers have been widely used in the past to study retinal diseases. With the above developments in iPSC research and the availability of robust protocols to generate retinal cells and complex 3D organoids, the field has opened up the possibility of large-scale cell preparations, for applications in disease modeling, *in vitro* drug screening and for clinical applications. Also, the effects of individual point mutations and the variability in disease severities observed in patients cannot be truly replicated in limited knock out animal models. Patient-specific iPSCs and mutant retinal cups thus provide a valuable opportunity to study early developmental defects leading to retinal dystrophies in humans (Sinha *et al.* 2016; Yvon *et al.* 2015).

Human iPSCs derived from patients with inherited retinal disorders (IRD) may not only carry the known pathogenic mutation, but also can harbor other known and unknown genetic modification that can together contribute to the observed disease phenotypes. With

the emergence of genome editing tools such as, ZFNs, TALENs and CRISPR-Cas9 systems, it is now possible to correct or to create patient-specific mutations either in mutant or normal iPSC lines respectively. This enables the generation of multiple isogenic controls for patient-specific iPSC and allows for better understanding of disease mechanisms and their confirmation with better test accuracies (Niemitz 2014). In the recent years, several IRDs have been modeled using iPSCs and the details are enlisted in **Table 2.5.**

Table 2.5: List of inherited retinal diseases and patient-specific mutations modeled using iPSCs

Disease	Gene	Mutation	Drug discovery	Gene introduction	Gene discovery	Reference
RP	*RP2*	R120X	✔			(Schwarz *et al.* 2017)
	RHO	G188R		✔		(Jin *et al.* 2012)
	RHO	E181K	✔			(Yoshida *et al.* 2014)
	RP9	H137L	✔			(Jin *et al.* 2011)
	RP1	721Lfs722X				Jin *et al.* 2011)
	RDS/ PRPH2	W316G				(Jin *et al.* 2011)
	MFRP	IVS10+5G>A		✔		(Li *et al.* 2014)
		del492C		✔		(Li *et al.* 2014)
	MERTK	Ser331Cysfs*5				(Lukovic *et al.* 2015)
Sporadic RP	*MAK*	Alu insert			✔	(Tucker *et al.* 2011)
Usher	*USH2A*	Arg4192His			✔	(Tucker *et al.* 2013)
LCA	Unknown					(Lustremant *et al.* 2013)
	CEP290	*IVS26c.2991+ 1665A>G*				(Parfitt *et al.* 2016)
Gyrate atrophy	*OAT*	A226V	✔	✔		(Meyer *et al.* 2011)
Best	*BEST1*	A146K, N296H				(Singh *et al.* 2013) (Singh *et al.* 2013)
Juvenile NCL	*CLN2*		✔	✔		(Lojewski *et al.* 2014)

The disease specific iPSC-derived RPE models displayed one of the following characteristics leading to the disease.

1. Expressed high levels of oxidative stress markers
2. Disrupted fluid flux
3. Accumulation of auto-fluorescent material in long term cultures
4. Differences in stimulated calcium response post photoreceptor outer segment (POS) feeding
5. Defective POS phagocytosis
6. Actin cytoskeletal disorganization and abnormal apical microvilli

The disease specific iPS-photoreceptor models displayed one of the following characteristics leading to the disease.

1. Increased apoptosis or decreased photoreceptor cell survival, leading to reduction in retinal cell numbers, compared to the controls
2. Expression of oxidative stress markers
3. Stress in the endoplasmic reticulum
4. Abnormal photoreceptor development leading to cell death
5. Complete loss of a functional protein, due to unstable mutant mRNA or protein
6. Abnormalities in endosomal-lysosomal systems
7. Delay in POS degradation
8. Differentiation defects and formation of non-neuro-retinal tissues, when compared to controls

Thus, the retinal diseases can be modeled in a dish using patient-specific iPSCs to understand the pathophysiology of the disease and for *in vitro* drug screening, for testing of gene therapy vectors and for various cell therapeutic applications in patients with retinal disorders. Such tissue relevant *in vitro* models can greatly reduce the need for small and large animal models in research. However, the lack of neighboring cells and imperfect cell-cell organization within the stem cell-derived complex tissues can greatly alter various complex cellular behaviors and in turn can question their validity as *in vitro* models in drug screening/testing applications. Also, achieving complete tissue maturation still remains a challenge even with advanced and long-term 3D culture systems. This limits their use as disease models to study various alterations in mature cell functions *in vitro*. It is therefore ideal to use such iPSC-derived *in vitro* disease models to carry out preliminary evaluations and the key findings should be reevaluated in suitable *in vivo* animal models for a better understanding of disease physiology.

2.8. Zebrafish models to understand human retinal diseases

Zebrafish (*Danio rerio*) has its origin from the river Ganges in India. They are small, fresh water species that are widely used as a model organism to study embryology, developmental and reproductive biology, behavior science, neurobiology, immunology, toxicology, oncology stem cells and regenerative biology and also to study a wide range of human diseases. Their increasing popularity as a model system can be attributed to their small size, simpler maintenance and breeding requirements, large clutch size, external fertilization and development of embryos, shorter generation time from egg to adult stage, transparent and bigger embryos that are amenable for genetic manipulations, translucent body that allows for live cell imaging possibilities during early stages of development, availability of genomic sequence information and easily testable developmental behaviors. The zebrafish genome is well annotated and maintained by multiple databases like the National Center for Biotechnology Information (NCBI-USA), Ensembl-UK, the Zebrafish Information Network (ZFIN-USA), University of California Santa Cruz genome browser (UCSC-USA) and the Zebrafish Genome Initiative-USA. It has 25 sets of chromosomes and has 33% similarity with that of human DNA and 72% of the human genes have at least one ortholog in zebrafish.

Mutations in several genes result in a variety of heritable retinal dystrophies. An *in vivo* model system is therefore required to validate such mutations and to assess their effects on cellular functions and disease mechanisms. A zebrafish model offers a quick and simper alternative to study human diseases and also to test different therapeutic strategies. The visual system of zebrafishes are very similar to that of humans and are useful for modeling certain ocular conditions like myopia, ciliopathies, glaucoma, albinism, and different forms of retinal dystrophies (Link and Collery 2015). An adult zebrafish retina has a greater regenerative potential unlike that of humans. A needle prick injury in the retina is known to heal within a week without any visible signs of scarring, unlike in humans. Thus, zebrafishes have evolved as interesting models to address various research questions related to retinal wound healing, tissue regeneration and disease mechanisms.

2.8.1. Visual system in zebrafish

The visual system in zebrafish develops very fast and is near compete within 3 days post fertilization (dpf). This is required as there is a greater need for young ones to forage for food while avoiding predators in its natural habitat. Zebrafish are diurnal animals and have copious numbers of cone photoreceptors. There are four types of cone opsins and thus four

kinds of cone photoreceptors for red, green, blue and UV light, enables tetra-chromatic vision. Once the gene of interest is knocked out, the effects on the visual system can be easily tested using various methods such as, the moving patterns with varied brightness, resolution, sharpness and color. These behavioral studies are characterized as optokinetic response, escape response and visual motor response. To complement the visual behavior test, scotopic and photopic ERG responses can also be measured.

Many zebrafish models with reduced vision or total blindness have been reported so far. They were either naturally occurring or created by knocking down the gene of interest using morpholinos or by complete knock out of genes using ZFNs (zinc finger nucleases) or TALENs (Transcription Activator Like Effector Nucleases) or CRISPR-Cas9 mediated gene editing (**Table 2.6**).

Table 2.6: List of inherited retinal disease models of zebrafish and their phenotypes

Human disease	Gene	Zebrafish model	Phenotype	References
Choroiderma	*REP1*	*rep1*	Disordered RPE, disrupted retinal layers	(Moosajee *et al.* 2009)
Sveinsson's chorioretinal atrophy	*TEAD1*	*yap*	Severe loss of RPE cells	(Miesfeld *et al.* 2015)
Retinitis punctate albescens	*RLBP1*	*rlbp1a, rlbp1b*	Reduced levels of 11-cis retinal leading to reduced visual acuity	(Collery *et al.* 2008)
Oculocutaneous albinism 1	*TYR*	*tyr*	Absence of tyrosinase activity leading to lack of proper dopamine and reduced vision	(Page-McCaw *et al.* 2004)
Oculocutaneous albinism 2	*OCA/P*	*oca2/p*	Reduced pigmentation in RPE	(Beirl *et al.* 2014)
Retinitis pigmentosa 2	*RP2*	*rp2*	Small eyes, retinal lamination failure	(Shu *et al.* 2011)
Retinitis pigmentosa 3	*RPGR*	*rpgr*	Small eyes and lamination defects	(Shu *et al.* 2010)
Retinitis pigmentosa 4	*RHO*	*Tg (rho:Hsa. RH1_Q344X)*	Rod apoptosis upon mutant protein expression	(Nakao *et al.* 2012)
Retinitis pigmentosa 11	*PRPF31*	*prpf31*	Loss of outer segments and eventually photoreceptor cell loss	(Yin *et al.* 2011)
Retinitis pigmentosa 26	*CERKL*	*cerkl*	Increased retinal cell death, with signs of oxidative stress	(Riera *et al.* 2013)
Retinitis pigmentosa 31	*TOPORS*	*toporsa*	Small eyes, lamination defects and failure of POS development	(Chakarova *et al.* 2011)

Retinitis pigmentosa 54	*C2ORF71*	*c2orf71*	Shorter POS and reduced visual response.	(Nishimura *et al.* 2010)
Retinitis pigmentosa 58	*ZNF513*	*znf513*	Small eyes, reduced retinal thickness, loss of photoreceptors and reduction of rod and cone opsin expression	(L. Li *et al.* 2010)
Retinitis pigmentosa 59	*DHDDS*	*dhdds*	Loss of POS and loss of visual function	(Züchner *et al.* 2011)
Retinitis pigmentosa 68	*SLC7A14*	*slc7a14*	Abnormal eye phenotype and defective light-induced locomotor response	(Jin *et al.* 2014)
LCA type 1	*GUCY2D*	*gucy2f*	Reduced vision and aberrant retinal histology with shortening of outer segments and reduction in cone marker staining	(Stiebel-Kalish *et al.* 2012)
Cone dystrophy X3	*CACNA1F*	*cacna1fa*	Reduced and altered photoreceptor ribbon synapses leading to thinner outer plexiform layer and abnormal ERG	(Jia *et al.* 2014)
Cone dystrophy 4	*PDE6C*	*pde6c*	Rapid and early cone degeneration leading to a rod dominated retina	(Stearns *et al.* 2007)
Cone-rod dystrophy 6	*GUCY2D*	*Tg (3.2gnat2: RETGC-1 E837D R838S)*	Overexpression of mutant protein led to aberrant cone morphology, reduced cone cell density and shortening of outer segments	(Collery, Cederlund, and Kennedy 2013)
Achromatopsia	*GNAT2*	*gnat2*	Reduced visual function and inability to track moving stripes in behavioral assays	(Brockerhoff *et al.* 2003)

These zebrafish models have provided key understandings into the genetic, molecular and cellular mechanisms fundamental to the various blinding conditions. Some of them prove to be useful tools to conduct large scale screening of chemical libraries to identify novel compounds that can rescue retinal functions.

2.9. CRISPR-Cas9 mediated gene editing

Clustered regularly interspaced short palindromic repeats (CRISPRs) are repetitive DNA sequences present in the *Streptococcus* sp., that act along with CRISPR-associated

endonuclease (Cas9) act as an adaptive immune system in the bacteria against bacteriophages (Wiedenheft *et al.* 2012). As a part of the immune mechanism in *Streptococcus* sp., the genome of the invading bacteriophage is chopped into small DNA fragments that gets integrated in the CRISPR locus and are called the "protospacer elements" (Doudna and Charpentier 2014). The CRISPR locus gets transcribed as a single, non-coding pre-crRNA (precursor CRISPR-RNA) which is further processed to shorter RNA fragments (crRNA), with the protospacers being complementary to the invading viral genome. crRNA along with the non-coding and trans-activating crRNA (tracrRNA) and the Cas9 endonuclease forms an active ribonucleoprotein (RNP) complex, that in turn recognizes and cleaves the invading viral genome, specifically at the region complementary to the protospacer element.

In vitro transcription of the fused DNA sequences of crRNA and tracrRNA resulted in a single guide RNA that had the ability to recruit Cas9 endonuclease and created double strand breaks (DSBs) at the targeting genomic region (Jinek *et al.* 2012; Mali *et al.* 2013). In the absence of a homologous template, the DSBs are repaired by an error-prone DNA repair mechanism called the non-homologous end joining (NHEJ), that causes random insertions and deletions (in-dels) of nucleotides while randomly joining the broken DNA fragment. Such CRISPR-Cas9 induced indels can result in frame shifts/internal deletions at the targeted genetic loci, leading to gene knockouts. Alternately, the DSBs can be repaired by another mechanism called the homology directed repair (HDR). HDR usually uses the unmutated wild type allele as the repair template to bring about homologous recombination mediated absolute DNA repair. However, supplementation of a synthetic repair template after the formation of DSBs also can mediate HDR events. Using such novel gene editing tools and native DNA repair mechanisms, it is now possible to introduce specific base-pair changes in the genomes of any cell lines and individual animal models.

2.10. Gene therapy for autosomal recessive retinal dystrophies

A gene therapy aims to supplement the mutant cells with a normal and functional copy of the mutated gene to restore normal cellular functions. This approach is more suitable for the treatment of autosomal recessive diseases, wherein, the disease manifests only when both the alleles are mutated in a homozygous state, while the heterozygous carriers are usually asymptomatic. However, in case of dominant disorders, even a single allele mutation can manifest a serious disease due to dosage insufficiencies or due to dominant negative effects

of the mutant protein. Therefore, a gene therapy for dominant disorder is more complex and requires a complete knock out of the mutant gene, prior to wild type gene supplementation.
A successful gene supplementation therapy requires a normal gene copy to be delivered efficiently into the target cell of interest. This requires the design of efficient gene expression cassettes that drives the expression of a transgene in a tissue-specific manner and at optimal physiological levels for a long period of time *in vivo*. This is made possible by the use of appropriate promoters to drive the transgene expression. A wide variety of promoters such as the ubiquitous and constitutively active cytomegalovirus immediate early enhancer and promoter (*CMV*), Chicken β actin promoter (*CBA*), eukaryotic elongation factor 1α promoter (*eEF1α*) and the hybrid *CMV* enhancer/chicken beta-actin promoter (*CAG*) have been used in the past to drive abundant transgene expression. Retinal tissue-specific promoters such as the human *RPE65* promoter, *GRK1* promoter, cone opsin (L-opsin & S-opsin) promoters, rhodopsin promoter, *IRBPe/GNAT2* chimeric promoter (enhancer element of the inner-photoreceptor retinoid binding protein (IRBP) promoter/human transducin alpha-subunit minimal promoter, cone arrestin promoter…etc. (Boye *et al.* 2012; Dyka *et al.* 2014; Khani *et al.* 2007; Kostic *et al.* 2013; Li *et al.* 2008; Miyoshi *et al.* 1997; Pierce and Bennett 2015; Zhu *et al.* 2002), have also been tested and used to confer tissue specificity and optimal transgene expression in various trials for *RPE65*, *RPGR*, *BEST1*, *ABCR*, *RHO*, *CHM*, *AIPL1* and *CNGB3* delivery (Auricchio, Trapani, and Allikmets 2015; Barnard, Groppe, and MacLaren 2014; Beltran *et al.* 2017; Cideciyan *et al.* 2018; Guziewicz *et al.* 2018; Jacobson *et al.* 2012; Miraldi Utz *et al.* 2018; Pang *et al.* 2010). Also, the choice of suitable gene delivery vectors can influence the efficiency and cell type specificity of *in vivo* gene delivery systems. For a stable and efficient retinal gene delivery, third generation lentiviral vectors and adeno-associated virus-based vectors of specific serotypes (AAV2, AAV5, AAV8) are a preferred choice.

With the availability of patient-specific iPSCs and iPSC-derived retinal tissues, it may now be possible to carry out *in vitro* gene correction in a combined gene and cell therapeutic strategies for autologous applications. This can be achieved by engineering patient cells *in vitro* to enable mutation correction, either by whole gene supplementation or by adopting targeted *in situ* gene editing using ZFNs or TALENs or CRISPR/Cas9 systems.

CHAPTER 3

METHODOLOGY

3. Methodology

3.1 Ethics statement

The study protocol followed the principles of the Declaration of Helsinki and ethical approval for this study was obtained from the Institutional Review Board of the L.V. Prasad Eye Institute. A written informed consent was taken from all the study participants prior to their enrolment in the study. Animal experiments were conducted in accordance with the approval of the Institutional Animal Ethics Committee (AEC) and Association for Research in Vision and Ophthalmology (ARVO) guidelines for the use of animals in eye research.

3.2 Recruitment of patient volunteers and mutation validation

The purpose of the study, need for the biological samples, the broad outline of work flow, sample storage, indirect benefits out of study outcomes, rights of participants, confidentiality of personal information…. etc., were clearly explained to all the volunteers before obtaining their consents and recruitment into the study. A copy of the ethics committee approved informed consent form (ICF) executed in the study is attached (**Annexure I**). The LCA and ARRD patients (VS and KR) were counseled as above and requested to visit the LV Prasad Eye Institute, Hyderabad to provide blood samples to re-confirm their genetic changes reported earlier in *RD3* and *ABCA4* respectively (Friedman *et al.* 2006, Singh *et al.* 2006). About 5 mL blood and a 2x2 mm full thickness punch biopsy of the retro-auricular skin was collected from all the study volunteers, including a healthy control individual (F2), for comparative studies.

3.2.1 Isolation of blood genomic DNA (deoxyribonucleic acid)

The blood samples were collected in VACUETTE® tubes containing anti-coagulant (EDTA) and stored in -20° C until further use. For genomic DNA isolation, blood was thawed completely on ice and transferred to a 15 mL centrifuge tube. Three volumes of cold 1X PBS was added and mixed well by vortexing the tube till the solution appeared clear. The tubes were incubated on ice for 20 minutes and then spun at 3000 rpm for 15 minutes. The supernatant was discarded and a reddish-brown pellet was obtained. The pellet was repeatedly washed with 1X PBS until it becomes pinkish white and then resuspended in 3.75 mL of **Genomic DNA extraction buffer** (per 5 mL of blood) containing 18.75 µL of 20 mg/mL Proteinase K and 7.5 µL RNase A (10 mg/mL). The solution was incubated at 37ºC overnight in water bath. The next day, equal volumes of phenol:chloroform:isoamyl alcohol (25:24:1) was added and mixed gently by inverting the tube until an emulsion is seen to

ensure complete mixing of the solutions. The tube was then centrifuged at 2500 rpm for 10 minutes. After centrifugation, the upper phase (aqueous) was transferred to a separate tube and equal volume of chloroform:isoamyl alcohol (24:1) was added. The contents were mixed by inverting the tube and centrifuged again at 2500 rpm for 10 minutes. The aqueous phase (supernatant) containing DNA was transferred to a fresh 15 mL centrifuge tube. A little amount of supernatant was left to avoid organic phase contamination. Two volumes of chilled absolute ethanol and 10 µL of 10 M ammonium acetate was added and inverted gently. The precipitating genomic DNA that appeared as thin threads were then spooled out gently, either using a glass rod or a cut pipette tip and then transferred to fresh 1.5 mL centrifuge tubes. The DNA was then washed with 1 mL of 70% ethanol and spun at 8000 rpm for 15 minutes. The supernatant was discarded and the DNA pellet was air dried. To re-suspend the DNA pellet, 200 µL of TE buffer was added. The tube was kept overnight at room temperature to dissolve the DNA completely. Vortexing was avoided to prevent the mechanical shearing of the purified genomic DNA.

3.2.2 Agarose gel electrophoresis (AGE)

AGE is the commonly used method to check the quality and quantity of DNA. The percentage of agarose used to make the gel depends on the size of the DNA to be analyzed. To analyze the genomic DNA isolated from the patients and the control, 0.4 grams of agarose was melted in a conical flask containing 50 mL of 1X **TAE buffer** (0.8% agarose gel) using the microwave oven for 2 minutes. The solution appears clear after all the agarose is melted. Once the temperature of the solution came down to ~60° C, 1 µL of 10 mg/mL ethidium bromide (EtBr) was added and swirled gently until all of the EtBr is completely mixed in the agarose gel solution. Care was taken not to introduce air bubbles. The agarose gel solution was poured on a gel casting tray with suitable combs based on the number of wells required. Once the gel was solidified, it was transferred to the electrophoresis tank containing 1X TAE buffer. The DNA samples were then diluted ten times in **TE buffer** in a separate vial and 1 µL of it was mixed with 5 µL of (6X) DNA loading dye and loaded in the wells of the agarose gel. 3 µL (250 ng) of DNA molecular weight marker was also loaded in a separate well. The gel was run at 120 V until the dye front reached half the distance of the complete gel. The gel (**Fig 3.1**) was then visualized using a UV transilluminator (Biorad, USA).

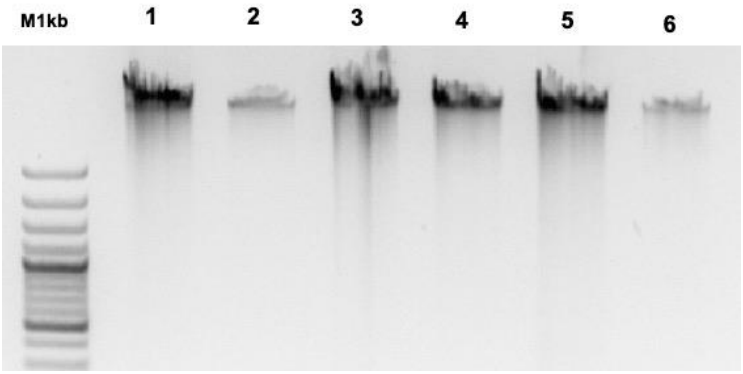

Figure 3.1: Agarose gel electrophoresis of genomic DNA isolated from the blood of patients and healthy control

3.2.3 Quantification of genomic DNA by AGE and NanoVue™ Plus

The amount of DNA can be approximately quantified by running a known amount of molecular marker (250 ng) side by side to the DNA to be quantified. When the DNA marker resolves, each band's intensity with known quantity can be compared with the test DNA sample (diluted 1:10) and the test DNA was approximately quantified.

Alternatively, for better quantification NanoVue™ Plus (GE Lifesciences, USA) was used, which works on the principle of Beer-Lambert law of absorption of light by molecules. Blanking was done using TE buffer in which the DNA was dissolved. Then 1-2 µL of diluted DNA was loaded onto the sample loading area and the DNA was quantified by measuring the optical density (OD) at both 260nm and 280 nm. The OD at 260 nm is used to measure the DNA yield and the ratio of OD at 260/280 nm gives the quality of the DNA. A good quality DNA has an OD ratio of ~1.8 at 260/280 nm and a good quality ribonucleic acid (RNA) has an OD ratio of ~2.0. Values less than 1.8 indicate the presence of phenol and protein contamination in the DNA sample.

3.2.4 Polymerase chain reaction (PCR) based DNA amplification

PCR based DNA amplification of the region of interest is the first step before DNA sequencing and is required to generate enough copies of the targeted DNA region of interest. The processes of unwinding of the DNA double helix by helicases, topoisomerases and priming by RNA primase during DNA replication *in vivo* are simulated by PCR amplification conditions in a thermal cycler. A thermal cycler is just like a dry bath which can heat up and cool down within few seconds. The only enzyme that a PCR reaction requires is the Taq DNA polymerase (isolated from *Thermus aquaticus*) that can withstand the extreme DNA denaturation temperature of 95º C. PCR reaction also requires a set of DNA primers

(forward and reverse - for the sense and anti-sense strands), deoxyribonucleotide triphosphate (dNTPs) and the DNA template from which the region of interest must be amplified. As two primers defines the DNA region to be amplified and every PCR cycle results in the amplification of double the number of DNA fragments, all of which serves as a template for the next cycle resulting in a chain reaction. This results in exponential increase of the DNA fragments after every cycle. Hence this *in vitro* reaction is called a polymerase chain reaction (PCR). Therefore, at the end of "n" number of cycles, N x 2^n copies of the targeted DNA region gets amplified in a PCR reaction, where 'N' is the number of template DNA molecules present initially.

The reaction mix shown in **Table 3.1**, was prepared in a 200 µL PCR tube, vortexed for even mixing and briefly centrifuged to collect the contents to the bottom of the tubes. The sequencing primers used to screen the mutations are listed in **Annexure V.** PCR reaction was then carried out by placing the tube in a thermal cycler (Applied Biosystems, USA) with the program mentioned in **Table 3.2**.

Table 3.1: PCR reaction mix

S. No.	Reagents	Concentration	Volume (µL)
1	Genomic DNA	100 ng	2.0
2	Taq buffer	10X	2.5
3	dNTPs	2 mM	2.5
4	Forward primer	5 pmol	1.2
5	Reverse primer	5 pmol	1.2
6	Taq polymerase	0.5 U/µL	0.5
7	Deionized water	-	15.1
		Total volume	**25.0**

Table 3.2: Thermal cycler program

S. No.	Amplification steps	Temperature (°C)	Duration (sec)
1	Initial denaturation	95	300
2	Denaturation	95	30-45
3	Annealing	X	30
4	Extension	72	60 per kb amplicon
Steps 2-4 for 35 cycles			
5	Final extension	72	300-600
6	Hold	4	300

3.2.5 AGE of the amplified PCR products

The amplification of desired DNA fragments of known sizes was confirmed by running 5 µL of PCR product with 1 µL of 6X DNA loading dye on AGE as described above (**section 3.2.2**). The percentage of agarose gels was determined based on the size of amplicons to be resolved. A 100 bp or 1 kb marker ladder was used for checking the size of amplicons.

3.2.6 Sanger's chain termination method of DNA sequencing

This method of DNA sequencing uses only one primer (either for the sense or the anti-sense strand) and therefore is not a chain reaction. The number of amplicons increases linearly after each cycle and not exponentially as in PCR. Therefore, at the end of "n" number of cycles, N x n copies of the targeted DNA region gets amplified, where 'N' is the number of template DNA molecules present initially. Another major difference is the use of fluorescently labeled ddNTPs (distinct fluorescent tags for each nucleotide: ddATP, ddTTP, ddGTP and ddCTP) along with regular dNTPs in the reaction mix. The sequencing reaction mix shown in **Table 3.3** was prepared in a PCR tube or a 96well sequencing plate. The sequencing reaction condition for the thermal cycler is shown in **Table 3.4.** In sequencing reaction, primer annealing and extension takes place just like PCR until the ddNTP is incorporated and terminates the extension of the DNA fragment. In this fashion, DNA fragments that had terminated at different base positions with a fluorescently labeled ddNTP at the 3' end are synthesized.

Table 3.3: Sequencing reaction mix

S. No.	Reagents	Concentration	Volume (µL)
1	PCR product	5-20 ng	0.5-1.0
2	Sequencing buffer	5X	2.0
3	BigDye Terminator	-	0.2
4	Forward/Reverse primer	5 pmol	1.0
5	Deionized water	-	5.8-6.3
		Total volume	**10.0**

Table 3.4: Sequencing reaction condition

S. No.	Amplification steps	Temperature (°C)	Duration (sec)
1	Initial denaturation	96	120
2	Denaturation	96	10
3	Annealing	56	6
4	Extension	72	240
Steps 2-4 for 30 cycles			
5	Hold	4	300

3.2.7 Precipitation of sequencing reaction products

The DNA fragments of different lengths obtained by the sequencing reaction were purified prior to subjecting to capillary electrophoresis. The elimination of unincorporated dNTPs, ddNTPs and unused primers is essential, because their contamination will result in noisy signals in early part of the chromatogram.

Purification of the DNA fragments after sequencing reaction was carried out in the sequencing plate itself or in a centrifuge tube by adding 1 µL of 125 mM EDTA (pH 8.0) and 1 µL of 3M sodium acetate (pH 5.2). After brief spinning to bring all the solution to the bottom of the tube/plate, 50 µL of 100% chilled ethanol was added to the plate/tube for DNA precipitation. The plate is then wrapped with aluminum foil and placed on a rocker for 20 minutes at room temperature (RT). The plate/tubes were then spun at 4000 rpm (11000

rpm in case of tubes to precipitate shorter fragments less than 50 bp) for 30 minutes in a refrigerated centrifuge (Eppendorf, Germany), set at 4° C to obtain the DNA pellet. The plate/tubes were inverted carefully on a paper towel to remove the ethanol without losing the pellet. The pellet was washed with 50 µL of 70% ethanol and spun at 4000 rpm for 20 minutes at 4° C. The ethanol was drained on a paper towel, air dried for 10-15 minutes to remove any residual ethanol and suspended in 10 µL of Hi-Di Formamide. The DNA suspended in Hi-Di Formamide was denatured at 95° C. Although most of the DNA fragments synthesized (fragments other than the ones synthesized in the last cycle) would be single stranded, denaturation step helps to keep the DNA linear and single stranded. HiDi-formamide helps in slowing down the renaturation of the DNA amplicons with the template DNA and also prevents sample evaporation during capillary electrophoresis.

3.2.8 Capillary electrophoresis mediated sequencing

The purified DNA fragments that had terminated at different base pair positions with a fluorescently labeled ddNTP at the 3' end was subjected to capillary electrophoresis in which the fragments were sorted based on their sizes in a sequential order of +1 bp. This was achieved using the 3130xl Genetic Analyzer (Applied Biosystems, USA). The shorter fragments run first forming a gradient of fragments that are 1 bp longer than the previous ones, forming a queue of DNA fragments. Before the fragments reach the anode, they move across a path of laser beam that excites the fluorescent dyes of the ddNTPs at the 3'end of each fragment. Each of the 4 types of ddNTPs fluoresces at different wavelengths that are detected by the detector and converted into digital data that is presented by the analyzer in the form of a chromatogram.

3.2.9 Sequence analysis

The raw data (.ab1 files) obtained from 3130xl Genetic Analyzer was analyzed using the softwares Chromas (version 2.6.4) or SnapGene Viewer (version 3.2.1). The software provides the data both in chromatogram format and in FASTA text format. The sequence was compared with the wild type sequence obtained from NCBI or Ensembl genome browser to validate the presence of reported base pair changes.

3.3 Culture and expansion of human dermal fibroblasts (HDFs)

Once the reported mutations were confirmed, full-thickness punch biopsies of skin were taken from patient volunteers (VS, KR) and healthy volunteer (F2). The biopsies were used to establish human dermal fibroblast (HDF) cultures.

3.3.1 Obtaining skin biopsy

The region with thin skin behind the ear pinna (periorbital skin) was selected as the area to be biopsied and was cleansed with povidone-iodine solution and anesthetized using a topical gel containing 2% lidocaine with epinephrine. The punch biopsy device (2 mm) was placed firmly against the skin and rotated against the skin with a gentle pressure until the device reached the subcutaneous fat and quickly pulled out to obtain the full thickness skin biopsy. An antibiotic ointment was then applied to the biopsied region and was covered by bandage. The skin biopsy was collected immediately in collection vials containing sterile **cDMEM with 20% FBS** on ice.

3.3.2 Matrigel™ coating of the culture dishes

We used Matrigel™ for coating the culture dishes. Matrigel is a solubilized ECM preparation obtained from Engelbreth-Holm-Swarm (EHS) mouse sarcoma, a tumor rich in ECM proteins. It majorly consists of laminin (60%), collagen IV (30%), and entactin (8%). The concentration of Matrigel™ varies from batch to batch and the average concentration is 10 mg/mL. A 20X stock concentration of 2 mg/mL was prepared and 500 µL aliquots were made in 1.5 mL vials and stored at -80° C freezer. For coating the wells of a 6-well plate, an aliquot of Matrigel™ (500 µL of 2 mg/mL) was thawed on ice and then diluted in 10 mL of ice cold DMEM-F12 and mixed using a pre-chilled pipette to prepare a 100 µg/mL working solution (1X). About 1-1.5 mL of 1X solution was added to each well of the 6-well plate and incubated at 37° C to ensure uniform coating of the culture surfaces.

3.3.3 Dissection of the skin biopsy

The skin biopsies from both the patients and control sample were taken inside a biosafety cabinet (Telstar, Japan) and placed in a 100 mm cell culture dish using sterile forceps. Using a dissection microscope (Olympus, Japan) placed inside the biosafety cabinet, the 2 mm skin biopsy was cut into 12-15 evenly sized pieces using a No. 21 surgical blade. It was made sure that sharp cuts were made resulting in biopsy pieces with sharp edges. (Biopsy pieces with blunt edges do not really adhere well in the culture dish). 2-3 biopsy pieces were picked carefully using a needle and placed onto the center of Matrigel™ coated wells of a 6-well plate. The tissue explants were held in place and made to stick to the bottom of the dish by placing a clean and sterile glass coverslip on the top and the cultures were maintained in **fibroblast growth medium, FGM** and placed in a CO_2 incubator (Thermo Fisher Scientific, USA) at 37° C with 5% CO2 supply. The cultures were monitored daily for a week, with fresh media changes on alternate days. During the first week, the biopsy pieces firmly get

attached to the dish and leave out fibroblast cell outgrowths that migrate on to the dish and expand all around the explants until they become confluent.

3.3.4 Passaging

Once the fibroblasts were confluent and reached the peripheral edges of the wells, the media was aspirated and washed with 1X DPBS to get rid of the leftover media. The serum in the media contains protease inhibitors that may hinder the trypsin activity. A saline wash prior to trypsin treatment helps to overcome this problem. After the saline wash, 0.5 mL of **Trypsin-EDTA** or 1X TrypLE was added to the wells and incubated at 37° C for 5 minutes. The plates were then gently tapped to detach the cells, quickly visualized under the microscope and then 2 mL of **cDMEM** was added to the wells to arrest the trypsin activity and triturated gently with 1 mL tip for 4-6 times to create single cell suspension. The cell suspension from all the wells was then transferred to a 15 mL tube and centrifuged at 1000 rpm for 4 minutes to obtain a cell pellet. The supernatant media was discarded and the pellet was re-suspended in required volume of cDMEM and plated onto two T75 flasks.

3.3.5 Cryopreservation

The cells were further passaged and used for further experiments or cryopreserved. Once the flasks were 90-95% confluent, they were trypsinized and passaged as mentioned in **section 3.3.4** and for freezing, the cell pellet was suspended in **cryopreservation medium** at about 1 million cells/mL and at least 0.5 mL of the above cryosolution containing the cells were transferred to duly labeled 2 mL cryovials, which were then closed airtight and kept on ice. The vials were then packed inside Mr. Frosty and stored in -80º C overnight, before transferring them to the vapor phase of liquid nitrogen container, for their long-term storage and cryopreservation.

3.4 Production of lentivirus with *hOCT4*, *hSOX2*, *hcMYC* and *hKLF4*

The plasmids mentioned in **Table 3.5** were obtained from Addgene. Addgene provides plasmids in the form of stab culture of DH5α cells containing the plasmid of interest. The stab cultures were streaked on to Luria-Bertani plates with Ampicillin (100 µg/mL) and incubated at 37° C for 16 hours. Single colonies that had appeared the next day were picked and cultured in 2 mL of Luria-Bertani broth, containing 100 µg/mL Ampicillin, for 16 hours at 37° C in a shaking incubator (Thermo Scientific, USA) at 220 rpm.

Table 3.5: Plasmids used for lentiviral production

Addgene ID	Plasmid	Gene/Insert	Vector type
17217	pMXs-hOCT3/4	OCT3/4 (Homo sapiens)	Mammalian Expression, Retroviral
17218	pMXs-hSOX2	SOX2 (Homo sapiens)	Mammalian Expression, Retroviral
17219	pMXs-hKLF4	KLF4 (Homo sapiens)	Mammalian Expression, Retroviral
17220	pMXs-hc-MYC	c-MYC (Homo sapiens)	Mammalian Expression, Retroviral

3.4.1 Plasmid amplification and purification from bacterial cultures (miniprep)

After 16 hours of incubation, the 2 mL bacterial cultures containing the specific plasmids were transferred to a 1.5 mL centrifuge tube inside the laminar hood. About 100-200 µL of the same culture was also used as a starter culture for a parallel 100 mL midiprep culture (**section 3.4.3**). The 1.5 mL bacterial culture was spun at 12000 rpm for 10 minutes. The spent media was discarded in a beaker containing diluted bleach. The cell pellet in the microfuge tubes were suspended in 300 µL of **plasmid isolation solution I** and vortexed vigorously to create a nice bacterial cell suspension. Later, another 300 µL of **plasmid isolation solution II** was added to the bacterial cell suspension and gently inverted 6-8 times to lyse the cells without shearing the bacterial genomic DNA. The detergent, SDS in solution 2 lyses the bacteria and releases the cellular contents. Also, the NaOH makes the solution alkaline in which genomic DNA, plasmid DNA and proteins are denatured. Further, 300 µL of **plasmid isolation solution III** was added to the tube and gently inverted 6-8 times and kept on ice for 10 minutes. 5M potassium acetate is used to create a high salt concentration that precipitates sodium dodecyl sulphate (SDS), lipids and proteins. Acetic acid neutralizes the pH of the solution resulting in renaturation of plasmid DNA, whereas the large genomic DNA is captured in the white DNA-Protein precipitate. The precipitate is then cleared from the solution by centrifuging the tube at 12000 rpm for 10 minutes. The supernatant with the plasmid DNA was then transferred to a fresh 1.5 mL centrifuge tube and 600 µL of 100% isopropanol was added to precipitate the plasmid DNA, mixed well and

kept at RT for 10 minutes. The precipitated plasmid DNA was then pelleted by spinning the tube at 12000 rpm for 10 minutes. The plasmid DNA pellet was washed with 500 µL of 70% ethanol and spun at 12000 rpm for 5 minutes. The ethanol containing supernatant was decanted and the excess solutions were blotted out. The pellet was air dried at room temperature until all the ethanol had evaporated. The transparent, plasmid DNA pellet at the bottom is dissolved in 50 µL of **TE-RNase** and incubated at 37° C for an hour to digest all the bacterial RNAs that got co-precipitated along with the plasmid DNA. The plasmid DNA was then run on AGE to check for their quality and quantity.

3.4.2 Restriction digestion and confirmation of Yamanaka plasmids

The plasmids were then digested with the restriction enzymes BglII (R0144S) and SalI (R0138S) from NEB to confirm their identity. The digestion reaction mix composition is given in **Table 3.6**. The digested plasmids were then run on AGE to analyze the restriction patterns.

Table 3.6: Restriction digestion reaction

S. No.	Reagents	Concentration	Volume (µL)
1	NEB buffer 3.1	10X	2.0
2	BglII	10000 U/mL	0.5
3	SalI	2000 U/mL	2.5
4	Plasmid DNA	1 µg/µL	1.0
5	Nuclease free water	-	11.0
		Total volume	**20.0**

3.4.3 Plasmid amplification and purification from large volume bacterial cultures (midiprep)

Once the plasmids were confirmed by restriction digestion checks, 100 mL bacterial cultures were processed for midi-preps using NucleoBond® Xtra Midi kit, as per the manufacturer's instructions. Briefly, 100 µL of the starter culture (**section 3.4.1**) was inoculated into 100 mL of LB-broth with Ampicillin (100 µg/mL) and incubated in shaker incubator (220 rpm) at 37° C for 16 hours or until the culture reached the required optical density of interest (OD at 600 nm). For high copy number plasmids (several hundred copies/cell), the bacterial culture was grown until OD_{600} = 2 and for low copy number plasmids (<20 copies/cell), the

bacterial culture was grown until OD_{600} = 8. The bacterial cultures were then transferred to 50 mL centrifuge tubes and centrifuged at 4000 rpm for 15 minutes at 4° C. The spent media was discarded and the remaining bacterial culture was added to the same tube and spun to collect the total cell pellet. The bacterial pellet weighing about 0.75 grams was then used for plasmid DNA isolation.

The bacterial pellet was suspended in 8 mL of resuspension buffer RES + RNase A, by vortexing thoroughly. Lysis buffer LYS (8 mL) was added to the suspension, mixed gently by inverting the tube for 5 times, until the suspension became blue and incubated at RT for 5 minutes. Meanwhile, the NucleoBond® Xtra Column along with the filter was equilibrated with 12 mL of equilibration buffer, EQU. The column was allowed to empty by gravity. Neutralization buffer NEU (8 mL) was added to the suspension and mixed gently by inverting the tube for 5 times until the suspension solution became colorless and a white precipitate was obtained. This solution with precipitate was either loaded directly on to the filter of the column or centrifuged at 4000 rpm for at least 10 minutes and the clear supernatant was then loaded. The sample flowed through the filter and the plasmid DNA in the suspension got bound to the column containing silica-based anion exchange resin. The column being highly positively charged at acidic pH holds on to negatively charged nucleic acids with high affinity. The column was then washed with 5 mL of equilibration buffer EQU**.** The filter was discarded and the column was washed with 8 mL of wash buffer WASH. To elute the DNA from the column, about 5 mL of the elution buffer, ELU was added to the column. The high nucleic acid affinity of the column was lost at slightly alkaline pH and that allowed the column bound DNA to flow through, which was then collected in a 15 mL centrifuge tubes. About 3.5 mL of isopropanol at RT was added to the DNA containing elution solution to precipitate the plasmid DNA, which was then spun down at 4000 rpm for 30 minutes at 4° C. Plasmid DNA pellet was washed with 2 mL of 70% ethanol, air dried and dissolved in 200 μL of nuclease free water or TE buffer. The highly concentrated plasmid preparation was further diluted ten times and run on agarose gels for visual quantifications.

3.4.4 Preparation of recombinant retroviral vectors

Platinum-A (Plat-A) cell line was used to produce lentiviruses that can deliver the Yamanaka factors into host cells. Plat-A cells are modified HEK-293T cells containing packaging constructs (gag, pol and amphoteric env) that are used for packaging potent amphotropic retroviruses that can tranduce both human and rodent cells efficiently. Alternately, HEK

cells were co-transfected with helper plasmids: pCMV-VSV-G (coding for the pantropic envelope protein VSV-G) and pDR8.2-GPRT (coding for gag and pol). These helper constructs were co-transfected along with the retroviral construct carrying the Yamanaka genes (or other retroviral constructs mentioned in **section 3.12.1**). The "gag" codes for a group of proteins that form the viral core structure. The "pol" codes for reverse transcriptase and integrase and forms a nucleoprotein complex. The VSV-G envelope protein renders pantropism and allows for receptor independent viral uptake and transduction of a wide range of cell types across species. Since the helper plasmids do not have a packaging signal (PsiΨ), their mRNA will not be packed within the viral genome. However, the RNA transcribed from the retroviral transgene construct (containing Ψ) will be packed into the viral core, resulting in recombinant retroviral particles that are infectious, but are replication incompetent.

The retroviral constructs and the helper plasmids were lipofected into HEK or PLAT-A cells using Lipofectamine 3000 as per the manufacturer's instructions. Briefly, 2.5 x 10^5 cells were seeded in each well of a six-well plate and allowed to adhere to the surface. The contents of tube A and B in **Table 3.7** were mixed together and incubated for 30 minutes at RT. The incubated transfection mix was added onto 60-70% confluent packaging cells and distributed evenly. After 24 hours, the cells were treated with 1 mM sodium butyrate to boost viral particle production and packaging. 12 hours after sodium butyrate treatment, the spent media was removed and fresh medium was added and incubated for further 12 hrs. The spent medium containing the released retroviral particles were collected at 48 hrs after transduction in a BSL-II hood, by following appropriate bio-safety precautions. The viral supernatant was filtered using 0.45 μm filters to remove larger cell debris and the cleared solution supernatant was made into 0.5 mL aliquots in sterile, well labeled cryovials, snap frozen with liquid nitrogen and stored at -80° C. Fresh media was added to the packaging cells and a second and third collection of virus was done for up to 72 hrs post transfection, at 12 hrs intervals and the stock aliquots were prepared and stored at -80° C, as explained above.

Table 3.7 Transfection reaction mix

Tube A	
Basal medium	100 µL
Purified plasmid DNA of interest	1 µg
pCMV-VSV-G	250 ng
pDR8.2-GPRT	750 ng
p3000 transfection reagent	2 µL

Tube B	
Basal medium	100 µL
Lipofectamine 3000	3 µL

3.5 Generation of induced pluripotent stem cells (iPSCs) from human dermal fibroblasts (HDFs)

About $1X10^5$ fibroblast cells were seeded and cultured in 6-well plates at least one day prior to transduction experiments or until the cells were 60-70% confluent. The spent media was removed and fresh FGM was added and a cocktail of *OCT4*, *SOX2*, *cMYC* and *KLF4* expressing lentiviral supernatants was added to the cells along with 10 µg/mL polybrene, to promote better transduction efficiencies. To reduce cytotoxicity, care was taken that the volume of viral supernatant does not exceed 50% of the total culture volume. The plates were then kept at 37° C with 5% CO_2 supply. The FGM was replaced with **mTeSR™1-hiPSC maintenance medium (mTeSR)** the next day. Media was changed every alternate day until the ESC-like colonies were observed at about 3-4 weeks post transduction. The reprogramming patches were allowed to develop further and well grown, ESC-like colonies with clear margins were manually picked and cut into small pieces using a flame-pulled glass Pasteur pipette under a stereo microscope placed inside the BSL-II hood. The pieces of colonies were then collected in a 15 mL tube with 2 mL mTeSR and triturated gently to get smaller clumps of 3-4 cells and plated onto a fresh Matrigel coated-well (**section 3.3.2**) of a 6-well plate. Each of the clones were individually passaged by manual picking and colony cutting, for about 4-5 passages or until they reached stable expansion.

3.5.1. Passaging of stable iPSC lines

Once the iPSC clones have become stable and crossed 4-5 passages, the clones were sub-cultured using **cell dissociation solution**, **CDS**. Briefly, the spent media from 80-90% confluent iPSC cultures were aspirated out and 1 mL of CDS was added to each well of the 6-well plate and kept at 37° C for 5-6 minutes. After incubation, the CDS was removed carefully and 1 mL of fresh mTeSR was added to the wells and gently triturated to lift the cells off the plate and the cell suspension collected in a 15 mL centrifuge tube. The cells were then spun at 1000 rpm for 4 minutes. The supernatant was discarded and the pellet was re-suspended in required volume of mTeSR and plated onto fresh 6-well plates or cryopreserved as in **section 3.3.5**. A standard split ratio of 1:6 or 1:10 were maintained for the routine passaging of stable iPSC lines. The stable iPSC lines were maintained in mTeSR.

3.6 Characterization of iPSCs

3.6.1 Genomic PCR to check transgene integration

Genomic DNA was isolated from the three iPSC lines and PCR was carried out to check for transgene integration using transgene specific primer sets listed in **Annexure V**. The amplicons were run on an AGE for further analysis.

3.6.2 Semi-quantitative RT-PCR to check for transgene and endogenous gene expression

3.6.2.1 RNA isolation

Total RNA was isolated from the iPS cells using TRIzol™. cDNA synthesis and further gene expression comparisons were done by semi-quantitative RT-PCR. Briefly, the iPS cells cultured in 6-well plates were washed once with ice cold 1X DPBS. The DPBS was aspirated and 1mL of TRIzol™ reagent was added per well, directly onto the cells, to lyse them for about 5 minutes. The lysed cells were then scraped using a cell scraper and the lysed solution was collected in a 1.5 mL centrifuge tubes and 0.2 mL of chloroform per 1 mL of TRIzol™ reagent was added, vortexed vigorously for 15 seconds and incubated at RT for 3 minutes. The tubes were then centrifuged at 12000 rpm for 15 minutes at 4° C. The mixture got separated into a phenol-chloroform phase at the bottom, a protein and chromatin containing thick interphase in the middle and an aqueous phase at the top. The aqueous phase of about 0.6 mL containing the RNA was carefully transferred to a fresh microfuge tube. About 0.5 mL of isopropyl alcohol was added to the aqueous phase in the fresh tube and incubated at RT for ten minutes to precipitate the RNA. Following the incubation, the RNA was pelleted

by centrifuging at 12000 rpm for 10 minutes at 4° C. A gel-like translucent RNA pellet appeared on the side walls, at the bottom of the microfuge tubes. The pellet was washed with 1 mL of 75% ethanol and air dried to let the ethanol evaporate and escape, while keeping the tubes on ice. Care was taken that the pellet was not completely dried and was re-suspended in nuclease free molecular grade water for further quantification and experimentations.

3.6.2.2 First strand complementary DNA synthesis- Reverse transcription reaction

The total RNA obtained above was then converted to complementary DNA using SuperScript™ III Reverse Transcriptase for further semi-quantitative gene expression analysis. The reaction mix shown in **Table 3.8** was prepared in a PCR tube and heated at 65° C for 5 minutes and incubated on ice for a minute.

Table 3.8: Reaction Mix 1 for first-strand cDNA synthesis

S. No.	Reagents	Concentration	Volume (µL)
1	Oligo $(dT)_{20}$	50 µM	1.0
2	Total RNA	10 pg – 5 µg	5.0
3	dNTP mix	10 mM	1.0
4	Nuclease free water	-	3.0
		Total volume	10.0

The tube was then briefly spun and the reaction mix 2 shown in **Table 3.9** was added sequentially, mixed gently, spun and incubated at 50° C for 30-60 minutes. The reaction was terminated by heat inactivating the reverse transcriptase at 70° C for 15 minutes. The cDNA thus obtained was used as templates for semi-quantitative PCR analysis to quantify the transcripts from different cells and tissues.

Care was taken to design exon spanning primers for semi-quantitative PCR mainly to distinguish the cDNA derived amplicons from that of the genomic DNA contaminants. A PCR reaction from a contaminated genomic DNA would result in a long PCR product size due to the presence of introns and would help in easy identification and quantification of gene expression products derived from cDNA templates. The primers used for semi-quantitative PCR are listed in **Annexure V**. The PCR reactions were similar to those described in **section 3.2.4** and the amplicons were analyzed using AGE, as described in **section 3.2.5.**

Table 3.9: Reaction Mix 2 for first-strand cDNA synthesis

S. No.	Reagents	Concentration	Volume (µL)
1	RT buffer	10X	2.0
2	DTT	0.1M	2.0
3	MgCl2	25 mM	4.0
4	RNase out	40U/µL	1.0
5	Reverse transcriptase	200U/ µL	1.0
		Total volume	10.0

3.6.3 Immunostaining and fluorescence imaging of cells

Immunofluorescence staining method was used to confirm the presence of pluripotency and lineage-specific markers in iPSCs and in iPSC-derived ocular cells. $2x10^5$ iPS cells were counted and seeded onto Matrigel coated cover slips placed inside the wells of 12-well plates. Once the cells adhered and formed colonies covering 50% of the cover slip, the cover slips with iPSCs (or iPSC derived ocular cells) were washed thrice with 1X PBS (this wash step was carried out between every subsequent steps), fixed in 4% formaldehyde and permeabilized using 0.5% Triton™ X-100 for ten minutes. The cells were then blocked with either 2.5% BSA or 10% FBS (blocking solution) for 30-45 minutes. Required primary antibodies (listed in **Annexure VI**) were diluted in the blocking solution, as per the manufacturer's instruction and added just onto the cover slips kept inside a moist chamber and were incubated at 4° C overnight. The next day the coverslips were washed thrice with 1X PBS and then a suitable secondary antibody with a fluorescent tag or a biotin label (listed in **Annexure VI**) was added and incubated for further 45 minutes at room temperature. For samples labeled with secondary antibodies with a biotin conjugate, an additional incubation step with streptavidin (conjugated with fluorescent tags) was considered for 45 minutes. After final washing, the samples were counter stained using either DAPI (in blue) or PI (in red) to mark all the cell nuclei based on suitable color choices and the coverslips were mounted onto a glass slide using 90% glycerol and 10% PBS containing mountant. The slides were then imaged using either an upright fluorescent microscope (Olympus IX71, Japan) or a confocal microscope (Zeiss LSM 880, Germany).

3.6.4 Karyotyping

iPS cells at passage 8 and 20 were subjected to karyotyping analysis to check the chromosomal stability of the reprogrammed cells. When the cells became 70-80% confluent, they were treated with colcemid (0.1 μg/mL) for 2-3 hours to arrest the cells at metaphase stage. The cells were then washed with 1X DPBS and trypsinized to prepare a single-cell suspension. The cell suspension was then treated with a hypotonic solution, fixed and then carefully dropped onto a clean glass slide for the cells to burst and to spread the chromosomes evenly on the glass slide. After a brief trypsin treatment, the slide was air dried and stained with Giemsa stain and analyzed using CytoVision automated (Leica Biosystems, Germany).

3.6.5 Embryoid body formation assay

When the iPS cells were 60-70% confluent, they were passaged and grown as suspension cultures on non-adherent dishes containing **embryoid body formation medium, EBM/differentiation medium, DM**. After 2 weeks, the spherical embryoid bodies (EBs) that grew in suspension culture were plated on to Matrigel™ coated dishes. The EBs, attached to the dishes and a wave of randomly differentiating heterogeneous populations of cells migrated out of the EBs making the cultures confluent within a week. Total RNA isolated from this mixture of cells were subjected to semi-quantitative RT-PCR analysis, as described in **section 3.6.2**, using primer sets specific for ectoderm, mesoderm and endoderm specific genes (listed in **Annexure V**).

3.6.6 Teratoma assay

The growing cultures of stably reprogrammed iPSCs at passage 25 were taken and treated with CDS to make single cell suspension, as explained in **section 3.5.1**. The cells were counted using a hemocytometer and about 10 million cells were suspended in 1 mL of DMEM/F12 containing 20 % Matrigel™ and kept on ice. 200 μL of the above cell suspension containing about 2 million cells was aspirated into 1 mL syringes fitted with a 26G needle and injected under the skin (in the subcutaneous region of the rear right haunch) of 6 weeks old nude mice (n=8). The mice that developed teratoma at around 6-8 weeks after injection were sacrificed and the teratomas obtained from three different iPSC lines were subjected to histopathological analysis and H&E staining to check for the presence of cell types of all three lineages (ectoderm, mesoderm and endoderm).

3.6.7 Histopathological analysis of tissues and Immunohistochemistry

Paraffin embedded sections (5 μm thickness) were taken on to positive charged silane-coated microscopic slides using a microtome. Tissue sections were deparaffinized by heating the slides at 70° C on a heat block, followed by treating the slides with xylene for 3 minutes for the complete removal of paraffin. After that, the sections on the slides were hydrated sequentially with different percentages of ethanol, with 3 minutes incubation at each step (100 % Ethanol, 95 % Ethanol, 80 % Ethanol) followed by a distilled water wash. The slides were further processed as described in **section 3.6.7.1** for hematoxylin and eosin (H&E) staining or as in **section 3.6.7.2** for immunohistochemistry.

3.6.7.1. H&E staining

After deparaffinization and hydration, the tissue sections were incubated in **hematoxylin staining solution** for 2-5 minutes. After washing in running tap water, the slides were dipped in **hydrochloric acid (1%) - ethanol solution** to remove the nonspecific staining. The slides were then washed thoroughly in running tap water. Tissue slides were then counterstained in **eosin staining solution** for 2 minutes. The tissue sections were dehydrated and cleared through 2 changes each of 95%, 100% ethanol and xylene for 5 minutes each. Slides were then dried and mounted with DPX mountant and observed under a light microscope.

3.6.7.2. Immunohistochemistry

Prior to antigen retrieval, the Coplin jars containing the **sodium citrate buffer** (pH 6.0) was preheated until it reached 95-100° C. Slides were immersed in preheated Coplin jar and heated in a microwave oven at medium heat for 15 minutes for antigen retrieval, after which the Coplin jar was removed from the microwave oven and allowed to cool down to RT. Tissue sections were then treated with 1:1 ratio of methanol and hydrogen peroxide (H_2O_2) to block the endogenous peroxidases. Sections were washed with 1X PBS followed by permeabilization with 0.5% Triton™ X-100 for 15 minutes. To block nonspecific binding of the primary antibody, tissue slides were incubated with blocking buffer (10% FBS or 2.5% BSA) for an hour. Sections were then incubated with the required primary antibodies **(Annexure VI)** diluted in the blocking buffer for an hour at RT or overnight at 4° C, followed by three PBS washes, for 5 minutes each. Tissue sections were then incubated with appropriate secondary antibodies **(Annexure VI)** for 45 minutes at RT and thoroughly washed for 3 times. For DAB staining, the appropriate secondary body from the kit (EnVision™ FLEX Mini Kit) was used followed by addition of the chromogenic substrate

DAB, 3-3- diamidino benzidine and incubating for approximately 5-8 minutes. The sections were washed with tap water for 1 minute and counter staining was done for the nucleus using DAPI/PI/hematoxylin and mounting was done using a resinous DPX mountant or using 90% glycerol containing 10% PBS. Further, the slides were imaged using a confocal microscope (Zeiss, Germany) or an upright fluorescence microscope (Zeiss, Germany).

3.7. Differentiation of human iPSCs into ocular lineages

Differentiation towards ocular lineage was initiated by detaching the hiPSC lines from adherent cultures and culturing them in suspension on non-adherent dishes containing **differentiation medium, DM**. The EBs obtained after 1-2 weeks were plated onto a Matrigel™ coated dishes containing **neural induction medium, NIM**. After a week, NIM was replaced with **retinal differentiation medium, RDM** in which the cultures were grown for 3 more weeks to obtain eye field clusters. Alternately, near confluent hiPSC cultures were directly transferred to NIM to induce neural induction and then to RDM for eye field induction.

3.8 Establishment of monolayer cultures of RPE and neuro-retinal cells

The well characterized human embryonic stem cell line, BJNhem20 that was maintained in the same method as iPSCs (**section 3.5.1)**, was differentiated towards ocular lineage as in **section 3.7**. The eye field clusters obtained were allowed to mature in RDM for another month to form neuro-retinal (NR) islands surrounded by pigmented RPE cells. The NR islands were manually scooped out using a flame-pulled glass Pasteur pipette and were plated onto Matrigel™ coated dishes or cover slips containing **neuro-retinal medium, NRM**, and grown as adherent cultures to obtain enriched neuro-retinal (NR) cells. Similarly, the pigmented RPE cells surrounding the NR islands were manually picked using a flame-pulled glass Pasteur pipette and plated onto Matrigel™ coated dishes or trans-well plates containing **RPE maturation medium, RPEM**, and grown as adherent cultures to obtain enriched RPE cells. To check the polarity, the RPE cells were also grown over 1.9 mg/mL of rat tail collagen-I matrix. The NR cells grown on cover slips and the RPE cells grown on trans-wells were fixed and processed for immunocytochemistry, as described in **section 3.6.3**. Total RNA was isolated and RT-PCR profiling was done, as described in **section 3.6.2**. Histological sections of the RPE cells cultured on collagen-I matrix were obtained and processed as described in **section 3.6.7** for H&E staining. The phagocytic ability of the RPE cells was tested by phagocytosis assay as described in **section 3.8.1**. The spent media

obtained from enriched and mature RPE cultures were subjected to ELISA analysis, to check the presence of secreted growth factors: vascular endothelial growth factor (VEGF) and pigment epithelium derived factor (PEDF), as described in **section 3.8.2**.

3.8.1. Phagocytosis assay

RPE cells were cultured on glass chamber slides coated with Matrigel™; and FITC labeled green fluorescent latex beads of 1 μm diameter were added on to the cells at a concentration of $1x10^6$ beads/mL. The RPE cells with the beads were incubated at 37° C for 6 hours after which the cells were washed thoroughly with 1X PBS five times to get rid of free-floating and non-internalized beads. The cells were then processed for ICC and ZO-1 staining, as described in **section 3.6.3** and were imaged using a confocal microscope.

3.8.2. Enzyme linked immunosorbent assay (ELISA)

ELISA assay for secreted VEGF and PEDF was performed using Human VEGF DuoSet ELISA kit and Human PEDF DuoSet ELISA kit as per the manufacturer's instructions. All steps in ELISA were performed at RT, and each step was followed by three PBS wash. Initially, capture antibodies (α-VEGF, α-PEDF) were diluted to working concentrations in 1X PBS and 100 μL of it was added onto 96-well microplate and incubated overnight. The plates were blocked with 300 μL of Reagent Diluent provided in the kit and incubated for an hour. A set of VEGF/PEDF standards (as per manufacturer's instructions) in 100 μL diluent and 100 μL of samples (spent media) from hESC-RPE were added in triplicates and incubated for 2 hours. The same was done for the spent media from ARPE19 and HEK cells. After 2 hours, 100 μL of diluted detection antibody was added and incubated for 2 hours, followed by the addition of 100 μL of streptavidin-HRP conjugate and were incubated for 20 minutes. The substrate solution (100 μL) was added to each well of the microplate and incubated for further 20 minutes. The reaction was arrested using the stop solution provided in the kit and the absorbance at 450 nm was measured using a ELISA microplate reader (Bio-Rad, USA).

3.9. Establishment of three-dimensional cultures and miniature organoids

In order to obtain three dimensional cultures of ocular tissues, hiPSC-F2-3F was subjected to neuro-ectodermal commitment and early eye-field differentiation to form eye field clusters as described in **section 3.7**. These eye field clusters gave rise to retinal and corneal organoids upon culturing them in different suspension culture conditions as described below.

3.9.1. Generating floating corneal organoids

About 40% of the eye field clusters in suspension also gave rise to transparent corneal primordia along with the retinal primordia. The delicate, transparent and fluid filled corneal primordia was dissected and cultured in suspension on non-adherent culture dishes containing **corneal differentiation medium, CDM**. After 4 weeks in CDM, the corneal primordia matured into compact and well-organized corneal organoids. The corneal organoids were subjected to IHC analysis, as explained in **section 3.6.7.**

3.9.1.1. Generating transplantable sheets of corneal epithelium from human iPSC derived corneal organoids

The processed human amniotic membrane (hAM) was obtained from our in-house eye bank (RIEB) and de-epithelialized using **Trypsin-EDTA solution** and washed three times to remove the enzymes and the denuded epithelial cells thoroughly. Corneal organoids at 10 weeks of development were chopped into fine pieces and cultured as explants on the denuded hAM matrix in **human corneal epithelial medium, HCEM**, similar to that of human limbal epithelial cultures described elsewhere (Mariappan *et al.* 2010). The uniform sheets of corneal epithelium obtained after 2 weeks of explant culture was processed for IHC analysis, as explained in **section 3.7.**

3.9.2. Generating miniature eye-like structures and adherent corneal organoids

When the eye field clusters were allowed to mature in adherent culture for 4 months in NRM, rare EFP developed into miniature eye-like structures with transparent cornea on the surface, neuro-retinal tissue on the posterior side and pigmented neural crest cells at the corneal margin. These corneal organoids were dissected out and subjected to IHC analysis, as explained in **section 3.6.7.**

3.9.3. Generating optic cups and retinal organoids

The distinct, oval eye field clusters were manually scooped and cultured in suspension on non-adherent dishes containing NRM. After 1 week of suspension culture in NRM, the NR islands developed into single or symmetrically arranged double optic vesicle-like structures on either side of the eye field cluster in suspension. The retinal primordia were dissected out and grown in suspension to develop into optic cup-like structures. The optic cups when cultured in NRM for further 4 weeks, matured into well-organized retinal organoids. The optic cups and the retinal organoids were subjected to IHC analysis and RT-PCR profiling as explained in **sections 3.6.7** and **3.6.2** respectively.

3.10. Characterization of patient-specific iPSCs with mutation in *ABCA4*

The hiPSC-F2-RPE and hiPSC-KR-RPE cells on trans-wells were subjected to ICC and RT-PCR profiling as in **sections 3.6.3** and **3.6.2** respectively. The hiPSC-F2-RPE cells and hiPSC-KR-RPE cells were also characterized by scanning electron microscopy (SEM), transmission electron microscopy (TEM) and electrophysiological studies.

3.10.1. Electron microscopy

The hiPSC-F2-RPE and hiPSC-KR-RPE cells on trans-well inserts were fixed in 0.1 M sodium cacodylate buffer containing 2.5% paraformaldehyde and 2.5% glutaraldehyde for 2 hours at RT. After fixation, the culture inserts were washed for 5 minutes thrice with 1X PBS. The cells on the inserts were then coated with 1% ice-cold osmium tetroxide (in 1X PBS) for an hour. After osmication, the inserts were rinsed with 1X PBS and subjected to dehydration by a series of increasing concentrations of ethanol dips (50%, 70%, 85% and 100% ethanol). For TEM analysis, plastic embedding was done and routine TEM protocol was used to obtain the RPE cross-section micrographs. For SEM analysis the dehydrated culture inserts were dried using a 'critical point dryer' to avoid surface tension artifacts. The culture inserts were then coated with a very thin film of gold using a sputter coater and routine SEM protocol was used to obtain the RPE apical surface micrographs.

3.10.2. Electrophysiology

Confluent monolayers of hiPSC-F2-RPE and hiPSC-KR-RPE grown on trans-well membranes were carefully removed from the trans-wells and were mounted onto Ussing chambers containing an apical bath and a basal bath of **Ringer's solution**. Electrical networks to the apical and basal chambers were provided by Ringer-agar bridges in series with calomel electrodes that measured the trans-epithelial potential (TEP) in mV. Pulses of bipolar current ranging from 2-8 μA were passed through the RPE cell sheets on the membrane and the ability of the cell sheets to resist the flow of current through them was measured as resistance ($\Omega.cm^2$). To achieve decreased concentration of K^+ ions in the apical bath, the KCl in Ringer's solution of the apical bath was replaced with equimolar amounts of NaCl. To induce ATP mediated response, 100 μM ATP was added to the Ringer's solution in the apical bath.

3.11. Characterization of patient-specific iPSCs with mutation in *RD3*

The hiPSC-F2-OCs and hiPSC-VS-OCs were subjected to IHC and RT-PCR profiling as in **sections 3.6.7** and **3.6.2** respectively, for characterizations and comparative studies.

Similarly, the hiPSC-F2-RPE cells and hiPSC-VS-RPE cells were subjected to ICC, RT-PCR profiling and phagocytosis assay as explained in **sections 3.6.3, 3.6.2** and **3.8.1** respectively.

3.12. Characterization of human *RD3* promoter for the construction of retina-specific gene expression cassette

3.12.1. Cloning

Genomic regions upstream to human *RD3* was obtained from NCBI nucleotide database. The promoter region of two different lengths, a full length *RD3* promoter (*RD3PFL* up to -2054 bp upstream to the *RD3* transcription start site) and a minimal *RD3* promoter (*RD3PM* up to -400 bp upstream to the *RD3* transcription start site) were analyzed for potential retina specific transcription factor binding sites using the Genomatix-Matinspector software. The *RD3PFL* and *RD3PM* regions were PCR amplified using the primers listed in **Annexure V** and cloned into pMOS-Blue blunt cloning vector to obtain pMOS-*RD3PFL* and pMOS-*RD3PM*. The *RD3PFL* and *RD3PM* fragments from pMOS vector were then mobilized into pGL3 basic vector, by restriction digestion and cloning, to obtain pGL3_*RD3PFL*/*luc* and pGL3-*RD3PM*/*luc* (the constructs used in luciferase reporter assays).

The internal ribosomal entry site and enhanced green fluorescent protein (*IRES-EGFP*) regions were obtained by restriction digestion from pIRES2-*EGFP* vector and were cloned downstream to the *CMV* promoter of pLNCX2 vector to obtain pLNCX2-*CMV*/*IRES-EGFP* lentiviral vector. The *RD3PM* fragment obtained from pMOS-*RD3PM* was mobilized into pLNCX2-*CMV*/*IRES-EGFP* vector replacing the constitutive *CMV* promoter to obtain pLNCX2-*RD3PM*/*IRES-EGFP* vector. These constructs were used to prepare retroviral vectors (**section 3.4.4**) that were tested in HEK and Y79 cells and in cadaveric retinal explant cultures.

In order to obtain a complete, tissue-specific *RD3* expression cassette, the human *RD3* was PCR amplified using the primers listed in **Annexure V** and cloned into pMOS-Blue vector. The *RD3* encoding region was then mobilized into pLNCX2-*RD3PM*/*IRES-EGFP* vector, downstream to *RD3PM*, to obtain pLNCX2-*RD3PM*/*RD3-IRES-EGFP* lentiviral vector containing a complete *RD3* expression cassette.

3.12.2. Luciferase reporter assay

The luciferase reporter constructs containing *RD3* minimal promoter (pGL3-*RD3PM*/*luc*) and full-length promoter (pGL3-*RD3PFL*/*luc*) were transfected into the non-ocular cell line, HEK 293T and also the ocular cell lines such as: HCE, ARPE19 and Y79, using

Lipofectamine 3000 Transfection Reagent. The transfected cells were also treated with 1 mM sodium butyrate for 12 hours to test the effect of HDAC inhibition on promoter activities. After 48 hours, cell lysates were collected and luciferin substrate was added to the cell lysates. The promoter activity was assayed as a proportion of the amount of luciferase enzyme expressed and in turn the amount of light emitted that was measured using a GloMax® 20/20 Luminometer (Promega, USA). Relative fold change values were calculated after normalizing the individual promoter activities over the basal values of the promoter less pGL3-Basic vector.

3.13. Zebrafish maintenance

As Zebrafish is a fresh water animal, it was maintained in UV treated, reverse osmosis (RO) water containing 0.3 g/L of sodium chloride (fish water) to mimic fresh water conditions and 0.0002% methylene blue as an anti-fungal agent. The fishes were maintained under strict day and night cycles of 14 hrs of light and 10 hrs of dark, using an automated timer-controlled lighting system.

3.13.1. Breeding

Zebrafish display a photoperiodic behavior. Hence, they have the tendency to mate in the early morning during the dawn. On the night prior to the day of breeding, the males and females were separated and kept in isolated tanks. The next morning, when the lights were on (mimicking dawn) the males and the females were mixed in 2:3 ratios respectively in breeding tanks, to initiate the breeding process. Due to photo-induction, both the males and females release their gametes (the sperm and the egg) in water and the fertilization happens externally. The net in the breeding tank allowed the dropping eggs to pass through, while blocking the adult fishes. This is important to prevent the adult mating fishes from feeding on their own progenies.

3.13.2. Egg collection

After one hour, the breeder fishes were transferred to their respective maintenance tanks and the eggs were collected using a sieve, rinsed gently to get rid of the food and fecal matter at the bottom and placed in a 100 mm petri dish containing fish water. If the breeding was done for the purpose of microinjection, then the eggs were transferred to an agarose mold and arranged in neat rows. If the embryos were collected for the routine fish maintenance cultures, then the petri plates with the eggs were kept inside a cooling incubator (Naanolab India) set at 28.5° C for 4 days or until the larvae hatched out of the chorion.

3.13.3. Larvae maintenance

Once the swim bladder developed in the larvae (usually takes about 5-6 days post fertilization, dpf), the larvae were transferred to 2-liter trays where they could swim around freely. The larvae were then fed with PL150 in the morning and evening and the live brine shrimp larvae, *Artemia naupli* (Artemia) once during the day. Extreme care was taken for the first 15 days post fertilization. As a part of regular maintenance, excess feed floating on the top were blotted out using a paper towel. The feed and fecal waste that accumulate at the

bottom of the tanks were suctioned out using a 10 mL pipette fitted with a rubber pressure bulb. The tank water was changed whenever it became turbid (usually once in every 4 days).

3.13.4. Juvenile maintenance

One-month post fertilization, the larvae had developed into juveniles and were transferred to juvenile tanks of 5-liter capacity. The juveniles were fed with live Artemia twice a day (morning and evening) and PL150 in the afternoon. PL500 was introduced now and then, so that the juveniles get habituated to feeds bigger than PL150. Tank scrubbing and water change was done twice a week.

3.13.5. Adults maintenance

After 3 months, the juveniles had developed into fully mature and sexually active adults and were transferred to the adult fish tanks of 10-liter capacity. At this point, the males and females were easily distinguishable. The males were long and slender with silver and gold lines on their body and yellow pigmentation in the anal fins. The females had enlarged bellies due to the presence of egg pouch with hundreds of eggs. The females had silver and blue lines on their body. The adults were fed with live Artemia twice a day (morning and evening) and PL500 in the afternoon. The adults between the ages of 6-12 months were used for all breeding experiments.

3.14. Generation of mutant disease models in Zebrafish

3.14.1. CRISPR guide RNA designing

The guides targeting the gene of our interest were designed using UCSC genome browser, track hub-Burgess lab zebrafish genomics resources. The CRISPR guides were designed to target the genomic regions adjacent to the translation start site at exon 2 of the zebrafish *rd3* gene. Two CRISPR guides with maximum efficiency and no off targets were selected and the following oligos were synthesized:

The sequence identities are color coded as mentioned below.

T7 promoter, target gRNA sequence, overlapping crRNA-tracrRNA sequence

ZF *RD3* oligoA1:

5'-TAATACGACTCACTATAGGCAGCATGTCGTGGTTCAGCGTTTTAGAGCTAGAAATAGC-3'

ZF *RD3* oligoA2:

5'-TAATACGACTCACTATAGGCTGAGCTGGCAAATAAAAGGTTTTAGAGCTAGAAATAGC-3'

Generic oligoB containing remaining tracrRNA sequence:

5'-AAAACCACCGACTCGGTGCCACTTTTTCAAGTTGATAACGGACTAGCCTTATTTTAACTTGCTATTTCTAGCTCTAAAAC-3'

3.14.2. Oligo annealing and extension to generate dsDNA templates

The reaction mix listed in **Table 3.10** was assembled in a PCR tube and the tubes were kept in a thermal cycler with the conditions mentioned in **Table 3.11** for annealing and extension of the single stranded oligos to form double stranded, DNA oligo templates for sgRNA1 and sgRNA2.

Table 3.10: Oligo annealing reaction mix

S. No.	Reagents	Concentration	Volume (µL)
1	Phusion Buffer	5X	5.0
2	dNTP	10 mM	0.5
3	Oligo1	10 µM	1.0
4	Oligo2	10 µM	1.0
5	Phusion Polymerase	2 U/µL	0.5
6	Water (RNAse free)		17.0
		Total volume	**25.0**

Table 3.11: Thermal cycler conditions for oligo extension

S. No.	Conditions	Temperature (°C)	Duration (minutes)
1	Denaturation	98	2
2	Annealing	50	10
3	Extension	72	10

3.14.3. gRNA preparation by in vitro transcription and purification

The sgRNAs 1 and 2 were synthesized by *in vitro* transcription (IVT) using MAXIscript™ T7 Transcription Kit as per the manufacturer's guidelines. Briefly the reaction mix in **Table 3.12** was assembled in a PCR tube and kept at 37° C for an hour. The reaction was arrested by adding 1 µL of 0.5 M EDTA and the remnant oligo DNA template was removed from the reaction mix by TURBO DNase (1 µL) treatment at 37° C for 15 minutes.

Table 3.12: IVT reaction mix

S. No.	Reagents	Concentration	Volume (µL)
1	Transcription buffer	10 X	2.0
2	ATP	10 mM	1.0
3	CTP	10 mM	1.0
4	GTP	10 mM	1.0
5	UTP	10 mM	1.0
6	Enzyme mix		2.0
7	Annealed oligo template		5.0
8	Nuclease free water		7.0
		Total volume	**20.0**

In order to purify the synthesized sgRNA transcripts, the reaction mix post IVT was made up to 50 µL with nuclease free water. 5M ammonium acetate (5 µL) was added to the reaction mix, vortexed and 3 volumes of 100% ethanol was added and kept at -20° C for 30 minutes or longer, for the precipitation of the sgRNAs. The precipitated sgRNAs were pelleted by centrifuging at 14000 rpm at 4° C for 30 minutes. The RNA pellets were then washed with 70% ice-cold ethanol, air dried and dissolved in 20 µL of nuclease free water. The quality of the synthesized guide oligos was checked by running it on a 2.5% agarose gel and the concentration was determined using NanoVue™ as discussed in **section 3.2.3**. The synthesized and purified sgRNAs 1 and 2 were aliquoted (5 µl into each vial) and stored at -80° C until further use.

3.14.4. In vitro cleavage assay

The ability of the sgRNAs 1 and 2 to create double strand break at the targeted genomic locus was tested by *in vitro* cleavage assay. For this, the sgRNA:Cas9 protein:DNA substrates were taken in 10:10:1 molar ratios. The sgRNA and Cas9 protein were incubated at 25° C for 10 minutes along with 1X ***in vitro* cleavage assay buffer** for the formation of a ribonucleoprotein (RNP) complex. The PCR amplified target DNA substrate was then added to this RNP complex and the reaction mixture was incubated at 37° C for 1 hour. The cleaved products were then analyzed on 2% agarose gels.

3.14.5. Microinjection

Freshly laid zebrafish embryos were collected and the RNP mix (containing sgRNA (15-20 ng) and Cas9 protein (300 ng)) along with 0.05% phenol red (for visual tracking) was injected into the yolk sac or the animal pole region of embryos, at the single cell stage. After 24 hours of microinjection, the dead and unfertilized eggs were removed and the live embryos were maintained as described in **section 3.13.3** for further experiments.

3.14.6. T7 endonuclease assay

The presence of in-dels in the injected batch of embryos was confirmed by T7 endonuclease assay. Briefly, genomic DNA was isolated from the embryos and their *rd3*-exon2 region was amplified by region specific primers **(Annexure V)**. The *rd3*-exon2 amplicons from each of the embryos were mixed with the *rd3*-exon2 amplicon of uninjected/wildtype zebrafish embryo. This mixture was denatured at 95° C for 5 minutes and allowed to renature by cooling down gradually to RT. About 200 ng of DNA from the above reaction was incubated in a reaction mix (20 µl) containing 0.5 µl of T7 endonuclease (10U/µl) and 1X NEB Buffer 2.1 at 37° C for 3 hours. The reaction mix was then run on a 2% agarose gel to check for the presence of in-dels and successful DNA template cleavage.

3.14.7. Genomic screening of F_0 fishes to identify mosaic founders

The RNP2 microinjected embryos that showed the presence of in-dels by T7 endonuclease assay was allowed to mature for a month to attain the juvenile stage. Upon maturation, the tail clips (obtained by anesthetizing the juveniles using 0.02% tricaine) were used for genomic DNA isolation. Briefly, the tail clips were lysed using a 100 µL of **lysis buffer** and 10 µL of 20 mg/mL proteinase K was added to the lysate and incubated at 56° C overnight. Later, 10 µL of 5M NaCl was added to the proteinase K-treated lysate and an equal volume of isopropanol was added. The contents of the tubes were properly mixed by gentle inversion and were incubated at 4° C for 10 minutes and then centrifuged at 12000 rpm for 15 minutes. The DNA pellet thus obtained, was washed with 70% ethanol, air dried, dissolved in TE-RNase and incubated overnight at RT. The obtained genomic DNA was run on 1% agarose gel to check for the quality and quantity. The *rd3*-exon2 region (sgRNA2's target site) was then PCR amplified and checked on AGE. The PCR amplicons were sequenced to check and identify the F_0 founders. The type of in-dels generated in F_0 founders was also identified by cloning the *rd3*-exon2 amplicon into pMOS-Blue vector and sequence confirmed using the M13 forward and T7 reverse primers (**Annexure V**).

3.14.8. Generation of homozygous recessive mutants in F_2 generation

The F_0 founder identified to carry gene disruptive in-dels was allowed to mature to adult stage. Once the F_0 founder matured into a sexually active adult, it was back crossed with *wt* animals to obtain F_1 heterozygotes. The F_1 progenies were genotyped as explained in **section 3.14.7**, in order to confirm the germ line transmissibility of the mutant allele and also to identify heterozygous mutants. The confirmed F_1 heterozygotes ($rd3^{+/-}$) were then interbred with each other and the progenies were genotyped as in **section 3.14.7**, to obtain 25% of *rd3* homozygous recessive mutants ($rd3^{-/-}$). The ($rd3^{+/+}$), ($rd3^{+/-}$) and ($rd3^{-/-}$) fishes at different stages of their development were fixed in 4% formaldehyde and their heads were subjected to IHC analysis, as described in **section 3.6.7** involving H & E staining and cone-arrestin antibody staining.

CHAPTER 4

RESULTS

4. Results

4.1. Generation of RP patient-specific iPSCs as *in vitro* disease models

Induced pluripotent stem cells are somatic cell-derived and their genomes are near identical to that of the parental cells. Therefore, patient-specific iPSCs can serve as useful *in vitro,* developmental disease models to understand the physiology of diverse genetic disorders. Long-term genetic studies on hundreds of retinal dystrophic patients treated at our clinic have identified many novel and reported mutations in several genes linked to autosomal recessive retinitis pigmentosa (ARRP), Leber congenital amaurosis (LCA) and age-related macular degeneration (AMD) (Biswas *et al.* 2016; Falk *et al.* 2012; Friedman *et al.* 2006; Kannabiran, H.P. Singh, *et al.* 2012a; Kannabiran, Palavalli, *et al.* 2012; Kannabiran, H. P. Singh, *et al.* 2012b; Lalitha *et al.* 2002; Singh *et al.* 2006, 2009). Based on the above information, this study was planned to generate patient-specific iPSCs to evaluate them as *in vitro* disease models. Such patient-specific iPSCs can serve as valuable tools to establish the proof-of-concept of mutation correction, either by whole gene delivery or by *in situ* gene sediting. To understand the effect of *RD3* and *ABCA4* mutations in retinal development, function and maintenance, this study has generated and characterized patient-specific iPSCs as described below.

4.1.1. Ethical approvals

All experiments with human samples were conducted according to the tenets of the declaration of Helsinki and were approved by the Institutional Review Board of LV Prasad Eye Institute and the human Ethics Committee (IRB & EC) and also by the Institutional Committee for Stem Cell Research (IC-SCR). All animal experiments were carried out at the National Center for Laboratory Animal Sciences (NCLAS), National Institute of Nutrition (NIN) in accordance to the animal ethics guidelines and with the approval of the Animal Ethics Committee (AEC).

4.1.2. Identification and recruitment of patients

Earlier, genetic studies by Dr. Kannabiran's group have identified probands carrying specific pathogenic mutations in genes associated with LCA12 and ARRD (Friedman *et al.* 2006; Singh *et al.* 2006). Using the patient record details, the families were contacted to explain the study purpose and the need for blood and skin biopsy samples. Informed consents were obtained from study volunteers prior to sample collection. A copy of the Informed Consent Form (ICF) executed is shown in **Annexure I**.

4.1.3. Collection of blood and skin biopsy samples

About 4 mL peripheral blood was collected by venipuncture in VACUETTE® tubes and processed for genomic DNA isolation and genotyping. Human dermal fibroblasts obtained from skin biopsies are an excellent source of somatic cells that can be successfully reprogrammed into iPSCs. HDFs are easy to expand and are amenable for cryopreservation and establishment of a bank of patient-specific somatic cells. A small skin biopsy of 2 mm size is adequate to establish good fibroblast cultures. Therefore, a full thickness punch biopsy was taken from the periorbital skin aseptically, under local anesthesia. At the end of the procedure, an antibiotic cream and bandage was applied and the wound did not require any stitch for closure. The open wound healed within 4-5 days without any infection or pain for the patient. The biopsied skin tissues were collected in vials containing **cDMEM with 20% FBS** and transferred to the cell culture lab for further processing. As a part of this study, three volunteers were recruited: a healthy control patient (from herein referred to as F2), an LCA12 proband with a reported mutation in *RD3* (hereinafter referred to as VS) (Friedman *et al.* 2006) and an ARRP proband with a reported mutation in *ABCA4* (hereinafter referred to as KR) (Singh *et al.* 2006).

4.1.3.1. Confirmation of patient-specific gene mutations

The blood samples were used to isolate genomic DNA and gene-specific PCR was carried out, as explained in the methods **section 3.2**. The PCR amplicons were Sanger sequenced to confirm the mutations reported in respective patients. The sequencing results confirmed that the LCA12 patient (VS) carried a c.296 + 1 G→A mutation in *RD3* (Friedman *et al.* 2006) and ARRD patient (KR) carried a c.6088C>T mutation in *ABCA4* (Singh *et al.* 2006), as reported earlier.

4.1.4. Culture and expansion of human dermal fibroblasts (HDFs)

The skin biopsies from all three individuals VS, KR and F2 were chopped into small pieces using a surgical blade and cultured in 6-well plates containing **fibroblast growth medium, FGM**. The minced tissue pieces adhered to the culture plate firmly during the first two days in culture and fibroblast cells were seen emerging out from day 3 (**Fig 4.1.A**). On day 10, the P0 culture reached 80-90% confluence and was passaged at 1:3 ratios. The P0 culture was a mix of both the fibroblasts and epithelium. In subsequent passages, the epithelial cells were lost, resulting in homogenous cultures with distinct spindle shaped cells and fibroblast cell

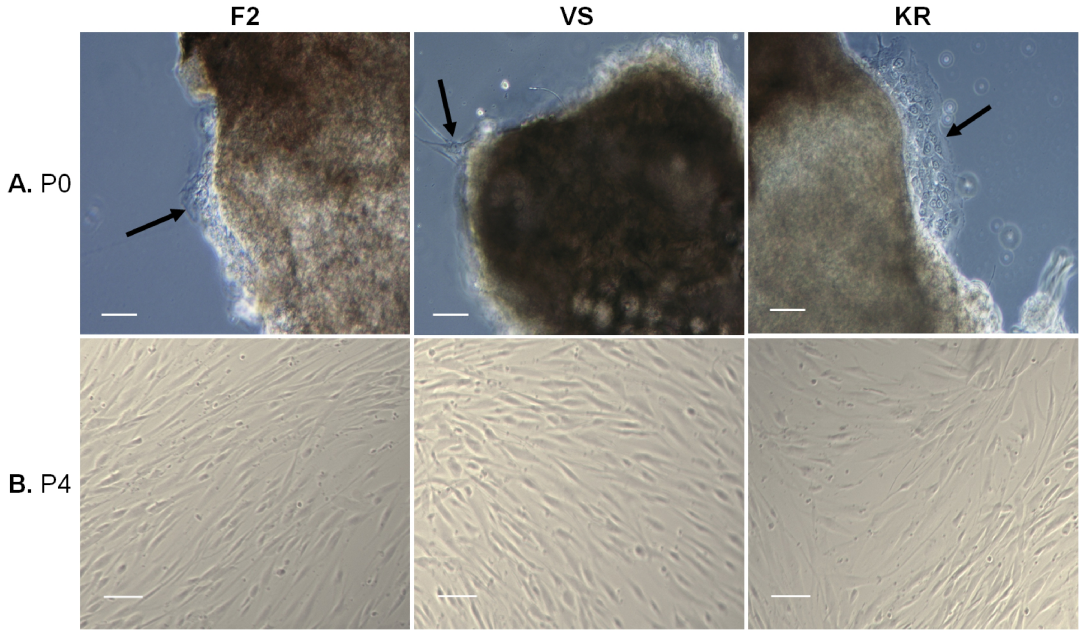

Figure 4.1: Patient-specific dermal fibroblast cultures. *Phase contrast images of explant cultures of skin biopsy of patient samples, F2, VS and KR.* ***A****. P0 cultures showing fibroblasts and epithelial cells emerging out of explants on day 3 (arrows).* ***B****. Homogenous human dermal fibroblast cultures at passage 4. Scale bar, 10 µm.*

morphology (**Fig 4.1.B**). The fibroblast cultures of all three patient donors were expanded until passage 10 and a batch of cells from each passage from P1 to P10 were cryopreserved.

4.1.5. Reprogramming of HDFs into iPSCs

A stem cell is considered to be pluripotent if it has the ability to generate cell types of all three lineages namely, the ectoderm, the mesoderm and the endoderm. In a developing embryo, the inner cell mass (ICM) of the blastocyst has the ability to generate the whole body. The embryonic stem cells (ESCs) derived from ICM are therefore pluripotent. However, a landmark report has shown that the pluripotency can be induced in fate-committed adult somatic cells by ectopic introduction of transcription factors such as, OCT4, SOX2, KLF4 and cMYC (OSKM) or collectively called as Yamanaka factors (Takahashi *et al.* 2007). These transcription factors erase and reset the epigenetic signature of somatic cells and reprogram them to an ESC-like state. The cells thus obtained after genetic reprogramming are referred to as induced pluripotent stem cells, or iPSCs. To generate iPSCs, the patient-specific fibroblasts were transduced with a cocktail of recombinant lentiviruses carrying *OSKM* genes. Individual recombinant viruses were prepared as described in the methods **section 3.4**. The entire gamut of molecular events during reprogramming is yet to be elucidated. However, some of the key events that take place during the reprogramming process have been identified. Post-transduction there is a dramatic change in the transcriptional profile of dermal fibroblasts (Sridharan *et al.* 2009). Initially, the lineage specific markers get downregulated and a genetic program is activated that changes the morphology of cells (Samavarchi-Tehrani *et al.* 2010a). This transition termed as the mesenchymal to epithelial transition (MET), is the effect of inhibition of TGF-beta pathway or the activation of BMP/Smad signaling and the upregulation of E-cadherin (R. Li *et al.* 2010; Maherali and Hochedlinger 2009; Samavarchi-Tehrani *et al.* 2010b). Additionally the cells undergoing reprogramming becomes smaller in size, acquire an increased nuclear to cytoplasmic ratio and generate ESC-like colonies that are very compact, with well-defined margins over a period of 20-30 days (Sampath *et al.* 2008; Smith *et al.* 2010). In this study, the transduced fibroblast cells were maintained in **mTeSR.** Small patches of tightly packed and reprogramming cells, with altered morphology could be observed at two weeks post transduction (**Fig 4.2.A**), which indicates an active reprogramming process. At 3 weeks post transduction, some clusters had formed well grown colonies of tightly packed cells with smaller cell size and high nuclear to cytoplasmic ratio (**Fig 4.2.B**). These colonies were manually picked and passaged clonally on Matrigel™ coated plates. Around passage 3,

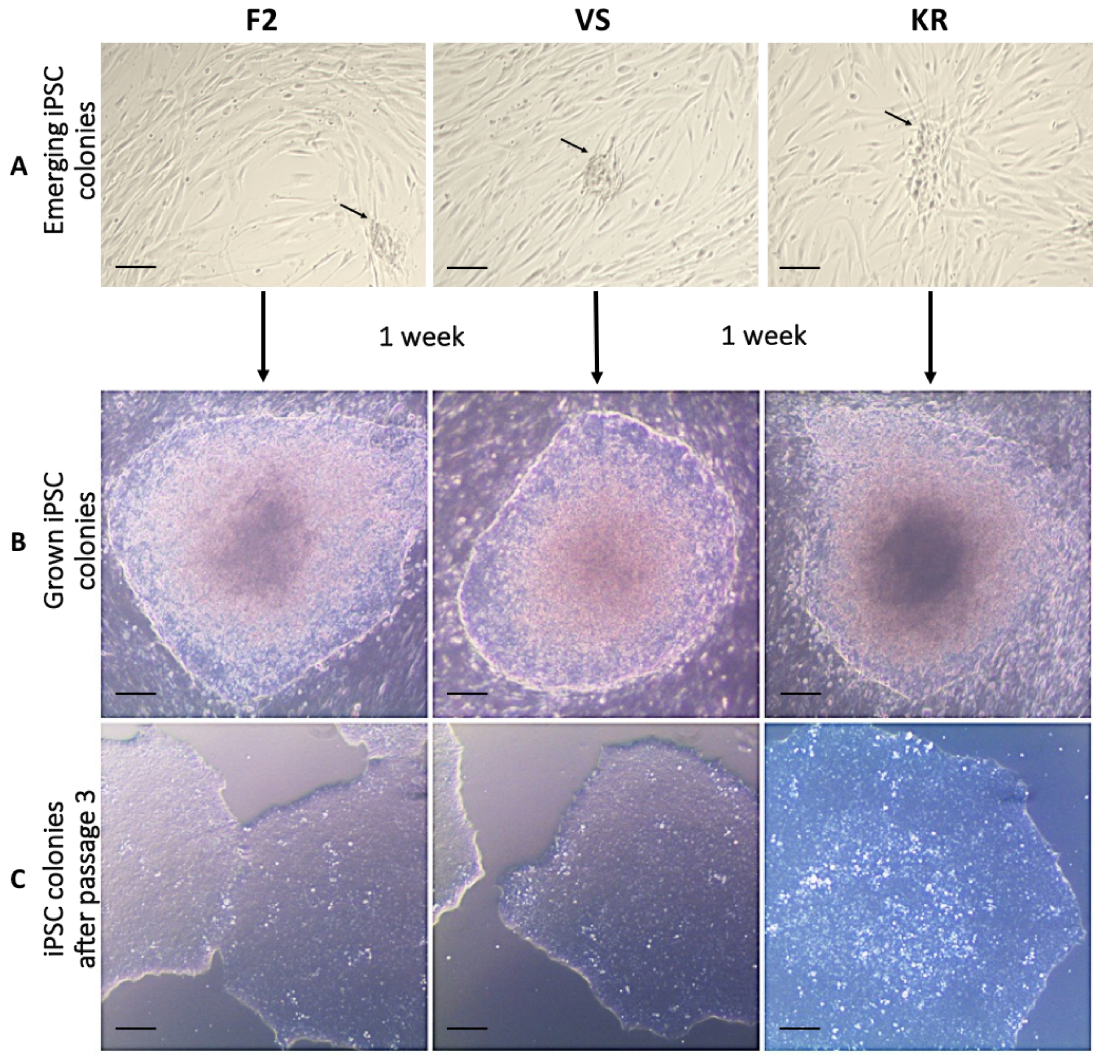

Figure 4.2: Reprogramming of HDFs into iPSCs. *Phase contrast images of newly emerging and expanded iPSC clones of F2, VS and KR specific cells.* ***A.*** *Tightly packed cells with altered morphology appeared at 2 weeks post transduction (Arrows).* ***B.*** *Well reprogrammed ESC-like iPSC colonies that newly emerged amongst the fibroblast cells in the background.* ***C.*** *Expanded, feeder free ESC-like iPSC cultures at passage 3. Scale bar, 10 µm.*

well reprogrammed clones proliferated well and maintained an ESC-like morphology (**Fig 4.2.C**).

4.1.6. Expansion and cryopreservation of patient-specific iPSCs

For each reprogramming experiment, several ESC-like colonies were picked and expanded clonally. Many clones tended to differentiate and failed to expand or lost their ESC-like morphology. Fully reprogrammed iPSC colonies had reduced doubling time. They continued to maintain the ESC-like morphology and possessed an indefinite self-renewing capacity. Successful reprogramming efficiency was observed to be approximately 0.01%. Stable clones that expanded beyond passage 10 were maintained as in **section 3.5.1** and were subjected to detailed molecular characterizations. For each patient line, at least 3-6 stable clones were expanded and cryopreserved at every passage as in **section 3.3.5**.

4.1.7. Characterization of patient-specific iPSCs

Although stable iPSC lines derived from HDFs of VS, KR and F2 maintained an ESC-like morphology and expanded well beyond passage 10, it is important to characterize them for **i**) the presence of patient specific mutations, **ii**) transgene integration and expression, **iii**) endogenous expression of Yamanaka factors, **iv**) maintenance of stemness, **v**) genomic integrity, **vi**) pluripotency and **vii**) the cells' ability to differentiate to ocular lineages.

4.1.7.1. Confirmation of patient-specific mutation

A newly derived iPSC-line should be genetically near identical to the parental HDFs and carry the same patient-specific mutation and STR (short tandem repeats) profiles. To check this, genomic DNA was isolated from VS-iPSCs, KR-iPSCs and F2-iPSCs at passage 10. The exon2-intron2 junction of *RD3* was PCR amplified from VS-iPSCs and F2-iPSCs and the PCR product was sequenced as in methods **section 3.2**. Sequence analysis confirmed the presence of c.296 + 1 G→A mutation in *RD3* (**Fig 4.3.A**). This is a splice junction mutation predicted to disrupt exon2-exon3 splicing and result in intron2 inclusion. An immediate in-frame stop codon within intron2 will result in pre-mature translation termination and generation of a truncated RD3 protein with only 99 amino acids (**Fig 2.4**) when compared to that of the wild type with 197 amino acids.

Similarly, the exon44 of *ABCA4* was PCR amplified from KR-iPSCs and F2-iPSCs and the PCR product was sequenced. Sequence analysis confirmed the presence of c.6088C>T non-sense mutation in *ABCA4* (**Fig 4.3.B**). This mutation results in a truncated ABCA4 protein of 2030 amino acids, whereas the wild type consists of 2273 amino acids (**Fig 2.3**). The

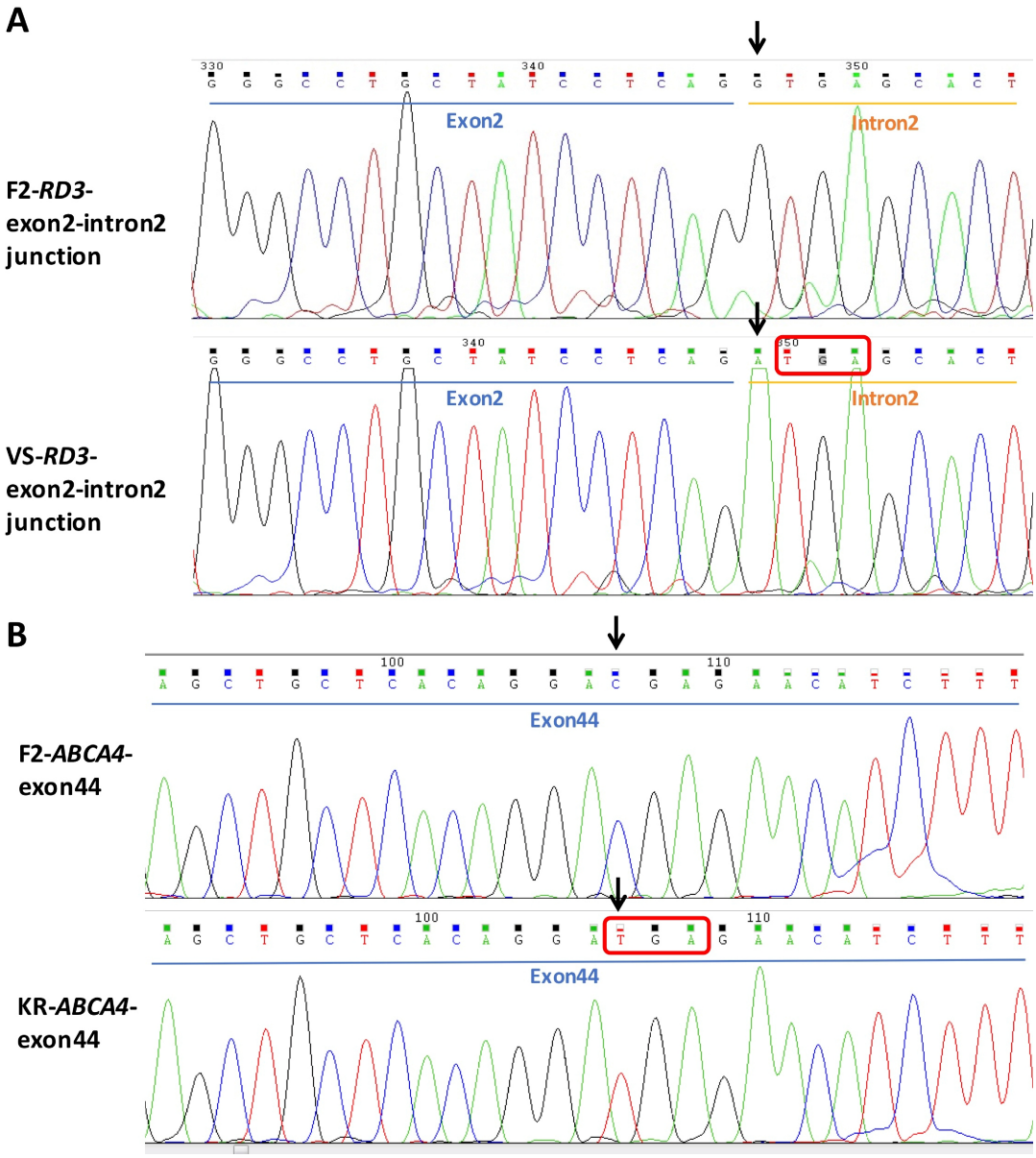

Figure 4.3: Confirmation of patient-specific mutations in iPSC lines. ***A****. Chromatograms from hiPSC-F2 and hiPSC-VS lines showing the G→A transition in c.296 + 1 splice donor position (arrows) in hiPSC-VS. Red box indicates an immediate, in-frame stop codon within the intron2 of RD3. Blue line spans the exon2 region and the yellow line spans the intron2 region.* ***B.*** *Chromatograms from hiPSC-F2 and hiPSC-KR lines showing C→T transition within exon44 of hiPSC-KR (arrows). Red box shows the mutation induced stop codon within ABCA4.*

presence of patient-specific mutation in the respective iPSC lines confirmed their genetic identity and absence of chance culture contaminations.

4.1.7.2. Evaluation of transgene integration and expression

Lentiviral mediated gene delivery results in the integration of the transgene into the host genome (Naldini *et al.* 1996). As it is not a targeted gene delivery, the viral-delivered transgene could integrate anywhere in the host genome. If the transgene integration happens at genomic regions that contain housekeeping genes that are required for cell survival and proliferation regulation, then it can lead to cell death. Thus, number of copies of transgene integration and the site of integration together dictates stable reprogramming, abnormal cell behavior and fate decisions. Also, it is important to check if all the four transgenes have integrated into the host genome. Stable integration and random activation of cMYC, a known oncogene has been a cause of concern with lenti and retroviral reprogramming (Okita, Ichisaka, and Yamanaka 2007). Reports have shown that introduction of only three Yamanaka factors (*O*, *S* and *K*) or just *OCT4* alone, along with a cocktail of small molecules is sufficient to reprogram the somatic cells to iPSCs, albeit at a very low efficiency, when compared to 4 factor reprogramming (Nakagawa *et al.* 2008).

To check for transgene integration in the patient-specific iPSCs derived in the lab, genomic DNA was analyzed by PCR using transgene-specific forward and flanking lentivector-specific reverse primer sets (**Annexure VI**).

Genomic PCR profiles of transgene specific amplicons confirmed genomic integration of three Yamanaka transgenes – *OCT4*, *SOX2* and *KLF4* but not *cMYC* in all the three lines generated (**Fig 4.4.A**). Thus, all the three iPSC lines generated are 3 factors lines and will be hereinafter referred to as, hiPSC-VS-3F, hiPSC-K4-3F and hiPSC-F2-3F respectively.

Stably integrated viral transgenes are known to get silenced during subsequent passages. Silencing of transgenes and activation of endogenous gene expression are an hallmark of stable reprogramming (Hotta and Ellis 2008). In order to confirm the expression of the integrated transgenes, transgene-specific PCR was done using the cDNA of VS-3F, K4-3F and F2-3F as template. RT-PCR profiles of transgene-specific amplicons showed the expression of human *OCT4* and *KLF4* but not *SOX2* and *cMYC* in all the 3 iPSC lines (**Fig 4.4.B**). The expression of transgene during early stages of reprogramming is sufficient to activate the endogenous stem cell factor genes. Stable and continued expression of endogenous factors ensures stable reprogramming. Hence, the endogenous OSKM gene expression profiles were checked by RT-PCR using distinct primer sets. The results

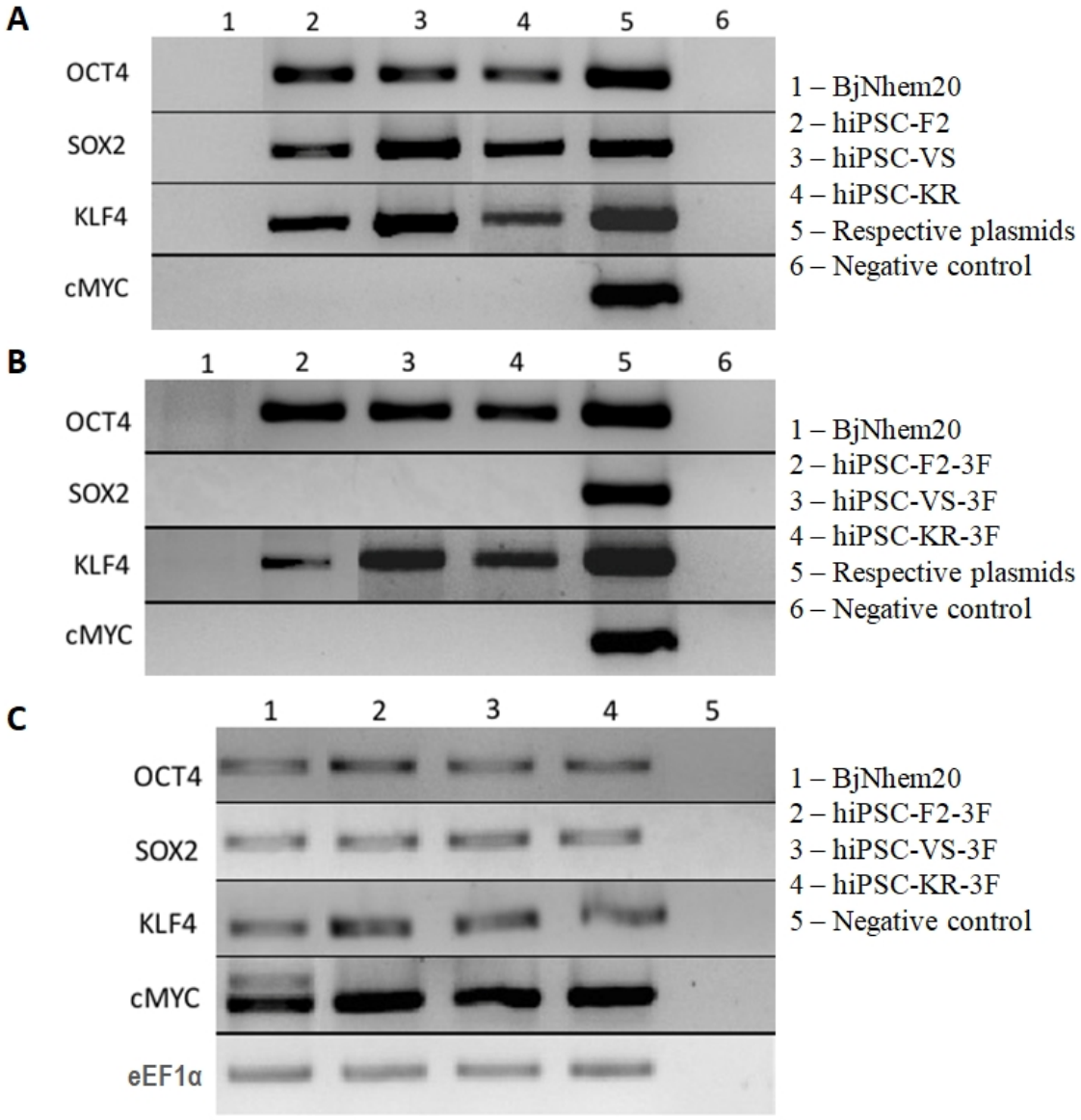

Figure 4.4: Confirmation of integration and expression of lentiviral delivered transgenes. *Agarose gel images showing the integration and expression of Yamanaka factor genes.* ***A.*** *Genomic PCR profiles of transgene specific amplicons confirmed stable genomic integration of human OCT4, SOX2 and KLF4 but not cMYC in all three iPSC lines.* ***B.*** *RT-PCR profiles of transgene-specific amplicons confirmed the expression of all transgenes except cMYC in all three iPSC lines at passage 20.* ***C.*** *RT-PCR profiles of endogenous stem cell factor gene-specific amplicons confirmed the expression of all four transcripts in all the lines at passage 20, at levels comparable to that of BJNhem20, hESCs. The cDNA samples were normalized using eEF1α as the loading control.*

confirmed the expression of *OSKM* Yamanaka genes in all three iPSC lines tested at passage 20 (**Fig 4.4.C**).

Taken together, the results confirmed that exogenous expression of three factors (OSK) is sufficient to completely reprogram HDFs. It is possible that the *SOX2* transgene must have been active at early stages of reprogramming to support iPSC induction. However, it may have got silenced at a later passage and is compensated by endogenous *SOX2* expression for stable iPSC generation. To summarize, all the iPSC lines derived in the lab were stably reprogrammed and expressed the endogenous pluripotent genes (*OSKM*) at passage 20.

4.1.7.3. Confirmation of stemness

The key pluripotency genes – *OCT4* and *NANOG* are highly expressed in growing cultures of ESCs and their promoters are maintained in a demethylated state (Hotta and Ellis 2008). However, upon differentiation and lineage commitment, the regulatory regions of pluripotency genes are methylated and silenced. In fully reprogrammed iPSCs, the epigenetic status of the stemness genes must be similar to that of the proliferating ESCs (Maherali *et al.* 2007; Mikkelsen *et al.* 2008; Okita *et al.* 2007; Wernig *et al.* 2007). Similar to human ESCs (Thomson *et al.* 1998), completely reprogrammed iPSCs depend on basic fibroblast growth factor (bFGF) for proliferation and maintenance of stemness and self-renewal abilities. Removal of bFGF from the culture medium results in differentiation of human pluripotent cells.

In order to check for the expression of stemness genes and the response of cells to differentiating culture conditions, the iPSC lines were cultured both in bFGF containing growth medium (mTeSR) and in bFGF lacking differentiation induction medium (**DM**). Total RNA was isolated from well grown cultures and the expression of stemness genes were evaluated by RT-PCR analysis. Proliferating cultures of human iPSCs have flat, circular and compact colonies of undifferentiated cells, with smooth margins. Upon bFGF withdrawal, the cells undergo spontaneous differentiation and the colonies begin to appear as loose clusters. Gene expression profiling by RT-PCR showed the expression of key stemness genes OCT4, SOX2, NANOG, hTERT in undifferentiated state (UD) and their complete down regulation at 30 days of spontaneous differentiation (**Fig 4.5.A**).

Stemness marker protein expression (OCT4 and SSEA4) was also checked by immunofluorescence staining (**section 3.6.3)**. As shown in **Fig 4.5.B**, all the three iPS lines – hiPSC-VS-3F, hiPSC-KR-3F and hiPSC-F2-3F expressed OCT4 and SSEA4 at levels comparable to that of the hESC line, BJNhem20.

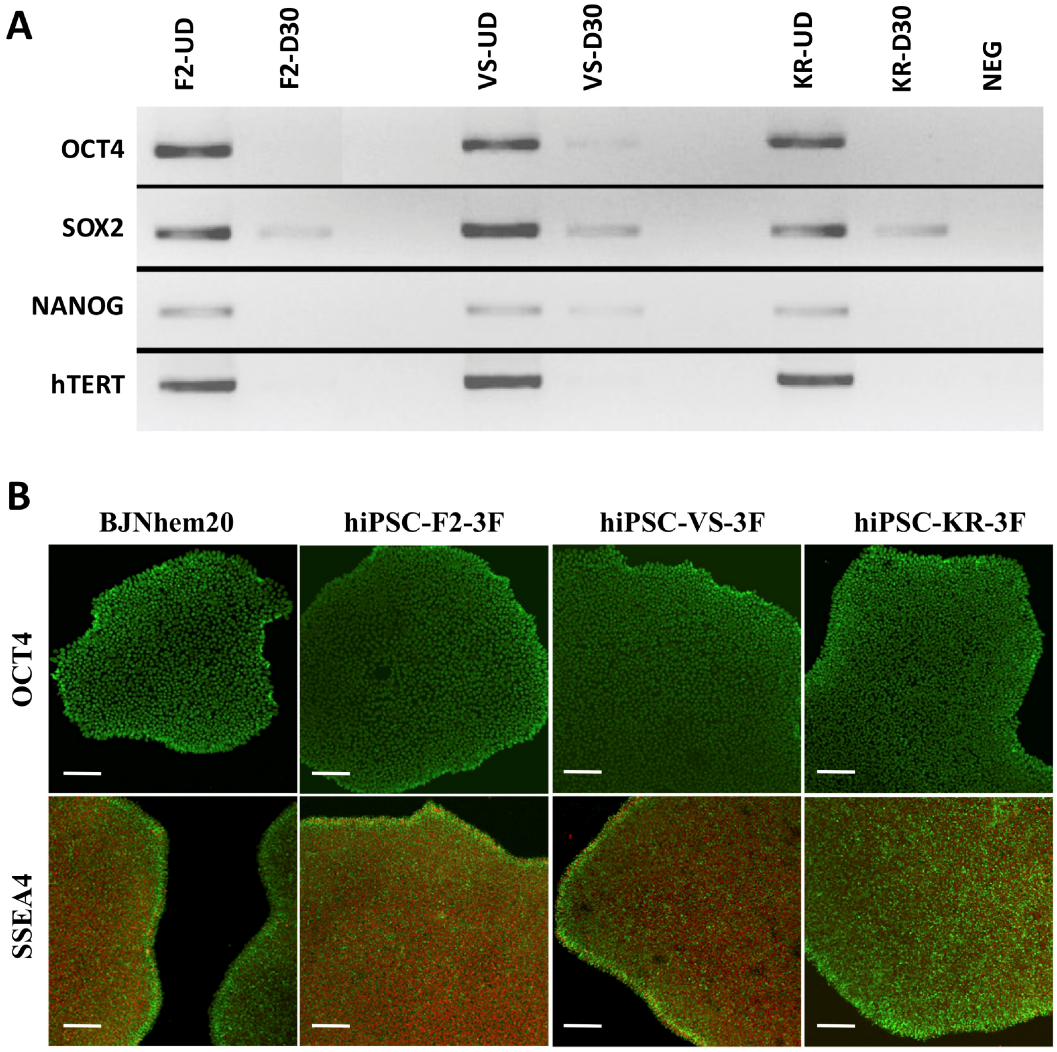

Figure 4.5: Confirmation of stemness marker expression. A. *RT-PCR profiles of stemness genes in undifferentiated (UD) growing cultures and in spontaneously differentiated cultures at day 30 (D30) of all the three iPSC lines are shown. All the three lines expressed key stemness factors in undifferentiated state (UD). bFGF withdrawal resulted in differentiation and loss of stemness marker expression in D30 cultures.* ***B.*** *Confocal images of immuno-stained cells of the human ESC line and the three iPSC lines showing the expression of stemness markers, OCT4 and SSEA4 (in green). OCT4 being a transcription factor is expressed inside the nucleus. SSEA4 is a cell surface marker expressed on the cell membranes. The cells are counter stained with propidium iodide (PI) stain in red. Scale bar, 10 µm.*

4.1.7.4. Confirmation of genomic integrity

ESCs maintained in culture for long term have been reported to acquire various chromosomal abnormalities including point mutations, deletions, insertion, copy number variations and gene amplifications (Draper *et al.* 2004). Such mutations conferring growth advantages get frequently selected in long term cultures and affect their pluripotency. Similarly iPSCs have also been reported to have copy number variations and deletions of chromosomal regions during reprogramming (Laurent *et al.* 2011). Indefinitely self-renewing pluripotent cells can carry karyotype aberrations that may induce tumor formation (Baker *et al.* 2007). Therefore, it is important to monitor the genomic integrity of stably reprogrammed, induced pluripotent cells, to ensure phenotypic stability and clinical safety.

Karyotyping assay helps to assess any gross chromosomal aberrations such as, large duplications, deletions, translocations and copy number variations. Hence, karyotyping by G-banding was employed to assess the genomic integrity of the stably reprogrammed, patient-specific iPSCs at different passages (p10 and p20). It was found that a majority of cells of all the three lines displayed normal karyotypes containing 23 pairs of chromosomes. Also, the results confirmed that the healthy control iPSC line, hiPSC-F2-3F is a female line, with 46, XX karyotype (**Fig 4.6.A**). The two RP patient-specific lines were confirmed to be male lines, with 46, XY karyotype (**Fig 4.6.B**, **4.6.C**). Thus, the karyotype assay confirmed the genetic identity and gross genetic integrity of all the three iPSC lines tested.

4.1.7.5. Confirmation of pluripotency

The iPSCs expressed all the important pluripotent stemness markers, as shown in **Fig 4.5**. However, the real test of pluripotency is the ability of stem cells to differentiate into cell types of all three lineages. Two major methods have been widely employed to assess the pluripotency of iPSCs.

The first method known as the embryoid body (EB) formation assay, is an *in vitro* technique that tests the ability of iPSC line to differentiate into cell types of all three lineages (Itskovitz-Eldor *et al.* 2000). Briefly, the cells are grown in suspension in non-adherent dishes, using **EBM/DM**. Under these conditions, the proliferating and differentiating cells form aggregates that gradually grow in size (2-5 mm). Mature EBs develop fluid filled cysts around 1-2 weeks in culture. Such EBs carry differentiating cells of all three lineages. Upon culture on Matrigel-coated plates, the EBs adhere and give rise to a wave of differentiated cells growth, resulting in heterogeneous cultures of cells of all three lineages.

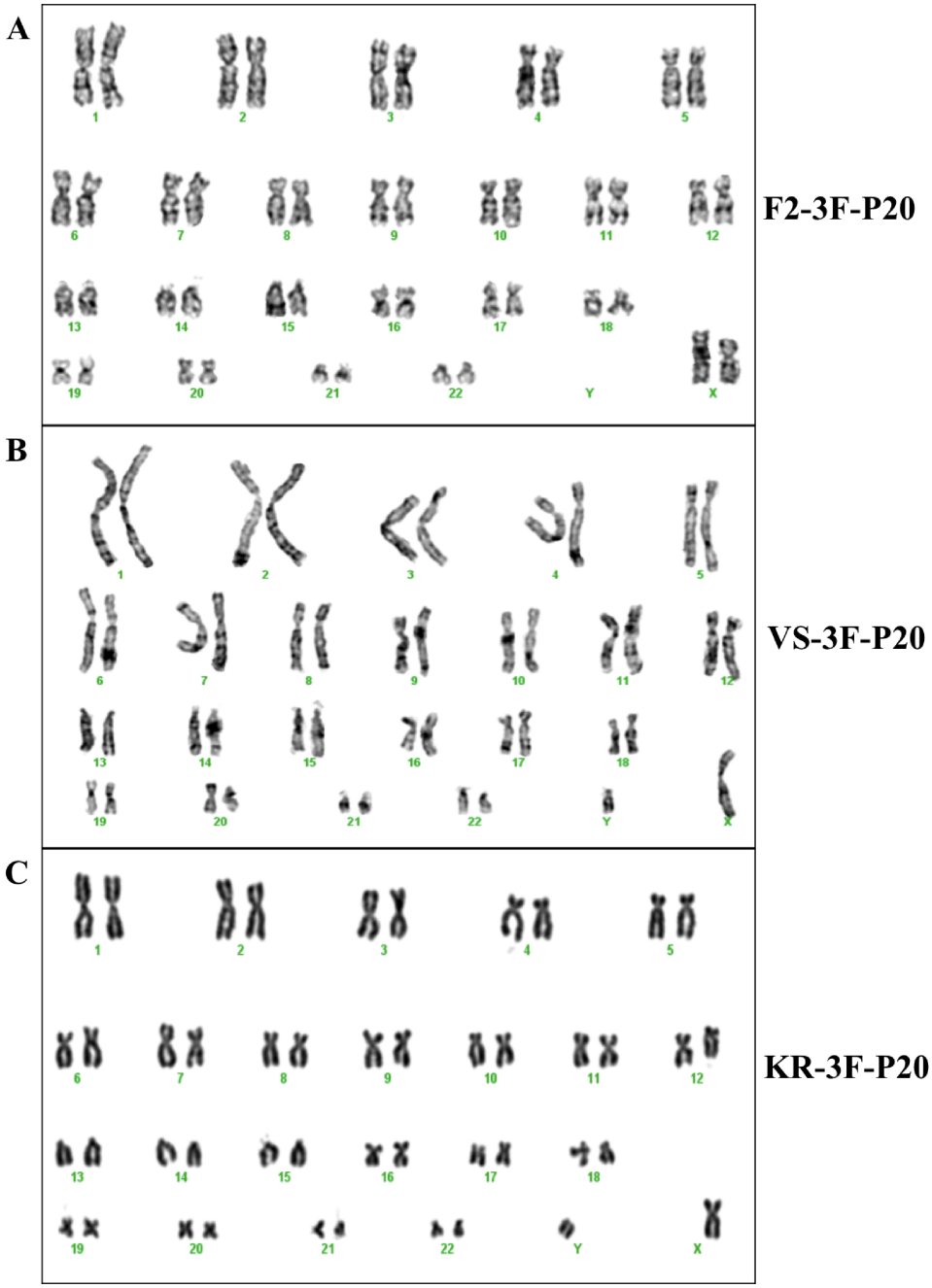

Figure 4.6: Karyotypes of patient-specific iPSCs. *Karyotypes of giemsa stained chromosomes of all three iPSC lines at passage 20 are shown.* ***A.*** *Karyotype of hiPSC-F2-3F, 46, XX, Female line.* ***B.*** *Karyotype of hiPSC-VS-3F, 46, XY, Male line.* ***C.*** *Karyotype of hiPSC-KR-3F, 46, XY, Male line.*

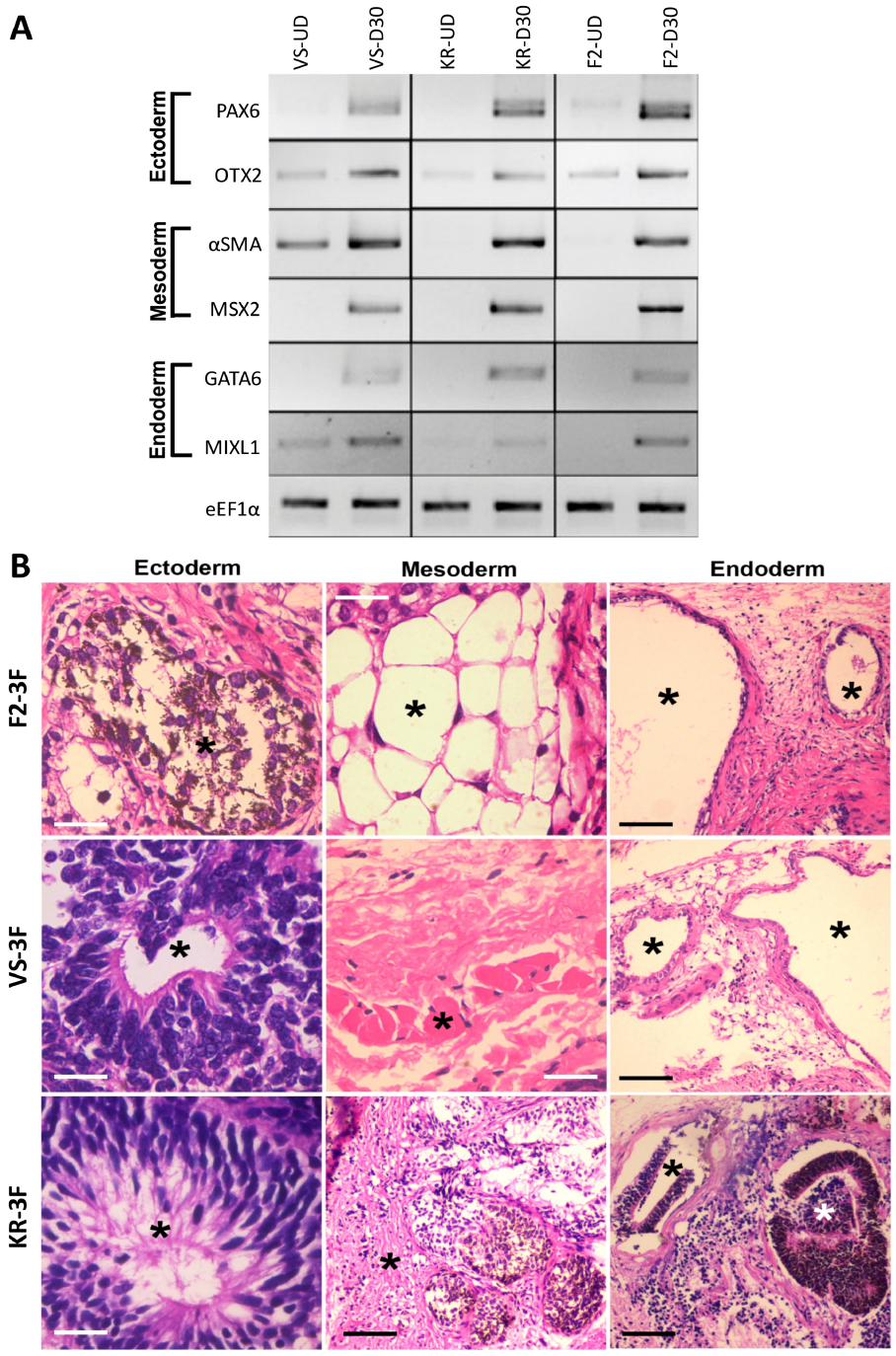

Figure 4.7: Pluripotency of patient-specific iPSCs. *Three lineage differentiation potential of all three iPSC lines were confirmed by RT-PCR and teratoma assay.* ***A.*** *RT-PCR profile showing the expression of all three lineage markers in undifferentiated cells and in EBs at 30 days of differentiation. The cDNA samples were normalized using eEF1α as the loading control.* ***B.*** *H&E sections of a teratoma showing cell types of all three germ layers.hiPSC-F2-3F formed pigmented cells of ectodermal lineage, adipose cells of mesodermal lineage and gut-epithelial-like structures of endodermal lineage. hiPSC-VS-3F formed neural rosette like structures of ectodermal lineage, muscle bundles of mesodermal lineage and gut-epithelial structures of endodermal lineage. hiPSC-KR-3F formed neural rosettes, pigmented cells and eye cup-like structures of ectodermal lineage and connective tissues of mesodermal lineage. Endoderm lineage structures could not be detected in the teratomas analyzed. ('*' indicates the lineage-specific structures of interest). Scale bars: White bar: 20 µm, Black bar: 100 µm.*

To check the pluripotency of the iPSC lines *in vitro*, the cells were cultured to form EBs as described in **section 3.6.5**. Lineage-specific marker expression analysis by RT-PCR confirmed the presence of cell types expressing the ectodermal markers (*PAX6* and *OTX2*), mesodermal markers (*SMA* ad *MSX2*) and the endodermal markers (*GATA6* and *MIXL1*) in 30-day old EBs of all iPSC lines tested (**Fig 4.7.A**).

However, the most reliable and the gold standard test of pluripotency is the teratoma formation assay (Takahashi *et al.* 2007). This method involves the sub-cutaneous injection of iPS cells in nude mice and checking for the ability of the cells to proliferate *in vivo* and differentiate into cell types of all three lineages and form a complex, well differentiated and encapsulated tumor called a teratoma.

To confirm the pluripotency of iPSC lines, teratoma assay was carried out by injecting the iPSCs of all the three lines in the sub-cutaneous space of immune compromised nude mice, as detailed in **section 3.6.6**. The injected cells survived, proliferated and remained confined to the site of injection and formed benign teratomas of variable sizes. 8 weeks post injection, the animals were sacrificed and the teratomas were excised for histopathological analysis. H&E stained sections revealed well differentiated nature of tumors and showed the presence of cell types derived from all three germ layers (marked by '*'), thus confirming the pluripotency of all the three iPSC lines tested (**Fig 4.7.B**). To summarize, a normal healthy control and two RP-patient-specific iPSC lines were generated and genotyped to confirm the presence of patient-specific mutations. Transgene integration check confirmed that only 3 of the 4 transgenes (*OSK*) were integrated in the genomes of the iPSCs, thus confirming that they are 3 factor lines. Transgene expression check by RT-PCR confirmed that only two out of 4 transgenes (*O* and *K*) were active at passage 20. However, the four endogenous stem cell factors (OSKM) were highly expressed in all the iPSC lines at passage 20, thus confirming their stably reprogrammed state. The stable iPSC lines expressed the stemness markers at comparable levels as that of the human ESC control line. The karyotypes of these lines were normal and confirmed the absence of any major chromosomal aberrations. All the lines successfully generated EBs *in vitro* and teratomas in nude mice that contained cell types of all three lineages, thus confirming their pluripotency.

4.1.7.6. Differentiation of human iPSCs into ocular lineages

To study tissue-specific effects of gene mutations and to test the usefulness of RP patient-specific iPSCs as *in vitro* disease models, it is important to establish efficient retinal differentiation protocols. During embryonic development, various signaling pathways, like

FGF, IGF, EGF, BMP, Wnt, Notch and Nodal signaling pathways dictate ectoderm lineage and anterior early eye field commitment, formation of optic vesicle, retinal progenitor cell proliferation and finally resulting in the development of a mature retina (Atkinson-Leadbeater, Hehr, and Mcfarlane 2014; Heavner and Pevny 2012; Huang et al. 2015; Lad, Cheshier, and Kalani 2009; Linker et al. 2004; Messina et al. 2015; Mills and Goldman 2017; Nishihara et al. 2012; Perea-Gomez et al. 2002; Reh 2013; Shen 2007; Streit and Stern 1999).

These developmental events *in vivo* could be recapitulated in a dish, by the addition of various growth factors, supplements and small molecules to the culture medium, either to stimulate or to suppress the activities of various signaling cascades, thus directing the differentiation of pluripotent stem cells towards an ocular lineage (Bertacchi *et al.* 2015) (Mellough *et al.* 2015) (Lupo *et al.* 2013) (Ikeda *et al.* 2005) (Osakada *et al.* 2009). Most of the ectoderm and neural differentiation medium cocktail contains the N2 and B27 growth supplements. In addition, various growth factors are included at different stages of differentiation to promote step-wise lineage commitment and cell maturation. For example, Noggin, a BMP antagonist helps to block mesoderm and endoderm fate and to induce ectoderm commitment (Messina *et al.* 2015). Similarly, LEFTY, a nodal antagonist, DKK1, a canonical Wnt pathway inhibitor and IGF-1 play an important role in retinal stem cell fate commitment (Ikeda *et al.* 2005; Perea-Gomez *et al.* 2002; Shen 2007). Further, exposure to bFGF induces neuro-retinal (NR) fate and Activin A mediated TGFβ signaling induces the retinal pigmented epithelial (RPE) fate of committed retinal stem cells (Pittack *et al.* 1997). Treatment of committed neuro-retinal precursors with retinoic acid was shown to promote further differentiation and morphological maturation (Zhong *et al.* 2014). Recent culture methods have adopted the inclusion of various small molecule analogues as cost effective replacements for recombinant growth factors to enable directed differentiation of PSCs (Osakada *et al.* 2009).

The iPSCs derived in the lab were subjected to differentiation by initial EB formation (**section 3.6.5**) in suspension cultures for 3 days in **DM** (DMEM-F12 medium containing 4% KOSR, 100 U/mL pen-strep solution, 1X NEAA, 2mM GlutaMAX™). Well-developed EBs were then transferred to a Matrigel coated dish and were grown as adherent cultures **NIM** (DM supplemented with 1% N2 and 100 ng/mL Noggin). Noggin is a BMP antagonist known to induce dorsal ectoderm and neural differentiation (Messina *et al.* 2015). The EBs in NIM adhered to the Matrigel coated plates and a concentric wave of cells emerged out of EBs resulting in a confluent culture of differentiated cells within two days. After a week in NIM, neural rosettes (**Fig 4.8.A**) were observed (marked by '*'), thus marking the first step in ocular lineage differentiation – the neural induction (**Fig 4.8.A**).

When these neural rosettes were maintained in **RDM** (DM supplemented with 2% B27 and 10ng/mL DKK1) for further 3 weeks, the hiPSC-VS-3F and hiPSC-F2-3F lines formed distinct, raised, circular to oval eye field-like, self-organized structures, which were termed as eye field primordia (EFP) (**Fig 4.8.A**). Starting with about 1 million iPSCs, about 20-30 EFP clusters emerged per well of a 6-well plate of both hiPSC-VS-3F and hiPSC-F2-3F cultures. RT-PCR profiling of these EFP showed the expression of OTX2 in all the lines, indicating the anterior neural fate specification. Early committed eye-field precursors express a set of eye field transcription factors (EFTFs) such as ET, PAX6, RX1, SIX3, SIX6, LHX2, TLL and OPTX2 (Zuber *et al.* 2003). When examined by RT-PCR, one-month old EFP expressed RX, PAX6 and SIX6, thus confirming an eye lineage commitment (**Fig 4.8.B**). The expression of these early eye field transcription factors got down regulated at 2 months of differentiation, as the EFP begin to differentiate into committed, post-mitotic cell types of the retina. Such step-wise lineage differentiation *in vitro* truthfully recapitulated the sequence of events that occur during embryonic eye development *in vivo* (Zagozewski, Zhang, and Eisenstat 2014). The EFP were surrounded by a monolayer of epithelial cells that later attained hexagonal morphology and pigmentation to form the retinal pigment epithelial cell monolayers (**Fig 4.9.A**).

However, the hiPSC-KR-3F line displayed a striking difference in their ability to differentiate into ocular cells. Although this iPSC line could form neural rosettes within a week of differentiation, it was inefficient in generating EFP (**Fig 4.8.A**). Only rare clusters (2-3 nos) of poorly organized EFP were noted per well of a 6-well plate. When such EFP-like clusters were manually picked and cultured, the retinal precursors preferentially differentiated towards RPE lineage over neuro-retinal lineage. Also, the expression of RX was delayed and was observed only after 2 months of differentiation (**Fig 4.8.B**). The RPE precursors developed intense pigmentation earlier than the other two lines. As explained earlier in **section 2.5.1.1**, the well characterized function of ABCA4 is to flip the visual pigment intermediates from the inside of the discs to the cytoplasm of the photoreceptors. It is unclear why a truncation mutation in *ABCA4*, would result in preferential differentiation towards RPE fate and defective neuro-retinal differentiation of retinal stem cells. The characterization of the RPE cells derived from hiPSC-KR-3F is further detailed in **section 4.1.10**.

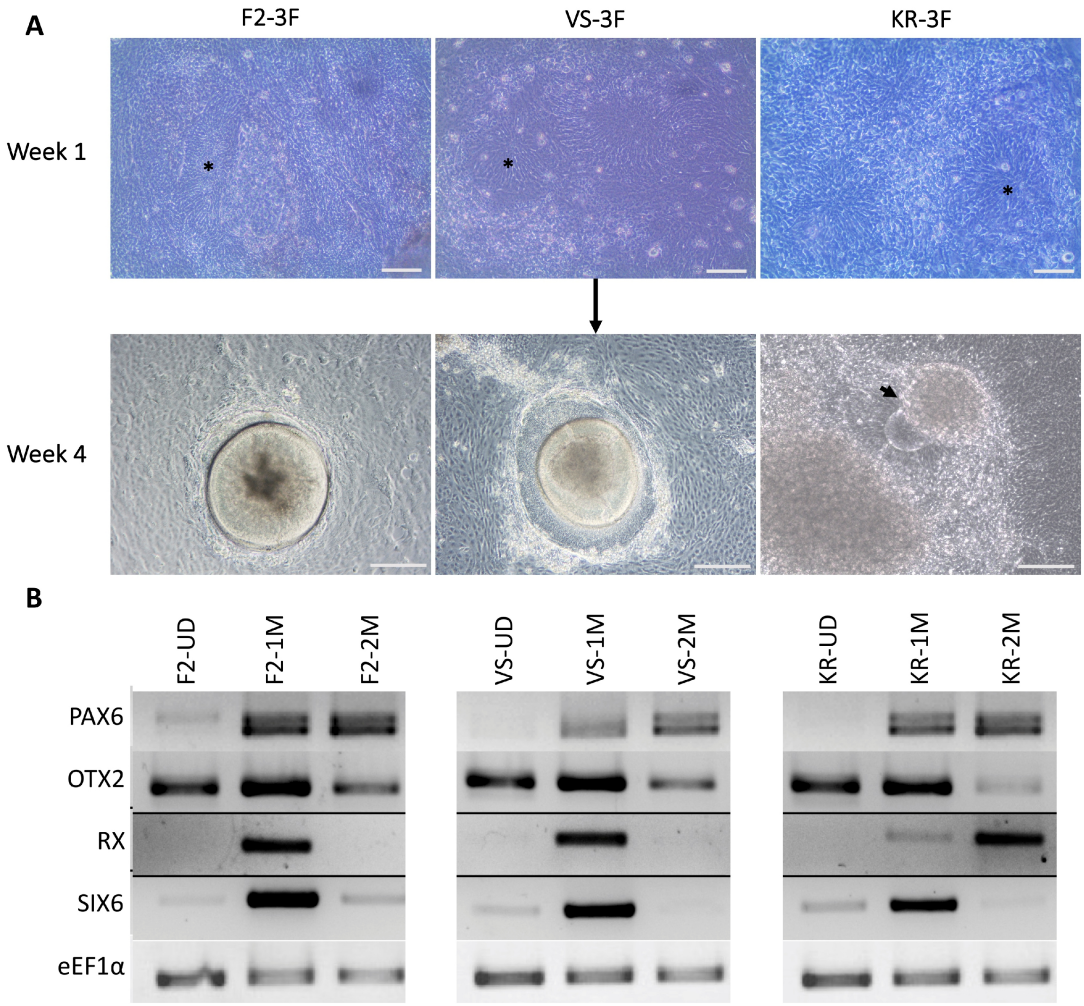

Figure 4.8: Retinal differentiation and early eye field commitment. *Phase contrast images showing the emerging eye fields and confirmation of expression of eye field specific genes by RT-PCR.* ***A.*** *Phase contrast images of differentiating cultures of iPSCs showing the emergence of neural rosettes (*) at 1 week post differentiation (top panel) and distinct self-organized, eye field primordia (EFP) at 4 weeks of differentiation. hiPSC-KR-3F formed poorly organized EFP that preferentially differentiated to RPE on manual passaging. Scale bars, 100 µm.* ***B.*** *RT-PCR profiles of 1 month old EFP of hiPSC-VS-3F, hiPSC-KR-3F and hiPSC-F2-3F showing the expression of EFTFs – PAX6, OTX2, RX and SIX6. The expression of RX was delayed by a month in KR. The cDNA samples were normalized using eEF1α as the loading control. Scale bars-1mm.*

Such EFP generated using patient-specific iPSCs can serve as excellent *in vitro* models to study retinal degeneration (Jin *et al.* 2011; Li *et al.* 2017; Sharma *et al.* 2017; Tang *et al.* 2016; Wiley *et al.* 2015). Further enriched cultures of retinal precursors and patient-specific retinal cells are valuable tools for preliminary drug screening *in vitro.* In order to characterize the effects of pathogenic mutations in retinal development and maturation, pure cultures of mature retinal pigment epithelium and neuro-retinal cells were established using all the three human iPSC lines.

4.1.8. Establishment of monolayer cultures of RPE and neuro-retinal cells

It is well established that during early retinal development and optic vesicle maturation stage, the bFGFs secreted by the ocular surface ectoderm play a crucial role in neuro-retinal lineage differentiation (Nguyen and Arnheiter 2000; Pittack *et al.* 1997) and TGFβ family of proteins (like Activin A) secreted by the periocular mesenchyme promotes RPE lineage differentiation of retinal stem cells (Fuhrmann 2010; Fuhrmann, Levine, and Reh 2000). Also, inhibition of wnt signaling is necessary to promote terminal differentiation and maturation of neuro retinal cells (Inoue *et al.* 2006; Kubo 2003).

To establish and standardize the retinal differentiation and cell enrichment protocols using pluripotent stem cells, differentiation cultures were initiated using the well characterized normal control, human embryonic stem cell line, BJNhem20 (Inamdar *et al.* 2009; Shetty and Inamdar 2012; Venu, Chakraborty, and Inamdar 2010). The eye field clusters obtained (as in **section 4.1.7.6**), were allowed to mature in RDM for another month to form neuro-retinal (NR) islands surrounded by pigmented RPE cells (**Fig 4.9.A**). The NR islands were manually scooped out using a pulled glass capillary pipette and were plated onto Matrigel™ coated dishes or cover slips containing **neuro-retinal medium, NRM** (DM supplemented with 1% N2, 2% B27 and 5 ng/mL bFGF as neural growth supplement), and grown as adherent cultures to obtain enriched neuro-retinal (NR) cells. Cells with neuron-like morphology with very long axons and dendrites were seen migrating out of the adhered NR islands within a day (**Fig 4.9.B**). These neurons expressed the early neuro-retinal precursor markers, PAX6 and CHX10 as shown in **Fig 4.9.D**, **E**. The expression of CHX10/VSX2 (an homeodomain containing transcription factor) and MITF (a basic helix-loop-helix leucine zipper containing, microphthalmia-associated transcription factor) in retinal stem cells are mutually exclusive and they negatively regulate each other resulting in either the neuro-retina or the RPE fate commitment respectively (Fuhrmann 2010; Horsford *et al.* 2004; Nguyen and Arnheiter 2000; Zagozewski, Zhang, and Eisenstat 2014b). These neural cells became confluent

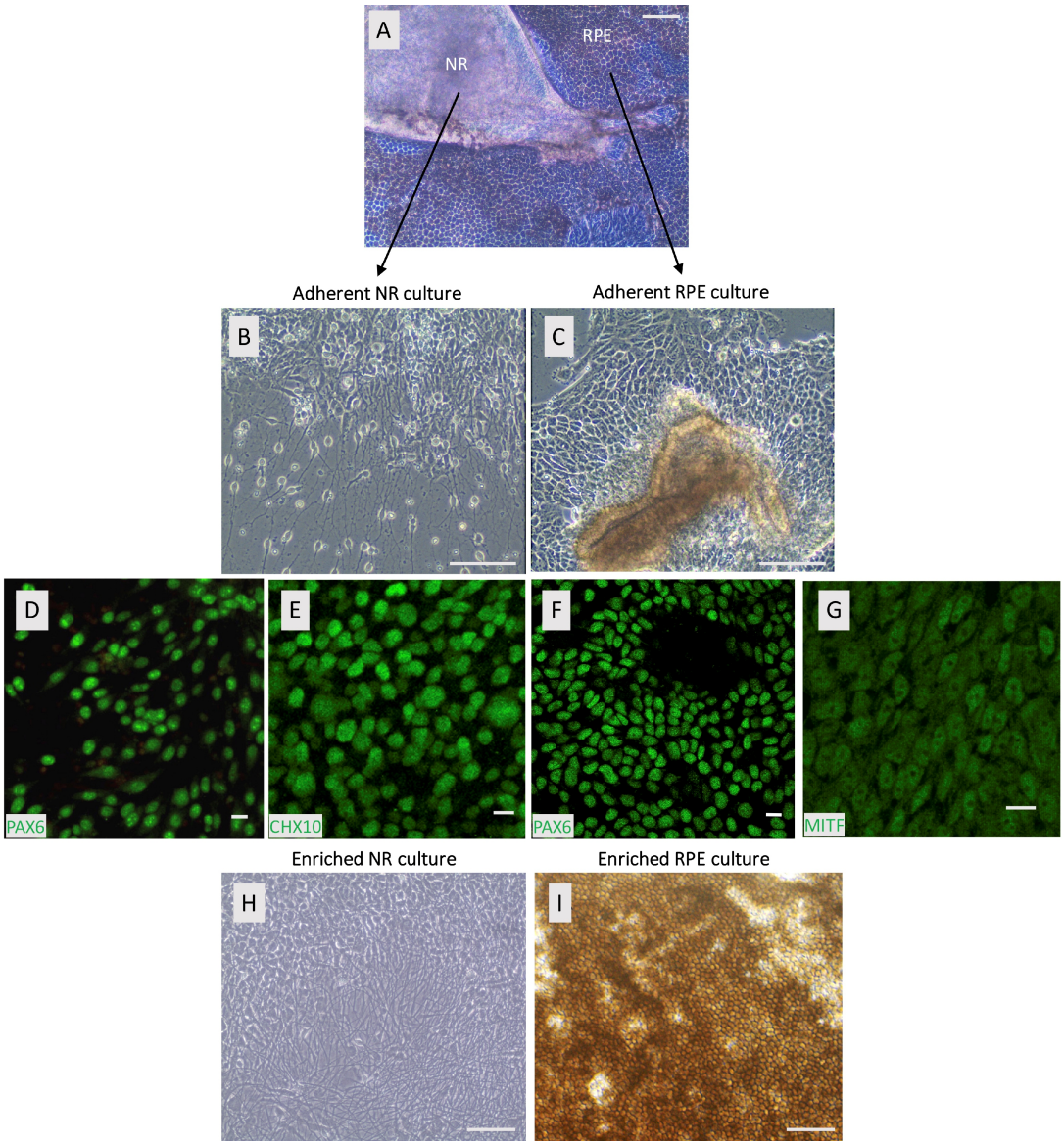

Figure 4.9: Establishment of monolayer cultures of neuro-retinal and RPE cells. *Phase contrast images of enriched NR and RPE culture and immunofluorescence staining confirming the early NR and RPE identity.* ***A****. EFPs that matured to form NR island surrounded by pigmented RPE cells.* ***B****. Adherent cultures of neurospheres containing NR progenitors.* ***C****. Adherent cultures of manually isolated RPE cell clusters on Matrigel™ coated surfaces.* ***D, E.*** *Early NR progenitors showing nuclear expression of PAX6 and CHX10 respectively.* ***F,G****. Early RPE progenitors showing nuclear expression of PAX6 and MITF respectively.* ***H****. 2 months old enriched NR culture showing mixed population of neuro-retinal cells.* ***I****. 3 months old enriched RPE culture showing a compact monolayer of highly pigmented epithelial cells with typical cobblestone morphology. Scale bars: A-C, H,I – 100 µm, D-G, 20 µm.*

within three days and were maintained in NRM for up to 2 months, to establish mature retinal cultures comprising of different neuro-retinal cells (**Fig 4.9.H**).

Similarly, the pigmented RPE progenitors surrounding the NR islands were also manually picked using the Pasteur pipette and seeded on to Matrigel coated dish in **retinal pigment epithelium maturation medium, RPEM** (DM supplemented with 2% B27, 10 ng/mL activin A as growth supplements and 10 μM Y-27632). The addition of Y-27632, a Rho-associated protein kinase (ROCK) inhibitor is known promote cell proliferation, reduces cell death and also prevents epithelial to mesenchymal transition (EMT) during RPE progenitor cell expansion (Croze *et al.* 2014). Upon culture of isolated RPE progenitors in RPEM, they adhered and proliferated to attain an elongated fibroblast-like cell morphology (**Fig 4.9.C**) and expressed PAX6 and MITF (**Fig 4.9.F**, **G**), thus confirming their RPE identity. Upon continued culture, the RPE cultures became confluent, established cell-cell contacts, tight junctions and formed a monolayer of hexagonal shaped and highly pigmented monolayer of mature RPE cell sheets (**Fig 4.9.I**).

4.1.8.1. Characterization of monolayer culture of neuro-retinal cells

The neuro-retinal culture that had matured in dish for 2-3 months in NRM contained heterogeneous population of NR cells. The NR cells were characterized for their individual cell identity by immunocytochemistry and semi-quantitative RT-PCR. Immunostaining of 3 months old cultures confirmed that a majority of cells expressed the general neuron-specific markers such as, MAP2, β-III tubulin and acetylated tubulin (**Fig 4.10.i.A**-**C**). A sub-set of these neurons also expressed the committed photoreceptor precursor marker, CRX (**Fig 4.10.i.D**). CRX (cone-rod homeobox) is a transcription factor, required for the rod and cone photoreceptor commitment of early NR cells (Croze *et al.* 2014). The CRX and PAX6 expressing NR precursors also co-expressed other committed photoreceptor markers such as, Recoverin and Rhodopsin, thus confirming the cell identity (**Fig 4.10.i.E**-**I**). Also, the asymmetric distribution of Rhodopsin within individual cells indicated some level of morphological maturation of committed photoreceptors (**Fig 4.10.i.E**). RT-PCR profiling (**Fig 4.10.ii**) of these cells also revealed the expression of early retinal markers such as, CHX10, CRX and visual transduction pathway genes such as, RLBP1 (retinaldehyde binding protein 1), Rhodopsin, PDE6C (phosphodiesterase 6C), PKC-β (protein kinase C beta), OPN1MW (middle wavelength opsin1 or green opsin) and RHOK (rhodopsin kinase). Together, the results confirmed that the in-house retinal differentiation and cell enrichment protocol was efficient in establishing monolayer cultures of mature NR cells from PSCs.

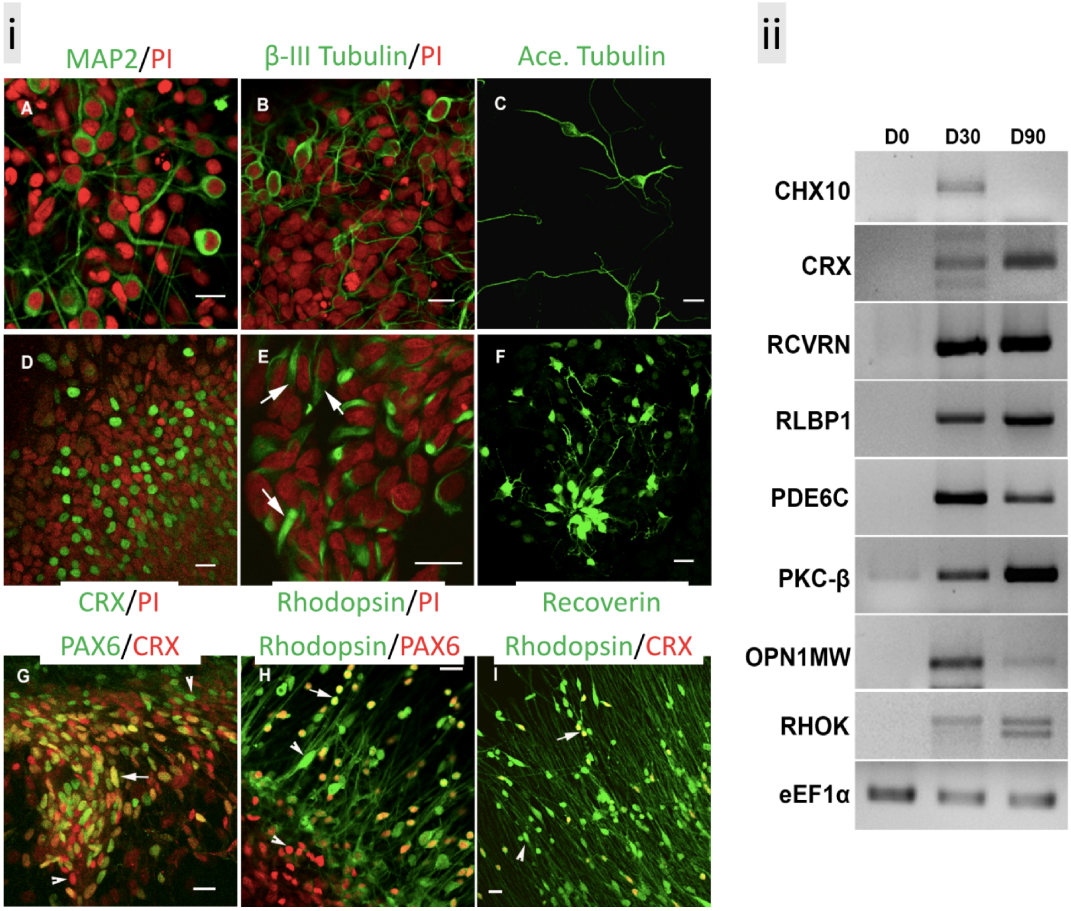

Figure 4.10: Characterization of mature neuro-retinal cells. *Confirmation of the presence of mature NR cell specific markers by* ***(i)****immunofluorescence and* ***(ii)*** *RT-PCR.* ***i)****The NR cells after 2 months in NRM expressed general neural markers MAP2 (****A****), β-III tubulin (****B****) acetylated tubulin (****C****) and photoreceptor specific markers, CRX (****D****), Rhodopsin (****E****) and Recoverin (****F****) (in green). Arrows mark the asymmetrically localized rhodopsin. The cells are counterstained with PI in (****A****,****B****,****D****,****E****) to mark the nuclei in red. Retinal cells co-expressing the markers PAX6 (green) and CRX (red) (****G****), Rhodopsin (green) and PAX6 (red) (****H****), Rhodopsin (green) and CRX (red) (****I****). (****G,H,I****): Arrows indicate dual positive cells. Arrowheads indicate the cells expressing a single marker. Scale bar, 20 µm.* ***ii)*** *RT-PCR profiles of NR cells at 30 and 90 days of differentiation showing the expression of early and mature retinal markers: CHX10, CRX, RCVRN (Recoverin), RLBP1 (Retinaldehyde binding protein 1), PDE6C (Phosphodiesterase 6C), PKC-β (Protein kinase C beta), OPN1MW (Opsin, medium wavelength) and RHOK (Rhodopsin kinase). The cDNA samples were normalized using eEF1α as the loading control.*

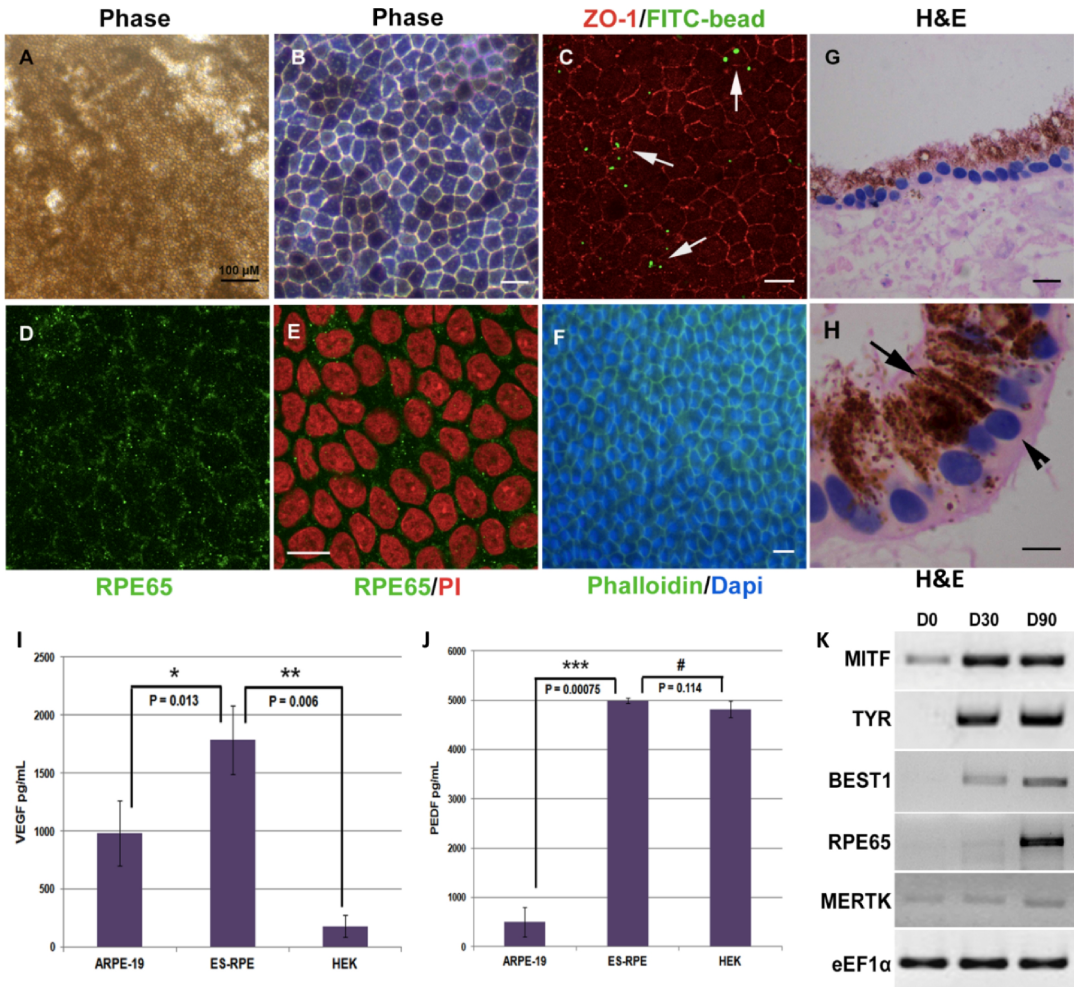

Figure 4.11: Characterization of mature RPE cells. ***A****. Monolayers of 3-months-old, highly pigmented RPE cells.* ***B****. Mature RPE cells at higher magnification showing cobble stone morphology.* ***C****. ZO-1 staining to label the intact tight junctions. Phagocytosed and internalized FITC labeled beads could be seen inside the RPE cells (arrows).* ***D-E****. Mature cells expressing cytosolic and membrane localized RPE65 (green). The cells are counter stained with PI in red.* ***F.*** *Well organized actin cytoskeletal bundles are marked by Phalloidin-green staining. The cells are counter stained with DAPI in blue.* ***G****. Histology and hematoxylin and eosin-stained section of RPE cells cultured on collagen I matrix.* ***H****. Higher magnification of G shows a polarized layer of mature RPE cells with basally located nucleus (arrowhead) and apically positioned melanosomes and the microvilli structures (arrow).* ***I-J****. Bar graphs showing ELISA-based quantification of the mean expression of basally secreted VEGF and apically secreted PEDF proteins detected in the spent medium of ARPE-19, HEK293T and PSC-derived RPE cells, n=3. Error bars represent the ± SD.* ***K****. RT-PCR profiles of 0, 30 and 90 days old RPE cells showing the expression of RPE-specific markers: MITF (microphthalmia associated transcription factor), TYR (Tyrosinase), BEST1 (Bestrophin1), RPE65 (Retinoid isomerohydrolase), MERTK (Receptor tyrosine kinase). The cDNA samples were normalized using eEF1α as the loading control. Scale bar: 20 µm, unless otherwise specified.*

4.1.8.2. Characterization of monolayer cultures of RPE cells

The RPE cells that had matured in RPEM, for 3 months became highly pigmented and attained cobblestone morphology (**Fig 4.11.A**, **B**). The RPE cells were characterized for their identity by immunocytochemistry (ICC), phagocytosis assay, ELISA and semi-quantitative RT-PCR. Immunostaining experiments confirmed that the compact epithelial sheets of RPE expressed ZO-1 in hexagonal patterns indicating the establishment of well-formed tight junctions between the cells (**Fig 4.11.C**). The presence of tight junctions is crucial to establish epithelial barrier functions and to ensure polarized secretion of growth factors and transport of ions across cell membranes. The 3-month-old mature RPE cells also expressed the key RPE-specific marker, RPE65 (**Fig 4.11.D**, **E**). RPE65 is an isomerohydrolase enzyme present in native RPE cells that converts all-trans retinol to 11-cis retinal as a part of the visual cycle. RPE65 exists both in cytosolic form and membrane bound form and similar localization was observed in three-month-old cultures of PSC-derived RPE cells (**Fig 4.11.D**, **E**). Native RPE cells are highly phagocytic and their important function is to clear the photoreceptor cell outer segments that are shed regularly in the sub-retinal space, by phagocytosis. To assess the phagocytic activity of the mature RPE cells, fluorescent beads of 1 μm size were added in culture and checked for internalization after 12 hrs. Upon confocal microscopic evaluation, the internalized FITC-labeled beads could be seen within the cells, thus confirming that the PSC-derived RPE cells are functional and carry phagocytic activity (**Fig 4.11.C**). The cell boundaries are marked by an orderly arrangement of actin cytoskeletal bundles marked by Phalloidin-FITC staining (**Fig 4.11.F**). The RPE cells cultured on collagen I matrix formed intact, monolayer sheets of RPE. On histopathological analysis, these cells appeared to be highly polarized with basally positioned nuclei and apically positioned pigmented melanosomes in the cytosol and numerous apical microvilli structures (**Fig 4.11.G**, **H**). It was also found that the mature RPE cells cultured on transwell membranes secreted significantly higher levels of PEDF on the apical side and VEGF on the basal side when compared to ARPE-19 and HEK293T cells, thus validating the maturity and highly polarized functions of RPE cells (**Fig 4.11.I**, **J**). RT-PCR profile of RPE cells at day 30 after differentiation showed the expression of early RPE markers MITF (microphthalmia-associated transcription factor) and TYR (tyrosinase) (**Fig 4.11.K**). The 90 days old RPE cells expressed the mature RPE markers such as, BEST1 (bestrophin1), RPE65 (retinoid isomerohydrolase and MERTK (a membrane-bound receptor tyrosine kinase). Together, the results confirmed that our retinal differentiation and cell enrichment protocol was efficient in establishing monolayer cultures of mature and functional RPE cells from human PSCs.

4.1.9. Establishment of three-dimensional cultures and miniature organoids

As described earlier (**section 2.2.2**), the neuro retina develops from the inner layer of the double walled optic cup and the RPE from the outer layer. The neuro retinal primordial tissue, at the inner layer of the optic cup, further develops into a complex tissue consisting of six different neuro-retinal cells and glial cells that are spatially organized into three distinct retinal layers. The monolayer cultures of neuro-retinal cells that was discussed earlier in **section 4.1.8.1**, do not truly represent a complex native retina. In 2011, a path breaking study reported a suspension culture method (serum-free floating culture of embryoid-body-like aggregates, SFEB) (Eiraku *et al.* 2008), by which self-formed optic cups were obtained from mouse embryonic stem cells (Eiraku *et al.* 2011). These optic cups truly recapitulated the different stages of embryonic retinal development. Following that, the same group and many other groups have published modified versions of the protocol with varied ECM proteins, growth factors and culture conditions to derive three dimensional retinal tissues from human ESCs and human iPSCs (Nakano *et al.* 2012;Assawachananont *et al.* 2014; Hiler *et al.* 2015; Kaewkhaw *et al.* 2015; Reichman *et al.* 2014; Völkner *et al.* 2016; Zhong *et al.* 2014;Reichman *et al.* 2014). Most of the protocols were laborious making it difficult for scaling up. To overcome that, this study came up with a simple protocol which involved obtaining the EFP by adherent culture followed by manual picking of the central islands of EFP and culturing them as suspension on non-adherent dishes.

To establish and standardize the generation of self-organizing optic cups using pluripotent stem cells, differentiation experiments were initiated with the well characterized, normal control human iPSC line, hiPSC-F2-3F. The EFP were obtained (**Fig 4.12.B**) as in **section 4.1.7.6** and the central neuro-retinal island of EFP were manually picked using a pulled glass pipette and grown as suspension culture in **neuroretinal medium, NRM** (DM supplemented with 1% N2, 2% B27 and 5 ng/mL human recombinant bFGF) in non-adherent dishes. EFP in NRM suspension culture formed three dimensional self-formed optic cups or retinal primordia within a week (**Fig 4.12.C**). The retinal primordia was excised from the rest of the ocular structures and allowed to mature in NRM (**Fig 4.12.D**). The characterization of these retinal primordia is discussed in detail in **section 4.1.9.2**.

Occasionally the EFP were left to mature in adherent culture and surprisingly, a few and rare EFP showed higher order organization in 3D and developed into miniature eye like structures (15 weeks old), with neuro-retinal primordia on the basal side, translucent corneal primordia on the anterior side, pigmented neural crest at corneal margins and RPE cells migrating out as adherent monolayer cells surrounding the posterior neuro-retina of the eye

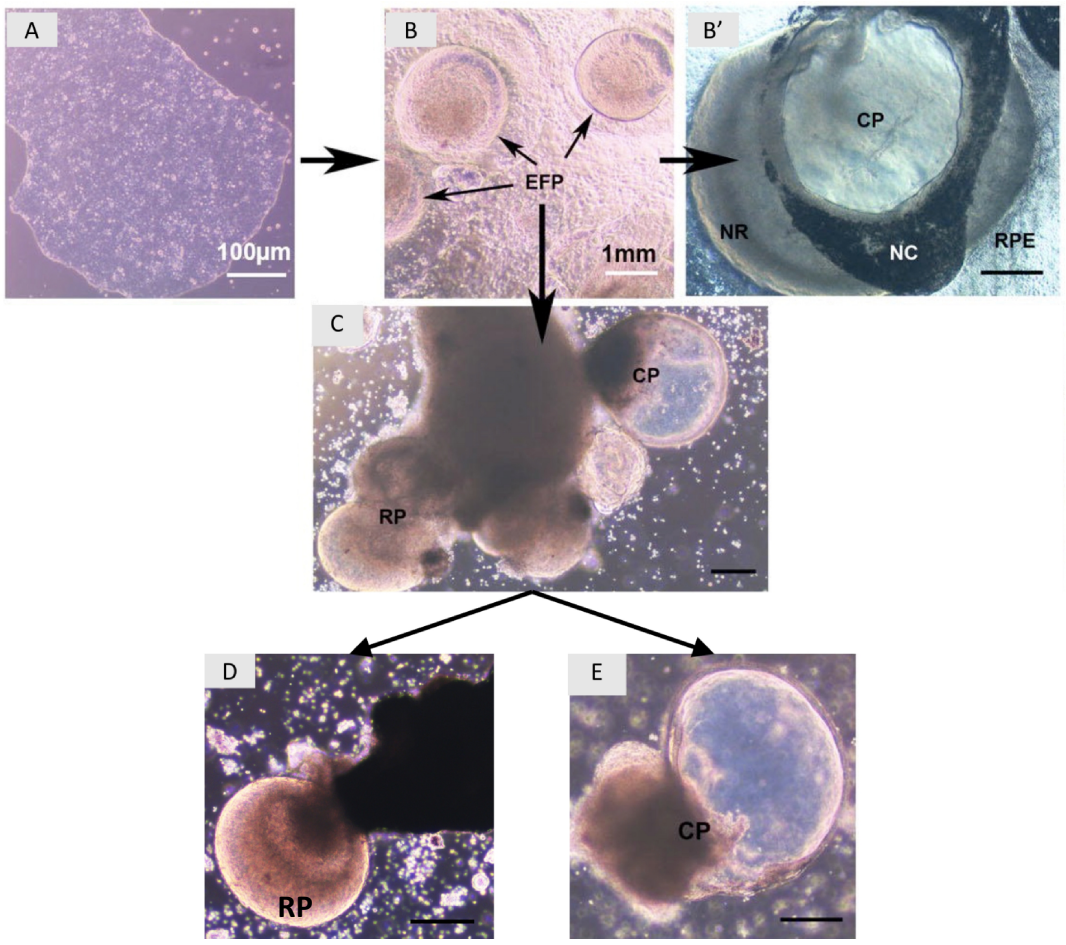

Figure 4.12.Establishment of three dimensional cultures of miniature retinal and corneal organoids. *Phase contrast images showing different stages of development of PSC-derived corneal and retinal organoids.* ***A****. Growing culture of hiPSC-F2-3F. Scale bar: 100 µm.* ***B****. Distinct EFP clusters (arrows) that emerged at 4 weeks in RDM.* ***B'****. Whole eyeball like structures with corneal primordia (CP) on the anterior side and neuro-retinal (NR) primordia on the basal side, with pigmented neural crest (NC) at corneal margins and migrating-out monolayers of RPE cells all around.* ***C.*** *Suspension culture of EFPs showing a well-organized retinal primordia (RP) and transparent corneal primordia (CP).* ***D****. Isolated suspension culture of RP in RDM for further maturation.* ***E****. Isolated suspension culture of CP in CDM for further maturation. Scale bar (B-E): 1 mm.*

primordia (**Fig 4.12.B'**). Another study had showed the appearance of self-formed ectodermal autonomous multi-zones (SEAM) of ocular cells in adherent, differentiation cultures of human iPSCs (Hayashi *et al.* 2016). The SEAM essentially consists of the neuro-ectoderm in the center, surrounded by concentric layers of cells of neuro-retinal and RPE precursors, neural crest cells, lens ectoderm, ocular surface ectoderm cells and finally the head surface ectoderm in an order that mimics embryonic anterior and posterior eye development. The miniature eye like structure that was observed in adherent cultures further confirmed that following eye field commitment, the precursor cells undergo sequential fate specifications into multiple cell types, which then signal each other and can self-organize to form complex three-dimensional mini eye-like structures *in vitro*. Though this was a rare observation, it opens up the possibility of developing improved culture methods for whole eye organogenesis, in future. This corneal primordium was dissected out and processed for histopathological analysis. The characterization of this adherent, miniature eye primordia-derived, complex corneal tissue is discussed in detail in **section 4.1.9.1b**.

To establish robust protocols to generate corneal primordial structures and to understand their step-wise development and maturation *in vitro*, hiPSC-F2-3F line was differentiated into EFP without the addition of Noggin, a BMP inhibitor. The EFP that emerged at 4 weeks of differentiation, when allowed to continue in adherent cultures, gave rise to SEAM-like outgrowths as reported earlier (Hayashi *et al.* 2016) (**Fig 4.12.B**). However, when the EFP at 4 weeks were immediately scooped and cultured in suspension, about 40.05±3.89% EFP gave rise to distinct, transparent, fluid-filled corneal primordial (CP) structures, along with the retinal primordia (RP) (n=6) (**Fig 4.12.C**). These RPs and CPs were then dissected out and cultured in isolation for their further maturation *in vitro* and for stage specific characterizations (**Fig 4.12.D, E**). It was observed that, it was critical to excise EFP and initiate suspension cultures before the surface ectodermal cells and neural crest cells migrate out of the EFP to ensure proper self-organization of different retinal cell types, resulting in successful induction and generation of complex 3D corneal organoids.

The delicate corneal primordia (CP) like structures (**Fig 4.13.i.A**), when excised and fixed for histopathological analysis, collapsed immediately due to leakage of fluids, resulting in loss of structural integrity (**Fig 4.13.i.B**). On histopathological analysis, it was found that these CPs contained a bi-layered epithelium that did not express PAX6 or TP63, but the peripheral cells expressed vimentin (**Fig 4.13.i.C**, **D**, **F**) at this early developmental stage. Further, two niche-like organizers were also observed at the stalk ends of the corneal primordia which contained actively dividing cells, as marked by Ki67 expression (**Fig 4.13.i.B, E**). Together it

was clear that the fluid filled corneal primordia is at an early developmental phase and were, therefore, allowed to mature in **corneal differentiation medium, CDM** – DMEM-F12 containing EGF (10 ng/mL), FGF (5 ng/mL), insulin (5 µg/mL) and N2 supplement (1%) (**Fig 4.12.E**). The characterization of these corneal primordia is discussed in detail in **section 4.1.9.1a**.

4.1.9.1. Characterization of 3D corneal organoids

4.1.9.1a. Floating corneal organoids

The transparent and fluid-filled corneal primordia at 2 weeks in suspension culture (**Fig 4.13.ii.A**), when further allowed to mature in CDM, grew in size, lost the transparency and became stable structures at about 6 weeks (**Fig 4.13.ii.B**). Histopathological analysis of 6-weeks old floating corneal primordia grown in CDM revealed that they had matured and displayed a stratified epithelium on the surface and a thick stroma that replaced the fluid filled lumen to confer structural rigidity (**Fig 4.13.ii.B**). Almost all the cells of the stratified epithelium expressed corneal epithelial markers PAX6/K12; and P63 expression was observed in the basal epithelial cells (**Fig 4.13.ii.D**-**F**). The $PAX6^+$, $K12^+$ epithelial cells had a distinct basement lining that clearly demarcated the epithelium from the $Vimentin^+$ stromal cells (**Fig 4.13.ii.C**). Although obtaining a miniature eye like structure and a well-developed minicorneal organoid in adherent cultures was a rare event (**Fig 4.12.B'**), we consistently obtained minicorneal organoids in about 40% of the EFP in suspension culture, as shown in **Fig 4.13.i.A**. The organoids were just about 2 mm in diameter (roughly about $1/6^{th}$ the size of an adult human cornea) and cannot serve as direct and immediate substitutes of adult donor corneas in surgical applications. However, they carry cornea-specific stem cells at early developmental stages that can be used in various regenerative applications. Therefore, it was checked if the epithelial cells of the developing minicorneal organoids could form uniform sheets of corneal epithelium similar to that of adult limbal stem cell derived tissue grafts, when grown on human amniotic membrane (hAM)(Fatima et al. 2006; Mariappan et al. 2010). For this, the floating corneal primordia cultured in CDM for 6 weeks were taken and dissected to separate the niche-like organizers and the corneal epithelial region. This corneal epithelial region of the CP was further cut into fine pieces and cultured as explants on de-epithelialized hAM. Epithelial cells migrated out of the explants and formed uniform cell sheets covering the entire hAM (**Fig 4.14.iii.A**). IHC examination of these cell sheets for the expression of PAX6, P63 and K12 confirmed their corneal epithelial cell identity (**Fig 4.14.iii.B**, **C**). Such corneal epithelial cell sheets have great value in basic research and in

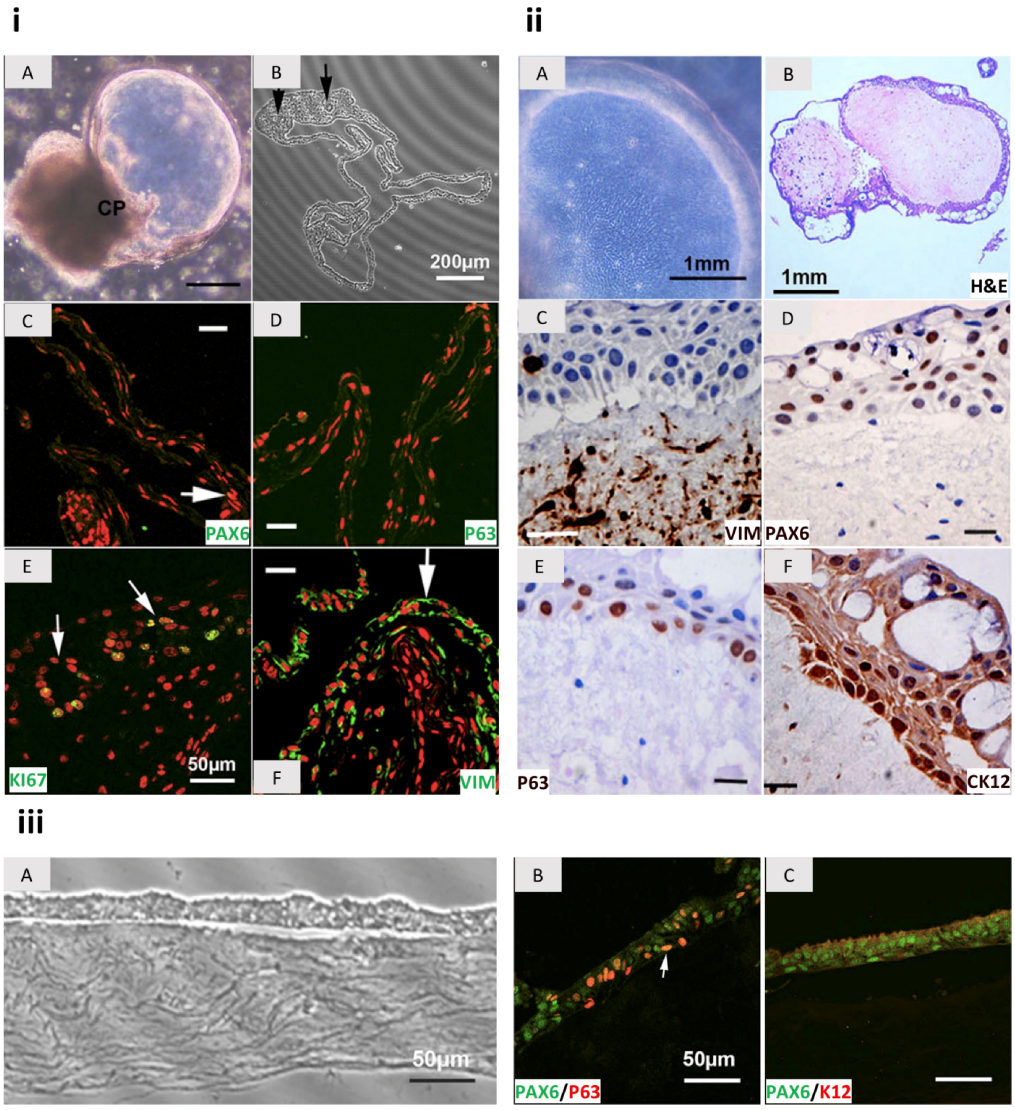

Figure 4.13: Characterization of floating mini-corneal organoids obtained by suspension culture. *i) Corneal primordia excised from 4 weeks old EFPs were maintained in suspension culture for further 2 weeks.* ***A****. Phase contrast image of fluid-filled, transparent, fragile corneal primordia (Scale bar: 1mm)* ***B****. Phase contrast image of 6 weeks old CP showing a bi-layered epithelium and a fluid filled lumen that collapsed upon fixation due to leakage of internal fluid. Arrows indicate the 'niche' like organizers* ***C, D****. Fluorescence microscopic images showing the absence of expression of PAX6 and TP63 in the cells of the bi-layered epithelium.* ***E****. Dividing cells at the niche are marked by Ki67 expression.* ***F****. Peripheral cells close to the niche-like organizers express Vimentin in 6 weeks old, floating CPs. (Scale bars* ***C-F****: 50 µm).* ***ii)*** *Matured corneal organoid cultured in CDM suspension for further 4 weeks.* ***A****. Phase contrast image of 10 weeks old corneal organoid showing an highly organized stratified squamous epithelial cells.* ***B****. H&E stained section of a 10 weeks old corneal organoid showing stratified epithelium and a thick stroma that replaced the fluid filled lumen.* ***C****. The stroma is clearly demarcated and is marked by Vimentin expression.* ***D, F****. The cells of the epithelial layer expressed PAX6 in the nucleus and K12 in the cytoplasm, thus confirming their corneal identity.* ***E****. The basal cells of the epithelium expressed TP63, as in native corneal tissues. (Scale bars* ***C-F****: 20 µm)* ***iii)*** *Corneal organoid derived epithelial sheets on hAM.* ***A****. Phase contrast image of a section of corneal organoid derived epithelial sheet grown on denuded hAM.* ***B, C****. The epithelial cells grown as sheets on hAM expressed the corneal epithelial markers, PAX6, TP63 and K12. Arrow indicate the cells expressing both PAX6 and P63. (Scale bars: 50 µm)*

regenerative applications for the treatment of corneal surface defects such as the limbal stem cell deficiency (LSCD) (Ramachandran *et al.* 2014).

4.1.9.1b. Adherent corneal organoid

The corneal primordia that had developed on the anterior side of the miniature eye-like structure (**Fig 4.12.B'**, **4,14.A**) was rigid and was cut into four quadrants using a surgical blade and processed for histopathological analysis. H&E stained section of one of the quadrants of corneal primordia displayed a striking similarity to an adult cornea and thus confirming the possibility of generating fully developed corneal organoid *in vitro* (**Fig 4.14.B**). This corneal organoid consisted of a central corneal region and a peripheral conjunctival region with a limbus like transition zone in between. The corneal region possessed stratified epithelium that expressed PAX6, P63 and CK12 and the conjunctival epithelial cells expressed MUC2 (**Fig 4.14.C.i-iii**,**v**). CK12 expression was confined to corneal epithelium and MUC2 expressing goblet cells were confined to the conjunctival epithelium and displayed a higher order cellular organization, in striking similarity to that of a native cornea. The stroma was clearly demarcated marked by the expression of Vimentin (**Fig 4.14.C.iv**). Such well-developed 3D corneal organoids of such complexity can serve as excellent *in vitro* models to study human corneal development, corneal diseases and also for testing promising drugs in pre-clinical screening and validations.

4.1.9.2. Characterization of 3D retinal organoids

The retinal primordial structures that were excised and cultured in NRM suspension organized themselves into well laminated complex structures in 1 month (**Fig 4.15.i.A**). Histological analysis of these structures revealed developing optic cup morphology with an inner and an outer layer (**Fig 4.15.i.B**). Upon immunohistochemistry it was found that the cells in the inner layer of the cups were CHX10, Recoverin and PAX6 positive indicating their neuro-retinal commitment, thus mimicking the early embryonic retinal development (**Fig 4.15.i.C, D**). These optic cups also expressed the general neuron-specific markers acetylated tubulin and Nestin and photoreceptor precursor marker CRX (**Fig 4.15.i.E-G**). These optic cups when allowed to mature in RDM for another month, showed visible lamination and cellular organization, with developing photoreceptor precursor cells lining the outer margins and immature precursors on the basal side. This was confirmed by PAX6 positive retinal precursor with Recoverin expressing photoreceptors lined on the outer margins of maturing retinal organoids as shown in **Fig 4.15.i.D**. IHC analysis of these two months old retinal organoids also revealed that they contained almost all the retinal cell types

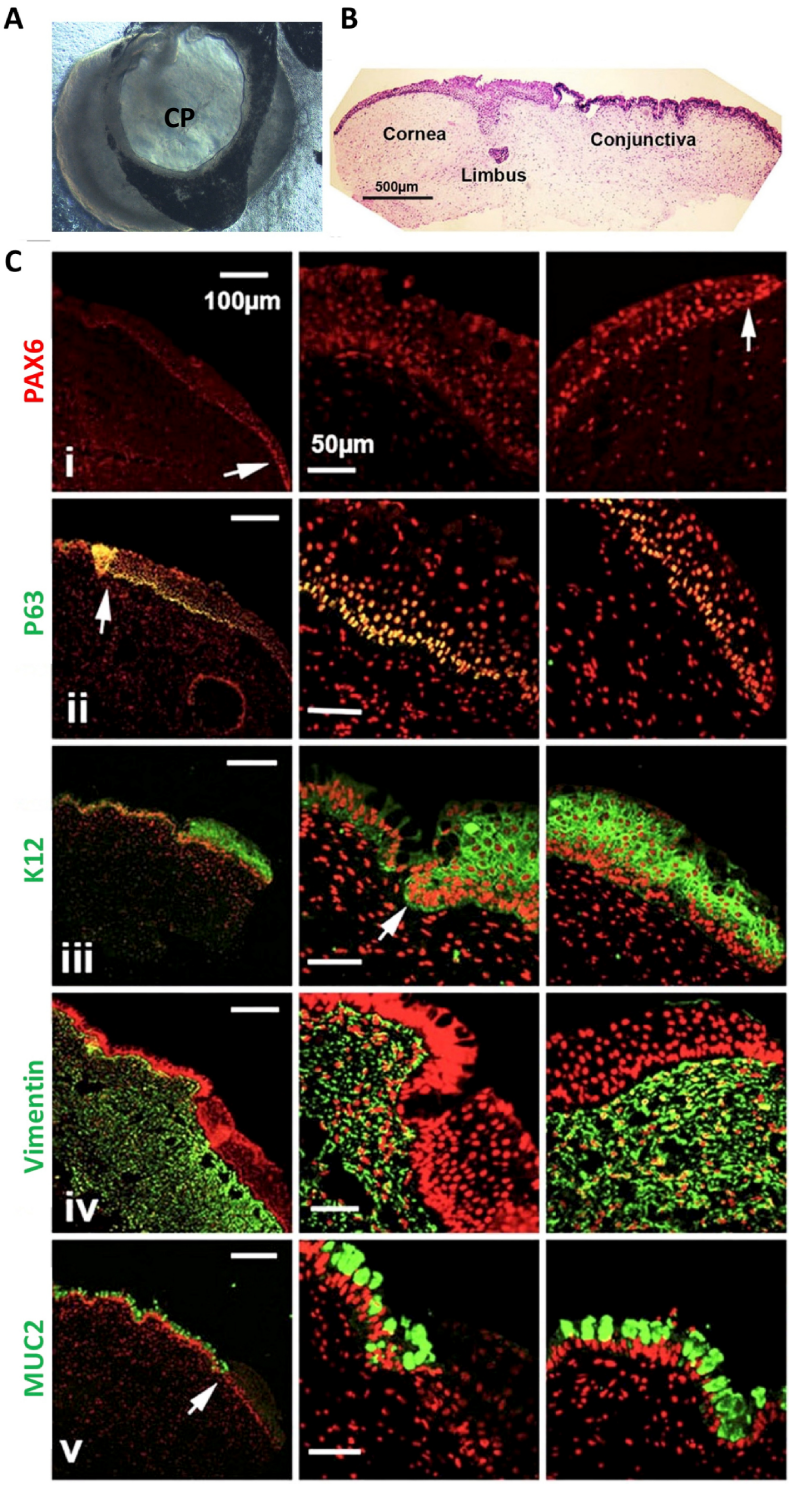

Figure 4.14: Characterization of a four months-old mature corneal organoid that developed in adherent cultures.

A. *Phase contrast image of a miniature eye-like primordia showing a transparent cornea-like structure (CP) developing on the anterior surface.*

B*. H&E stained section of the corneal organoid showing the central corneal region, the peripheral conjunctival region and a limbus-like transition zone.*

C*. Confocal images of tissue sections of the corneal organoid showing the expression of various corneal markers.* ***i)*** *PAX6 expression (in red) confirms the corneal identity of the surface epithelium (arrows).* ***(ii-v)*** *Other corneal markers stained in green and counterstained with PI in red.* ***ii)*** *Basal epithelial cells expressed p63 and* ***iii)*** *the supra-basal differentiated epithelial cells expressed K12, in the corneal region.* ***iv)*** *Vimentin^{+} cells filled the entire stroma, thus confirming their neural-crest origin.* ***v)*** *MUC2^{+} goblet cells were observed only within the peripheral conjunctival epithelium. (arrows indicate the limbal-transition zone). Scale bar, First column: 100 µm, second and third column: 50 µm.*

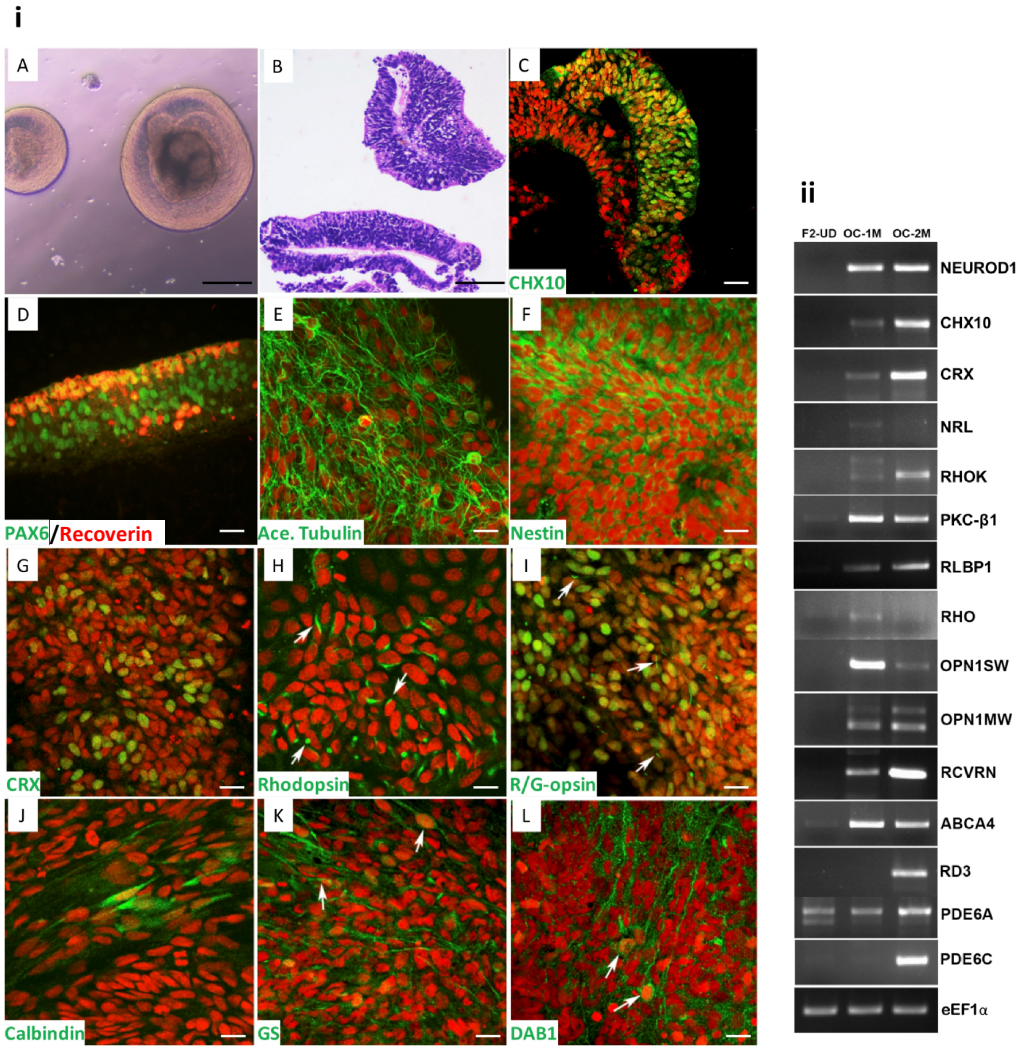

Figure 4.15: Characterization of three dimensional optic cups and retinal organoids. i) A. *Phase contrast image of 3D optic cups in suspension culture.* ***B.*** *H&E stained section of optic cups showing laminated arrangement of cells in double layers.* ***C.*** *Confocal images of 1 month old optic cup section showing the expression of neuro-retinal commitment marker, CHX10 (in green), exclusively in the inner layer and the sections were counter stained with PI (in red).* ***D.*** *The 3D optic cups cultured for 1 month on a collagen matrix showed the presence of early neuro retinal precursors on the basal side, as marked by the expression of PAX6 (in green) and developing photoreceptor precursors on the outer surface, as marked by the expression of Recoverin (in red). When the OCs were allowed to adhere and grow on Matrigel coated plates, the precursor cells differentiated into various retinal cell types and expressed the general neuron-specific markers acetylated tubulin (**E**) and Nestin (**F**) and early photoreceptor marker CRX (**G**). The optic cups that had matured into retinal organoids after 2 months in suspension culture expressed mature rod photoreceptor marker Rhodopsin (**H**), mature cone photoreceptor marker R/G-opsin (**I**), (Arrows indicate the outer segment like projections that are stained positive for Rhodopsin and R/G-opsin, **H, I**), bipolar cell marker, Calbindin (**J**), muller glia marker, glutamine synthetase, GS (**K**) and the retinal ganglion cell marker, DAB1 (**L**). Arrows indicate the neuronal cell body (**K,L**). Scale bars **A,B**: 0.5 mm **C**:100 µm, **D**: 50 µm, **E-L**: 20 µm.* ***ii)*** *RT-PCR profiles of optic cups at 1 month and retinal organoids at 2 months of differentiation showing the expression of early and mature neuro-retinal markers: NEUROD1, CHX10, CRX, NRL and visual transduction genes: RHOK, PKCβ1, RLBP1, RHO, OPN1SW, OPN1MW, RCVRN, ABCA4, RD3, PDE6A and PDE6C. The cDNA samples were normalized using eEF1α as the loading control.*

such as the rod cells (Rhodopsin$^+$), the cone cells (R/G-opsin$^+$), the bipolar cells (Calbindin$^+$), Müller glial cells (GS$^+$) and the retinal ganglion cells DAB1$^+$ (**Fig 4.15.i.H-L**). RT-PCR profiling of these organoids (**Fig 4.15.ii**) revealed the expression of early neuro-retinal markers, CHX10, NEUROD1, NRL and CRX; and visual transduction genes such as, RLBP1, RHO, RCVRN, PDE6A, PDE6C, PKC-β1, OPN1SW, OPN1MW, RHOK and more importantly, ABCA4 (ATP binding cassette, subfamily A member 4) and RD3 (retinal degeneration 3).

These results confirmed that the EFP self-organized to form optic cups in suspension cultures, which further matured to become retinal organoids containing all the cell types of an adult retina. The expression of ABCA4 and RD3 in the retinal organoids provided the assurance that such retinal organoids when derived from hiPSC-KR-3F and hiPSC-VS-3F would serve as ideal *in vitro* models of ARRD and LCA12.

4.1.10. Characterization of patient-specific iPSCs with mutation in *ABCA4*

As mentioned earlier in **section 4.1.7.6**, hiPSC-KR-3F differentiated into poorly organized EFP that when manually picked and cultured, preferentially differentiated towards RPE lineage over neuro-retinal lineage. The RPE precursors developed intense pigmentation at an early time point compared to the other two lines. Recent reports have confirmed that ABCA4 is also expressed in RPE cells and functions as the retinal flippase as it does in the photoreceptors (Lenis *et al.* 2018). Therefore, the enriched RPE cultures derived from hiPSC-KR-3F cells were further compared with that of hiPSC-F2-3F cells. On phase contrast imaging, unlike the compact hiPSC-F2-RPE sheet, the hiPSC-KR-RPE cells displayed illuminated boundaries that could be due to compromised cell-cell junctions that allowed the light to pass through them (**Fig 4.16.A**). On RT-PCR profiling (**Fig 4.16.E**), it was found that both iPSC-KR-RPE and hiPSC-F2-RPE expressed RPE specific markers MITF, TYR and RPE65. However, iPSC-KR-RPE clearly showed reduced levels of ABCA4 transcripts, when compared to hiPSC-F2-RPE. This was further confirmed by quantitative RT-PCR which showed a four-fold decrease in the ABCA4 transcript levels in hiPSC-KR-RPE, when compared to hiPSC-F2-RPE ($p=0.03$) (**Fig 4.16.F**). This could be due to nonsense mediated decay of ABCA4 transcripts, triggered by the premature stop codon generated due to c.6088C>T variation in hiPSC-KR-RPE. By immunocytochemistry, ABCA4 protein expression could be detected, and its localization was confined to to apical membranes and cell-cell boundaries, in hiPSC-F2-RPE cells, thus confirming the earlier reports about the presence of ABCA4 in RPE cells (Lenis *et al.* 2018).

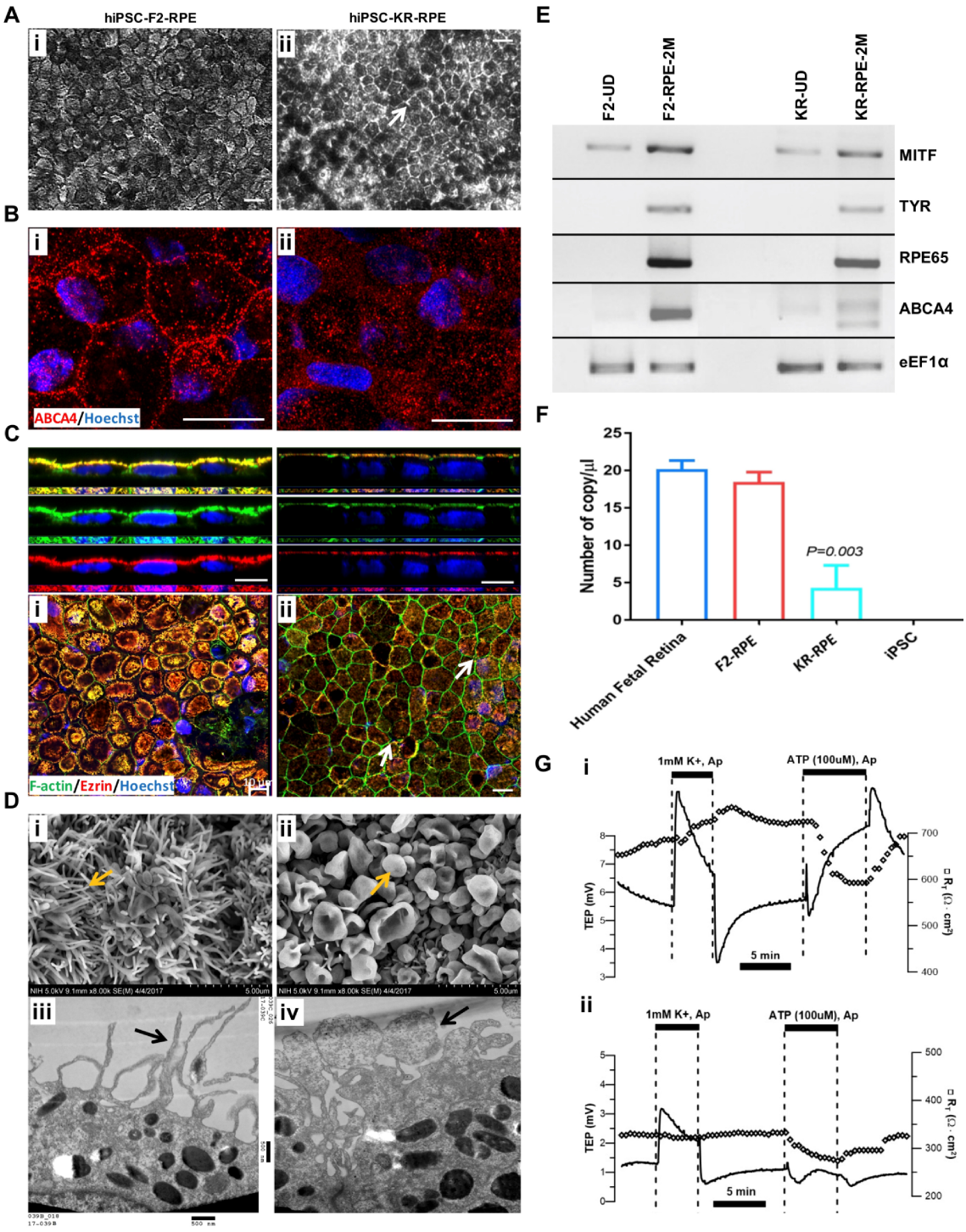

Figure 4.16: Validation of hiPSC-KR-RPE as in vitro ARRD model. *Comparative analysis of the RPE cell morphology, cell surface marker protein expression, apical structural integrity, gene expression and ion transport between hiPSC-KR-RPE and hiPSC-F2-RPE cells cultured on trans-well membranes in RPEM medium.* ***A****. Phase contrast images showing hexagonal shaped, tightly packed hiPSC-F2-RPE cells* ***(i)*** *and hexagonal hiPSC-KR-RPE cells with illuminated cell boundaries, indicating compromised cell-cell junctions (arrows)* ***(ii)****.(Scale bar: 20µm)* ***B****. Immunostaining for ABCA4 showing the presence of ABCA4 (in red) at cell boundaries and on*

*apical membrane surfaces of hiPSC-F2-RPE (**i**) and its near absence in hiPSC-KR-RPE cell (**ii**). Scale bar: 10 µm. **C**. Confocal images of RPE cells immune-stained for F-actin, the cytoskeletal protein (in green) and Ezrin, the cross linker protein between the plasma membrane proteins and the actin cytoskeleton (in red). The cells were counter stained with Hoechst dye in blue. Merged and single channel z-plane images are displayed in the top panels and the 2D images are displayed in the bottom panels. The levels of both F-actin and Ezrin were significantly lower in hiPSC-KR-RPE (**ii**) when compared with hiPSC-F2-RPE cells (**i**). Gaps were observed between cell boundaries (arrows) indicating that hiPSC-KR-RPE cells were not tightly packed. Scale bar: 10 µm. **D**. Scanning electron microscopy (**i,ii**) and transmission electron microscopy (**iii,iv**) images of hiPSC-F2-RPE (**i,iii**) and hiPSC-KR-RPE (**ii,iv**) showing finger like apical villi-projections (arrows) in hiPSC-F2-RPE and a distorted apical surface, with blob like apical projections in hiPSC-KR-RPE (arrows). Scale bars: 5 µm (**i,ii**), 500 nm (**iii,iv**). **E**. RT-PCR profiles of 2 months old hiPSC-F2-RPE and hiPSC-KR-RPE cells showing the expression of RPE-specific markers MITF, TYR, RPE65 and ABCA4. The transcript levels of ABCA4 were lower in hiPSC-KR-RPE when compared to hiPSC-F2-RPE cells. The cDNA samples were normalized using eEF1α as the loading control. **F**. Bar graph representing the transcript levels of ABCA4 quantified by real time PCR. ABCA4 levels in hiPSC-KR-RPE were four times lower than that of hiPSC-F2-RPE cells. P=0.003. **G**. Electrophysiological readings show significantly decreased resting TEP, trans-epithelial potential (solid line) and TER, trans-epithelial resistance (◇) and weakened electrical responses to external physiological stimuli (reduction in K^+ ion concentration and addition of ATP in the apical bath) in hiPSC-KR-RPE cells when compared to hiPSC-F2-RPE cells, which signifies impaired electrophysiological functioning of hiPSC-KR-RPE cells. Horizontal bars indicate the duration of presentation of the external stimuli.*

The ABCA4 protein was almost absent and the staining appeared to be more diffused in hiPSC-KR-RPE. Thus, this study was successful in deriving monolayers of hiPSC-KR-RPE cells, as an *in vitro* model system of ARRD with c.6088C>T variation in the *ABCA4* gene.

Further comparative analysis of hiPSC-KR-RPE cells with hiPSC-F2-RPE cells was done by immunostaining for RPE specific membrane proteins and SEM/TEM imaging of the apical processes. Upon immunostaining, it was found that hiPSC-KR-RPE cells were not as tightly packed as hiPSC-F2-RPE and had disorganized actin cytoskeletal bundles, marked by F-actin, and reduced expression and mislocalization of Ezrin, a cell membrane-cytoskeleton cross linker protein (**Fig 4.16.C**). SEM and TEM analysis of RPE cell surface showed a completely distorted apical membrane surface, with microvilli projections that were modified into blob like structures in hiPSC-KR-RPE cells, whereas the hiPSC-F2-RPE cells had a typical finger like apical microvilli projections (**Fig 4.16.D**).

This study also checked and compared the epithelial barrier function and ion-transport function of hiPSC-KR-RPE cells with that of hiPSC-F2-RPE cells by electrophysiology experiments (Blenkinsop *et al.* 2015; Maminishkis *et al.* 2006; Miyagishima *et al.* 2016; Quinn R H and Miller 1992). Confluent monolayers of hiPSC-F2-RPE and hiPSC-KR-RPE grown on trans-well membranes were carefully removed from the trans-wells and were mounted in Ussing chambers containing an apical bath and a basal bath of Ringer's solution (Quinn R H

and Miller 1992). Two electrodes, one in the apical bath and the other in the basal bath were used to measure the trans-epithelial potential (TEP) (mV). Pulses of current ranging from 2-8 μA were passed through the RPE cell sheets grown on membranes and the ability of the cell sheets to resist the flow of current was measured as trans-epithelial resistance, TER ($\Omega.cm^2$). TEP and TER measurements together, demonstrate the integrity and tight packing of RPE cells and ultimately signifying the maturity and proper functioning of the cells. The apical and basal electrode measurements showed that the resting TEP of hiPSC-F2-RPE were in the range of 5.5-6.5mV and the resting TER was between 650-700 $\Omega.cm^2$ (**Fig 4.16.G.i**). The hiPSC-KR-RPE possessed a drastically decreased resting TEP in the range of 1.2-1.3 mV and a correspondingly decreased resting TER in the range of 300-330 $\Omega.cm^2$ (**Fig 4.16.G.ii**), thus confirming that the barrier functions are compromised in hiPSC-KR-RPE cells.

Further, to validate the electrophysiological response of the RPE cells to external physiological stimuli, K^+ ion concentration in the apical bath was reduced. This mimics the reduction in the K^+ ion concentration in the interstitial/sub-retinal space (space between RPE and photoreceptors) *in vivo* during the transition from the dark phase to the light phase. Native RPE cells respond to the decreased K^+ concentration in the sub-retinal space by Kir7.1 channel protein (located in the apical membrane) mediated effluxing of K^+ ions into the sub-retinal space, to maintain K^+ ion homeostasis in the sub-retinal space (Pattnaik *et al.* 2013; Shahi *et al.* 2017; Yang *et al.* 2003). In the electrophysiology experiments of the present study, upon replacing the apical bath with Ringer's solution containing reduced K^+ concentration (1 mM), the TEP of hiPSC-F2-RPE membrane sheets spiked to 9 mV from 5.5 mV, which then steadily lowered down to the resting phase-TEP levels, whereas in hiPSC-KR-RPE membrane sheets, the TEP rose only to 3.1 mV from 1.2 mV, which then gradually lowered up to 2 mV, without restoring the resting phase transmembrane potential. This result confirmed an impaired apical Kir7.1 channel protein activity in hiPSC-KR-RPE cells.

It has been well established that RPE cell sheets respond to adenosine triphosphate (ATP) and evoke a purine receptor (located in the RPE apical membrane) mediated electrophysiological response, and releases Ca^{2+} ions in the apical bath (Peterson *et al.* 1997). The presence of ATP in the sub-retinal space could be from the damaged photoreceptors (Peterson *et al.* 1997) or from the RPE cells itself (Mitchell and Reigada 2008). Continuing with the electrophysiological experiments, the apical bath of the Ussing chamber was replaced with Ringer's solution containing 100 μM ATP. hiPSC-F2-RPE cells displayed

characteristic electrophysiological response to ATP as reported previously (Blenkinsop *et al.* 2015; Maminishkis *et al.* 2006; Miyagishima *et al.* 2016; Peterson *et al.* 1997). However, the hiPSC-KR-RPE displayed a negligible response to ATP (**Fig 4.16.G**). Taken together, the electrophysiological experiments confirmed that hiPSC-KR-RPE cells had a significantly impaired membrane integrity and showed poor response to external stimuli. These results correlate well with the observation of distorted apical processes and tight junctions (**Fig 4.16.C,D**) in hiPSC-KR-RPE, thus affecting the functioning of membrane bound channel proteins.

Together the above results confirmed that the expression of ABCA4 is crucial for normal RPE cellular functions, apart from its well-known functions in photoreceptors. Further global gene expression studies on hiPSC-KR-RPE cells and neuro-retinal precursors is required to elucidate the exact mechanisms leading to preferential RPE cell fate commitment and maturation defects upon ABCA4 loss of expression and function.

4.1.11. Characterization of patient-specific iPSCs with mutation in *RD3*

With the optimized retinal differentiation protocol discussed earlier (**sections 4.1.8 and 4.1.9**), mature RPE cells and three-dimensional retinal organoids were obtained from hiPSC-VS-3F and the control line, hiPSC-F2-3F. The hiPSC-VS-3F derived retinal organoids, hiPSC-VS-OC (**Fig 4.17.A.ii**) and mature RPE cells, hiPSC-VS-RPE (**Fig 4.17.B.ii**) were then compared with that of hiPSC-F2-3F derived retinal organoids (hiPSC-F2-OC) (**Fig 4.17.A.i**) and mature RPE cells (hiPSC-F2-RPE)(**Fig 4.17.B.i**).

The hiPSC-VS-RPE cells did not display any significant difference in their differentiation timeline when compared to hiPSC-F2-RPE cells. The hiPSC-VS-RPE cells exhibited typical cobblestone morphology (**Fig 4.17.B.ii**), expressed tight junction marker, ZO-1 (**Fig 4.17.B.iv**), and had comparable pigmentation levels as that of hiPSC-F2-RPE (**Fig 4.17.B.i,ii**). Also, the hiPSC-VS-RPE cells expressed mature RPE marker, RPE65 (**Fig 4.17.B.vi**) and exhibited phagocytic activity, as marked by the internalization of FITC-beads (**Fig 4.17.B.viii**). RT-PCR profiling confirmed the expression of early commitment RPE marker (MITF) and RPE-specific, mature cell markers (TYR and RPE65) in hiPSC-VS-RPE, at levels comparable to that of hiPSC-F2-RPE cells (**Fig 4.17.C.ii**). In short, there was no significant difference between hiPSC-VS-RPE and hiPSC-F2-RPE in the differentiation timelines, RPE cell morphology, pigmentation, gene expression profiles, presence of tight junctions, expression of early and late RPE-specific markers and phagocytic activity.

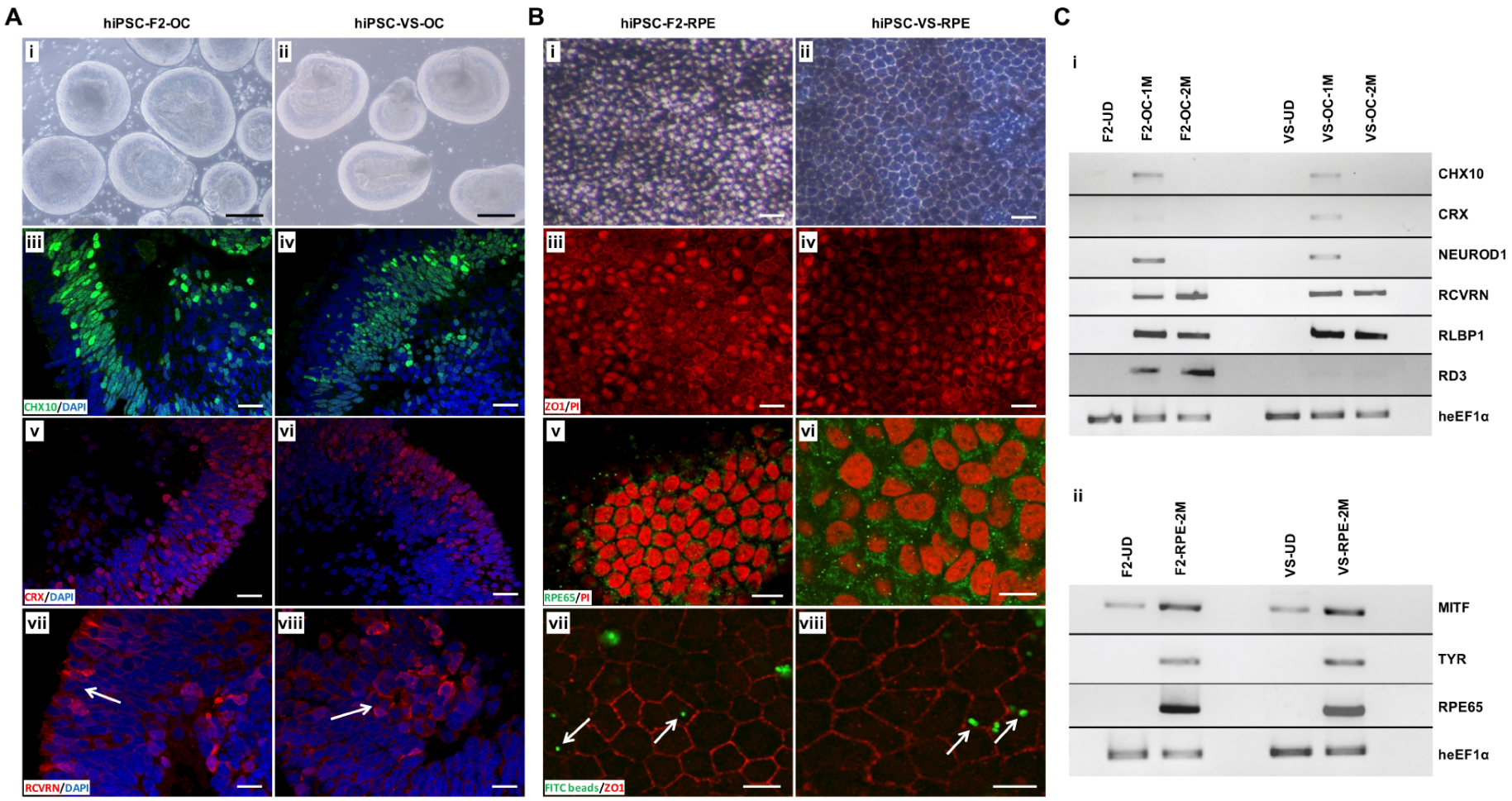

Figure 4.17: Validation of hiPSC-VS-OC as in vitro LCA12 model. A. *Comparison of hiPSC-VS-OCs with hiPSC-F2-OCs. Phase contrast images of 1 month old optic cups in suspension culture* ***(i,ii)****. Confocal images of OC sections immuno-stained for retinal markers and counter stained with DAPI (in blue)* ***(iii-viii)****. One month old optic cups expressing the early neuro-retinal marker CHX10 (in green)* ***(iii,iv)*** *and committed photoreceptor marker, CRX (in red)* ***(v,vi)****.* ***(vii,viii)****. Two months old retinal organoids, expressing mature photoreceptor marker, RCVRN (Recoverin in red)* ***(vii, viii)****. Arrows indicate cellular lamination and organization*

*of photoreceptor precursor cells on the outer layers of hiPSC-F2 retinal organoids (**vii**). hiPSC-VS retinal organoids display altered lamination (arrows) and randomly arranged photoreceptors (**viii**). Scale bars: 1mm (**i,ii**), 20 μm (**iii-viii**). **B**. Comparison of 2 months old hiPSC-VS-RPE and hiPSC-F2-RPE cells. Phase contrast image of RPE monolayers matured on trans-wells showing intense pigmentation and cobblestone morphology (**i,ii**). Confocal images of RPE cell sheets immuno-stained with mature RPE markers and counter stained with PI (in red) (**iii-vi**). Both hiPSC-F2-RPE and hiPSC-VS-RPE cells expressed tight junction marker, ZO-1 (in red) (**iii,iv**) and mature RPE-specific marker, RPE65 (in green) (**v,vi**). Both hiPSC-F2-RPE and hiPSC-VS-RPE cells exhibited phagocytic ability, as marked by the internalized FITC labeled 1 micron sized latex beads (green). Arrows indicate the internalized FITC beads and the cell boundaries are marked by ZO-1 in red (**vii,viii**). Scale bars: 20 μm (**i-vi**), 10 μm (**vii,viii**). **C.** RT-PCR profiles of retinal organoids (**i**) and RPE monolayers (**ii**) derived from hiPSC-F2-3F and hiPSC-VS-3F. Both hiPSC-VS-OCs and hiPSC-F2-OCs expressed the early retinal markers CHX10 and NEUROD1; early photoreceptor marker, CRX and mature photoreceptor markers, Recoverin and RLBP. The RD3 transcript levels were significantly low in hiPSC-VS-OCs when compared to hiPSC-F2-OCs (i). Both hiPSC-VS-RPE and hiPSC-F2-RPE cells expressed RPE specific markers, MITF, TYR and RPE65 at comparable levels, with no significant difference (ii). The cDNA samples were normalized using eEF1α as the loading control.*

The hiPSC-VS-OCs appeared very similar to hiPSC-F2-OC with a defined spherical morphology (**Fig 4.17.A.i,ii**). By immunohistochemistry (**Fig 4.17.A.iii**-**viii**) and RT-PCR profiling (**Fig 4.17.C.i**) it was found that the hiPSC-VS-OCs expressed both the early photoreceptor (CHX10, NEUROD1, CRX) and mature photoreceptor markers (RCVRN, RLBP1) at levels comparable to that of hiPSC-F2-OCs.

However, the RD3 transcripts in hiPSC-VS-OCs were significantly less and almost negligible when compared to its levels in hiPSC-F2-OCs (**Fig 4.17.C.i**). This could be attributed to nonsense mediated decay of RD3 transcript due to the presence of premature stop codon in intron 2, which is included in the transcript due to the donor splice site c.296.G→A mutation in hiPSC-VS-OCs.

The presence of RD3 protein could not be confirmed even in hiPSC-F2-OC due to lack of suitable antibodies and other technical difficulties. However, a significantly altered lamination pattern was noticed in hiPSC-VS-OC when compared to hiPSC-F2-OC (**Fig 4.17.A.vii**, **viii**). The RCVRN positive photoreceptor cells were neatly arranged in the outer layers of the mature hiPSC-F2-OCs and displayed proper lamination (**Fig 4.17.A.vii**). In contrast, the photoreceptor cells of hiPSC-VS-OC were distributed throughout the retinal organoid indicating the inability of hiPSC-VS-OCs to form properly laminated retinal organoids (**Fig 4.17.A.viii**). An in-depth molecular characterization on hiPSC-VS-OCs is required in future to fully elucidate the exact roles of RD3 in retinal progenitor cell maturation, lamination and function.

4.1.12. Characterization of human *RD3* promoter for the construction of retina-specific gene expression cassette

LCA12 is an autosomal recessive cone/rod dystrophy caused by homozygous mutations in *RD3* gene. This gene encodes a small protein of 195 amino acids and therefore a good candidate to test the proof-of-concept of *in vitro* gene therapy by transgene delivery into patient-specific cells, to rescue normal cellular functions. This requires the design of a suitable gene expression cassette and a vector system to achieve efficient transgene delivery, stable and optimal transgene expression in patient-specific iPSCs and/or retinal cells.

Since the disease affects both the rod and cone cells, it is preferable to consider a tissue-specific promoter that can drive optimal and stable RD3 expression in all photoreceptor cells. Hence, an attempt was made to clone and characterization the genes' own promoter and to validate its activity in different retinal and non-ocular cell types.

The genomic regions immediately upstream to human *RD3* gene was obtained from NCBI nucleotide database. A full length promoter (*RD3PFL* up to -2054 bp upstream to the *RD3* gene transcription start site, TSS) and a minimal RD3 promoter (*RD3PM* up to -400 bp upstream to the *RD3* gene TSS) was analyzed using Genomatix-Matinspector software and was found that both the *RD3PFL* and *RD3PM* promoter regions contained numerous retina-specific transcription factor binding sites such as, CRX, PAX6, RXR, NEUROD1 and VSX/CHX10 indicating that the promoters might confer high levels of retina specific activity (**Fig 4.18.A**).

RD3PFL and *RD3PM* promoter regions were PCR amplified and cloned upstream to the luciferase (*luc*) reporter gene of pGL3_basic vector and were transfected into non-retinal cell lines HEK, HCE and also into retinal cell lines ARPE-19 and Y79. After 48 hours, cell lysates were collected and subjected to luciferase reporter assay. The promoter strength and activity was quantified by a luminometer that measures the light emitted upon addition of luciferin (the substrate for luciferase). Relative light intensity differences were calculated as fold change values over a promoter less pGL3-Basic vector. The results revealed that the *RD3PM* is highly active in retinal cell lines, ARPE19 and Y79 cells, when compared to non-retinal cell lines, HEK 293T and HCE cells. Histone deacetylase (HDAC) inhibition by sodium butyrate (NaB) treatment was earlier shown to activate *CRX* and induce rod and cone specific gene expression and differentiation in Y79 cells (Peng and Chen 2007). The results of the present study also confirmed that NaB treatment of transfected cells significantly upregulated the *RD3PM* (4 fold) and *RD3PFL* promoters (6 fold) in retinal cells ($P<0.001$), while it repressed the promoter activity in HEK cells (2 fold) ($P<0.001$) and

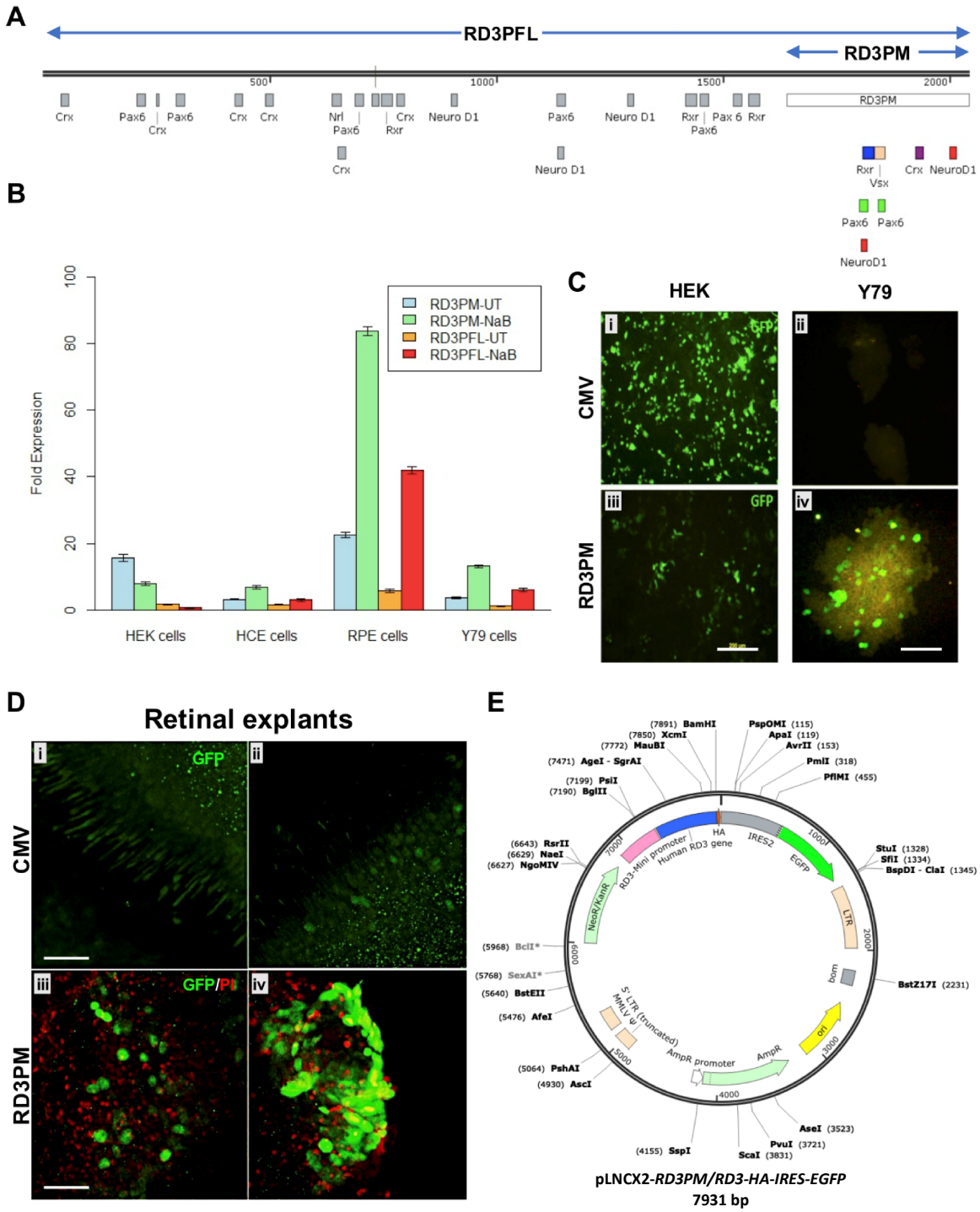

Figure 4.18: Characterization of human RD3 promoter and construction of retina-specific gene expression cassette. A. *Pictorial representation of the genomic regions upstream of human RD3 gene showing different retina specific transcription factor binding sites, as analyzed by Genomatix-Matinspector software. RD3 promoter full length, RD3PFL (-2054 bp upstream to RD3 transcription start site, TSS) and RD3 promoter minimal, RD3PM (-400 bp upstream to RD3 TSS).* ***B****. Bar graph representing the fold change in RD3 promoter activities (RD3PM and RD3PFL) with and without the addition of the HDAC inhibitor, sodium butyrate (NaB), in non-retinal and retinal cell lines. Error bars represents ± S.D. n=3.* ***C.*** *Anti-GFP immunostaining showing the levels of CMV and RD3PM promoter activities in HEK 293T and Y79 cells. Scale bars: 200µm (ii-iv).* ***D.*** *Anti-GFP immunostained images showing the activity of CMV and RD3PM promoters in cadaveric, retinalexplant cultures. Scale bar: 100 µm.* ***E****. Vector map of RD3 minimal promoter driven RD3 gene expression cassette cloned into the lentiviral vector, pLNCX2.*

the difference was low in HCE cells (P<0.05) (**Fig 4.18.B**). The *RD3PM* activity was 3-fold higher than *RD3PFL* without NaB treatment (P<0.001) and 2-fold higher with NaB treatment (P<0.001). Since the nucleotide sequence length of *RD3PM* was 5 times shorter than *RD3PFL* and its activity was 2-3 times higher than *RD3PFL* in retinal cells, the *RD3PM* promoter was considered for further characterization and validation.

Moving forward, the *RD3PM* promoter region was cloned upstream to an enhanced green fluorescent protein reporter (*EGFP*) gene, in place of the constitute *CMV* promoter of a lentiviral vector pLNCX2. The pLNCX2-*CMV*/EGFP construct was used as a positive control for comparative analysis. Both the pLNCX2-*CMV*/EGFP and pLNCX2-*RD3PM*/EGFP constructs were transfected to HEK and Y79 lines. After 48 hours of transfection, live-cell fluorescence imaging of GFP protein expression was checked in HEK and Y79 cells. As expected, the activity of *CMV* promoter was significantly higher than the activity of *RD3PM* in HEK cells (**Fig 4.18.C.i**, **iii**), measured by the intensity of GFP signal. GFP reporter expression in Y79 cells was weak, thus making it difficult to capture live cell images of floating cell clusters. In order to amplify and detect the GFP signal, the transfected cells were immuno-stained with anti-GFP and the results confirmed that *RD3PM* was significantly active in Y79 cells (**Fig 4.18.C.iv**) and the constitutive *CMV* promoter remained completely inactive (**Fig 4.18.C.ii**).

To confirm the activity of *RD3PM* in human retinal cells, native retinal tissue cultures were established, using retinal tissues isolated from cadaveric donor eye balls. Three days old cultures were transduced with lentiviruses prepared (**section 3.4.4**) from pLNCX2-*CMV*/EGFP and pLNCX2-*RD3PM*/EGFP constructs. After 72 hours following transduction, the retinal tissues were fixed and whole mounts were prepared and immuno-stained with anti-GFP. The results confirmed a significantly higher activity of *RD3PM* in the outer layers of the human retinal whole mounts (**Fig 4.18.D**), whereas the constitutive and ubiquitous *CMV* promoter showed an almost negligible activity. The higher activity of *RD3PM* in the outer retinal layers indicates its specific activity in photoreceptors cells.

Once the retina specific activity of *RD3PM* was confirmed, a complete *RD3* gene expression cassette containing the *RD3*-minimal promoter driving the expression of *RD3* gene was constructed as shown in **Fig 4.18.E**. The retina specific activity of *RD3PM* promoter will be further tested in iPSC-derived retinal organoids and in rat eyes. Further, the recombinant lentiviral vector containing the retina-specific *RD3* gene expression cassette will be used in proof-of-concept gene supplementation studies in hiPSC-VS-3F and in hiPSC-VS-OCs to evaluate the reversal of disease phenotype upon wild type gene supplementation.

4.2. Generation of an *in vivo* LCA12 disease model in Zebrafish

Recent reports have shown that iPSC-derived retinal organoids could be maintained in culture for longer durations to achieve morphological and functional maturation (Zhu *et al.* 2018). However, their gene expression signature mostly matches that of fetal stage retinal cells. Incomplete maturation of iPSC-derived tissues *in vitro* therefore has limitations to be considered as disease models to understand mature cell-specific functions and disease phenotypes. This requires a simpler *in vivo* animal model that would allow carrying out quick validations of several disease-specific mutations in fully developed adult retinal tissues.

Zebrafish models have various advantages owing to their small size, which enables easy maintenance, short generation time, high breeding ability and hence, relatively large clutch size, external fertilization, rapid development, transparent embryos, efficient genetic manipulations with simpler tools and easily testable developmental behaviors. With the advent of CRISPR-Cas9 based genome editing systems, zebrafishes have proven to be useful models in forward genetic studies to understand the functions of various genes and to elucidate the mechanisms behind inherited disease pathogenesis (Link and Collery 2015).

Further the visual system of zebrafish is strikingly similar to that of humans and 72% of the human genes have at least one ortholog in zebrafish. Few reports have shown them to be useful models to study various ocular disease conditions such as, retinoblastoma, glaucoma, retinitis pigmentosa (RP), ciliopathies and albinism (Link and Collery 2015). Therefore, mutant fishes with retinal dystrophy related gene-specific edits would serve as valuable *in vivo* models to understand the development of disease. Keeping this in mind, this study aimed to create *rd3* knock out models of zebrafish to be used as *in vivo* models of LCA12.

4.2.1. Sequence alignment of human *RD3* and zebrafish *rd3* loci

Human *RD3* sequence (Gene ID: 343035) and zebrafish *rd3* sequence (Gene ID: 791149) were obtained from the NCBI nucleotide database. Upon sequence alignment, it was found that the zebrafish *rd3* gene sequence was 74.76% identical to that of human *RD3* (**Fig 4.19.A**). Sequence alignment of human RD3 and zebrafish rd3 proteins showed 53% similarity (**Fig 4.19.B**).

A

Alignments | Download | GenBank | Graphics

Description	Max Score	Total Score	Query Cover	E value	Per. Ident	Accession
Danio rerio strain Tuebingen chromosome 20, GRCz11 Primary Assembly	1075	91314	0%	0.0	74.76%	NC_007131.7

B

Score	Expect	Method	Identities	Positives	Gaps
205 bits(522)	3e-72	Compositional matrix adjust.	109/207(53%)	141/207(68%)	20/207(9%)

```
Query  4    ISWLRWNEAPSRLSTRSPAEMVLETLMMELTGQMREAERQQRERSNAVRKVCTGVDYSWL  63
            +SW  WNE   R   R P+E+V +TLM+EL+ Q++EAER QRER N  R++ +GVDYSWL
Sbjct  1    MSWFSWNEPYYRSGRREPSEVVSDTLMLELSWQIKEAERLQRERDNEYRRLKSGVDYSWL  60

Query  64   ASTPRSTYDLSPIERLQLEDVCVKIHPSYCGPAILRFRQLLAEQEPEVQEVSQLFRSVLQ  123
             +TPRS+YD+SP ERL LED+C K+ PS+CG  I RFRQ+L E EPEVQEVS LFRSVL
Sbjct  61   MNTPRSSYDISPGERLGLEDLCSKVPPSHCGSVIQRFRQVLMENEPEVQEVSGLFRSVLV  120

Query  124  EVLERMKQEEEAHKLTRQWSLRPRGSLA--TFKTRARISPFAS----------------D  165
            E LER+ +E+EA +LT+QWS R   SL+  +F++  RI+PF S                D
Sbjct  121  ESLERVHEEQEAQRLTQQWSNRRSISLSLMSFRSGVRINPFGSTLGLKSNSYGSEEDGVD  180

Query  166  IRTISEDVERD--TPPPLRSWSMPEFR  190
            ++T+ EDVE+        R WSMPEFR
Sbjct  181  VKTVCEDVEKGQTAEKTRRVWSMPEFR  207
```

Figure 4.19: ***A.*** *Sequence alignment of human RD3 (Gene ID: 343035) with zebrafish rd3 (Gene ID: 791149) genes showing 74.76% identity (in red box).* ***B****. Sequence alignment of human and zebrafish rd3 proteins showing 53% identity (in red box).*

4.2.2. Design and generation of CRISPR guide RNAs to target zebrafish *rd3*

Two single guide RNAs (sgRNA) targeting the genomic regions adjacent to the *rd3* translation start site were designed using UCSC genome browser. Care was taken to exclude the guides that may have off-targets. Single stranded (ss) DNA oligos A containing the minimal T7 promoter sequence, sgRNA (target) sequence and a partial tracrRNA sequence, and a universal ss oligo B with a complementary tracrRNA sequence were synthesized (**section 3.14.1**). Oligo A and Oligo B were annealed (**section 3.14.2**) and extended to obtain the double stranded guide DNA template (Varshney *et al.* 2015) containing the T7 promoter region, the sgRNA sequence and the tracrRNA sequence as shown in **Fig 4.20.A.i**. The ds DNA oligo templates for the guides 1 and 2 were *in vitro* transcribed using T7 RNA polymerase (**section 3.14.3**) to obtain sgRNAs 1 and 2 (**Fig 4.20.A.ii**). The synthesized sgRNAs were checked for the quality and quantity as in **section 3.2.3** and stored in -80° C as 5 μL aliquots.

4.2.3. Validation of gRNAs by *in vitro* cleavage assay

Though the sgRNAs designed showed high efficiency *in silico* score to create double strand DNA breaks, it is important to check the actual DNA cleaving ability and target specificity of the synthesized sgRNAs *in vitro*.To check the target site DNA cleaving ability of the sgRNAs 1 and 2, the ribonucleoprotein (RNP) complex 1 and 2 was prepared by incubating sgRNAs 1 and 2 respectively with Cas9 protein at room temperature. Further, the RNP1 and RNP2 complexes were incubated with the target site DNA substrate (*rd3*-exon2 amplicon) in separate tubes and the cleavage products were analyzed in agarose gels (**section 3.14.4**). The results confirmed that both the RNP complexes were efficient in creating double strand break at the targeted genomic locus (**Fig 4.20.B**). The size of the *rd3*-exon 2 amplicon was 396 bp. The target site of sgRNA1 was 61 bp away from the first nucleotide of the amplicon. Agarose gel electrophoresis (AGE) after *in vitro* cleavage (IVC) assay, showed the presence of two cleaved products of sizes 335 bp and 61 bp. Similarly, the target site of sgRNA2 was 152 bp away from the first nucleotide of the amplicon. IVC assay resulted in two cleaved products of sizes 244 bp and 152 bp. Thus, both the sgRNAs were tested and proved to be efficient in creating double strand breaks at the targeted genomic locus.

4.2.4. Genome editing of zebrafish embryos

Once the efficiency of the sgRNAs 1 and 2 to create double strand DNA breaks at the genomic region of interest was confirmed, genome editing of zebrafish embryos was carried

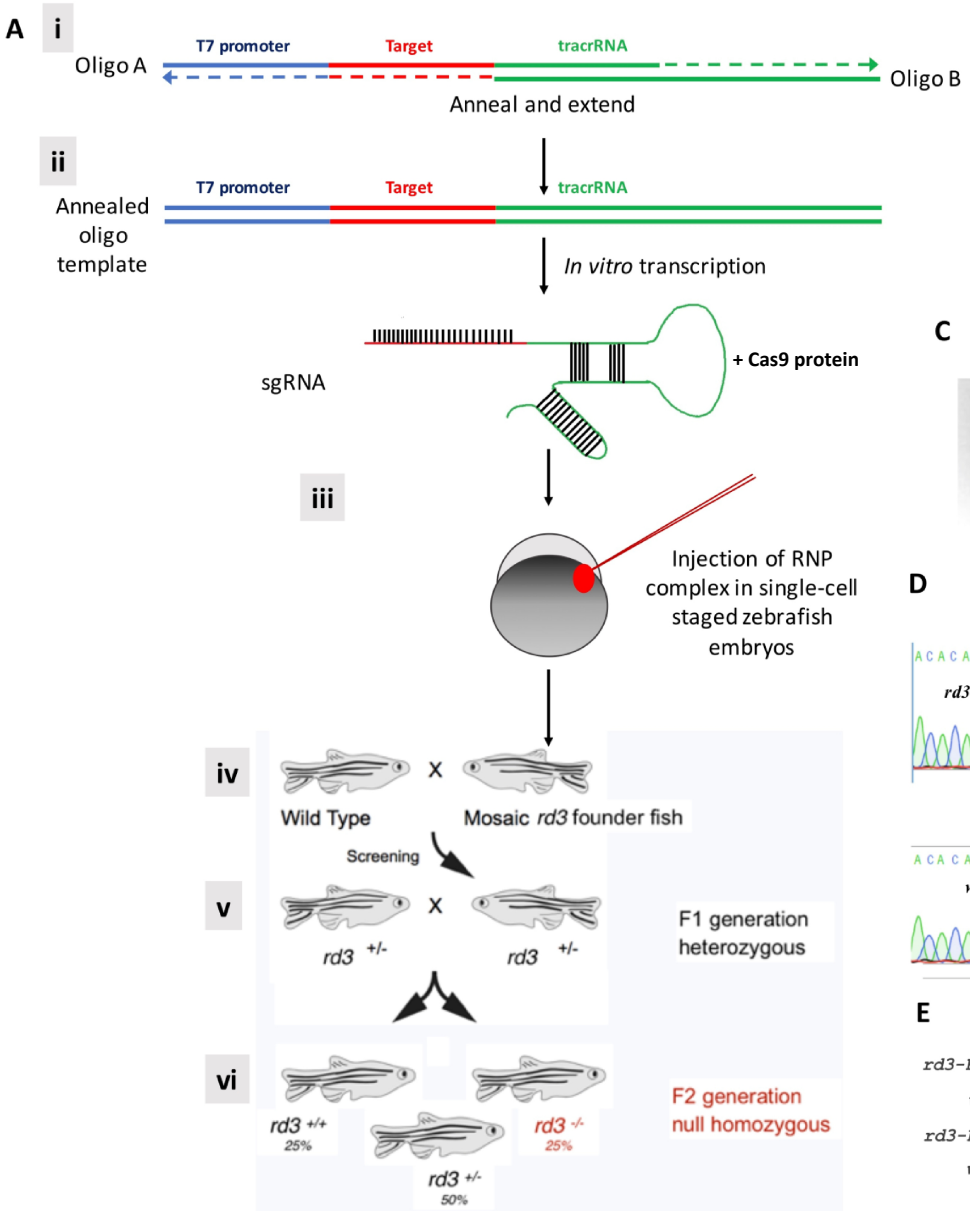
A
i
Oligo A
T7 promoter
Target
tracrRNA
Oligo B
Anneal and extend
ii
Annealed oligo template
T7 promoter
Target
tracrRNA
In vitro transcription
sgRNA
+ Cas9 protein
iii
Injection of RNP complex in single-cell staged zebrafish embryos
iv
Wild Type
X
Mosaic rd3 founder fish
Screening
v
rd3 +/-
X
rd3 +/-
F1 generation heterozygous
vi
rd3 +/+ 25%
rd3 +/- 50%
rd3 -/- 25%
F2 generation null homozygous

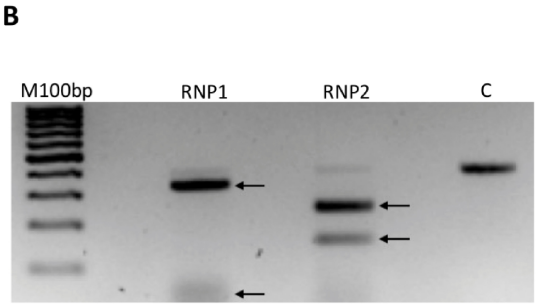
B
M100bp
RNP1
RNP2
C

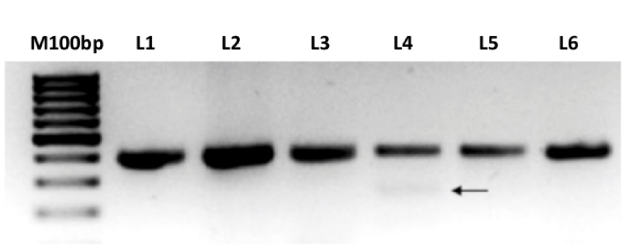
C
M100bp
L1
L2
L3
L4
L5
L6

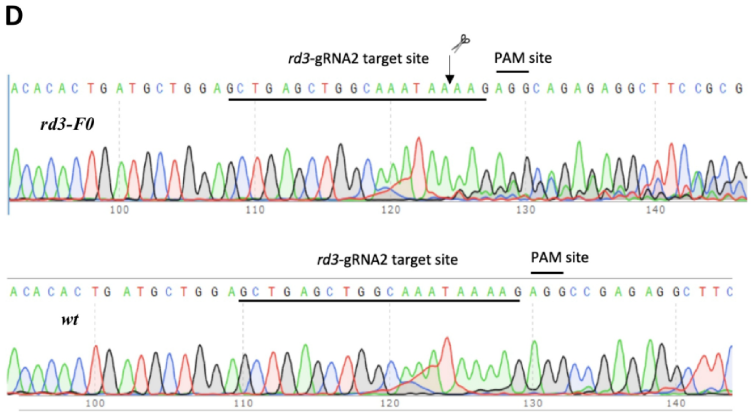
D
rd3-gRNA2 target site
PAM site
rd3-F0
wt

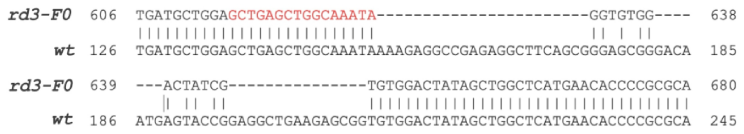
E
rd3-F0 606 TGATGCTGGAGCTGAGCTGGCAAATA---------- GGTGTGG---- 638
wt 126 TGATGCTGGAGCTGAGCTGGCAAATAAAAGAGGCCGAGAGGCTTCAGCGGGAGCGGGACA 185
rd3-F0 639 ---ACTATCG---------- TGTGGACTATAGCTGGCTCATGAACACCCCGCGCA 680
wt 186 ATGAGTACCGGAGGCTGAAGAGCGGTGTGGACTATAGCTGGCTCATGAACACCCCGCGCA 245

Figure 4.20: Generation and validation of CRISPR guide RNAs to target zebrafish rd3 and screening of F_0 founders. A. *Cartoon representing the overall work-flow of CRISPR-Cas9 mediated gene editing to obtain rd3 gene knockouts (null homozygotes in F_2 generation).* ***i****. Annealing and extension of single stranded, oligo A and oligo B to obtain double stranded template containing T7 promoter, specific gRNA sequence targeting zebrafish rd3-exon 2 and an universal tracrRNA sequence.* ***ii****. In vitro transcription of the double stranded DNA template to obtain single gRNA targeting zebrafish rd3.* ***iii.*** *Micro-injection of ribonucleoprotein (RNP) complex containing gRNA and Cas9 protein, into fertilized, single cell staged, zebrafish embryos.* ***iv.*** *Back crossing F_0 founders with wt zebrafish, to obtain F_1 heterozygotes.* ***v****. Interbreeding of F_1 heterozygotes to obtain F_2 null homozygotes.* ***vi****. F_2 generation producing 25% homozygous null progenies.* ***B.*** *Agarose gel electrophoretic image showing site-specific DNA cleaving ability of both RNP1 (sgRNA1 + Cas9) and RNP2 (sgRNA2 + Cas9) complexes. The rd3-exon 2 amplicon of 396 bp was cleaved into 335 bp & 61 bp fragments by RNP1 and 244 bp & 152 bp fragments by RNP2, as marked by the arrows.* ***C.*** *Agarose gel electrophoretic image of T7 endonuclease assay showing the cleavage of rd3-exon 2 amplicon of the larva no. 4 (L4), thus confirming the presence of in-del edits in L4.* ***D****. Sequence chromatogram of rd3-exon2 region of F_0 founder and wt zebrafish. Appearance of double peaks immediately upstream of the protospacer adjacent motif (PAM) site indicates either the presence of in-dels in mosaic pattern or in heterozygous state.* ***E****. BLAST analysis of the DNA sequences of the rd3-KO allele of the F_0 founder and that of the rd3-wt allele showed a 13 bp insertion and 58 bp deletion in rd3-exon 2 region of the F_0 founder zebrafish.*

out (**section 3.14.5**). Single cell-staged fertilized embryos were collected from breeding pairs and were arranged in neat rows in an agarose mold. 2-3 nL of micro-injection mix containing either sgRNA1 or sgRNA2 along with the recombinant Cas9 protein was injected into 80-100 single-cell staged embryos, at the interface region (junction between the egg yolk and the cell) (**Fig 4.20.A.iii**). The injected embryos were then incubated at 28° C to develop and hatch. Three days after injection, around 60 embryos survived and had hatched. Genomic DNA was isolated individually from 10% of the surviving embryos (6 nos) for amplifying the *rd3*-exon2 region, to screen for the presence of insertions-deletions (in-dels) by T7 endonuclease assay (**section 3.14.6**). T7 endonuclease is an enzyme that cleaves double stranded DNA molecules with base mismatch. When the edited DNA amplicons with in-dels were mixed with a control DNA amplicon, followed by denaturation and renaturation steps, hybrid DNA fragments with base mismatches (due to the presence of in-dels) were created. These base mismatches were identified and cleaved by T7 endonuclease enzyme. Out of the 6 larvae screened from the RNP2 injected batch, one of the larva L4 contained in-dels – as seen by the presence of cleaved DNA fragment in AGE (**Fig 4.20.C**). This confirmed that 16.66% ($1/6^{th}$) of the embryos injected with RNP2 contained in-dels and the remaining embryos were allowed to mature until juvenile stage to be screened for F0 founders carrying *rd3* gene edits.

4.2.5. Screening of embryos to identify F_0 mosaic founders

The RNP2 injected embryos developed into juveniles within a month. At the juvenile stage, individual fishes were anesthetized with tricaine and tail fin clips were taken for genomic

DNA isolation (**section 3.14.7**). Amplification of *rd3*-exon2 region from each of these fishes and sequencing of the PCR amplicons identified an F_0 founder fish with in-dels at the sgRNA2 cleavage site. The sequence chromatogram of *rd3*-exon2 of F_0 founder showed double peaks starting from the sgRNA2 target site (**Fig 4.20.D**). The presence of double peaks might indicate: 1: The presence of mosaic pattern of edits in the cell of the F_0 founder fish, 2: The presence of in-dels in only one of the alleles of the *rd3* gene of the F_0 founder fish (heterozygous condition). To identify the kind of in-dels that had occurred in F_0 founder fish, the *rd3*-exon2 region was PCR amplified and the amplicon was cloned into the pMOS-Blue vector for sequence confirmation. Sequence analysis confirmed the presence of a 13 bp insertion and a 58 bp deletion in the *rd3*-exon2 region of F_0 founder fish (**Fig 4.20.E**). Thus, the in-del had resulted in a cumulative nucleotide loss of 45 bp, which corresponded to a 15 amino acids deletion from 35^{th} to 49^{th} position of the zebrafish rd3 protein. The genotype of this F_0 mutant founder fish could be identified as double bands in agarose gels (396 bp and 351 bp), represented in **Fig 4.21.A** (marked by '*').

4.2.6. Breeding of founder fishes to generate *rd3* homozygous recessive mutants

The F_0 founder identified to carry the in-del was allowed to mature to adult stage until it became sexually active. Back crossing F_0 founder with *wt* animals (**section 3.14.8**) gave rise to 50% of F_1 fishes that were heterozygous for the in-dels (**Fig 4.20.A.v**), as marked by the appearance of double bands, represented in **Fig 4.21.A** (marked by '*'). This confirmed that the F_0 founder carried the edit in germ line cells, in only one of the two alleles, thus resulting in 1:1 ratio of allelic segregation. The heterozygosity of F_1 fishes was also confirmed by sanger sequencing. The confirmed F_1 heterozygotes were then interbred with each other to obtain F_2 progenies, with 25% of them being homozygous for the in-dels observed in the F_0 founder (**Fig 4.20.A.vi**). Agarose gel analysis of the PCR amplicons of the targeted *rd3*-exon2 region easily identified the heterozygotes with double bands (396 bp and 351 bp) and the recessive homozygotes with a single band of 351 bp (**Fig 4.21.A**). The heterozygotes and the recessive homozygotes from the F_2 progenies were sequence confirmed as shown in **Fig 4.21.B.ii**, **iii**. Since the heterozygotes carried a 13 bp insertion and a 58 bp deletion in only one of the two *rd3* alleles, the resulting PCR products will be of two different sizes (396 bp and 351 bp) which therefore caused the appearance of double peaks right after the sgRNA2 target site (**Fig 4.21.B.ii**). Since the homozygotes carried the same mutation in both the alleles, the resulting sequence was clean, with single peaks throughout the chromatogram (**Fig 4.21.B.iii**). Thus, *rd3* homozygous recessive mutants were successfully obtained in the F2 generation.

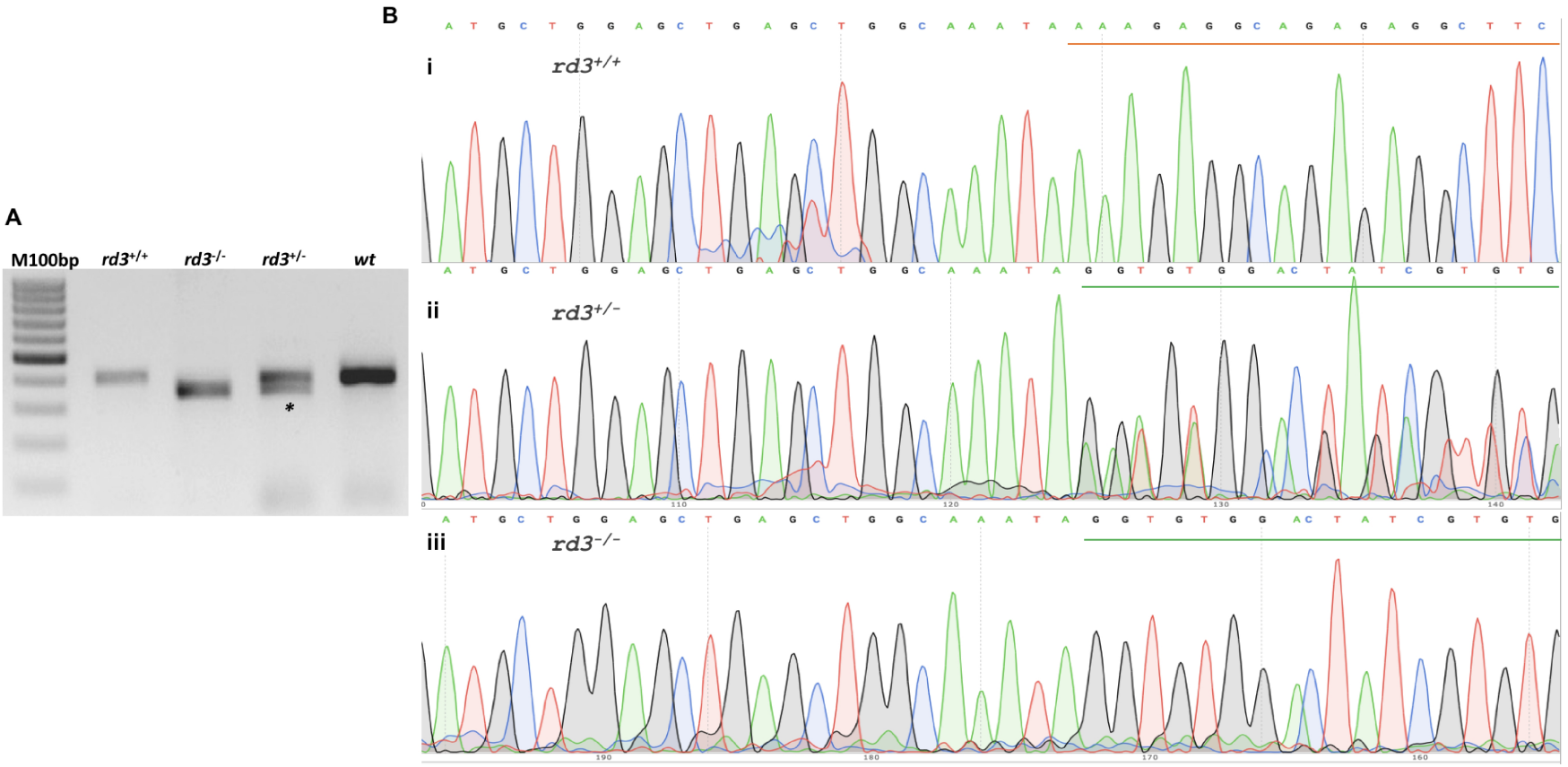

Figure 4.21: Genotyping of F2 generation. ***A***. *Agarose gel electrophoretic image of rd3-exon 2 amplicons from* $rd3^{+/+}$ *(396 bp),* $rd3^{+/-}$ *(396 bp and 351 bp) and* $rd3^{-/-}$ *(351 bp) zebrafish progenies. '*' indicates the heterozygosity, which enabled easy identification of* F_0 *founders and* F_1 *heterozygotes.* ***B***. *Sequence chromatograms of homozygous wild type* $rd3^{+/+}$*, heterozygous mutants* $rd3^{+/-}$ *and homozygous mutants* $rd3^{-/-}$*. Orange line in wt sequence marks the rd3 sequences deleted in homozygous mutants. Heterozygosity of* $rd3^{+/-}$ *fishes is marked by the appearance of double peaks at the edit locus (green line in* $rd3^{+/-}$ *sequence). Homozygosity of* $rd3^{-/-}$ *fishes is marked by the appearance of clear peaks at the edit locus (green line in* $rd3^{-/-}$ *sequence).*

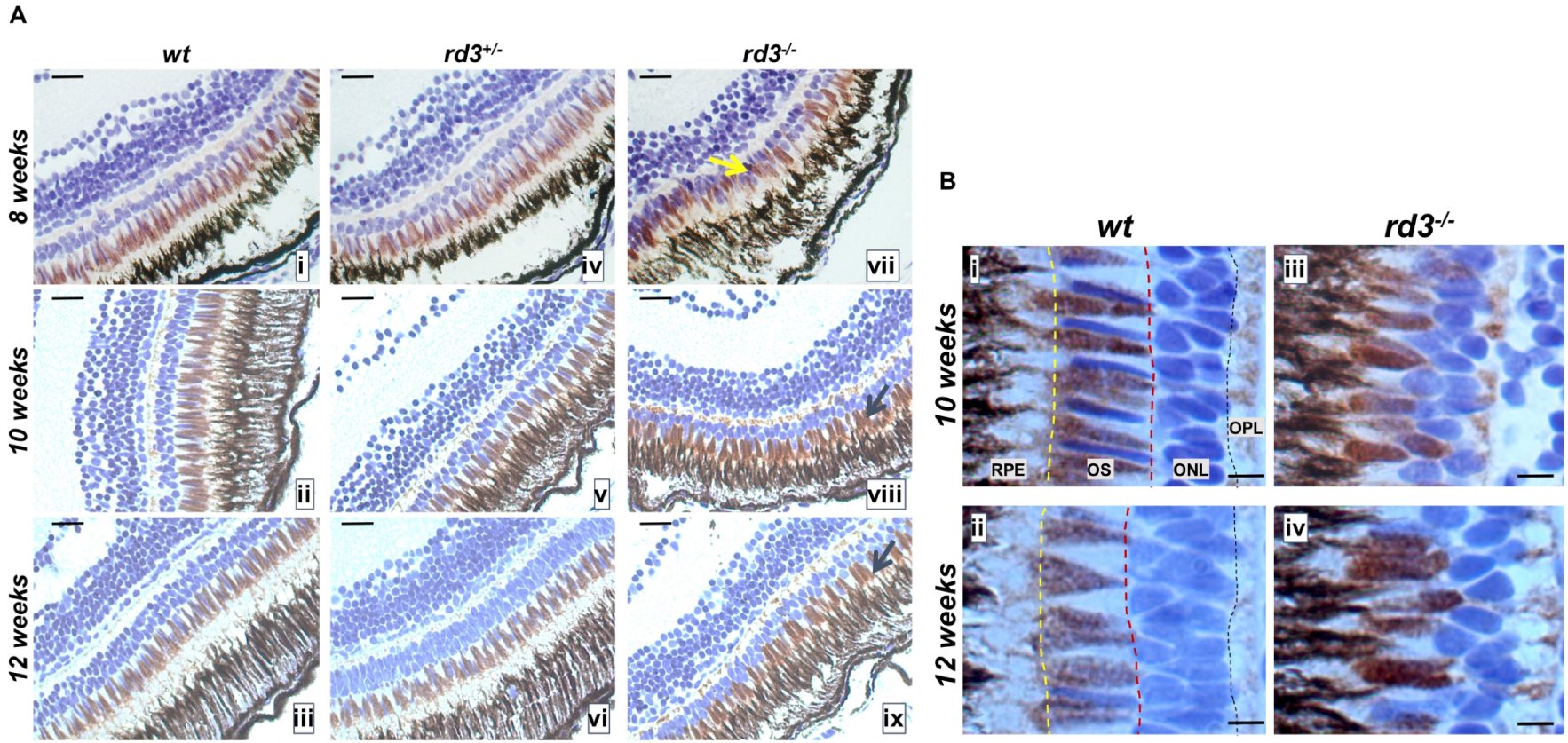

Figure 4.22. Characterization of rd3 homozygous null mutants. ***A***. *IHC evaluation of wt and mutant zebrafish retinal sections at different developmental time points (8, 10, 12 weeks post fertilization). DAB staining of cone-specific arrestin is marked in brown and the sections were counter-stained with hematoxylin in blue. The outer segments of rd3$^{-/-}$ retina appeared shorter and the cells of the ONL showed significant lamination defects (arrows). Scale bars: 40 µm.* ***B***. *Magnified view of wt and rd3$^{-/-}$ retinal ONL region at 10 and 12 weeks post fertilization. The outer retina of wt fishes (i, ii) displayed a clear line of demarcation between the RPE cells and the outer segments (OS) (as marked by the yellow dotted line); the outer limiting membrane (OLM) (as marked by the red dotted line) between the outer segments and the outer nuclear layer (ONL); and the outer plexiform layer (OPL) (as marked by the black dotted line). This orderly arrangement and lamination of cone photoreceptor cells in the outer nuclear layer was completely distorted in rd3$^{-/-}$ retina. Scale bars: 15 µm.*

4.2.7. Characterization of retinal phenotypes of homozygous recessive mutants

To study the effect of *rd3* gene mutations on retinal development, the homozygous recessive mutants were characterized by IHC examination of their retinas at various stages of development and were compared with age matched heterozygous and wild type control fishes.

Cone-arrestin staining of the retinal sections of *wt* and *rd3*$^{+/-}$ fishes at different time points (8, 10 and 12-weeks post fertilization) showed that the retinal cells were arranged in neat rows indicating proper lamination (**Fig 4.22.A.i**-**vi**). The magnified view of the outer layers of the retina showed clear stratification and demarcation between the RPE, OS, OLM, ONL and OPL (**Fig 4.22.B.i**, **ii**). However, cone-arrestin stained retinal sections of *rd3*$^{-/-}$ mutant fishes at different time points (8, 10 and 12 weeks) showed that the lamination and organization of cells within the ONL of the retina is significantly altered, as marked by a disorderly arrangement of outer segments and the absence of OLM (**Fig 4.22.A.vii**-**ix**). Magnified images of the outer retina confirmed that the outer segments of mutant animals were shorter than the wild type and heterozygotes. Also, the cells of the ONL are organized in a random fashion, with outer segments of some of the cells were noted within the ONL layer. The thickness of the OPL layer was also found to be reduced in mutants (**Fig 4.22.B.iii**, **iv**). These observations were in confirmation with the lamination defects seen in hiPSC-VS-OC (**Fig 4.17.A.viii**). Taken together, the results confirm an early retinal developmental anomaly in *rd3* mutants. However, understanding the exact molecular mechanisms leading to the defects in retinal progenitor maturation and lamination in *rd3* mutants (VS-OCs & *rd3*$^{-/-}$ fishes), warrants thorough molecular characterizations to understand disease pathogenesis resulting in retinal degeneration.

CHAPTER 5

DISCUSSIONS

5. Discussions

Patient volunteers for the current study were identified and recruited based on mutation screening data from a previous molecular genetics study (Friedman *et al.* 2006; Singh *et al.* 2006). Blood and full thickness skin biopsy samples were taken from study participants, with their informed consents and the approvals of IRB and IC-SCR. Region-specific PCR and sequencing of genomic DNA isolated from the blood samples of F2 (normal control), KR (*ABCA4*$^{-/-}$) and VS (*RD3*$^{-/-}$) confirmed the presence of patient-specific mutations reported earlier (Friedman *et al.* 2006; Singh *et al.* 2006). The skin biopsies were used to establish human dermal fibroblast (HDF) cultures of all the three volunteers (**Fig 4.1**). The HDF cells were then successfully reprogrammed to induced pluripotent stem cells (iPSCs) using lentiviral vectors to deliver the four Yamanaka factors (*OCT4, SOX2, KLF4* and *cMYC*, shortly OSKM) (**Fig 4.2**). The reprogrammed iPSC lines derived from all the three patient-specific HDFs were characterized for, their identity (**Fig 4.3**), transgene integration and silencing (**Fig 4.4.A**,**B**), endogenous Yamanaka factor expression (**Fig 4.4.C**), stemness (**Fig 4.5**), absence of major chromosomal aberrations (**Fig 4.6**), pluripotency (**Fig 4.7**) and for their ability to differentiate into ocular lineages (**Fig 4.8**) . The results confirmed that the iPSCs harbored the same patient-specific mutations (**Fig 4.3**), with only three of the transgenes integrated into their genomes (**Fig 4.4.A**). Out of the integrated transgenes, *SOX2* was silenced whereas the *OCT4* and *KLF4* were found to be active in stably expanded iPSC lines (**Fig 4.4.B**). However, all the four endogenous copies of the Yamanaka factors were stably activated and expressed in the stable lines, at levels comparable to that of the hESC line, BJNhem20 (**Fig 4.4.C**). Thus, all the three iPSC lines generated were 3 factors lines and were referred to as hiPSC-KR-3F, hiPSC-VS-3F and hiPSC-F2-3F; and shortly as KR, VS, F2 cells respectively. All the three patient-specific iPSC lines expressed the key stemness markers such as, OCT4, NANOG, hTERT and SSEA4 (**Fig 4.5**). Gross karyotypes of all the three stable lines confirmed the genomic integrity and absence of major chromosomal aberrations (**Fig. 4.6**). The iPSCs exhibited pluripotency and differentiated into cell types of all three lineages both in embryoid body (EB) and in teratoma formation assays (**Fig 4.7**). Further the ability of the iPSC lines to differentiate into ocular lineage was assessed by directed differentiation of near confluent adherent cultures.

Upon retinal differentiation, the VS and F2 lines formed distinct, raised, circular to oval shaped, self-organized structures that are termed as "eye field primordia" (EFP) (**Fig 4.8.A**). The cells of the EFP expressed the early retinal progenitor marker, *RX* at one-month post

differentiation (**Fig 4.8.B**). However, the KR line was inefficient in generating EFP and the rare ones that developed were found to be poorly organized (marked by arrow in **Fig 4.8.A**) and expressed *RX* only after 2 months of differentiation (**Fig 4.8.B**). Also, the retinal precursors of KR preferentially differentiated towards RPE over the neuro-retinal lineage. The well characterized function of ABCA4 is to flip the visual cycle intermediate, all-trans retinal (**section 2.5.1.1**) from the inside of the discs to the cytoplasm of the photoreceptors (Quazi, Lenevich, and Molday 2012). It is unclear why the non-sense mutation observed in this patient would result in preferential differentiation of retinal stem cells towards an RPE fate and also cause defective neuro-retinal cell organization. This requires further detailed evaluation to understand the exact molecular mechanisms leading to the developmental defects observed so far. Such EFP generated using patient-specific iPSCs can thus serve as excellent *in vitro* models to study retinal degeneration (Jin *et al.* 2011; Li *et al.* 2017; Sharma *et al.* 2017; Tang *et al.* 2016; Wiley *et al.* 2015).

The protocols for retinal differentiation and further enrichment of RPE and NR precursors in monolayer cultures were first standardized using a well characterized, normal control, human embryonic stem cell line, BJNhem20 (Inamdar *et al.* 2009; Shetty and Inamdar 2012; Venu *et al.* 2010). The eye field clusters obtained (as in **section 4.1.7.6**) from BjNhem20, when allowed to mature in RDM for another month, formed neuro-retinal (NR) islands surrounded by pigmented RPE cells (**Fig 4.9.A**). The NR islands and the surrounding RPE cells were manually picked and cultured on Matrigel^{TM} coated plates containing NRM and RPEM respectively. The NR (**Fig 4.9.B**) and RPE (**Fig 4.9.C**) progenitor cultures expressed the early NR (**Fig 4.9.D**,**E**) and RPE markers (**Fig 4.9.F**,**G**) respectively, which later matured to form enriched cultures of NR (**Fig 4.9.H**) and RPE cells (**Fig 4.9.I**).

The enriched, neuro-retinal cultures contained different retinal neurons that expressed the general neuron-specific markers such as, MAP2, β-III tubulin and acetylated tubulin (**Fig 4.10.i.A**-**C**); committed photoreceptor precursor markers such as, CRX (**Fig 4.10.i.D**); and mature photoreceptor markers such as, Recoverin and Rhodopsin (**Fig 4.10.i.E**,**F**). RT-PCR profiling (**Fig 4.10.ii**) of these cells also revealed the expression of early retinal markers such as, CHX10, CRX, visual transduction pathway genes such as, RLBP1 (retinaldehyde binding protein 1), Rhodopsin, PDE6C (phosphodiesterase 6C), PKC-β (protein kinase C beta), OPN1MW (medium wavelength opsin 1 or green opsin) and RHOK (rhodopsin kinase).

The enriched RPE cells, formed a uniform monolayer that matured in the dish for 3 months and developed intense pigmentation (**Fig 4.11.A**) and displayed cobblestone morphology

(**Fig 4.11.B**) with an orderly arrangement of actin cytoskeletal bundles, marked by Phalloidin staining (**Fig 4.11.F**). The cells also expressed the epithelial tight-junction marker, ZO-1 (**Fig 4.11.C**), the key RPE specific marker, RPE65 (**Fig 4.11.D**,**E**) and could internalize 1-micron sized fluorescent labeled latex beads, thus confirming their phagocytic activity (**Fig 4.11.C**). The RPE cells cultured on thick Collagen I gels were highly polarized, with basally positioned nuclei and apically positioned cytosolic melanosomes and numerous apical microvilli structures (**Fig 4.11.G**,**H**). The secretion of VEGF and PEDF by mature RPE cells cultured on trans-wells further validated the RPE cell identity (**Fig 4.11.I**,**J**). RT-PCR profiles of RPE cells (**Fig 4.11.K**) at day 30 post differentiation showed the expression of early RPE progenitor markers, MITF (microphthalmia-associated transcription factor) and TYR (tyrosinase). The 90 days old RPE cells expressed the mature RPE markers such as, BEST1 (bestrophin1), RPE65 (retinoid isomerohydrolase) and MERTK (a membrane-bound receptor tyrosine kinase). Together, the results confirmed that our retinal differentiation and cell enrichment protocol was efficient in establishing monolayer cultures of both mature neuro-retinal cells and RPE cells from human pluripotent stem cells (PSCs).

The enriched NR cultures established a complex network of axonal connections, which when disrupted by regular passaging techniques resulted in their massive cell death and therefore, unsuitable for cell preparations meant for transplantation purposes - which require rigorous cell-enrichment and expansion protocols. Few groups had earlier reported protocols for developing three dimensional ocular tissue from human ESCs and iPSCs (Assawachananont *et al.* 2014; Eiraku *et al.* 2011; Hiler *et al.* 2015; Kaewkhaw *et al.* 2015; Nakano *et al.* 2012; Reichman *et al.* 2014; Völkner *et al.* 2016; Zhong *et al.* 2014). These protocols were laborious, involving various ECM proteins, growth factors and complex culture conditions and cell sorting strategies, making it difficult for scaling up. Therefore, this study has come up with a simple modified protocol which involved generating EFP in adherent cultures (as in **section 4.1.7.6**), followed by manual picking of the central NR islands and culturing them in suspension to generate enriched NR cups and 3D retinal organoids.

To establish and standardize the self-formed optic cup derivation using pluripotent stem cells, differentiation was initiated using a well characterized normal control, human iPSC line, hiPSC-F2-3F (**Fig 4.12**). This culture technique resulted in formation of corneal primordia, miniature eye like structures and retinal primordia, as described in **section 4.1.9.**

Upon differentiation in the absence of Noggin, a BMP inhibitor, the developing EFP gave rise to a peripheral rim of migrating cells that contributed to ocular surface development. This outgrowth was described as self-formed, ectodermal, autonomous multi-zones (SEAMs) elsewhere (Hayashi *et al.* 2016). When these EFP along with the SEAMs (**Fig 4.12.B**) were manually picked and cultured in suspension, they formed transparent, fluid-filled and delicate bubble-like, corneal primordial (CP) structures along with the optic cups (retinal primordia, RP) (**Fig 4.12.C**). Fixation of these CP for histopathological analysis resulted in their rupture and release of their internal fluids. Further, it was found that these CPs are made of bi-layered epithelium (**Fig 4.13.B**) that expressed Vimentin in the periphery but neither PAX6 or P63 at this early developmental stage (**Fig.4.13.i.C**,**D**,**F**). Also two niche like organizers were observed at the stalk end of the CP, which contained actively dividing cells, as marked by Ki67 expression (**Fig 4.13.i.B**,**E**). Upon extended culture for up to 6 weeks in suspension, the CPs matured in the dish and developed a stratified epithelium (**Fig 4.13.ii.A**), above a well-developed thick stroma (**Fig 4.13.ii.B**,**C**). The epithelial cells expressed the corneal identity markers such as, PAX6, P63 and CK12 (**Fig 4.13.ii.D**-**F**). Such corneal primordia, when cut into small pieces and grown as explants cultures on denuded human amniotic membrane (hAM), formed transplantable, uniform sheets of corneal epithelial cells that expressed PAX6, TP63 and CK12 (**Fig 4.13.iii**), at levels comparable to that of adult limbal tissues. Such iPSC-derived corneal organoids and the engineered corneal epithelial cell sheets have immense potential as *in vitro* models in basic research applications and in regenerative medicine for the treatment of blinding conditions such as limbal stem cell deficiency (LSCD).

Rare EFP that was left to mature in adherent culture, surprisingly, matured into a miniature eye like structures, with neuro-retinal primordia on the basal side, translucent corneal primordia on the anterior side, pigmented neural crest cells at corneal margins and migrating RPE cells surrounding the basally located neuro-retina (**Fig 4.12.B'**). The formation of such miniature eye-like structure was a rare event in adherent cultures. However, it highlights the possibility of whole eye organogenesis in future, with improved protocols and better 3D culture conditions. The corneal organoid that was dissected out of the miniature eye like structure (**Fig 4.14.A**) displayed a high level of self-organization and striking similarity to the native ocular surface, with distinct cornea and conjunctival-like regions separated by a limbal-like margin (**Fig 4.14.B**). There was a clear demarcation between the corneal epithelial region (containing $PAX6^+$, $P63^+$, $K12^+$ epithelial cells) and the conjunctival region ($Muc2^+$ goblet

cells) (**Fig 4.14.C**). The stromal cells were distinct from the surface epithelium and expressed Vimentin, thus confirming their neural crest and mesenchymal origin. Corneal organoids of such complexity, although rare to obtain, are excellent *in vitro* models to study human corneal development and function.

The retinal primordial structures that were excised and cultured in RDM in suspension, organized themselves into laminated and circular cup-like structures within a week (**Fig 4.15.i.A**). Histological analysis of these structures revealed a developing optic cup morphology with an inner layer and an outer layer (**Fig 4.15.i.B**) and the cells of the inner layer were $CHX10^+$ and $PAX6^+$ indicating their neuro-retinal commitment. (**Fig 4.15.i.C**,**D**). These optic cups also expressed the general neuron-specific markers, acetylated tubulin and Nestin and photoreceptor precursor marker, CRX (**Fig 4.15.i.E**-**G**). These optic cups when allowed to mature in NRM formed retinal organoids that contained almost all the neuro-retinal cell types (**Fig 4.15.i.H**-**L**). RT-PCR profiling of these organoids (**Fig 4.15.ii**) revealed the expression of early neuro-retinal markers at one month after differentiation and also expressed the visual transduction genes, including the *ABCA4* and *RD3* at 2 months after differentiation. These results confirmed that the self-organized optic cups formed by EFP in suspension culture, undergo some level of lamination and maturation in the dish to form a near complete retinal graft and can serve as excellent *in vitro* models to study retinal development and disease.

Once the protocols were established for generating mature retinal organoids, the patient-specific iPSC lines (KR and VS) were differentiated into retinal lineages. As mentioned earlier in **section 4.1.7.6**, the hiPSC-KR-3F line differentiated into poorly organized EFP (**Fig 4.8.A**), which when picked and cultured further, differentiated preferentially towards the RPE lineage. The RPE precursors developed intense pigmentation at an early time point, when compared to the normal control cells. Recently it was reported that the ABCA4 is expressed not only in photoreceptors, but also in RPE cells and carry out the same function as the retinal flippase in RPE cells (Lenis *et al.* 2018). Hence, enriched cultures of RPE cells derived from the KR line were further compared with that of the normal control cells.

On phase contrast imaging, the hiPSC-KR-RPE cells displayed illuminated boundaries due to compromised cell-junctions that allowed the light to pass through, in contrast to the compact cell-cell junctions observed in hiPSC-F2-RPE cells (**Fig 4.16.A**). RT-PCR profiling of both hiPSC-KR-RPE and hiPSC-F2-RPE cells showed that they both expressed the RPE markers such as, MITF, TYR and RPE65 at comparable levels (**Fig 4.16.E**). However, the

ABCA4 transcript was expressed at significantly lower levels in hiPSC-KR-RPE cells. A quantitative PCR analysis showed a four-fold decrease in the ABCA4 transcript levels in hiPSC-KR-RPE compared to hiPSC-F2-RPE (p=0.03) (**Fig 4.16.F**). This could be due to nonsense mediated decay of ABCA4 transcript owing to the premature stop codon generated due to c.6088C>T variation in hiPSC-KR-RPE. The absence of ABCA4 protein expression was also confirmed in hiPSC-KR-RPE cells by immunocytochemistry (**Fig 4.16.B**). Further morphological comparisons revealed that the hiPSC-KR-RPE cells were not tightly packed as that of hiPSC-F2-RPE and showed a disorderly arrangement of actin cytoskeletal bundles, as marked by abnormal Phalloidin staining and damaged apical surface, as marked by reduced Ezrin staining (**Fig 4.16.C**). SEM and TEM analysis of RPE cell surface showed a completely distorted apical surface, with blob like apical microvilli projections in hiPSC-KR-RPE cells, as opposed to the typical finger like, microvilli structures seen in normal control cells (**Fig 4.16.D**). The epithelial barrier functions and transmembrane ion-transport function of hiPSC-KR-RPE and hiPSC-F2-RPE cells were checked by electrophysiological experiments and found that the barrier functions of hiPSC-KR-RPE cells were highly compromised and the ion-transport was almost nil (**Fig 4.16.G**). This could be attributed to the compromised cell-cell tight junctions and apical surface abnormalities seen in hiPSC-KR-RPE cells, as discussed above. Together these results showed that the presence of ABCA4 and its normal functioning is not only essential for photoreceptors, but also for RPE cells. Further studies on hiPSC-KR-RPE cells would help in better understanding of the role of ABCA4 in RPE cell development, maturation and function. Thus, this study was successful in establishing hiPSC-KR-RPE cultures as patient-specific, *in vitro* model of ARRD.

The hiPSC-VS-3F line differentiated normally into mature RPE cells (hiPSC-VS-RPE) and optic cups (hiPSC-VS-OC) at efficiencies comparable to that of the normal control line, hiPSC-F2-3F. The hiPSC-VS-RPE cells showed no significant difference in their differentiation timelines, RPE morphology, pigmentation, phagocytic activity, presence of tight junctions and in the expression of RPE-specific markers such as, MITF, TYR and RPE65, when compared to hiPSC-F2-RPE (**Fig 4.17.B,C.ii**). The morphology of hiPSC-VS-OCs appeared very similar to hiPSC-F2-OCs in phase contrast imaging (**Fig 4.17.A.i**,**ii**). Immunohistochemistry (**Fig 4.17.A.iii**-**viii**) and RT-PCR profiling (**Fig 4.17.C.i**) confirmed that the hiPSC-VS-OCs expressed both the early photoreceptor precursor markers (CHX10, NEUROD1, CRX) and the mature photoreceptor markers (RCVRN, RLBP1) at levels

comparable to that of hiPSC-F2-OCs. However, the transcript levels of RD3 were almost negligible in hiPSC-VS-OC compared to hiPSC-F2-OC (**Fig 4.17.C.i**). This could again be attributed to the splicing defects caused by c.296+1G→A variation in hiPSC-VS-OCs, leading to nonsense mediated decay of RD3 transcripts. The presence of RD3 protein could not be confirmed even in hiPSC-F2-OC due to lack of suitable antibodies. However, a significantly altered lamination pattern was noticed in hiPSC-VS-OCs (**Fig 4.17.A.viii**) when compared to hiPSC-F2-OCs (**Fig 4.17.A.vii**), which warrants further in-depth molecular characterizations to elucidate the exact molecular mechanisms that led to the severe form of congenital retinal dystrophy, LCA12.

LCA12 is an autosomal, recessive, cone/rod dystrophy caused by homozygous mutations in *RD3* (Friedman *et al.* 2006). This gene encodes a small protein of 195 amino acids (**Fig 2.4**) and therefore an ideal candidate for *in vitro* gene correction in patient-specific cells, by whole gene supplementation and rescue of normal cellular functions. This required the design of a suitable gene expression cassette and a vector system to achieve efficient transgene delivery, stable and optimal transgene expression in patient-specific iPSCs and/or retinal cells. Since the disease affects the rod and cone cells, a tissue-specific promoter that can drive optimal and stable *RD3* expression in all the photoreceptor cells and RPE cells was preferred. Hence, an attempt was made to clone and characterize the endogenous *RD3* promoter.

The retina-specific activity of two different lengths of *RD3* promoter (*RD3PFL* and *RD3PM*) (**Fig 4.18.A**) was validated using luciferase reporter gene expression, in retinal and non-retinal cell lines. The *RD3PM* promoter was 5 times shorter, but resulted in 2-3 times higher activity than *RD3PFL* in retinal cells and therefore considered for further characterization and validations.GFP reporter assays comparing the *RD3PM* promoter strength with that of the *CMV* promoter revealed that the widely used ubiquitously expressed and constitutively active *CMV* promoter was almost inactive in retinal cell lines and in native retinal tissues, indicating their non-suitability for retina specific applications. The *RD3PM* was highly active in the retinoblastoma line, Y79 and in photoreceptor rich, outer nuclear layers of cultured cadaveric retinal explants (**Fig 4.18.C,D**). Further, to test the proof-of-concept of gene supplementation therapy, a lentivirus-based vector system, carrying the *RD3* promoter driven *RD3* expression cassette, was designed and constructed (**Fig 4.18.E**). This *RD3* delivery vector needs further evaluation in rat models to assess for sustained and optimal transgene expression in native retinal tissues.

To establish a zebrafish model of retinal dystrophy, the NCBI database was analyzed to identify the zebrafish orthologs of human *RD3* (NCBI gene id: NC_007131.7). Sequence alignment confirmed that the zebrafish *rd3* and the encoded protein were 74.76% and 53% identical to those of humans respectively (**Fig 4.19**). CRISPR-Cas9 guide RNAs were designed using UCSC genome browser and the oligos were synthesized to target the regions downstream of the translational start site. *In vitro* cleavage assay using *rd3* region-specific PCR products confirmed that, the guide RNAs were efficient in creating double strand breaks at the targeted genomic locus (**Fig 4.20.B**).

Microinjection of validated CRISPR-Cas9/RNP complexes in single-cell staged zebrafish embryos and their screening confirmed that about 16.66% of the injected embryos carried in-dels at the targeted genomic loci (**Fig 4.20.C**). Screening of embryos that developed to juvenile stage identified an F_0 founder that carried a 13 bp insertion and 58 bp deletion, causing a cumulative nucleotide loss of 45 bp, which corresponds to a 15 amino acids deletion from 35^{th} to 49^{th} position of the zebrafish rd3 protein (**Fig 4.20.E**).

The F_0 founder when back crossed with *wt* partners resulted in 50% of F_1 progenies that were heterozygous for the mutation ($rd3^{+/-}$). This suggested that the in-dels observed in the F_0 founder was not due to mosaic pattern of somatic cell edits, but due to single allele edits in most cells, including the germ line cells. Interbreeding of $rd3^{+/-}$ F_1 animals resulted in 25% of F_2 progenies that were homozygous mutants ($rd3^{-/-}$) that carried the same in-dels in both the alleles of *rd3*. Thus, homozygous *rd3* knock out model of zebrafish was created.

Histopathological analysis of the retinal sections of $rd3^{-/-}$ fishes showed significant differences in the organization of retinal cell layers when compared to $rd3^{+/-}$ and *wt* fishes. Cone-arrestin staining of retinal tissues of 8-12 weeks old adult $rd3^{-/-}$ fishes showed that the cellular organization and lamination was significantly altered in the ONLs of the retina (**Fig 4.22.A.vii-ix**). Magnified view of the ONL layer of the retina showed that the outer segments were shorter and failed to establish boundaries between different cell layers, possibly due to the loss of outer limiting membrane (OLM) (**Fig 4.22.B.iii,iv**). Loss of rd3 in zebrafish retina resulted in lamination defects similar to the phenotypes observed in patient-specific, hiPSC-VS-OCs with *RD3* mutation. A detailed molecular characterization of these disease models would help in further understanding of the role (s) of *rd3* mutations in LCA12 pathogenesis.

CHAPTER 6

CONCLUSIONS

6. Conclusions

The major objectives of the aim 1 has been achieved by generating and characterizing three patient specific iPSC lines and by establishing patient-specific retinal cultures and 3D organoids as *in vitro* models of retinal degeneration. The key observations of the study are listed below:

1. Three human iPSC lines were derived from patient-specific HDFs and were characterized for their stemness, pluripotency, genetic identity and genome stability.
2. Retinal differentiation protocols to generate monolayer cultures of both RPE and neuro-retinal cells were established.
3. A suspension culture system to generate 3D retinal and corneal organoids was established. These miniature organoids were very similar to adult tissue and can therefore serve as *in vitro* disease models for basic science needs and for drug screening applications.
4. Patient-specific iPSC line carrying mutation in *ABCA4* was defective in optic cup formation and the retinal progenitors exhibited preferential fate commitment towards RPE lineage.
5. The patient-specific RPE cells with *ABCA4* mutation displayed abnormal tight junctions and microvilli projections that resulted in severely altered epithelial barrier functions and ion transport functions.
6. Patient-specific iPSC line carrying mutation in *RD3* showed normal eye field commitment. But the optic cups and retinal organoids indicated possible lamination defects.
7. To test the proof-of-concept of gene supplementation therapy, a lentivirus-based vector system, encoding the *RD3* promoter driven transgene was designed that will be checked for tissue-specific expression in hiPSC-derived retinal cups and rat models.

The major objective of the aim 2 has been achieved by generating and characterizing an *rd3*$^{-/-}$ mutant model of zebrafish to serve as an *in vivo* model of retinal degeneration. The key observations are listed below:

1. A stable zebrafish mutant model with a homozygous mutation in *rd3* (*rd3*$^{-/-}$) was successfully created using CRISPR/Cas9 based genome editing of fertilized embryos. The edit efficiency was found to be approximately 16%.
2. The *rd3*$^{-/-}$ animals displayed defective retinal lamination, with altered outer segment development, leading to gradual retinal degeneration.

CHAPTER 7

CONTRIBUTIONS

7. Contributions

This study has created patient-specific iPSC lines, iPSC-derived retinal cells and complex 3D ocular tissues or miniature organoids that are ideal model systems to understand the molecular mechanisms leading to inherited retinal degenerative conditions. These disease models are also ideal for potential drug screening and to carry out proof-of-concept gene correction/supplementation studies.

Apart from the *in vitro* models, the study has also created an *in vivo* zebrafish model of LCA12, an inherited and congenital form of retinal dystrophy. This model system is ideal to understand disease manifestations at various time points, right from early stages of retinal degeneration to its progression into late and severe form of the disease, leading to complete blindness.

The study also confirmed that the widely used *CMV* promoter is not suitable for retina-specific gene expression and further validated a retinal gene-specific promoter (*RD3PM*). Further, a photoreceptor-specific gene expression cassette, with a *GFP* reporter was constructed, for its applications in gene supplementation studies in future.

CHAPTER 8

LIMITATIONS OF THE STUDY

8. Limitations of the study

The present study was unable to confirm the presence of RD3 protein, even in control, hiPSC-derived retinal organoids, due to non-availability of suitable antibodies. Also, this study could not elucidate the exact molecular mechanism that cause: (i) preferential RPE lineage commitment of hiPSC-KR-3F derived retinal progenitors and (ii) the lamination defects observed in hiPSC-VS-3F derived optic cups.

CHAPTER 9

FUTURE SCOPES

9. Future scopes

1. Isogenic control lines for both the hiPSC-VS-3F and hiPSC-KR-3F lines have to be generated and characterized.
2. The retina-specific, *RD3* gene expression cassettes have to be evaluated in retinal organoids and in rat models.
3. The feasibility of mutation correction by gene editing and whole gene supplementation for disease reversal, have to be evaluated in hiPSC-3F-KR and hiPSC-3F-VS cells respectively.
4. Molecular mechanisms resulting in preferential RPE fate commitment and retinal lamination defects observed in *ABCA4* and *RD3* mutant iPSCs respectively need to be evaluated.

REFERENCES

Algvere P V, Berglin L, Gouras P, Sheng Y. Transplantation of fetal retinal pigment epithelium in age-related macular degeneration with subfoveal neovascularization. *Graefes Arch Clin Exp Ophthalmol* (1994) 232(12):707–16.

Aravindan S, Somasundaram DB, Kam KL, Subramanian K, Yu Z, Herman TS, *et al.* Retinal Degeneration Protein 3 (RD3) in normal human tissues: Novel insights. *Sci Rep.* (2017) 7(1):13154.

Asai-Coakwell M, March L, Dai XH, DuVal M, Lopez I, French CR, *et al.* Contribution of growth differentiation factor 6-dependent cell survival to early-onset retinal dystrophies. *Hum Mol Genet* (2013) 22(7):1432–42.

Assawachananont J, Mandai M, Okamoto S, Yamada C, Eiraku M, Yonemura S, *et al.* Transplantation of Embryonic and Induced Pluripotent Stem Cell-Derived 3D Retinal Sheets into Retinal Degenerative Mice. *Stem Cell Reports* (2014) 2(5):662–74.

Atkinson-Leadbeater K, Hehr CL, Mcfarlane S. Fgfr signaling is required as the early eye field forms to promote later patterning and morphogenesis of the eye. *Dev Dyn* (2014) 243(5):663–75.

Auricchio A, Trapani I, Allikmets R. Gene Therapy of ABCA4-Associated Diseases. *Cold Spring Harb Perspect Med.* (2015) 5(5):a017301.

Azadi S, Molday LL, Molday RS. RD3, the protein associated with Leber congenital amaurosis type 12, is required for guanylate cyclase trafficking in photoreceptor cells. *Proc Natl Acad Sci U S A* (2010) 107(49):21158–63.

Baehr W, Devlin MJ, Applebury ML. Isolation and characterization of cGMP phosphodiesterase from bovine rod outer segments. *J Biol Chem* (1979) 254(22):11669–77.

Baker DEC, Harrison NJ, Maltby E, Smith K, Moore HD, Shaw PJ, *et al.* Adaptation to culture of human embryonic stem cells and oncogenesis in vivo. *Nat Biotechnol* (2007) 25(2):207–15.

Barbieri AM, Lupo G, Bulfone A, Andreazzoli M, Mariani M, Fougerousse F, *et al.* A homeobox gene, vax2, controls the patterning of the eye dorsoventral axis. *Proc Natl Acad Sci U S A*(1999) 96(19):10729–34.

Barnard AR, Groppe M, MacLaren RE. Gene therapy for choroideremia using an adeno-associated viral (AAV) vector. *Cold Spring Harb Perspect Med* (2014) 5(3):a017293.

Behesti H, Holt JK, Sowden JC. The level of BMP4 signaling is critical for the regulation of distinct T-box gene expression domains and growth along the dorso-ventral axis of the optic cup. *BMC Dev Biol* (2006) 6(1):62.

Beirl AJ, Linbo TH, Cobb MJ, Cooper CD. oca2 regulation of chromatophore differentiation and number is cell type specific in zebrafish. *Pigment Cell Melanoma Res* (2014) 27(2):178–89.

Beltran WA, Cideciyan A V, Boye SE, Ye G-J, Iwabe S, Dufour VL, *et al.* Optimization of Retinal Gene Therapy for X-Linked Retinitis Pigmentosa Due to RPGR Mutations. *Mol Ther* (2017) 25(8):1866–80.

Bertacchi M, Lupo G, Pandolfini L, Casarosa S, D'Onofrio M, Pedersen RA, *et al.* Activin/Nodal Signaling Supports Retinal Progenitor Specification in a Narrow Time Window during Pluripotent Stem Cell Neuralization. *Stem cell reports* (2015) 5(4):532–45.

Bertuzzi S, Hindges R, Mui SH, O'Leary DDM, Lemke G. The homeodomain protein Vax1 is required for axon guidance and major tract formation in the developing forebrain. *Genes Dev* (1999) 13(23):3092–105.

Bilitou A, Ohnuma S. The role of cell cycle in retinal development: Cyclin-dependent kinase inhibitors co-ordinate cell-cycle inhibition, cell-fate determination and differentiation in the developing retina. *Dev Dyn* (2010) 239(3):727–36.

Biswas P, Chavali VRM, Agnello G, Stone E, Chakarova C, Duncan JL, *et al.* A missense mutation in ASRGL1 is involved in causing autosomal recessive retinal degeneration. *Hum Mol Genet* (2016) 25(12):ddw113.

Blenkinsop TA, Saini JS, Maminishkis A, Bharti K, Wan Q, Banzon T, *et al.* Human Adult Retinal Pigment Epithelial Stem Cell-Derived RPE Monolayers Exhibit Key Physiological Characteristics of Native Tissue. *Investig Ophthalmol Vis Sci* (2015) 56(12):7085–99

Bowne SJ, Sullivan LS, Mortimer SE, Hedstrom L, Zhu J, Spellicy CJ, *et al.* Spectrum and Frequency of Mutations in IMPDH1 Associated with Autosomal Dominant Retinitis Pigmentosa and Leber Congenital Amaurosis. *Investig Opthalmology Vis Sci* (2006) 47(1):34.

Boye SE, Alexander JJ, Boye SL, Witherspoon CD, Sandefer KJ, Conlon TJ, *et al.* The Human Rhodopsin Kinase Promoter in an AAV5 Vector Confers Rod- and Cone-Specific Expression in the Primate Retina. *Hum Gene Ther* (2012) 23(10):1101–15.

Brockerhoff SE, Rieke F, Matthews HR, Taylor MR, Kennedy B, Ankoudinova I, *et al.* Light stimulates a transducin-independent increase of cytoplasmic Ca2+ and suppression of current in cones from the zebrafish mutant nof. *J Neurosci* (2003) 23(2):470–80.

Brown A, McKie M, Van Heyningen V, Prosser J. The human PAX6 Mutation Database. *Nucleic Acids Res.* (1998) 26(1):259–64.

Brown A. The Human PAX6 Mutation Database. *Nucleic Acids Res*(1998) 26(1):259–64.

Bunt-Milam AH, Saari JC. Immunocytochemical localization of two retinoid-binding proteins in vertebrate retina. *J Cell Biol* (1983) 97(3):703–12.

Carl M, Loosli F, Wittbrodt J. Six3 inactivation reveals its essential role for the formation and patterning of the vertebrate eye. *Development* (2002) 129(17):4057–63.

Chakarova CF, Khanna H, Shah AZ, Patil SB, Sedmak T, Murga-Zamalloa CA, *et al.* TOPORS, implicated in retinal degeneration, is a cilia-centrosomal protein. *Hum Mol Genet* (2011) 20(5):975–87.

Chang B, Heckenlively JR, Hawes NL, Roderick TH. New Mouse Primary Retinal Degeneration (rd-3). *Genomics* (1993) 16(1):45–9.

Chen C-K, Inglese J, Lefkowitz RJ, Hurley JB. Ca-dependent Interaction of Recoverin with Rhodopsin Kinase. *J Biol Chem* (1995) 270(30):18060–6.

Chiang C, Litingtung Y, Lee E, Young KE, Corden JL, Westphal H, *et al.* Cyclopia and defective axial patterning in mice lacking Sonic hedgehog gene function. *Nature*. (1996) 383(6599):407–13.

Chow RL, Altmann CR, Lang RA, Hemmati-Brivanlou A. Pax6 induces ectopic eyes in a vertebrate. *Development* (1999) 126(19):4213–22.

Chung DC, Traboulsi EI. Leber congenital amaurosis: Clinical correlations with genotypes, gene therapy trials update, and future directions. *J Am Assoc Pediatr Ophthalmol Strabismus*(2009) 13(6):587–92.

Cideciyan A V., Sudharsan R, Dufour VL, Massengill MT, Iwabe S, Swider M, *et al.* Mutation-independent rhodopsin gene therapy by knockdown and replacement with a single AAV vector. *Proc Natl Acad Sci U S A* (2018) 115(36):E8547–56.

Collery R, McLoughlin S, Vendrell V, Finnegan J, Crabb JW, Saari JC, *et al.* Duplication and Divergence of Zebrafish CRALBP Genes Uncovers Novel Role for RPE- and Müller-CRALBP in Cone Vision. *Investig Opthalmology Vis Sci* (2008) 49(9):3812.

Collery RF, Cederlund ML, Kennedy BN. Transgenic zebrafish expressing mutant human RETGC-1 exhibit aberrant cone and rod morphology. *Exp Eye Res* (2013) 108:120–8.

Crouch RK, Hazard ES, Lind T, Wiggert B, Chader G, Corson DW. Interphotoreceptor retinoid-binding protein and alpha-tocopherol preserve the isomeric and oxidation state of retinol. *Photochem Photobiol* (1992) 56(2):251–5.

Croze RH, Buchholz DE, Radeke MJ, Thi WJ, Hu Q, Coffey PJ, *et al.* ROCK Inhibition Extends Passage of Pluripotent Stem Cell-Derived Retinal Pigmented Epithelium. *Stem Cells Transl Med* (2014) 3(9):1066–78.

Daiger S, Rossiter B, Greenberg J, Christoffels A, Hide W. Data services and software for identifying genes and mutations causing retinal degeneration. *Investig Ophthalmol Vis Sci.* 1998; 39:S295.

den Hollander AI, Koenekoop RK, Yzer S, Lopez I, Arends ML, Voesenek KEJ, *et al.* Mutations in the CEP290 (NPHP6) Gene Are a Frequent Cause of Leber Congenital Amaurosis. *Am J Hum Genet* (2006) 79(3):556–61.

Deterre P, Bigay J, Forquet F, Robert M, Chabre M. cGMP phosphodiesterase of retinal rods is regulated by two inhibitory subunits. *Proc Natl Acad Sci* (1998) 85(8):2424–8.

Dev Borman A, Ocaka LA, Mackay DS, Ripamonti C, Henderson RH, Moradi P, *et al.* Early Onset Retinal Dystrophy Due to Mutations in LRAT : Molecular Analysis and Detailed Phenotypic Study. *Investig Opthalmology Vis Sci* (2012) 53(7):3927.

Dharmaraj S, Leroy BP, Sohocki MM, Koenekoop RK, Perrault I, Anwar K, *et al.* The Phenotype of Leber Congenital Amaurosis in Patients With AIPL1 Mutations. *Arch Ophthalmol* (2004) 122(7):1029.

Ding SLS, Kumar S, Mok PL. Cellular Reparative Mechanisms of Mesenchymal Stem Cells for Retinal Diseases. *Int J Mol Sci* (2017) 18(8).

Doudna JA, Charpentier E. The new frontier of genome engineering with CRISPR-Cas9. *Science* (2014) 346(6213):1258096–1258096.

Draper JS, Smith K, Gokhale P, Moore HD, Maltby E, Johnson J, *et al.* Recurrent gain of chromosomes 17q and 12 in cultured human embryonic stem cells. *Nat Biotechnol* (2004) 22(1):53–4.

Driessen CA, Janssen BP, Winkens HJ, van Vugt AH, de Leeuw TL, Janssen JJ. Cloning and expression of a cDNA encoding bovine retinal pigment epithelial 11-cis retinol dehydrogenase. *Investig Ophthalmol Vis Sci* (1995) 36(10):1988–96.

Dryja TP, Adams SM, Grimsby JL, McGee TL, Hong D-H, Li T, *et al.* Null RPGRIP1 Alleles in Patients with Leber Congenital Amaurosis. Am J *Hum Genet* (2001) 68(5):1295–8.

Dryja TP, Rucinski DE, Chen SH, Berson EL. Frequency of Mutations in the Gene Encoding the α Subunit of Rod cGMP-Phosphodiesterase in Autosomal Recessive Retinitis Pigmentosa. *Investig Ophthalmol Vis Sci* (1999) 40(8):1859–65.

Dyka FM, Boye SL, Ryals RC, Chiodo VA, Boye SE, Hauswirth WW. Cone specific promoter for use in gene therapy of retinal degenerative diseases. *Adv Exp Med Biol* (2014) 801:695–701.

Ebert AD, Liang P, Wu JC. Induced pluripotent stem cells as a disease modeling and drug screening platform. *J Cardiovasc Pharmacol* (2012) 60(4):408–16.

Eiraku M, Takata N, Ishibashi H, Kawada M, Sakakura E, Okuda S, *et al.* Self-organizing optic-cup morphogenesis in three-dimensional culture. *Nature* (2011) 472(7341):51–6.

Eiraku M, Watanabe K, Matsuo-Takasaki M, Kawada M, Yonemura S, Matsumura M, *et al.* Self-Organized Formation of Polarized Cortical Tissues from ESCs and Its Active Manipulation by Extrinsic Signals. *Cell Stem Cell* (2008) 3(5):519–32.

Ekker SC, Ungar AR, Greenstein P, von Kessler DP, Porter JA, Moon RT, *et al.* Patterning activities of vertebrate hedgehog proteins in the developing eye and brain. *Curr Biol* (1995) 5(8):944–55.

Erter CE, Wilm TP, Basler N, Wright CVE, Solnica-Krezel L. Wnt8 is required in lateral mesendodermal precursors for neural posteriorization in vivo. *Development*(2001) 128(18):3571–83.

Falk MJ, Zhang Q, Nakamaru-Ogiso E, Kannabiran C, Fonseca-Kelly Z, Chakarova C, *et al.* NMNAT1 mutations cause Leber congenital amaurosis. *Nat Genet* (2012) 44(9):1040–5.

Fatima A, Sangwan VS, Iftekhar G, Reddy P, Matalia H, Balasubramanian D, *et al.* Technique of cultivating limbal derived corneal epithelium on human amniotic membrane for clinical transplantation. *J Postgrad Med* (2006) 52(4):257–61.

Fesenko EE, Kolesnikov SS, Lyubarsky AL. Induction by cyclic GMP of cationic conductance in plasma membrane of retinal rod outer segment. *Nature* (1985) 313(6000):310–3.

Freund CL, Wang Q-L, Chen S, Muskat BL, Wiles CD, Sheffield VC, *et al.* De novo mutations in the CRX homeobox gene associated with Leber congenital amaurosis. *Nat Genet* (1998) 18(4):311–2.

Friedman JS, Chang B, Kannabiran C, Chakarova C, Singh HP, Jalali S, *et al.* Premature Truncation of a Novel Protein, RD3, Exhibiting Subnuclear Localization Is Associated with Retinal Degeneration. *Am J Hum Genet* (2006) 79(6):1059–70.

Fu Y. Phototransduction in Rods and Cones [Internet]. Webvision: The Organization of the Retina and Visual System. University of Utah Health Sciences Center; (1995)

Fuhrmann S, Levine EM, Reh TA. Extraocular mesenchyme patterns the optic vesicle during early eye development in the embryonic chick. *Development* (2000) 127(21):4599–609.

Fuhrmann S. Eye Morphogenesis and Patterning of the Optic Vesicle. *Current topics in developmental biology* (2010) 61–84.

Garita-Hernandez M, Goureau O, Dalkara D. Gene and Cell Therapy for Inherited Retinal Dystrophies. In: eLS [Internet] (2016) p. 1–16.

Geng X, Speirs C, Lagutin O, Inbal A, Liu W, Solnica-Krezel L, *et al.* Haploinsufficiency of Six3 Fails to Activate Sonic hedgehog Expression in the Ventral Forebrain and Causes Holoprosencephaly. *Dev Cell.* (2008) 15(2):236–47.

Graw J. Genetic aspects of embryonic eye development in vertebrates. *Dev Genet* (1996) 18(3):181–97.

Grindley JC, Davidson DR, Hill RE. The role of Pax-6 in eye and nasal development. *Development* (1995) 121(5):1433–42.

Guziewicz KE, Cideciyan A V., Beltran WA, Komáromy AM, Dufour VL, Swider M, *et al.* BEST1 gene therapy corrects a diffuse retina-wide microdetachment modulated by light exposure. *Proc Natl Acad Sci* (2018) 115(12):E2839–48.

Haeseleer F, Huang J, Lebioda L, Saari JC, Palczewski K. Molecular Characterization of a Novel Short-chain Dehydrogenase/Reductase That Reduces All- trans -retinal. *J Biol Chem* (1998) 273(34):21790–9.

Hägglund A-C, Berghard A, Carlsson L. Canonical Wnt/β-Catenin Signalling Is Essential for Optic Cup Formation. Swaroop A, editor. *PLoS One* (2013) 8(12):e81158.

Hägglund A-C, Dahl L, Carlsson L. Lhx2 Is Required for Patterning and Expansion of a Distinct Progenitor Cell Population Committed to Eye Development. Reh TA, editor. *PLoS One* (2011) 6(8):e23387.

Hallonet M, Hollemann T, Pieler T, Gruss P. Vax1, a novel homeobox-containing gene, directs development of the basal forebrain and visual system. *Genes Dev* (1999) 13(23):3106–14.

Hayashi R, Ishikawa Y, Sasamoto Y, Katori R, Nomura N, Ichikawa T, *et al.* Co-ordinated ocular development from human iPS cells and recovery of corneal function. *Nature* (2016) 531(7594):376–80.

He W, Cowan CW WT. RGS9, a GTPase accelerator for phototransduction. *Neuron*(1998) (Jan;20(1)):95–102.

Heavner W, Pevny L. Eye Development and Retinogenesis. *Cold Spring Harb Perspect Biol* (2012) 4(12).

Heisenberg CP, Brand M, Jiang YJ, Warga RM, Beuchle D, van Eeden FJ, *et al.* Genes involved in forebrain development in the zebrafish, Danio rerio. *Development* (1996) 123:191–203.

Hiler D, Chen X, Hazen J, Kupriyanov S, Carroll PA, Qu C, *et al.* Quantification of Retinogenesis in 3D Cultures Reveals Epigenetic Memory and Higher Efficiency in iPSCs Derived from Rod Photoreceptors. *Cell Stem Cell* (2015) 17(1):101–15.

Hill RE, Favor J, Hogan BLM, Ton CCT, Saunders GF, Hanson IM, *et al.* Mouse Small eye results from mutations in a paired-like homeobox-containing gene. *Nature* (1991) 354(6354):522–5.

Hollander AI den, Heckenlively JR, van den Born LI, de Kok YJM, van der Velde-Visser SD, Kellner U, *et al.* Leber Congenital Amaurosis and Retinitis Pigmentosa with Coats-like Exudative Vasculopathy Are Associated with Mutations in the Crumbs Homologue 1 (CRB1) Gene. *Am J Hum Genet* (2001) 69(1):198–203.

Horsford DJ, Nguyen M-TT, Sellar GC, Kothary R, Arnheiter H, McInnes RR. Chx10 repression of Mitf is required for the maintenance of mammalian neuroretinal identity. *Development* (2004) 132(1):177–87.

Hotta A, Ellis J. Retroviral vector silencing during iPS cell induction: An epigenetic beacon that signals distinct pluripotent states. *J Cell Biochem* (2008) 105(4):940–8.

Huang J, Liu Y, Filas B, Gunhaga L, Beebe DC. Negative and positive auto-regulation of BMP expression in early eye development. *Dev Biol* (2015) 407(2):256–64.

Huang SH, Pittler SJ, Huang X, Oliveira L, Berson EL, Dryja TP. Autosomal recessive retinitis pigmentosa caused by mutations in the α subunit of rod cGMP phosphodiesterase. *Nat Genet* (1995) 11(4):468–71.

Hurley JB, Stryer L. Purification and characterization of the gamma regulatory subunit of the cyclic GMP phosphodiesterase from retinal rod outer segments. *J Biol Chem* (1982) 257(18):11094–9.

Hurley JB. Phototransduction. *Encyclopedia of Neuroscience* (2009) p. 687–92.

Ikeda H, Osakada F, Watanabe K, Mizuseki K, Haraguchi T, Miyoshi H, *et al.* Generation of Rx+/Pax6+ neural retinal precursors from embryonic stem cells. *Proc Natl Acad Sci* (2005) 102(32):11331–6.

Illing M, Molday LL, Molday RS. The 220-kDa Rim Protein of Retinal Rod Outer Segments Is a Member of the ABC Transporter Superfamily. *J Biol Chem* (1997) 272(15):10303–10.

Inamdar MS, Venu P, Srinivas MS, Rao K, VijayRaghavan K. Derivation and Characterization of Two Sibling Human Embryonic Stem Cell Lines From Discarded Grade III Embryos. *Stem Cells Dev* (2009) 18(3):423–34.

Inoue T, Kagawa T, Fukushima M, Shimizu T, Yoshinaga Y, Takada S, *et al.* Activation of Canonical Wnt Pathway Promotes Proliferation of Retinal Stem Cells Derived from Adult Mouse Ciliary Margin. *Stem Cells* (2006) 24(1):95–104.

Itskovitz-Eldor J, Schuldiner M, Karsenti D, Eden A, Yanuka O, Amit M, *et al.* Differentiation of human embryonic stem cells into embryoid bodies compromising the three embryonic germ layers. *Mol Med* (2000) 6(2):88–95.

Jacobson SG, Cideciyan A V., Ratnakaram R, Heon E, Schwartz SB, Roman AJ, *et al.* Gene Therapy for Leber Congenital Amaurosis Caused by RPE65 Mutations. *Arch Ophthalmol* (2012) 130(1):9.

Jean D, Ewan K, Gruss P. Molecular regulators involved in vertebrate eye development. *Mech Dev* (1998) 76(1–2):3–18.

Jia S, Muto A, Orisme W, Henson HE, Parupalli C, Ju B, *et al.* Zebrafish Cacna1fa is required for cone photoreceptor function and synaptic ribbon formation. *Hum Mol Genet* (2014) 23(11):2981–94.

Jin M, Li S, Moghrabi WN, Sun H, Travis GH. Rpe65 Is the Retinoid Isomerase in Bovine Retinal Pigment Epithelium. *Cell* (2005) 122(3):449–59.

Jin Z-B, Huang X-F, Lv J-N, Xiang L, Li D-Q, Chen J, *et al.* SLC7A14 linked to autosomal recessive retinitis pigmentosa. *Nat Commun* (2014) 5(1):3517.

Jin Z-B, Okamoto S, Osakada F, Homma K, Assawachananont J, Hirami Y, *et al.* Modeling Retinal Degeneration Using Patient-Specific Induced Pluripotent Stem Cells. Mattson M, editor. *PLoS One* (2011) 6(2):e17084.

Jin Z-B, Okamoto S, Xiang P, Takahashi M. Integration-Free Induced Pluripotent Stem Cells Derived from Retinitis Pigmentosa Patient for Disease Modeling. *Stem Cells Transl Med* (2012) 1(6):503–9.

Jinek M, Chylinski K, Fonfara I, Hauer M, Doudna JA, Charpentier E. A Programmable Dual-RNA-Guided DNA Endonuclease in Adaptive Bacterial Immunity. *Science* (2012) 337(6096):816–21.

Jones GJ, Crouch RK, Wiggert B, Cornwall MC, Chader GJ. Retinoid requirements for recovery of sensitivity after visual-pigment bleaching in isolated photoreceptors. *Proc Natl Acad Sci* (1989) 86(23):9606–10.

Kaewkhaw R, Kaya KD, Brooks M, Homma K, Zou J, Chaitankar V, *et al.* Transcriptome Dynamics of Developing Photoreceptors in Three-Dimensional Retina Cultures Recapitulates Temporal Sequence of Human Cone and Rod Differentiation Revealing Cell Surface Markers and Gene Networks. *Stem Cells* (2015) 33(12):3504–18.

Kang L, Wang J, Zhang Y, Kou Z, Gao S. iPS cells can support full-term development of tetraploid blastocyst-complemented embryos. *Cell Stem Cell* (2009) 5(2):135–8.

Kannabiran C, Palavalli L, Jalali S. Mutation of SPATA7 in a family with autosomal recessive early-onset retinitis pigmentosa. *J Mol Genet Med* (2012) 6:301–3.

Kannabiran C, Singh H, Sahini N, Jalali S, Mohan G. Mutations in TULP1, NR2E3, and MFRP genes in Indian families with autosomal recessive retinitis pigmentosa. *Mol Vis* (2012) 18:1165–74.

Kannabiran C, Singh HP, Jalali S. Mapping of locus for autosomal dominant retinitis pigmentosa on chromosome 6q23. *Hum Genet* (2012) 131(5):717–23.

Karlstrom RO, Trowe T, Klostermann S, Baier H, Brand M, Crawford AD, *et al.* Zebrafish mutations affecting retinotectal axon pathfinding. *Development* (1996) 123:427–38.

Kawamura S. Light-sensitivity modulating protein in frog rods. *Photochem Photobiol* (1992) 56(6):1173–80.

Kawamura S. Rhodopsin phosphorylation as a mechanism of cyclic GMP phosphodiesterase regulation by S-modulin. *Nature* (1993) 362(6423):855–7.

Keller SA, Jones JM, Boyle A, Barrow LL, Killen PD, Green DG, *et al.* Kidney and retinal defects (krd), a transgene-induced mutation with a deletion of mouse chromosome 19 that includes the pax2 locus. *Genomics.* (1994) 23(2):309–20.

Khan AO, Al Rashaed S, Neuhaus C, Bergmann C, Bolz HJ. Peripherin mutations cause a distinct form of recessive Leber congenital amaurosis and dominant phenotypes in asymptomatic parents heterozygous for the mutation. *Br J Ophthalmol* (2016) 100(2):209–15.

Khan FH, Pandian V, Ramraj SK, Aravindan S, Natarajan M, Azadi S, *et al.* RD3 loss dictates high-risk aggressive neuroblastoma and poor clinical outcomes. *Oncotarget* (2015) 6(34):36522–34.

Khani SC, Pawlyk BS, Bulgakov O V., Kasperek E, Young JE, Adamian M, *et al.* AAV-Mediated Expression Targeting of Rod and Cone Photoreceptors with a Human Rhodopsin Kinase Promoter. *Investig Opthalmology Vis Sci* (2007) 48(9):3954.

Kiecker C, Niehrs C. A morphogen gradient of Wnt/{beta}-catenin signalling regulates anteroposterior neural patterning in Xenopus. *Development* (2001) 128(21):4189–201.

Kim C. Disease modeling and cell based therapy with iPSC: future therapeutic option with fast and safe application. *Blood Res* (2014) 49(1):7–14.

Koenekoop RK, Wang H, Majewski J, Wang X, Lopez I, Ren H, *et al.* Mutations in NMNAT1 cause Leber congenital amaurosis and identify a new disease pathway for retinal degeneration. *Nat Genet* (2012) 44(9):1035–9.

Koenekoop RK. An overview of leber congenital amaurosis: a model to understand human retinal development. *Surv Ophthalmol* (2004) 49(4):379–98.

Kolesnikov A V., Tang PH, Kefalov VJ. Examining the Role of Cone-expressed RPE65 in Mouse Cone Function. *Sci Rep* (2018) 8(1):14201.

Koshiba-Takeuchi K. Tbx5 and the Retinotectum Projection. *Science* (2000) 287(5450):134–7. Available from: http://www.sciencemag.org/cgi/doi/10.1126/science.287.5450.134

Kostic C, Lillico SG, Crippa SV, Grandchamp N, Pilet H, Philippe S, *et al.* Rapid Cohort Generation and Analysis of Disease Spectrum of Large Animal Model of Cone Dystrophy. Stieger K, editor. *PLoS One* (2013) 8(8):e71363.

Kubo F. Wnt2b controls retinal cell differentiation at the ciliary marginal zone. *Development* (2003) 130(3):587–98.

Kühn H, Wilden U. Deactivation of photoactivated rhodopsin by rhodopsin-kinase and arrestin. *J Recept Res* (1987) 7(1–4):283–98.

Kukekova A V., Goldstein O, Johnson JL, Richardson MA, Pearce-Kelling SE, Swaroop A, *et al.* Canine RD3 mutation establishes rod-cone dysplasia type 2 (rcd2) as ortholog of human and murine rd3. *Mamm Genome* (2009) 20(2):109–23.

Lad EM, Cheshier SH, Kalani MYS. Wnt-Signaling in Retinal Development and Disease. *Stem Cells Dev* (2009) 18(1):7–16.

Lalitha K, Jalali S, Kadakia T, Kannabiran C. Screening for homozygosity by descent in families with autosomal recessive retinitis pigmentosa. *J Genet* (2002) 81(2):59–63.

Lamba DA, Reh TA. Microarray characterization of human embryonic stem cell derived retinal cultures. *Investig Ophthalmol Vis Sci* (2011) 52(7):4897–906.

Laurent LC, Ulitsky I, Slavin I, Tran H, Schork A, Morey R, *et al.* Dynamic Changes in the Copy Number of Pluripotency and Cell Proliferation Genes in Human ESCs and iPSCs during Reprogramming and Time in Culture. *Cell Stem Cell* (2011) 8(1):106–18.

Lekven AC, Thorpe CJ, Waxman JS, Moon RT. Zebrafish wnt8 Encodes Two Wnt8 Proteins on a Bicistronic Transcript and Is Required for Mesoderm and Neurectoderm Patterning. *Dev Cell.* (2001) 1(1):103–14.

Lenis TL, Hu J, Ng SY, Jiang Z, Sarfare S, Lloyd MB, *et al.* Expression of ABCA4 in the retinal pigment epithelium and its implications for Stargardt macular degeneration. *Proc Natl Acad Sci* (2018) 115(47):E11120–7.

Lerea C, Somers D, Hurley J, Klock I, Bunt-Milam A. Identification of specific transducin alpha subunits in retinal rod and cone photoreceptors. *Science* (1986) 234(4772):77–80.

Leskov IB, Klenchin VA, Handy JW, Whitlock GG, Govardovskii VI, Bownds MD, *et al.* The gain of rod phototransduction: reconciliation of biochemical and electrophysiological measurements. *Neuron* (2000) 27(3):525–37.

Li L, Nakaya N, Chavali VRM, Ma Z, Jiao X, Sieving PA, *et al.* A mutation in ZNF513, a putative regulator of photoreceptor development, causes autosomal-recessive retinitis pigmentosa. *Am J Hum Genet* (2010) 87(3):400–9.

Li Q, Timmers AM, Guy J, Pang J, Hauswirth WW. Cone-specific expression using a human red opsin promoter in recombinant AAV. *Vision Res* (2008) 48(3):332–8.

Li R, Liang J, Ni S, Zhou T, Qing X, Li H, *et al.* A Mesenchymal-to-Epithelial Transition Initiates and Is Required for the Nuclear Reprogramming of Mouse Fibroblasts. *Cell Stem Cell* (2010) 7(1):51–63.

Li Y, Sallam K, Schwartz PJ, Wu JC. Patient-Specific Induced Pluripotent Stem Cell-Based Disease Model for Pathogenesis Studies and Clinical Pharmacotherapy. *Circ Arrhythm Electrophysiol* (2017) 10(6).

Li Y, Wu W-H, Hsu C-W, Nguyen H V, Tsai Y-T, Chan L, *et al.* Gene Therapy in Patient-specific Stem Cell Lines and a Preclinical Model of Retinitis Pigmentosa With Membrane Frizzled-related Protein Defects. *Mol Ther* (2014) 22(9):1688–97.

Link BA, Collery RF. Zebrafish Models of Retinal Disease. *Annu Rev Vis Sci* (2015) 1(1):125–53.

Linker C, Stern CD, Steele K, George S, Smith WC. Neural induction requires BMP inhibition only as a late step, and involves signals other than FGF and Wnt antagonists. *Development* (2004) 131(22):5671–81.

Little CW, Castillo B, DiLoreto DA, Cox C, Wyatt J, del Cerro C, *et al.* Transplantation of human fetal retinal pigment epithelium rescues photoreceptor cells from degeneration in the Royal College of Surgeons rat retina. *Investig Ophthalmol Vis Sci* (1996) 37(1):204–11.

Liu IS, Chen JD, Ploder L, Vidgen D, van der Kooy D, Kalnins VI, *et al.* Developmental expression of a novel murine homeobox gene (Chx10): evidence for roles in determination of the neuroretina and inner nuclear layer. *Neuron* (1994) 13(2):377–93.

Liu J, Itagaki Y, Ben-Shabat S, Nakanishi K, Sparrow JR. The Biosynthesis of A2E, a Fluorophore of Aging Retina, Involves the Formation of the Precursor, A2-PE, in the Photoreceptor Outer Segment Membrane. *J Biol Chem* (2000) 275(38):29354–60.

Liu W, Lagutin O, Swindell E, Jamrich M, Oliver G. Neuroretina specification in mouse embryos requires Six3-mediated suppression of Wnt8b in the anterior neural plate. *J Clin Invest* (2010) 120(10):3568–77.

Lojewski X, Staropoli JF, Biswas-Legrand S, Simas AM, Haliw L, Selig MK, *et al.* Human iPSC models of neuronal ceroid lipofuscinosis capture distinct effects of TPP1 and CLN3 mutations on the endocytic pathway. *Hum Mol Genet* (2014) 23(8):2005–22.

Loosli F, Winkler S, Wittbrodt J. Six3 overexpression initiates the formation of ectopic retina. *Genes Dev.* (1999) 13(6):649–54.

Lu B, Malcuit C, Wang S, Girman S, Francis P, Lemieux L, *et al.* Long-Term Safety and Function of RPE from Human Embryonic Stem Cells in Preclinical Models of Macular Degeneration. *Stem Cells* (2009) 27(9):2126–35.

Lukovic D, Artero Castro A, Delgado ABG, Bernal M de los AM, Luna Pelaez N, Díez Lloret A, *et al.* Human iPSC derived disease model of MERTK-associated retinitis pigmentosa. *Sci Rep* (2015) 5(1):12910.

Lupo G, Novorol C, Smith JR, Vallier L, Miranda E, Alexander M, *et al.* Multiple roles of Activin/Nodal, bone morphogenetic protein, fibroblast growth factor and Wnt/ -catenin signalling in the anterior neural patterning of adherent human embryonic stem cell cultures. *Open Biol* (2013) (4):120167–120167.

Lustremant C, Habeler W, Plancheron A, Goureau O, Grenot L, de la Grange P, *et al.* Human Induced Pluripotent Stem Cells As a Tool to Model a Form of Leber Congenital Amaurosis. *Cell Reprogram* (2013) 15(3):233–46.

Macdonald R, Barth KA, Xu Q, Holder N, Mikkola I, Wilson SW. Midline signalling is required for Pax gene regulation and patterning of the eyes. *Development* (1995) 121(10):3267–78.

Maherali N, Hochedlinger K. Tgfβ Signal Inhibition Cooperates in the Induction of iPSCs and Replaces Sox2 and cMyc. *Curr Biol* (2009) 19(20):1718–23.

Maherali N, Sridharan R, Xie W, Utikal J, Eminli S, Arnold K, *et al.* Directly Reprogrammed Fibroblasts Show Global Epigenetic Remodeling and Widespread Tissue Contribution. *Cell Stem Cell* (2007) 1(1):55–70.

Mahla RS. Stem Cells Applications in Regenerative Medicine and Disease Therapeutics. *Int J Cell Biol* (2016) 2016:6940283.

Mali P, Yang L, Esvelt KM, Aach J, Guell M, DiCarlo JE, *et al.* RNA-Guided Human Genome Engineering via Cas9. *Science* (2013) 339(6121):823–6.

Malicki J, Neuhauss SC, Schier AF, Solnica-Krezel L, Stemple DL, Stainier DY, *et al.* Mutations affecting development of the zebrafish retina. *Development* (1996) 123:263–73.

Maminishkis A, Chen S, Jalickee S, Banzon T, Shi G, Wang FE, *et al.* Confluent Monolayers of Cultured Human Fetal Retinal Pigment Epithelium Exhibit Morphology and Physiology of Native Tissue. *Investig Opthalmology Vis Sci* (2006) 47(8):3612.

Mandai M, Watanabe A, Kurimoto Y, Hirami Y, Morinaga C, Daimon T, *et al.* Autologous Induced Stem-Cell–Derived Retinal Cells for Macular Degeneration. *N Engl J Med* (2017) 376(11):1038–46.

Mariappan I, Maddileti S, Savy S, Tiwari S, Gaddipati S, Fatima A, *et al.* In vitro culture and expansion of human limbal epithelial cells. *Nat Protoc* (2010) 5(8):1470–9.

Martínez-Mir A, Paloma E, Allikmets R, Ayuso C, Río T del, Dean M, *et al.* Retinitis pigmentosa caused by a homozygous mutation in the Stargardt disease gene ABCR. *Nat Genet* (1998) 18(1):11–2.

Mataftsi A, Schorderet DF, Chachoua L, Boussalah M, Nouri MT, Barthelmes D, *et al.* Novel TULP1 Mutation Causing Leber Congenital Amaurosis or Early Onset Retinal Degeneration. *Investig Opthalmology Vis Sci* (2007) 48(11):5160.

Mathers PH, Grinberg A, Mahon KA, Jamrich M. The Rx homeobox gene is essential for vertebrate eye development. *Nature.* (1997) 387(6633):603–7.

Maugeri A, van Driel MA, van de Pol DJR, Klevering BJ, van Haren FJJ, Tijmes N, *et al.* The 2588G→C Mutation in the ABCR Gene Is a Mild Frequent Founder Mutation in the Western European Population and Allows the Classification of ABCR Mutations in Patients with Stargardt Disease. *Am J Hum Genet* (1999) 64(4):1024–35.

McLaughlin ME, Sandberg MA, Berson EL, Dryja TP. Recessive mutations in the gene encoding the β–subunit of rod phosphodiesterase in patients with retinitis pigmentosa. *Nat Genet* (1993) 4(2):130–4.

Mehat MS, Sundaram V, Ripamonti C, Robson AG, Smith AJ, Borooah S, *et al.* Transplantation of Human Embryonic Stem Cell-Derived Retinal Pigment Epithelial Cells in Macular Degeneration. *Ophthalmology* (2018) 125(11):1765–75.

Mekala SR, Vauhini V, Nagarajan U, Maddileti S, Gaddipati S, Mariappan I. Derivation, characterization and retinal differentiation of induced pluripotent stem cells. *J Biosci* (2013) 38:123–34.

Mellough CB, Collin J, Khazim M, White K, Sernagor E, Steel DHW, *et al.* IGF-1 Signaling Plays an Important Role in the Formation of Three-Dimensional Laminated Neural Retina and Other Ocular Structures From Human Embryonic Stem Cells. *Stem Cells* (2015) 33(8):2416–30.

Messina A, Lan L, Incitti T, Bozza A, Andreazzoli M, Vignali R, *et al.* Noggin-Mediated Retinal Induction Reveals a Novel Interplay Between Bone Morphogenetic Protein Inhibition, Transforming Growth Factor β, and Sonic Hedgehog Signaling. *Stem Cells* (2015) 33(8):2496–508.

Meyer JS, Howden SE, Wallace KA, Verhoeven AD, Wright LS, Capowski EE, *et al.* Optic vesicle-like structures derived from human pluripotent stem cells facilitate a customized approach to retinal disease treatment. *Stem Cells* (2011) 29(8):1206–18.

Meyer JS, Shearer RL, Capowski EE, Wright LS, Wallace KA, McMillan EL, *et al.* Modeling early retinal development with human embryonic and induced pluripotent stem cells. *Proc Natl Acad Sci* (2009) 106(39):16698–703.

Miesfeld JB, Gestri G, Clark BS, Flinn MA, Poole RJ, Bader JR, *et al.* Yap and Taz regulate retinal pigment epithelial cell fate. *Development* (2015) 142(17):3021–32.

Mikkelsen TS, Hanna J, Zhang X, Ku M, Wernig M, Schorderet P, *et al.* Dissecting direct reprogramming through integrative genomic analysis. *Nature* (2008) 454(7200):49–55.

Mills EA, Goldman D. The Regulation of Notch Signaling in Retinal Development and Regeneration. *Curr Pathobiol Rep* (2017) 5(4):323–31.

Miraldi Utz V, Coussa RG, Antaki F, Traboulsi EI. Gene therapy for RPE65 -related retinal disease. *Ophthalmic Genet* (2018) 39(6):671–7.

Mitchell CH, Reigada D. Purinergic signalling in the subretinal space: a role in the communication between the retina and the RPE. *Purinergic Signal* (2008) 4(2):101–7.

Miyagishima KJ, Wan Q, Corneo B, Sharma R, Lotfi MR, Boles NC, *et al.* In Pursuit of Authenticity: Induced Pluripotent Stem Cell-Derived Retinal Pigment Epithelium for Clinical Applications. *Stem Cells Transl Med* (2016) 5(11):1562–74.

Miyoshi H, Takahashi M, Gage FH, Verma IM. Stable and efficient gene transfer into the retina using an HIV-based lentiviral vector. *Proc Natl Acad Sci* U S A (1997) 94(19):10319-23.

Mohamed MD, Topping NC, Jafri H, Raashed Y, McKibbin MA, Inglehearn CF. Progession of phenotype in Leber's congenital amaurosis with a mutation at the LCA5 locus. *Br J Ophthalmol* (2003) 87(4):473–5.

Molday RS, Zhong M, Quazi F. The role of the photoreceptor ABC transporter ABCA4 in lipid transport and Stargardt macular degeneration. *Biochim Biophys Acta* (2009) 1791(7):573–83.

Moosajee M, Tulloch M, Baron RA, Gregory-Evans CY, Pereira-Leal JB, Seabra MC. Single choroideremia Gene in Nonmammalian Vertebrates Explains Early Embryonic Lethality of the Zebrafish Model of Choroideremia. *Investig Opthalmology Vis Sci* (2009) 50(6):3009.

Mui SH, Hindges R, O'Leary DDM, Lemke G, Bertuzzi S. The homeodomain protein Vax2 patterns the dorsoventral and nasotemporal axes of the eye. *Development* (2002) 129(3):797–804.

Mui SH, Kim JW, Lemke G, Bertuzzi S. Vax genes ventralize the embryonic eye. *Genes Dev* (2005) 19(10):1249–59.

Nakagawa M, Koyanagi M, Tanabe K, Takahashi K, Ichisaka T, Aoi T, *et al.* Generation of induced pluripotent stem cells without Myc from mouse and human fibroblasts. Nat Biotechnol [Internet]. 2008 Jan 30 [cited 2019 Jun 4];26(1):101–6. Available from: http://www.ncbi.nlm.nih.gov/pubmed/18059259

Nakano T, Ando S, Takata N, Kawada M, Muguruma K, Sekiguchi K, *et al.* Self-Formation of Optic Cups and Storable Stratified Neural Retina from Human ESCs. *Cell Stem Cell* (2012) 10(6):771–85.

Nakao T, Tsujikawa M, Notomi S, Ikeda Y, Nishida K. The Role of Mislocalized Phototransduction in Photoreceptor Cell Death of Retinitis Pigmentosa. Koch K-W, editor. *PLoS One* (2012) 7(4):e32472.

Naldini L, Blömer U, Gage FH, Trono D, Verma IM. Efficient transfer, integration, and sustained long-term expression of the transgene in adult rat brains injected with a lentiviral vector. *Proc Natl Acad Sci U S A* (1996) 93(21):11382–8.

Nash BM, Wright DC, Grigg JR, Bennetts B, Jamieson R V. Retinal dystrophies, genomic applications in diagnosis and prospects for therapy. *Transl Pediatr* (2015) 4(2):139–63.

Nguyen M, Arnheiter H. Signaling and transcriptional regulation in early mammalian eye development: a link between FGF and MITF. *Development* (2000) 127(16):3581–91.

Niemitz E. Isogenic iPSC-derived models of disease. *Nat Genet* (2014) 46(1):7–7.

Nishihara D, Yajima I, Tabata H, Nakai M, Tsukiji N, Katahira T, *et al.* Otx2 Is Involved in the Regional Specification of the Developing Retinal Pigment Epithelium by Preventing the Expression of Sox2 and Fgf8, Factors That Induce Neural Retina Differentiation. *PLoS One* (2012) 7(11):e48879.

Nishimura DY, Baye LM, Perveen R, Searby CC, Avila-Fernandez A, Pereiro I, *et al.* Discovery and Functional Analysis of a Retinitis Pigmentosa Gene, C2ORF71. *Am J Hum Genet* (2010) 86(5):686–95.

Ohsaki K, Morimitsu T, Ishida Y, Kominami R, Takahashi N. Expression of the Vax family homeobox genes suggests multiple roles in eye development. *Genes Cells* (1999) 4(5):267–76.

Okita K, Ichisaka T, Yamanaka S. Generation of germline-competent induced pluripotent stem cells. *Nature* (2007) 448(7151):313–7.

Oliver G, Loosli F, Köster R, Wittbrodt J, Gruss P. Ectopic lens induction in fish in response to the murine homeobox gene Six3. *Mech Dev* (1996) 60(2):233–9.

Osakada F, Jin Z-B, Hirami Y, Ikeda H, Danjyo T, Watanabe K, *et al.* In vitro differentiation of retinal cells from human pluripotent stem cells by small-molecule induction. *J Cell Sci* (2009) 122(Pt 17):3169–79.

Page-McCaw PS, Chung SC, Muto A, Roeser T, Staub W, Finger-Baier KC, *et al.* Retinal network adaptation to bright light requires tyrosinase. *Nat Neurosci* (2004) 7(12):1329–36.

Pang J-J, Alexander J, Lei B, Deng W, Zhang K, Li Q, *et al.* Achromatopsia as a potential candidate for gene therapy. *Adv Exp Med Biol* (2010) 664:639–46.

Parfitt DA, Lane A, Ramsden CM, Carr A-JF, Munro PM, Jovanovic K, *et al.* Identification and Correction of Mechanisms Underlying Inherited Blindness in Human iPSC-Derived Optic Cups. *Cell Stem Cell* (2016) 18(6):769–81.

Park SS, Bauer G, Abedi M, Pontow S, Panorgias A, Jonnal R, *et al.* Intravitreal Autologous Bone Marrow CD34+ Cell Therapy for Ischemic and Degenerative Retinal Disorders: Preliminary Phase 1 Clinical Trial Findings. *Investig Ophthalmol Vis Sci* (2015) 56(1):81–9.

Pattnaik BR, Tokarz S, Asuma MP, Schroeder T, Sharma A, Mitchell JC, *et al.* Snowflake Vitreoretinal Degeneration (SVD) Mutation R162W Provides New Insights into Kir7.1 Ion Channel Structure and Function. Kanzaki M, editor. *PLoS One* (2013) 8(8):e71744.

Peng G-H, Chen S. Crx activates opsin transcription by recruiting HAT-containing co-activators and promoting histone acetylation. Hum Mol Genet [Internet]. 2007 Oct 15 [cited 2019 Jun 30];16(20):2433–52. Available from: https://academic.oup.com/hmg/article-lookup/doi/10.1093/hmg/ddm200

Perea-Gomez A, Vella FDJ, Shawlot W, Oulad-Abdelghani M, Chazaud C, Meno C, *et al.* Nodal antagonists in the anterior visceral endoderm prevent the formation of multiple primitive streaks. *Dev Cell* (2002) 3(5):745–56.

Perrault I, Estrada-Cuzcano A, Lopez I, Kohl S, Li S, Testa F, *et al.* Union Makes Strength: A Worldwide Collaborative Genetic and Clinical Study to Provide a Comprehensive Survey of RD3 Mutations and Delineate the Associated Phenotype. Brusgaard K, editor. *PLoS One* (2013) 8(1):e51622.

Perrault I, Hanein S, Gerber S, Barbet F, Ducroq D, Dollfus H, *et al.* Retinal Dehydrogenase 12 (RDH12) Mutations in Leber Congenital Amaurosis. *Am J Hum Genet* (2004) 75(4):639–46.

Perrault I, Hanein S, Gerber S, Lebail B, Vlajnik P, Barbet F, *et al.* A novel mutation in the GUCY2D gene responsible for an early onset severe RP different from the usual GUCY2D-LCA phenotype. *Hum Mutat* (2005) 25(2):222–222.

Peshenko I V., Olshevskaya E V., Azadi S, Molday LL, Molday RS, Dizhoor AM. Retinal Degeneration 3 (RD3) Protein Inhibits Catalytic Activity of Retinal Membrane Guanylyl Cyclase (RetGC) and Its Stimulation by Activating Proteins. *Biochemistry* (2011) 50(44):9511–9.

Peterson WM, Meggyesy C, Yu K, Miller SS. Extracellular ATP activates calcium signaling, ion, and fluid transport in retinal pigment epithelium. *J Neurosci* (1997) 17(7):2324–37.

Pierce EA, Bennett J. The Status of RPE65 Gene Therapy Trials: Safety and Efficacy. *Cold Spring Harb Perspect Med* (2015) 5(9):a017285.

Pittack C, Grunwald GB, Reh TA. Fibroblast growth factors are necessary for neural retina but not pigmented epithelium differentiation in chick embryos. *Development* (1997) 124(4):805–16.

Porter FD, Drago J, Xu Y, Cheema SS, Wassif C, Huang SP, *et al.* Lhx2, a LIM homeobox gene, is required for eye, forebrain, and definitive erythrocyte development. *Development* (1997) 124(15):2935–44.

Preising MN, Hausotter-Will N, Solbach MC, Friedburg C, Rüschendorf F, Lorenz B. Mutations in RD3 Are Associated with an Extremely Rare and Severe Form of Early Onset Retinal Dystrophy. *Investig Opthalmology Vis Sci* (2012) 53(7):3463.

Quazi F, Lenevich S, Molday RS. ABCA4 is an N-retinylidene-phosphatidylethanolamine and phosphatidylethanolamine importer. *Nat Commun* (2012) 3(1):925.

Quinn R H, Miller SS. Ion transport mechanisms in native human retinal pigment epithelium. *Investig Ophthalmol Vis Sci* (1992) 33(13):3513–27.

Ramachandran C, Basu S, Sangwan VS, Balasubramanian D. Concise review: the coming of age of stem cell treatment for corneal surface damage. *Stem Cells Transl Med* (2014) 3(10):1160–8.

Redmond TM, Poliakov E, Yu S, Tsai J-Y, Lu Z, Gentleman S. Mutation of key residues of RPE65 abolishes its enzymatic role as isomerohydrolase in the visual cycle. *Proc Natl Acad Sci* (2005) 102(38):13658–63.

Reichman S, Terray A, Slembrouck A, Nanteau C, Orieux G, Habeler W, *et al.* From confluent human iPS cells to self-forming neural retina and retinal pigmented epithelium. *Proc Natl Acad Sci* (2014) 111(23):8518–23.

Rembold M, Loosli F, Adams RJ, Wittbrodt J. Individual cell migration serves as the driving force for optic vesicle evagination. *Science* (2006) 313(5790):1130–4.

Riera M, Burguera D, Garcia-Fernàndez J, Gonzàlez-Duarte R. CERKL knockdown causes retinal degeneration in zebrafish. *PLoS One* (2013) 8(5):e64048.

Saari JC, Bredberg DL. Lecithin:retinol acyltransferase in retinal pigment epithelial microsomes. *J Biol Chem* (1989) 264(15):8636–40.

Saari JC, Bredberg L, Garwin GG. Identification of the endogenous retinoids associated with three cellular retinoid-binding proteins from bovine retina and retinal pigment epithelium. *J Biol Chem* (1982) 257(22):13329–33.

Saari JC, Nawrot M, Kennedy BN, Garwin GG, Hurley JB, Huang J, *et al.* Visual cycle impairment in cellular retinaldehyde binding protein (CRALBP) knockout mice results in delayed dark adaptation. *Neuron* (2001) 29(3):739–48.

Samavarchi-Tehrani P, Golipour A, David L, Sung H, Beyer TA, Datti A, *et al.* Functional Genomics Reveals a BMP-Driven Mesenchymal-to-Epithelial Transition in the Initiation of Somatic Cell Reprogramming. *Cell Stem Cell* (2010) 7(1):64–77.

Samavarchi-Tehrani P, Golipour A, David L, Sung H, Beyer TA, Datti A, *et al.* Functional Genomics Reveals a BMP-Driven Mesenchymal-to-Epithelial Transition in the Initiation of Somatic Cell Reprogramming. *Cell Stem Cell* (2010) 7(1):64–77.

Sampath P, Pritchard DK, Pabon L, Reinecke H, Schwartz SM, Morris DR, *et al.* A Hierarchical Network Controls Protein Translation during Murine Embryonic Stem Cell Self-Renewal and Differentiation. *Cell Stem Cell* (2008) 2(5):448–60.

Sasagawa S, Takabatake T, Takabatake Y, Muramatsu T, Takeshima K. Axes establishment during eye morphogenesis inXenopus by coordinate and antagonistic actions of BMP4, Shh, and RA. *Genesis* (2002) 33(2):86–96.

Schappert-Kimmijser J, Henkes H, Van Den Bosch J. Amaurosis congenita (Leber). *AMA Arch Ophthalmol* (1959) 61(2):211–8.

Schwartz SD, Hubschman J-P, Heilwell G, Franco-Cardenas V, Pan CK, Ostrick RM, *et al.* Embryonic stem cell trials for macular degeneration: a preliminary report. *Lancet* (2012) 379(9817):713–20.

Schwartz SD, Regillo CD, Lam BL, Eliott D, Rosenfeld PJ, Gregori NZ, *et al.* Human embryonic stem cell-derived retinal pigment epithelium in patients with age-related macular degeneration and Stargardt's macular dystrophy: follow-up of two open-label phase 1/2 studies. *Lancet* (2015) 385(9967):509–16.

Schwarz M, Cecconi F, Bernier G, Andrejewski N, Kammandel B, Wagner M, *et al.* Spatial specification of mammalian eye territories by reciprocal transcriptional repression of Pax2 and Pax6. *Development* (2000)127(20):4325–34.

Shahi PK, Liu X, Aul B, Moyer A, Pattnaik A, Denton J, *et al.* Abnormal Electroretinogram after Kir7.1 Channel Suppression Suggests Role in Retinal Electrophysiology. *Sci Rep* (2017) 7(1):10651.

Sergouniotis PI, Davidson AE, Mackay DS, Li Z, Yang X, Plagnol V, *et al.* Recessive mutations in KCNJ13, encoding an inwardly rectifying potassium channel subunit, cause leber congenital amaurosis. *Am J Hum Genet* (2011) 89(1):183–90.

Shahi PK, Liu X, Aul B, Moyer A, Pattnaik A, Denton J, *et al.* Abnormal Electroretinogram after Kir7.1 Channel Suppression Suggests Role in Retinal Electrophysiology. *Sci Rep* (2017) 7(1):10651.

Sharma R, Khristov V, Rising A, Jha BS, Dejene R, Hotaling N, *et al.* Clinical-grade stem cell–derived retinal pigment epithelium patch rescues retinal degeneration in rodents and pigs. *Sci Transl Med* (2019) 11(475):eaat5580.

Sharma TP, Wiley LA, Whitmore SS, Anfinson KR, Cranston CM, Oppedal DJ, *et al.* Patient-specific induced pluripotent stem cells to evaluate the pathophysiology of TRNT1-associated Retinitis pigmentosa. *Stem Cell Res* (2017) 21:58–70.

Shen MM. Nodal signaling: developmental roles and regulation. *Development* (2007) 134(6):1023–34.

Shen S, Sujirakul T, Tsang SH. Next-generation Sequencing Revealed a Novel Mutation in the Gene Encoding the Beta Subunit of Rod Phosphodiesterase. *Ophthalmic Genet* (2014) 35(3):142–50.

Shetty R, Inamdar MS. Derivation of Human Embryonic Stem Cell Lines from Poor Quality Embryos. *Methods in molecular biology* (2012) 873:151-61.

Shi Y, Inoue H, Wu JC, Yamanaka S. Induced pluripotent stem cell technology: a decade of progress. *Nat Rev Drug Discov* (2017) 16(2):115–30.

Shroyer NF, Lewis RA, Allikmets R, Singh N, Dean M, Leppert M, *et al.* The rod photoreceptor ATP-binding cassette transporter gene, ABCR, and retinal disease: from monogenic to multifactorial. *Vision Res* (1999) 39(15):2537–44.

Shu X, Zeng Z, Gautier P, Lennon A, Gakovic M, Cheetham ME, *et al.* Knockdown of the Zebrafish Ortholog of the Retinitis Pigmentosa 2 (RP2) Gene Results in Retinal Degeneration. *Investig Opthalmology Vis Sci* (2011) 52(6):2960.

Shu X, Zeng Z, Gautier P, Lennon A, Gakovic M, Patton EE, *et al.* Zebrafish Rpgr is required for normal retinal development and plays a role in dynein-based retrograde transport processes. *Hum Mol Genet* (2010) 19(4):657–70.

Simon A, Hellman U, Wernstedt C, Eriksson U. The retinal pigment epithelial-specific 11-cis retinol dehydrogenase belongs to the family of short chain alcohol dehydrogenases. *J Biol Chem* (1995) 270(3):1107–12.

Singh HP, Jalali S, Hejtmancik JF, Kannabiran C. Homozygous Null Mutations in the ABCA4 Gene in Two Families With Autosomal Recessive Retinal Dystrophy. *Am J Ophthalmol.* (2006) 141(5):906–13.

Singh HP, Jalali S, Narayanan R, Kannabiran C. Genetic analysis of Indian families with autosomal recessive retinitis pigmentosa by homozygosity screening. *Investig Ophthalmol Vis Sci* (2009) 50(9):4065–71.

Singh R, Shen W, Kuai D, Martin JM, Guo X, Smith MA, *et al.* iPS cell modeling of Best disease: insights into the pathophysiology of an inherited macular degeneration. *Hum Mol Genet* (2013) 22(3):593–607.

Sinha D, Phillips J, Joseph Phillips M, Gamm DM. Mimicking Retinal Development and Disease With Human Pluripotent Stem Cells. *Investig Opthalmology Vis Sci* (2016) 57(5):ORSFf1.

Siqueira RC, Messias A, Voltarelli JC, Scott IU, Jorge R. Intravitreal Injection Of Autologous Bone Marrow–Derived Mononuclear Cells For Hereditary Retinal Dystrophy. *Retina* (2011) 31(6):1207–14.

Smith ZD, Nachman I, Regev A, Meissner A. Dynamic single-cell imaging of direct reprogramming reveals an early specifying event. *Nat Biotechnol* (2010) 28(5):521–6.

Song WK, Park K-M, Kim H-J, Lee JH, Choi J, Chong SY, *et al.* Treatment of Macular Degeneration Using Embryonic Stem Cell-Derived Retinal Pigment Epithelium: Preliminary Results in Asian Patients. *Stem Cell Reports* (2015) 4(5):860–72.

Sowden JC. ESC-Derived Retinal Pigmented Epithelial Cell Transplants in Patients: So Far, So Good. *Cell Stem Cell* (2014) 15(5):537–8.

Sridharan R, Tchieu J, Mason MJ, Yachechko R, Kuoy E, Horvath S, *et al.* Role of the Murine Reprogramming Factors in the Induction of Pluripotency. *Cell* (2009) 136(2):364–77.

Stearns G, Evangelista M, Fadool JM, Brockerhoff SE. A Mutation in the Cone-Specific pde6 Gene Causes Rapid Cone Photoreceptor Degeneration in Zebrafish. *J Neurosci* (2007) 27(50):13866–74.

Stiebel-Kalish H, Reich E, Rainy N, Vatine G, Nisgav Y, Tovar A, *et al.* Gucy2f zebrafish knockdown – a model for Gucy2d-related leber congenital amaurosis. *Eur J Hum Genet* (2012) 20(8):884–9.

Stone EM. Leber Congenital Amaurosis–A Model for Efficient Genetic Testing of Heterogeneous Disorders: LXIV Edward Jackson Memorial Lecture. *Am J Ophthalmol* (2007) 144(6):791-811.e6.

Streit A, Stern CD. Neural induction: a bird's eye view. *Trends Genet* (1999) 15(1):20–4.

Sun H, Smallwood PM, Nathans J. Biochemical defects in ABCR protein variants associated with human retinopathies. *Nat Genet* (2000) 26(2):242–6.

Takahashi K, Tanabe K, Ohnuki M, Narita M, Ichisaka T, Tomoda K, *et al.* Induction of Pluripotent Stem Cells from Adult Human Fibroblasts by Defined Factors. *Cell* (2007) 131(5):861–72.

Takahashi VKL, Takiuti JT, Jauregui R, Tsang SH. Gene therapy in inherited retinal degenerative diseases, a review. *Ophthalmic Genet* (2018) 39(5):560–8.

Take-uchi M. Hedgehog signalling maintains the optic stalk-retinal interface through the regulation of Vax gene activity. *Development* (2003) 130(5):955–68.

Tang PH, Buhusi MC, Ma J-X, Crouch RK. RPE65 Is Present in Human Green/Red Cones and Promotes Photopigment Regeneration in an In Vitro Cone Cell Model. *J Neurosci* (2011) 31(50):18618–26.

Tang S, Xie M, Cao N, Ding S. Patient-Specific Induced Pluripotent Stem Cells for Disease Modeling and Phenotypic Drug Discovery. *J Med Chem* (2016) 59(1):2–15.

Thomson JA, Itskovitz-Eldor J, Shapiro SS, Waknitz MA, Swiergiel JJ, Marshall VS, *et al.* Embryonic stem cell lines derived from human blastocysts. *Science* (1998) 282(5391):1145–7.

Travis GH, Golczak M, Moise AR, Palczewski K. Diseases Caused by Defects in the Visual Cycle: Retinoids as Potential Therapeutic Agents. *Annu Rev Pharmacol Toxicol* (2007) 47(1):469–512.

Tucker BA, Mullins RF, Streb LM, Anfinson K, Eyestone ME, Kaalberg E, *et al.* Patient-specific iPSC-derived photoreceptor precursor cells as a means to investigate retinitis pigmentosa. *Elife* (2013) 2.

Tucker BA, Scheetz TE, Mullins RF, DeLuca AP, Hoffmann JM, Johnston RM, *et al.* Exome sequencing and analysis of induced pluripotent stem cells identify the cilia-related gene male germ cell-associated kinase (MAK) as a cause of retinitis pigmentosa. *Proc Natl Acad Sci U S A* (2011) 108(34):E569-76.

Turner DL, Cepko CL. A common progenitor for neurons and glia persists in rat retina late in development. *Nature* (1987) 328(6126):131–6.

Tzoulaki I, White IM, Hanson IM. PAX6 mutations: genotype-phenotype correlations. *BMC Genet* (2005) 6(1):27.

van Driel MA, Maugeri A, Klevering BJ, Hoyng CB, Cremers FP. ABCR unites what ophthalmologists divide(s). *Ophthalmic Genet* (1998) 19(3):117–22.

Varshney GK, Pei W, LaFave MC, Idol J, Xu L, Gallardo V, *et al.* High-throughput gene targeting and phenotyping in zebrafish using CRISPR/Cas9. *Genome Res* (2015) 25(7):1030–42.

Venu P, Chakraborty S, Inamdar MS. Analysis of long-term culture properties and pluripotent character of two sibling human embryonic stem cell lines derived from discarded embryos. *Vitr Cell Dev Biol Anim* (2010) 46(3–4):200–5.

Völkner M, Zschätzsch M, Rostovskaya M, Overall RW, Busskamp V, Anastassiadis K, *et al.* Retinal Organoids from Pluripotent Stem Cells Efficiently Recapitulate Retinogenesis. *Stem cell reports* (2016) 6(4):525–38.

Voronina VA, Kozhemyakina EA, O'Kernick CM, Kahn ND, Wenger SL, Linberg J V., *et al.* Mutations in the human RAX homeobox gene in a patient with anophthalmia and sclerocornea. *Hum Mol Genet.* 2004;13(3):315–22.

Wang H, den Hollander AI, Moayedi Y, Abulimiti A, Li Y, Collin RWJ, *et al.* Mutations in SPATA7 Cause Leber Congenital Amaurosis and Juvenile Retinitis Pigmentosa. *Am J Hum Genet* (2009) 84(3):380–7.

Warwick R. Eugene Wolff'S Anatomy Of The Eye And Orbit. 7th edition. *Saunders.* (1976)

Wenzel A, von Lintig J, Oberhauser V, Tanimoto N, Grimm C, Seeliger MW. RPE65 Is Essential for the Function of Cone Photoreceptors in NRL-Deficient Mice. *Investig Opthalmology Vis Sci* (2007) 48(2):534.

Wernig M, Meissner A, Foreman R, Brambrink T, Ku M, Hochedlinger K, *et al.* In vitro reprogramming of fibroblasts into a pluripotent ES-cell-like state. *Nature* (2007) 448(7151):318–24.

Westenskow P, Piccolo S, Fuhrmann S. -catenin controls differentiation of the retinal pigment epithelium in the mouse optic cup by regulating Mitf and Otx2 expression. *Development* (2009) 136(15):2505–10.

Wiedenheft B, Sternberg SH, Doudna JA. RNA-guided genetic silencing systems in bacteria and archaea. *Nature* (2012) 482(7385):331–8.

Wilden U, Hall SW, Kuhn H. Phosphodiesterase activation by photoexcited rhodopsin is quenched when rhodopsin is phosphorylated and binds the intrinsic 48-kDa protein of rod outer segments. *Proc Natl Acad Sci* (1986) 83(5):1174–8.

Wiley LA, Burnight ER, Songstad AE, Drack A V., Mullins RF, Stone EM, *et al.* Patient-specific induced pluripotent stem cells (iPSCs) for the study and treatment of retinal degenerative diseases. *Prog Retin Eye Res* (2015) 44:15–35.

Wimberg H, Janssen-Bienhold U, Koch K-W. Control of the Nucleotide Cycle in Photoreceptor Cell Extracts by Retinal Degeneration Protein 3. *Front Mol Neurosci* (2018) 11:52.

Wolf G. The Visual Cycle of the Cone Photoreceptors of the Retina. *Nutr Rev* (2004) 62(7):283–6.

Wu Q, Blakeley LR, Cornwall MC, Crouch RK, Wiggert BN, Koutalos Y. Interphotoreceptor Retinoid-Binding Protein Is the Physiologically Relevant Carrier That Removes Retinol from Rod Photoreceptor Outer Segments. *Biochemistry* (2007) 46(29):8669–79.

Yang D, Pan A, Swaminathan A, Kumar G, Hughes BA. Expression and Localization of the Inwardly Rectifying Potassium Channel Kir7.1 in Native Bovine Retinal Pigment Epithelium. *Investig Opthalmology Vis Sci* (2003) 44(7):3178.

Yau K-W, Nakatani K. Light-suppressible, cyclic GMP-sensitive conductance in the plasma membrane of a truncated rod outer segment. *Nature* (1985) 317(6034):252–5.

Yin J, Brocher J, Fischer U, Winkler C. Mutant Prpf31 causes pre-mRNA splicing defects and rod photoreceptor cell degeneration in a zebrafish model for Retinitis pigmentosa. *Mol Neurodegener* (2011) 6:56.

Yoshida T, Ozawa Y, Suzuki K, Yuki K, Ohyama M, Akamatsu W, *et al.* The use of induced pluripotent stem cells to reveal pathogenic gene mutations and explore treatments for retinitis pigmentosa. *Mol Brain* (2014) 7(1):45.

Young RW. Cell differentiation in the retina of the mouse. *Anat Rec* (1985) 212(2):199–205.

Yun S, Saijoh Y, Hirokawa KE, Kopinke D, Murtaugh LC, Monuki ES, *et al.* Lhx2 links the intrinsic and extrinsic factors that control optic cup formation. *Development* (2009) 136(23):3895–906.

Yvon C, Ramsden CM, Lane A, Powner MB, da Cruz L, Coffey PJ, *et al.* Using Stem Cells to Model Diseases of the Outer Retina. *Comput Struct Biotechnol J* (2015) 13:382–9.

Zagozewski JL, Zhang Q, Eisenstat DD. Genetic regulation of vertebrate eye development. *Clin Genet* (2014) 86(5):453–60.

Zhang N, Tsybovsky Y, Kolesnikov A V., Rozanowska M, Swider M, Schwartz SB, *et al.* Protein misfolding and the pathogenesis of ABCA4-associated retinal degenerations. *Hum Mol Genet* (2015) 24(11):3220–37.

Zhao J, Jiang W, Sun C, Hou C, Yang X-M, Gao J. Induced pluripotent stem cells: origins, applications, and future perspectives. *J Zhejiang Univ Sci B* (2013) 14(12):1059–69.

Zhong M, Molday LL, Molday RS. Role of the C Terminus of the Photoreceptor ABCA4 Transporter in Protein Folding, Function, and Retinal Degenerative Diseases. *J Biol Chem* (2009) 284(6):3640–9.

Zhong X, Gutierrez C, Xue T, Hampton C, Vergara MN, Cao L-H, *et al.* Generation of three-dimensional retinal tissue with functional photoreceptors from human iPSCs. *Nat Commun* (2014) 5:4047.

Zhong X, Gutierrez C, Xue T, Hampton C, Vergara MN, Cao L-H, *et al.* Generation of three-dimensional retinal tissue with functional photoreceptors from human iPSCs. *Nat Commun* (2014) 5:4047.

Zhu J, Reynolds J, Garcia T, Cifuentes H, Chew S, Zeng X, *et al.* Generation of Transplantable Retinal Photoreceptors from a Current Good Manufacturing Practice-Manufactured Human Induced Pluripotent Stem Cell Line. *Stem Cells Transl Med* (2018) 7(2):210–9.

Zhu X, Ma B, Babu S, Murage J, Knox BE, Craft CM. Mouse cone arrestin gene characterization: promoter targets expression to cone photoreceptors. *FEBS Lett* (2002) 524(1–3):116–22.

Znoiko SL, Crouch RK, Moiseyev G, Ma J-X. Identification of the RPE65 protein in mammalian cone photoreceptors. *Investig Ophthalmol Vis Sci* (2002) 43(5):1604–9.

Zuber ME, Gestri G, Viczian AS, Barsacchi G, Harris WA. Specification of the vertebrate eye by a network of eye field transcription factors. *Development* (2003) 130(21):5155–67.

Züchner S, Dallman J, Wen R, Beecham G, Naj A, Farooq A, *et al.* Whole-Exome Sequencing Links a Variant in DHDDS to Retinitis Pigmentosa. *Am J Hum Genet* (2011) 88(2):201–6.

ANNEXURES

I. Patient Volunteer Consent Form

Consent to participate in research

Title of Research: Generation of disease-specific induced pluripotent stem cells (iPSCs) from dermal fibroblasts of patients with retinal dystrophy.

Investigators: Dr. Indumathi Mariappan (Scientist-Cell Biologist)
Dr. Chitra kannabiran (Scientist-Geneticist)
Dr. Subhadra Jalali (Retina Consultant)
Dr. Milind N. Naik (Ophthalmic Plastic Surgeon).

Institute: L V Prasad Eye Institute
L V Prasad Marg
Road No: 2, Banjara Hills
Hyderabad, Telangana, India

Invitation: You are invited to participate in this research study as a volunteer. The investigator would like to take a sample of dermis of retro-auricular skin for its use in experiments involving human stem cell research.

The purpose of this study: The skin biopsy obtained would be used to derive patient-specific dermal fibroblast (hFib) cultures. The hFib cells obtained from a genetically defective patient can be eventually used for making a patient specific induced pluripotent stem cell line (iPS), which can be either used as an *in vitro* model system to study the disease or can be further manipulated to correct the genetic defect and use them in cell replacement therapy. The derivation of patient specific pluripotent stem cells would be carried out in collaboration with Prof. George Daley's Laboratory at Children's Hospital, Boston.

Pluripotent Stem Cells are "master cells" that can form many types of cells found in the body. Pluripotent stem cells come from at least two sources. One type of pluripotent stem cell, called an embryonic stem cell, is taken from early stage human embryos. Another type of pluripotent stem cell are made by inserting genes into matured cells from the body. This procedure is called "direct reprogramming" and it creates a type of cell called an "induced" Pluripotent Stem Cell (iPSCs). These pluripotent stem cells can be differentiated to specific human tissues, like blood, skin, heart muscle, neurons, insulin secreting pancreatic β-Cells and even photoreceptor cells of an eye.

We and other researchers want to make pluripotent stem cells from the skin tissue of patients with diseases to study the pathophysiology of the disease and hope to manipulate these cells to correct the genetic defect for possible cell replacement therapy. Pluripotent stem cells can also be used as a disease model to test the effectiveness of new drugs.

In this study, we request you to allow a doctor to take a sample of skin biopsy from your retro-auricular surface. The doctor will perform a 6mmX6mm skin biopsy under local anesthesia. The scientists would use the cells grown from the skin biopsy as a "somatic

donor cell" in their stem cell experiments. We also need information about your health so that any stem cells we isolate from your tissue would represent your disease or condition.

We also inform you that the cells taken from your skin tissue would be treated in tissue culture dishes with genes and/or chemicals to "reprogram" them into pluripotent stem cells. The stem cell lines that are made will contain your DNA and therefore will be a perfect genetic match of you.

This research study is aimed at advancing knowledge only, and may not result in any direct medical benefit to you or specific patients.

1. I **Dr. Indumathi Mariappan** have fully explained to _____
(name of person providing information) *(somatic cell donor, ID #)*

the nature and purpose of the research protocol and the procedures involved in obtaining somatic cells for human stem cell research.

Signed:_____ Date:_____

2. I _____confirm that **Dr. Indumathi Mariappan**
(name of donor) *(name of person providing information)*

A. has fully explained the nature and purpose of the research protocol in a plain and easy to comprehend manner.
B. has encouraged me to be actively involved during the consent process and has answered all of my questions and concerns in a satisfactory and respectful manner.
C. has offered me opportunities to consult with other persons prior to my providing consent and has given me adequate time to decide whether to provide consent.
D. has given me detailed and satisfactory explanations for each of the following points:

i. that the research is not intended to provide direct medical benefit to me or anyone else.
ii. that cells from a skin biopsy provided by me will be used to make human pluripotent stem cells through reprogramming.
iii. that my cells may be genetically manipulated before being used in experiments.
iv. that the stem cells or cell lines that are generated in these experiments will be genetically matched to me.
v. that the stem cells or cell lines that are generated in these experiments might be kept for many years and may be used for any legal research purpose (except those specifically excluded by this informed consent form) including research that may not presently be anticipated.
vi. that the stem cells or cell lines that are generated in these experiments might be used in research involving genetic or chemical manipulation of the cells.
vii. that the stem cells or cell lines that are generated in these experiments might be shared with researchers at other institutions.
viii. that even if the stem cells or cell lines that are generated in these experiments are limited to specific research purposes only, and not others, permission for broader uses may later be granted by an ethical or institutional review board.

ix. that researchers must tell me what medical or other information that might identify me or link me to the cells will be retained, and what specific steps they will take to protect the confidentiality of my retained information.
x. that researchers must tell me whether my identity will be readily available to those who make or work with the resulting stem cell lines, or any other entity or person, including specifically any oversight bodies and government agencies.
xi. that any resulting cells or cell lines may have commercial potential and that I will not claim financial benefits from any future commercial development and/or patents of discoveries.
xii. that there may be present or potential financial benefits to the investigator and the institution related to or arising from the proposed research.
xvi. that other research institutions or researchers at other institutions may have financial interests arising from discoveries made from these cells or cell lines.
xiii. that I will not claim any (cash or in kind) payments for donating my cells.
xiv. that somatic cell donation by skin biopsy sample may pose a minor discomfort.
xv. that I may withdraw my consent at any time prior to the point at which my cells are used in research.
xvi. that if I am uncomfortable with having my cells or DNA used in any form of stem cell research, or having my genetic material maintained as cells in a laboratory, that I should refuse to participate in this study.

3. I hereby give my voluntary and informed consent to donate my skin sample for the following human stem cell research protocol:

Generation of induced pleuripotent stem cells (iPSCs) from dermal fibroblasts of patients with retinitis pigmentosa,

Carried out by **Dr. M. Indumathi Mariappan**, Scientist, Stem Cell Biology Laboratory, LVPEI, Road No: 2, Banjara Hills, Hyderabad – 500 034, India.

Signed:_____ **Date:**_____
(somatic cell donor, ID #)

II. Media compositions

cDMEM
DMEM-F12 basal medium containing 10% Fetal bovine serum (FBS), 100 U/ml Penicillin-Streptomycin solution and 2 mM GlutaMax™

cDMEM with 20% FBS
DMEM-F12 basal medium containing 20% FBS, 100 U/ml Penicillin-Streptomycin solution and 2 mM GlutaMax™

Fibroblast growth medium, FGM
DMEM-F12 basal medium containing 10% Knockout serum replacement (KOSR), 100 U/ml Penicillin-Streptomycin solution, 2 mM GlutaMax™, 2 mM 1X NEAA, 1 μM hydrocortisone. 10 ng/mL bFGF and 100 ng/mL hEGF were freshly added just before use

Cryopreservation medium
DMEM-F12 basal medium containing 40% FBS and 10% DMSO

mTeSR™1-hiPSC maintenance medium
mTeSR™1 basal medium containing 1X mTeSR™1 supplement (provided with the kit) and 100 U/mL Penicillin-Streptomycin solution

Embryoid body formation, EBM/Differentiation medium, DM
DMEM-F12 basal medium containing 4% KOSR, 1X NEAA, 2 mM GlutaMAX™ and 100 U/mL Penicillin-Streptomycin

Neural induction medium, NIM
DM supplemented with 1% N2 and 100 ng/mL human recombinant Noggin

Retinal differentiation medium, RDM
DM supplemented with 2% B27 and 10 ng/mL human recombinant DKK1

Neuro-retinal medium, NRM
DM supplemented with 1% N2, 2% B27 and 5 ng/mL human recombinant bFGF

Retinal pigment epithelium maturation medium, RPEM
DM supplemented with 2% B27, 10 ng/mL human recombinant Activin A and 10 μM Y-27632

Corneal differentiation medium, CDM
DM supplemented with 1% N2, 10 ng/mL human recombinant EGF, 5 ng/mL human recombinant bFGF and 5 μg/mL human recombinant insulin

Human corneal epithelial medium, HCEM
DMEM/F12 basal medium containing 10% FBS, 2 mM GlutaMAX™, 100 U/mL Penicillin-Streptomycin solution, 10 ng/mL human recombinant EGF, 5 μg/mL human recombinant insulin

III. Reagents composiitions

Reagents used in molecular biology work

Genomic DNA extraction buffer
Tris-Cl – pH 8.0 (0.1mM), EDTA – pH 8.0 (0.1 M), Sodium dodecyl sulphate (0.025%) in de-ionized water

TAE (Tris acetate EDTA) buffer 50X Stock solution, pH 8.5
Tris (2M), glacial acetic acid (1M), EDTA, pH 8.0 (50mM) in de-ionized water

Plasmid isolation solution I
Glucose (50mM), Tris-Cl – pH 8.0 (25mM), EDTA – pH 8.0 (10mM) in de-ionized water

Plasmid isolation solution II
Sodium hydroxide (0.2N), Sodium dodecyl sulphate (1%) in de-ionized water

Plasmid isolation solution III
Potassium acetate (5M) in de-ionized water and adjusted to pH 5.5 with glacial acetic acid

TE buffer
Tris-Cl – pH 8.0 (10mM), EDTA – pH 8.0 (1mM) in de-ionized water

TE-RNase
RNase A (400 ug/mL) in TE buffer

Phosphate buffered saline 1X solution
Sodium chloride (137mM), Potassium chloride (2.7mM), Disodium phosphate (8mM), Potassium dihydrogen phosphate (2mM) in de-ionized water

Luria Bertani agar plates with Ampicillin
Luria Bertani agar powder (40g) suspended in 1000 ml distilled water. Heated to boiling to dissolve the medium completely. Sterilized by autoclaving at 15 lbs pressure (121°C) for 15 minutes. 100 ug/mL Ampicillin was added once the solution came down to 50-60° C. Mixed well and 20 ml of the media was poured onto sterile Petridishes (85mm)

Luria-Bertani broth with Ampicillin
Luria Bertani broth powder (25g) suspended in 1000 ml distilled water. Sterilized by autoclaving at 15 lbs pressure (121°C) for 15 minutes. 100 ug/mL Ampicillin was added prior to use

Hematoxylin staining solution (Stock)
Hematoxylin (0.5%), absolute ethanol (5%), ammonium aluminum sulphate (10%), Mercuric oxide (0.037%) in de-ionized water.

Hematoxylin staining solution (Working)
To 50 ml of the stock add 2-3 drops of glacial acetic acid

Hydrochloric acid (1%) - ethanol solution
Add 1 ml of Hydrochloric acid (12 N) in 99 ml of isopropyl alcohol (70%)
Eosin stain (Stock)
Eosin (1%) in 75% ethanol

Eosin staining solution (Working)
Add 25 ml of stock to 75 ml of 80% ethanol and 0.5ml of glacial acetic acid to obtain 100 ml of working solution of Eosin stain

Sodium citrate buffer – pH 6.0
Sodium citrate (10 mM), Tween 20 (0.05%) in de-ionized water. pH adjusted to 6.0 using 1N HCl.

Ringer's solution
Potassium chloride (5 mM), Magnesium chloride (0.8 mM), Sodium chloride (113.4 mM), Sodium bi-carbonate (26.2 mM), Sodium dihydrogen phosphate (1 mM), Glucose (5.6 mM) and Calcium chloride (1.8 mM)

***in vitro* cleavage assay buffer**
Tris-Cl – pH 8.0 (20 mM), Potassium chloride (200 mM) and Magnesium chloride (10 mM) in de-ionized water.

Lysis buffer
Tris – pH 8.0 (10mM), sodium dodecyl sulphate (1%) and EDTA (50 mM)

Reagents used in cell culture work

Cell dissociation solution, CDS
Cell culture grade EDTA (0.5 mM) in 1X PBS

Trypsin-EDTA
Trypsin (0.5%) and EDTA (0.5 mM) in 1X PBS

IV. Chemicals/Materials used in the study

Reagent / Materials	Company / Catalog number
0.45 μm filters	PALL Acrodisc / PN4614
1 mL syringes	DISPO-VAN / 1mL
1.5 mL centrifuge tubes	Tarson / 500010
100 mm cell-culture dish	TPP / 93100
100 mm petridish	Laxbro / PD-100
15 mL centrifuge tubes	Tarson / 546021
15 mL centrifuge tubes, cell-culture grade	BD / 352196
200 uL PCR tubes	ThermoFisher Scientific / AB0620
26G needle	DISPO-VAN / 26G
50 mL centrifuge tubes	Tarson / 546041
6-well plate	TPP / 92006
85 mm petridish	Laxbro / PD-85
96-well microplate	CELLSTAR / 655160
Acetic acid, glacial	SRL / 60363
Activin A	Bionova / A4941
Adenosine 5'-triphosphate, ATP	Sigma-Aldrich / FLAAS
Agarose	Lonza / 50004
Ammonium Acetate	Sigma / A1542
Ammonium aluminium sulphate	Sigma / A2140
Ampicillin	Himedia / MB104
Artemia nauplii	INVE Aquaculture
B27 supplement	Gibco / 17504044
bFGF, human recombinant protein	Sigma / F0291
BglII restriction enzyme	NEB / R0144S
Big Dye Terminator	Applied Biosystems / 4337455
Bleach (1% hypochlorite solution)	Loba chemie / 283
Bovine Serum Albumin	Sigma / A7906
Cell scraper	Corning® Costar® / 3010
Chloroform	Merck / 1.94506.0521
Colcemid	Sigma-Aldrich / 234109
Collagen-I matrix	life Technologies / A1048301
Coplin jar	Tarson / 480000
Cryovials	Nunc / V7884
DAB, 3-3- diamidino benzidine	DAKO / K0673
DAPI	Invitrogen™ / D1306
DEPC	Sigma / D5758
Disodium hydrogen phosphate	Sigma / S5136
DKK1, human recombinant protein	R&D systems / 5439-DK

DMEM-F12	Gibco / 10565-018
DMSO	Sigma / D8418
DNA ladder, 100bp	Thermo Fisher Scientific / SM0241
DNA ladder, 1kb	Thermo Fisher Scientific / SM0313
dNTPs	Bioline / BIO-39049
DPX mountant	SD fine chemicals / 46029-L02
Dulbecco's phosphate-buffered saline, DPBS	Sigma / D5652
EDTA	Sigma / E5134
EDTA, cell-culture grade	Gibco / 13151014
EGF, human recombinant protein	Biosource / PHG0311
Eosin - Y	Sigma / E4382
Ethanol	Changshu hongshen fine chemical ltd.
Ethidium bromide	Sigma / E7673
Fetal Bovine Serum, US origin	Gibco / 26140079
FITC beads	Millipore / L4655
Formaldehyde Solution	Merck / 1.94950.0521
Glass chamber slides	Corning / 354688
Glass coverslip, round, 18 mm	Blue star / 000871
Glass Pasteur pipette	Corning / 7095D-9
Glucose	SRL / 42738
GlutaMAX™	Gibco / 35050061
Glutaraldehyde	EMS / 16000
Glycerol	Sigma / G2025
Hematoxylin	Sigma / H3136
Hemocytometer	ROHEM INDIA / B.S. 748
Hi-Di Formamide	Applied Biosystems / 4311320
Human PEDF DuoSet ELISA kit	R&D / DY1177-05
Human VEGF DuoSet ELISA kit	R&D / DY293B-05
Hydrochloric acid	Thermo Fisher Scientific / A142-212
Hydrocortisone	Sigma / H0396
Hydrogen peroxide	Thermo Fisher Scientific / 18706
Insulin, human recombinant protein	Sigma / I2643
Isoamyl alcohol	Merck / 1.94608.0521
Isopropanol	Thermo Fisher Scientific / 26895
KnockOut Serum Replacement, KOSR	Gibco / 10828028
Lipofectamine 3000 Transfection Reagent	Invitrogen / L3000008
Luria Bertani agar	HIMEDIA / M1151
Luria Bertani broth	Himedia / M1245
Magnesium chloride	Merck / 1.93663.0521
MatrigelTM	Corning / 354277)
MAXIscript™ T7 Transcription Kit	Thermo Fisher scientific / AM1312

Mercuric oxide	Merck / 104466
Methanol	Thermo Fisher scientific / 43637G
Methylene blue	SRL / 60363
Minimum essential medium, MEM	Sigma / M0644
Mr. Frosty	Thermo Fisher scientific / 5100-0001
mTeSR™1 basal medium	Stem cell technologies / 85851
mTeSR™1 supplement	Stem cell technologies / 85852
N2 supplement	Gibco / 17502048
NEAA	Gibco / 11140050
NEB buffer 2.1	NEB / B7202S
NEB buffer 3.1	NEB / B7203S
No. 21 surgical blade	SURGEON / AF-055/2
Noggin, human recombinant protein	R&D systems / 6057-NG
Non-adherent dishes, 60mm	BD Falcon / 351007
NucleoBond® Xtra Midi kit	MN / 740410.100
Nutrient mixture, Ham's F-12	Sigma / N6760
Osmium tetroxide	EMS / 19100
Paraformaldehyde	EMS / 19200
pCMV_VSV-G	Addgene / 8454
pDR8.2_GPRT	Addgene / 8455
Penicillin-Streptomycin solution	Gibco / 15140122
pGL3 basic vector	Promega / E1751
Phenol	Sigma-Aldrich / P1037
Phenol red	Sigma / P0290
Phusion DNA polymerase	NEB / M0530S
pIRES2-EGFP vector	Clontech / 6029-1
PL150	RUDIRA AQUA / FRIPPAK RW +150
PL500	RUDIRA AQUA / FRIPPAK RW +500
pLNCX2 vector	Clontech / 6102-1
pMOS-Blue blunt cloning vector	Sigma / GERPN5110
Polybrene	Sigma / TR1003
Potassium acetate	Sigma / P1190
Potassium chloride	SRL / 38630
Potassium dihydrogen phosphate	Sigma / P5655
Propidium iodide, PI	Sigma / P4170
Proteinase K	Genei / 2150180251730
RNase A	Sigma / R6513
SalI restriction enzyme	NEB / R0138S
Sequencing buffer	Applied Biosystems / 4336697
Sodium acetate	Sigma / S2889
Sodium bicarbonate	Sigma / S5761

Sodium butyrate	Sigma-Aldrich / B5887
Sodium cacodylate buffer	EMS / 11650
Sodium chloride	SRL / 33205
Sodium dodecyl sulphate	SRL / 54468
Sodium hydroxide	Thermo Fisher Scientific / S320-1
SuperScript™ III Reverse Transcriptase	Thermo Fisher Scientific / 18080051
T7 endonuclease	NEB / M0302L
Taq Polymerase	Invitrogen / 610602400051730
Transwell plates	Nunc / 140652
Tricaine	Sigma-Aldrich / E10521
TRIS base	Thermo Fisher Scientific / BP152-1
Triton™ X-100	Sigma-Aldrich / X100
TRIzolTM	Invitrogen / 15596026
TrypLE 1X solution	Invitrogen / 12604
Trypsin	Sigma / T4799
VACUETTE® TUBE 3.5 mL K2E	Greiner Bio-one / 454235
Xylene	Thermo Fisher Scientific / 35417
Y-27632 (ROCK inhibitor)	Sigma / Y0503

V. Primers used in the study

Genes	Primer sequence	Product Size (bp)	NCBI Accession number
Mutation sequencing primers			
ABCA4 **Exon 44**	F: GGTCATCCCTCCACTCCTTG R: GCACTCTCATGAAACAGGCTT	261	Gene ID: 24
RD3 **Exon 2**	F: TTCCCAGGTTCCCCACTCTG R: CCACTGCAGCCACCTTTCCT	436	Gene ID: 343035
Primer sets to amplify Yamanaka transgenes			
OCT3/4	F: CCTCACTTCACTGCACTGTACTC L3205: CCCTTTTTCTGGAGACTAAATAAA	335	
SOX2	F: CCCAGCAGACTTCACATGTCC L3205: CCCTTTTTCTGGAGACTAAATAAA	348	
KLF4	F: GATCGTGGCCCCGGAAAAGGAC L3205: CCCTTTTTCTGGAGACTAAATAAA	455	
cMYC	F: GAACAGCTACGGAACTCTTGTGC L3205: CCCTTTTTCTGGAGACTAAATAAA	419	
RT-PCR loading control			
eEF1α	F: GAAGTCTGGTGATGCTGCCATTGT R: TTCTGAGCTTTCTGGGCAGACTTG	198	NM_001402
Primer sets to amplify endogenous Yamanaka genes			
OCT3/4	F: TCCCTTCGCAAGCCCTCATTT R: TCTGCAGAGCTTTGATGTCC	486	NM_002701
SOX2	F: CCCAGCAGACTTCACATGTCC R: GCGTGAGTGTGGATGGGATTG	287	NM_003106
KLF4	F: GATCGTGGCCCCGGAAAAGGAC R: GATTGTAGTGCTTTCTGGCTGG	394	NM_004235
cMYC	F: AGCTTGTACCTGCAGGATCT R: CTGCGTAGTTGTGCTGATGT	409	NM_002467

Stemness markers			
NANOG	F: ACCAGTCCCAAAGGCAAACA R: TGGTTGCTCCACATTGGAAG	389	NM_024865
hTERT	F: AGGTTTCACGCATGTGTGCT R: ATCAGTCCAGGATGGTCTTG	370	NM_198253
Ectodermal markers			
PAX6	F: ATAACCTGCCTATGCAACCC R: GGAACTTGAACTGGAACTGAC	208	NM_000280
OTX2	F: ACTTCGGGTATGGACTTGCT R: GTTCCACTCTCTGAACTCAC	350	NM_021728
Mesodermal markers			
αSMA	F: TCATCGGGATGGAGTCTGCT R: CCACAGGACATTCACAGTTG	385	NM_001141945
MSX2	F: GCGCTCATGTCCGACAAGAA R: GAACTCTGCACGCTCTGCAA	375	NM_002449
Endodermal markers			
GATA6	F: TGGATTGTCCTGTGCCAACT R: AGCCCATCTTGACCCGAATA	384	NM_005257
MIXL1	F: ACGTCTTTCAGCGCCGAACA R: TTTGGTTCGGGCAGGCAGTT	317	NM_001282402
Early eye field markers			
RX	F: GCAAGGTCAACCTACCAGA R: TCGTCCAGCGGGAACTTGT	439	NM_013435
SIX6	F: ATTTGGGACGGCGAACAGAA R: TGGATGGGCAACTCAGATGT	381	NM_007374
Neuro-retinal markers			
CHX10	F: CAAGTCAGCCAAGGATGGCA R: CTTGACCTAAGCCATGTCCT	382	NM_182894
CRX	F: TCAACGCCTTGGCCCTAAGT R: ACACATCTGTGGAGGGTCTT	357	NM_000554
NEUROD1	F: CGCGCTTAGCATCACTAACT R: GCGTCTCTTGGGCTTTTGAT	349	NM_002500

NRL	F: TTGGGGCTGAGTCCTGAAGA R: ACAGCGAGCCTTGTAGAGAT	396	NM_006177
RCVRN	F: AGACCAACCAGAAGCTGGAGT R: ACGGGTGTCATGTGAGTGGTA	367	NM_002903
RLBP1	F: TGCACCATTGAAGCTGGCTA R: AGAAGGGCTTGACCACATTG	361	NM_000326
PDE6A	F: TGCAACAGAATCCCATTCCC R: CTTCCACTGGCTTGAGTCAT	396	NM_000440
PDE6C	F: GTTGATGCCTGTGAACAAATGC R: ACCACTCAGCATAGGTGTGAT	351	NM_006204
PKC-β	F: AAAGGCAGCTTTGGCAAGGT R: CGAGCATCACGTTGTCAAGT	376	NM_212535
OPN1SW	F: TGCTTCATTGTGCCTCTCTC R: AGCTGCATGTGTCGGATTCA	373	NM_001708
OPN1MW	F: GATTGTCCTCATGGTCACCT R: TTCAGAGCCATCGTCAACCT	379	NM_000513
RHOK	F: CAAGCTGTATGCCTGCAAGA R: ATCCGGACATTGCCGTCATT	360	NM_002929
RHO	F: TTCGTGGTCCACTTCACCAT R: ATCGTCACCCAGTGGGTTCTT	372	NM_000539
ABCA4	F: CACCGTAGCAGGCAAGAGTATT R: AATGAGTGCGATGGCTGTGGAGA	271	NG_009073
RD3	F: ATGGTGCTGGAGACGCTTAT R: CTTCCTGCTTCATCCTCTCCA	328	NM_183059
RPE markers			
MITF	F: ACCGGCATTTGTTGCTCAGA R: AGTGTGCTCCGTCTCTTCCA	422	NM_198159
TYR	F: TGGACATAACCGGGAATCCT R: TTGGCCCTACTCTATTGCCT	364	NM_000372
BEST1	F: TATGTTGGCTGGCTGAAGGT R: GTTTGGTCCTTGAGTTTGCC	385	NM_004183
RPE65	F: TCTGTGCAGTGACGAGACTA R: GGGCAACTTCACTTAAGTCC	362	NM_000329

MERTK	F: ACTGTCTGTGTTGCGGACTT R: GCTGCAGCCTCAATACTGAA	355	NM_006343
Primers used in RD3 gene and promoter cloning			
RD3P-FL	F: CGATATCACAAGGGCAGTAATCTCATTCC R: CAAGCTTGCACCTAACAGACATTAGGTA	2054	
RD3P-M	F: GGATATCGTGCTGTGAACTGGTCAAGAGA R: CAAGCTTGCACCTAACAGACATTAGGTA	412	
***RD3* CDS**	F: GAAGCTTGCCAGGGGCTATGTCTCTCATCT R: GGCGGCCGCTCCGGTCACCGGCCTATCATT	679	NM_183059
Primer set used for zebrafish *rd3* exon2 in-del screening			
***rd3* exon 2**	F: ACAGGTCTCCACAGGTAAAAGC R: CAAAGAGACGCTAAAGTTGCAC	396	NM_001080631
Sequencing primers			
M13-Fwd	GTTTTCCCAGTCACGAC		
T7-Rev	TAATACGACTCACTATAGGG		

VI. Antibodies and stains used in the study

Antigen	Antibody	Manufacturer	Catalogue No.	Conc.	Dilution
OCT3/4	Mouse monoclonal	Millipore	MAB4419	1 mg/mL	1:300
SSEA4	Mouse monoclonal	Millipore	MAB4304	1 mg/mL	1:300
P63	Mouse monoclonal	Santa Cruz	sc-8431	0.2 mg/mL	1:100
PAX6	Mouse monoclonal	Santa Cruz	sc-81649	0.2 mg/mL	1:100
PAX6	Rabbit polyclonal	abcam	ab5790	1 mg/mL	1:250
K3/12	Mouse monoclonal	abcam	ab68260	1 mg/mL	1:300
Mucin2	Rabbit polyclonal	Santa Cruz	sc-15334	0.2 mg/mL	1:100
ZO-1	Rabbit polyclonal	Invitrogen	40-2200	0.25 mg/ml	1:100
Nestin	Rabbit polyclonal	Millipore	ABD69	1 mg/mL	1:300
Vimentin	Mouse monoclonal	BioGenex	AM074-5M	Diluted Ascites fluid	1:500
KI67	Mouse monoclonal	Dako	M724029	0.05 mg/mL	1:100
β-III tubulin	Mouse monoclonal	Millipore	MAB1637	1 mg/mL	1:300
Acetylated tubulin	Mouse monoclonal	Sigma	T6793	Ascites fluid	1:500
Recoverin	Rabbit polyclonal	Millipore	AB5585	1 mg/mL	1:300
CHX10	Mouse monoclonal	Santa Cruz	sc365519	200 µg/mL	1:100
MITF-A	Mouse monoclonal	Chemicon (Millipore)	MAB3747	1 mg/mL	1:100
Rhodopsin	Mouse monoclonal	Chemicon (Millipore)	MAB5356	1 mg/mL	1:200
CRX	Rabbit polyclonal	Santa Cruz	sc-30150	200 µg/mL	1:100
MAP2	Mouse Monoclonal	Millipore	MAB3418	1 mg/mL	1:200
RPE65	Mouse Monoclonal	Millipore	MAB5428	1 mg/mL	1:200
GFP	Mouse monoclonal	abcam	ab1218	1 mg/mL	1:1000
ABCA4	Mouse	My	MBS500001	-	1:300

	monoclonal	Biosource			
R/G Opsin	Rabbit polyclonal	Millipore	AB5405	1 mg/mL	1:300
Calbindin	Rabbit polyclonal	CST	2173	-	1:300
Glutamine synthetase, GS	Rabbit polyclonal	abcam	ab73593	1 mg/mL	1:200
DAB1	Rabbit polyclonal	Millipore	AB5840	-	1:500
Cone arrestin	Mouse monoclonal	abcam	ab174435	1 mg/mL	1:300
Ezrin	Mouse monoclonal	Santa Cruz	sc-58758	200 μg/mL	1:100
F-actin/ Phalloidin-Alexa Fluor 488 conjugate	-	Invitrogen	A12379	200 units/mL	1:200
Secondary Antibodies					
Alexa Fluor® 488-anti-Mouse IgG	Goat polyclonal	Invitrogen	A11001	2 mg/mL	1:300
Alexa Fluor® 488-anti-Rabbit IgG	Goat polyclonal	Invitrogen	A-11008	2 mg/mL	1:300
Alexa Fluor® 594-anti-Mouse IgG	Goat polyclonal	Invitrogen	A-11005	2 mg/mL	1:300
Alexa Fluor® 594-anti-Rabbit IgG	Goat polyclonal	Invitrogen	A-11012	2 mg/mL	1:300
Anti-Mouse IgGBiotin	Goat Polyclonal	Invitrogen	B-2763 626540	2 mg/ml	1:300
Anti-Rabbit IgG Biotin	Goat Polyclonal	Invitrogen	B-2770 656140	2 mg/ml	1:300
Streptavidin-Alexa 488	-	Invitrogen	S-11223	1 mg/mL	1:300
Streptavidin-Alexa 594	-	Invitrogen	S-11227	1 mg/mL	1:300
EnVision™ FLEX Mini Kit, High pH	-	DAKO	K8023	-	-
Counter stains					
Propidium iodide, PI	NA	Sigma	P4170	1 mg/mL	1:1000
DAPI	NA	Sigma	D8417	1 mg/mL	1:1000
Hoechst	NA	Sigma	382061	1 mg/mL	1:1000

Awards and Honors

International Awards

Fulbright Nehru Doctoral Research Fellowship (Sep 2016-May 2017) at the National Eye Institute, NIH, Bethesda, MD, USA

National Awards

- Got selected as the second finalist and received the TNQ-Cell Press, **Inspiring Science Award 2018** for best scientific papers in Life Sciences published from India, for the article Susaimanickam PJ et al., 2017, published in the journal *Development*.
- **Young Scientist Award** of Citation 2015-2016 from K. V. Rao Scientific Society, Hyderabad, India
- **Best poster** presentation award 2015 in India Eye Research Group ARVO India Chapter (IERG-ARVO-IC)
- **Best poster** presentation award 2016 in India Eye Research Group ARVO India Chapter (IERG-ARVO-IC)

List of Presentations

International conferences

Oral presentation of a paper titled *"Eye Field Differentiation and Generation of Corneal Organoids from Human Induced Pluripotent Stem Cells"* at the ARVO 2017-Baltimore, USA. This work earned a Hot Topic ribbon in the conference

National conferences

- **Oral presentation** of a paper titled "*Eye Field Differentiation and Generation of Corneal Organoids from Human Induced Pluripotent Stem Cells*" at the IERG-ARVO 2017-Madurai
- **Poster presentation** of a paper titled *"Retinal and corneal organoids generated from human induced pluripotent stem cells*" at the IERG-ARVO 2016-Hyderabad
- **Poster presentation** of a paper entitled "*Characterization of human RD3 promoter for the construction of retina-specific gene expression cassette*" in the All India Cell Biology conference, Trivandrum, India
- **Poster presentation** of a paper titled "*Construction of retina-specific gene expression cassette and a donor vector for its application in genome editing*" at the IERG-ARVO 2015-Hyderabad
- **Oral presentation** of a paper titled "*Characterization of human RD3 promoter for the construction of retina- gene expression cassette*" at the IERG-ARVO 2014-Hyderabad

List of Publications

Original research articles

- **Susaimanickam PJ**, Maddileti S, Pulimamidi VK, Boyinpally SR, Naik RR, Naik MN, Reddy BG, Sangwan VS and Mariappan I. Generating minicorneal organoids from human induced pluripotent stem cells. Development. 2017 Jul 1 [cited 2018 Feb 7];144(13):2338–51.

- Mariappan I, Maddileti S, **Joseph P**, Siamwala JH, Vauhini V. Enriched cultures of retinal cells from BJNhem20 human embryonic stem cell line of Indian origin. Investig Ophthalmol Vis Sci. 2015;56(11):6714–23.

- Dave VP, **Susaimanickam PJ**, Mir IA, Mariappan I, Basu S, Reddy GB, Pappuru RR, Jalali S and Das TP. Learning curve of a trained vitreo-retinal surgeon in sub-retinal injections in a rat model: Implications for future clinical trials. Indian J Ophthalmol 2019;XX:XX-XX. DOI:10.4103/ijo.IJO_317_19 (Manuscript accepted and in press).

- Dave VP, Maddileti S, **Susaimanickam PJ**, Pulimamidi VK, Boyinpally SR, Mishra DK, Naik RR, Jalali S, Das TP and Mariappan I. Validation of pluripotency of a newly generated human induced pluripotent stem cell line by teratoma assay. Indian J Ophthalmol 2019; (Manuscript under review).

Book chapter

- Vemuganti GK, Sangwan VS, Mariappan I, **Joseph P**, Balasubramanian D. Regenerative therapies for the ocular surface. In: Regenerative Medicine - from Protocol to Patient: 4 *Regenerative Therapies I: Third Edition. 2016.*

Meeting abstract

- **Susaimanickam PJ**, Maddileti S, Boyinpally SR, Naik RR, Naik MN, Mishra DK, Reddy GB, Sangwan VS, Mariappan I. Eye Field Differentiation and Generation of Corneal Organoids from Human Induced Pluripotent Stem Cells. *Investigative Ophthalmology & Visual Science*. 2017 Jun 23;58(8):1996-1996.

© 2017. Published by The Company of Biologists Ltd | Development (2017) 144, 2338-2351 doi:10.1242/dev.143040

Generating minicorneal organoids from human induced pluripotent stem cells

Praveen Joseph Susaimanickam[1,*], Savitri Maddileti[1,*], Vinay Kumar Pulimamidi[1], Sreedhar Rao Boyinpally[2], Ramavat Ravinder Naik[3], Milind N. Naik[4], Geereddy Bhanuprakash Reddy[5], Virender Singh Sangwan[1,6] and Indumathi Mariappan[1,6,‡]

ABSTRACT

Corneal epithelial stem cells residing within the annular limbal crypts regulate adult tissue homeostasis. Autologous limbal grafts and tissue-engineered corneal epithelial cell sheets have been widely used in the treatment of various ocular surface defects. In the case of bilateral limbal defects, pluripotent stem cell (PSC)-derived corneal epithelial cells are now being explored as an alternative to allogeneic limbal grafts. Here, we report an efficient method to generate complex three-dimensional corneal organoids from human PSCs. The eye field primordial clusters that emerged from differentiating PSCs developed into whole eyeball-like, self-organized, three-dimensional, miniature structures consisting of retinal primordia, corneal primordia, a primitive eyelid-like outer covering and ciliary margin zone-like adnexal tissues in a stepwise maturation process within 15 weeks. These minicorneal organoids recapitulate the early developmental events *in vitro* and display similar anatomical features and marker expression profiles to adult corneal tissues. They offer an alternative tissue source for regenerating different layers of the cornea and eliminate the need for complicated cell enrichment procedures.

KEY WORDS: Human induced pluripotent stem cells, Ocular differentiation, Organogenesis, Corneal organoids

INTRODUCTION

Cornea is the transparent, avascular tissue on the ocular surface through which light enters the eye. Any damage to its epithelial, stromal or endothelial cell layers can lead to visual impairment. The annular limbus surrounding the cornea harbors adult stem cells that regenerate different parts of the cornea (Schermer et al., 1986; Cotsarelis et al., 1989). Cell replacement therapy using autologous or allogeneic adult limbal grafts has been the standard treatment for patients with severe limbal stem cell deficiency (LSCD) (Rama et al., 2010; Sangwan et al., 2011; Basu et al., 2016). However, in the case of bilateral epithelial defects and for the treatment of conditions affecting the stromal and endothelial cell layers, alternative stem cell sources such as embryonic stem cells (ESCs) and induced pluripotent stem cells (iPSCs) have been explored with a view to generating the various corneal cell types (Ahmad et al., 2007; Shalom-Feuerstein et al., 2012; Hayashi et al., 2012; Sareen et al., 2014; Mikhailova et al., 2014; Chan et al., 2013; Zhang et al., 2014; Chen et al., 2015; McCabe et al., 2015).

A recent report has shown coordinated development of corneal epithelium, neural crest cells, lens epithelium and retinal cells from iPSCs in a two-dimensional (2D) culture system and employed FACS to establish pure cultures of corneal epithelial cells (Hayashi et al., 2016). However, the requirement of rigorous cell enrichment protocols imposes a major hurdle in tissue-specific cell expansion, but can be overcome by establishing three-dimensional (3D) culture systems. This method exploits the inherent self-organizing capacity of differentiating progenitor cell populations, together with the surrounding niche cells, to generate complex tissue structures *in vitro*. This has been demonstrated successfully with the generation of neuroretinal tissues using PSCs (Eiraku et al., 2011; Gonzalez-Cordero et al., 2013; Assawachananont et al., 2014; Reichman et al., 2014; Zhong et al., 2014; Hiler et al., 2015; Kaewkhaw et al., 2015; Völkner et al., 2016). A recent report has described a method of generating immature corneal organoids from human iPSCs and shown them to express a few corneal markers (Foster et al., 2017). We report here a much simpler and efficient culture method that can generate complex 3D corneal organoids from both human ESCs and iPSCs. We report the establishment of long-term cultures and the characterization of these organoids at different stages of maturation. The mature organoids developed into complex, multilayered, minicornea-like 3D tissues and recapitulated the early developmental events *in vitro*. We also show that they offer an alternative tissue source for various ocular cell types and report the generation of transplantable sheets of corneal epithelium suitable for regenerative applications.

RESULTS

Derivation and characterization of human iPSCs

As pluripotent stem cells are valuable cell sources for generating various ocular cell types and for the study of organ development *in vitro*, we derived and characterized several human iPSC lines from human dermal fibroblasts as described earlier (Takahashi et al., 2007). As shown in Fig. S1A, the hiPSC-F2-3F1 line formed typical ESC-like colonies both on mouse embryonic fibroblast (MEF) feeders and on Matrigel-coated surfaces. This line expanded well under standard human iPSC culture conditions and the cells were passaged more than 25 times. They remained pluripotent and expressed the stem cell markers OCT4 (POU5F1), SOX2, SSEA4 and alkaline phosphatase (Fig. S1B). When passage 25 cells were transplanted into the subcutaneous space of nude mice, they

[1]Sudhakar and Sreekanth Ravi Stem Cell Biology Laboratory, Prof. Brien Holden Eye Research Centre, Hyderabad Eye Research Foundation, L.V. Prasad Eye Institute, Hyderabad 500 034, India. [2]Ophthalmic Pathology Laboratory, L.V. Prasad Eye Institute, Hyderabad 500 034, India. [3]National Centre for Laboratory Animal Sciences, National Institute of Nutrition, Hyderabad 500 007, India. [4]Department of Ophthalmic Plastic and Facial Aesthetic Surgery, L.V. Prasad Eye Institute, Hyderabad 500 034, India. [5]Biochemistry Division, National Institute of Nutrition, Hyderabad 500 007, India. [6]Tej Kohli Cornea Institute, Centre for Ocular Regeneration, L.V. Prasad Eye Institute, Hyderabad 500 034, India.
*These authors contributed equally to this work

‡Author for correspondence (indumathi@lvpei.org)

P.J.S., 0000-0002-1567-1312; V.K., 0000-0002-1365-878X; S.R.B., 0000-0002-2136-4415; R.R.N., 0000-0003-3884-157X; I.M., 0000-0001-7059-3030

Received 30 July 2016; Accepted 19 May 2017

Development (2017) 144, 2338-2351 doi:10.1242/dev.143040

proliferated and developed into teratomas comprising all three germ layers within 6 weeks (n=8, 6/8 animals developed teratomas) (Fig. S1C). The gross karyotype of this female line was found to be normal at passage 20 (Fig. S1D). Genotype analysis confirmed the presence of integrated copies of the three transgenes *OCT4*, *SOX2* and *KLF4*, but not *cMYC*. The endogenous copies of all four genes were active in passage 25 cells and were expressed at levels comparable to that of the human ESC line BJNhem20 (Inamdar et al., 2009; Mariappan et al., 2015) (Fig. S1E).

Eye field differentiation of iPSCs and the development of corneal primordial structures

To induce ocular differentiation, the iPSCs and ESCs were grown to 70-80% confluence under feeder-free conditions and differentiation was initiated *in situ* as described in Fig. 1A. At 4 weeks of differentiation, distinct clusters of raised, circular to oval-shaped eye field primordial (EFP) clusters (or 'EFPs') had developed (Fig. S2A). Starting from 1×10^6 PSCs, an average of 27.33±13.63 EFP clusters could be generated from a well of a 6-well plate (n=6). To confirm that these are EFPs, we manually collected the clusters for total RNA isolation and marker expression analysis by reverse transcription PCR (RT-PCR). As shown in Fig. S2B, the expression of *PAX6*, *OTX2*, *SIX6* and *RX* (*RAX*) confirmed that these 3D clusters consisted of eye field-committed progenitor cells. When the EFPs were allowed to differentiate further *in situ*, they gave rise to lens epithelial clusters (Fig. S2C) and a SEAM (self-formed ectodermal autonomous multizone) of ocular surface epithelium by 6-8 weeks, as described by Hayashi et al. (2016). The central island of neuroretinal (NR) cells was CHX10 $(VSX2)^+$ and $RCVRN^+$, and the SEAM of ocular surface ectodermal (OSE) sheets was P63 $(TP63)^+$ (Fig. 1Bi,ii). A wave of $SOX10^+$ pigmented neural crest cells (NCCs) marked the boundary between NR and OSE cell zones (Fig. 1Biv). Retinal pigmented epithelial (RPE) cells emerged as a compact, non-pigmented epithelium surrounding the NR clusters and later matured to acquire pigmentation. Lentoid clusters expressing gamma-crystallin developed at a precise location adjacent to NR clusters (Fig. 1Bv, Fig. S2C). The NR clusters developed into optic cups and $CHX10^+$ precursors self-organized to form the NR layer (Fig. S2D). Pigmented melanocytes were also observed interspersed within the zone of migrating epithelial cells (Fig. 1Bvi, Fig. S2E).

Apart from the emergence of SEAMs, rare EFP clusters developed into 3D, miniature eyeballs, with transparent anterior-segment-like structures on the surface and complex NR structures beneath. A wave of pigmented NCCs set the boundary for the cornea-like structures (Fig. 2Aiii,iv). When the EFPs at 4 weeks were manually collected and cultured under suspension in non-adherent dishes, 40.05±3.89% gave rise to distinct corneal primordial (CP) structures distinct from the generally observed retinal primordia (RP) (n=6; Fig. 2Avi-ix). In the earlier method described by Hayashi et al. (2016), the corneal epithelial cell enrichment was achieved by approximate zoning of cell outgrowths within the SEAM region and by FACS of $SSEA4^+$ and $ITGB4^+$ cells. However, the method described here enables the self-organization of different CP cells (OSE cells and NCCs) into 3D minicorneal organoids that can directly serve as valuable tissue sources to study corneal development *in vitro* and also to establish pure cultures of different corneal cell types.

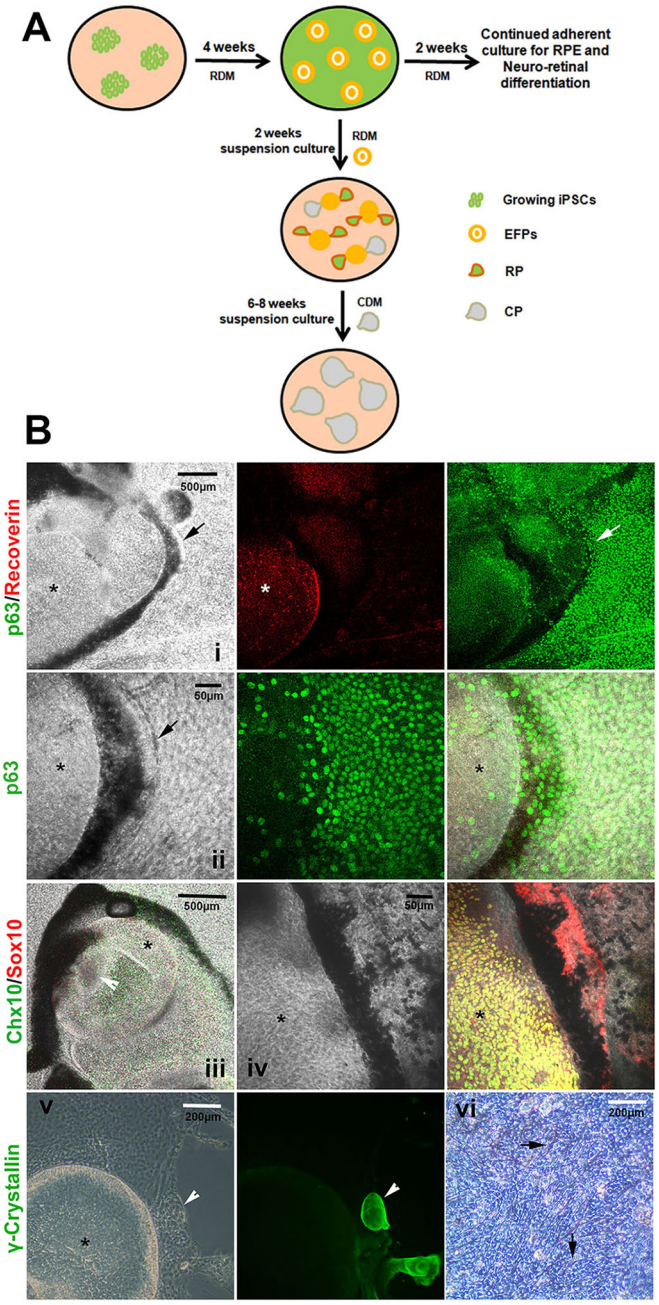

Fig. 1. Characterization of iPSC-derived eye field primordial (EFP) clusters. (A) Schematic representation of the stepwise differentiation of human iPSCs into retinal and corneal organoids. Growing iPSCs are first differentiated into EFPs, which upon isolation and suspension culture give rise to both retinal primordia (RP) and corneal primordia (CP). The dissected-out CP are cultured under corneal differentiation conditions for further maturation. CDM, corneal differentiation medium; RDM, retinal differentiation medium; RPE, retinal pigmented epithelium. (B) Distinct circular to oval-shaped EFPs encompassed a centrally located $CHX10^+$ $RCVRN^+$ neuroretinal (NR) cup (asterisks) (i). Pigmented neural crest-derived cells and $P63^+$ ocular surface ectodermal (OSE) cells appear to differentiate from the edges of EFP clusters. Arrows point to a distinct margin comprising a spindle-shaped melanocyte enriched-zone between the NR and OSE cells (i-iv). Arrowheads point to $crystallin^+$ lentoid clusters adjacent to NR cups (v) and a phase image showing the presence of pigmented melanocytes (arrows) over a layer of epithelial sheet within the migratory cell zone (vi).

Morphological features of minicorneas

The minicorneas (MCs) ranged from ~1-7 mm in diameter (Table S3). A magnified view of MCs revealed the presence of a uniform epithelial cell lining (Fig. 2Aix, Movie 1). Transmission electron microscopy images of an 8-week-old MC revealed the presence of a layer of epithelium with tight junctions and numerous

Development (2017) 144, 2338-2351 doi:10.1242/dev.143040

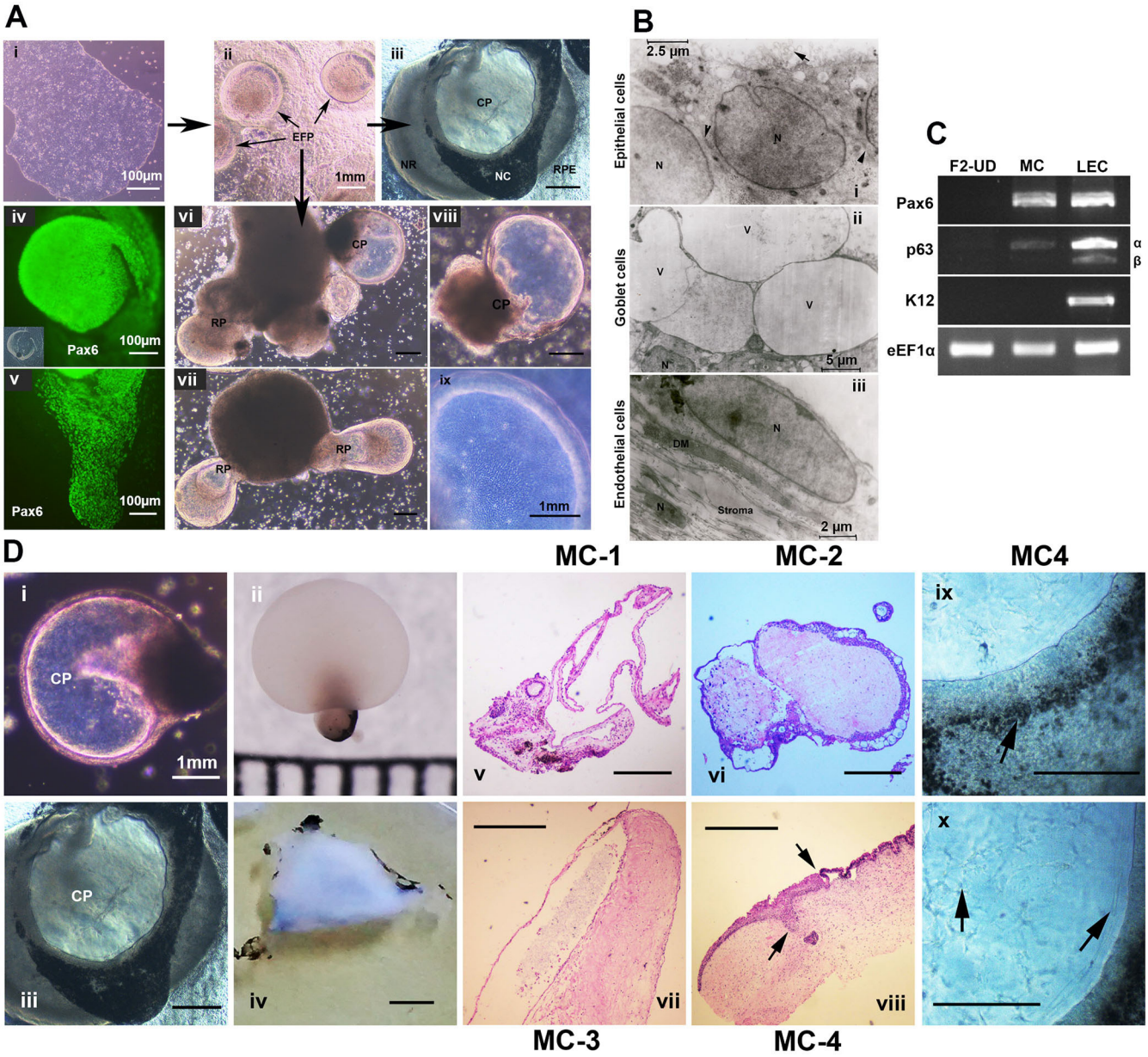

Fig. 2. Morphology of developing corneal organoids. (A) Growing iPSCs (i) differentiate into EFP clusters (ii), which further mature to form whole eyeball-like structures, with transparent CP on the surface and NR cup on the basal side. Pigmented neural crest (NC) cells mark the corneal boundary (iii). Pigmented RPE-like cells are seen migrating out of the NR tissue on the basal side. A subset of PAX6^{+} NR clusters was able to self-organize into optic vesicle-like structure with an optic stalk (iv, inset) and migrating OSE cells (v). Suspension cultures of EFPs gave rise to RP and CP structures (vi,vii), which were isolated and cultured separately for further maturation (viii,ix). *n*=6. (B) TEM images of an 8-week-old minicornea (MC) showing epithelial microvilli (arrow) and tight junctions between cells (arrowheads), cell nuclei (N), microvesicles (v) and Descemet's-like membrane (DM). (C) RT-PCR profiles of 8-week-old MCs, as compared with undifferentiated iPSCs (F2-UD) and primary limbal epithelial cultures (LEC). (D) Representative images of MCs at different stages of development under suspension culture (i,ii) and adherent culture (iii,iv). H&E-stained sections of MCs analyzed (v-viii), showing limbus-like margin (arrows). Magnified view of adherent MC, with pigmented melanocytes (arrows) observed around the corneal periphery and spindle-shaped stromal cell infiltration seen within the transparent CP (ix,x). Scale bars: 1 mm, unless otherwise specified.

apical microvilli, which is a feature of corneal epithelium but not that of lens epithelial cells. The mucin-secreting goblet cells had numerous microvesicles on the apical surface. The middle stromal layer consisted of well-organized collagen fibrils interspersed with stromal cells. A monolayer of flat endothelium-like cells was observed on the inner surface, with a Descemet's-like basement membrane (Fig. 2B). About 10-15 MCs at 8 weeks of differentiation were pooled for the isolation of total RNA, and RT-PCR analysis revealed the expression of the cornea-specific markers *PAX6* and *P63*, but not *K12* (*KRT12*). Variant-specific PCR indicated *P63*α as the major variant expressed in the developing corneas (Fig. 2C).

Maturation of MCs *in vitro*

Hematoxylin and Eosin (H&E) staining of immunohistochemical (IHC) sections of MCs at 6, 8, 10 and 15 weeks of maturation revealed a stepwise process of tissue layer development and self-organization of cells. The transparent MCs grew from 1 to 4 mm in diameter until 10 weeks of differentiation and developed into

Development (2017) 144, 2338-2351 doi:10.1242/dev.143040

opaque structures (Fig. 2Di-iv). The 6-week-old transparent MCs under suspension culture (MC-1) consisted of a double-layered epithelium and a fluid-filled lumen, without any stroma. These structures collapsed immediately after fixation, with leakage of internal fluids (Fig. 2Dv). At ∼8-10 weeks of differentiation, the MCs became strengthened by the subepithelial infiltration of spindle-shaped cells (MC-2), resulting in the development of a thick stromal cell layer, which occupied the entire fluid-filled lumen (Fig. 2Dvi). Surprisingly, IHC examination of intact MCs developing *in situ* in adherent cultures revealed complex tissue patterns, with orderly layers of different cell types that constitute a normal cornea. The adherent MCs at 10 weeks of differentiation (MC-3) revealed the formation of anterior-segment-like structure, consisting of a thin lid-like structure above a cornea-like tissue (Fig. 2Dvii). At 15 weeks of differentiation the adherent MCs exhibited mature corneal features (MC-4), with well-formed corneal and conjunctiva-like surface epithelia, separated by a limbal crypt-like margin zone (Fig. 2Dviii). Pigmented NCCs marked the boundary between the clear corneal surface and the surrounding epithelium (Fig. 2Dix).

Cornea-specific marker expression patterns in floating corneal organoids

To confirm that the MCs are authentic ocular structures and to understand the spatiotemporal distribution of cells within complex tissues, we carried out IHC examinations on MCs at different stages of development (n=8). At 6 weeks, the fragile MC1-1 comprises a double-layered epithelium, with a fluid-filled lumen (Fig. 3Ai). The epithelial cells were VIM$^+$ PAX6$^-$ P63$^-$, suggesting an undifferentiated primitive state (data not shown). Interestingly, a pair of circular niche-like organizers was observed at the connecting base, and Ki67$^+$ proliferating cells emerged from there (Fig. 3Aii). At 8 weeks, the MC1-2 showed significant stromal cell expansion and stratification of surface epithelium. The basal epithelial cells expressed P63α and PAX6 (Fig. 3Bi,ii) and the entire stroma was populated by VIM$^+$ cells (Fig. 3Biii). At 10 weeks, the MC-2 developed a thick stratified epithelium, with highly ordered collagen-filled stroma. The epithelial cells expressed P63α, PAX6 and the cornea-specific cytokeratins K3/12 and the stromal cells expressed VIM (Fig. 3C).

Characterization of MCs developing *in situ* on adherent EFPs

At 10 weeks, the MC-3 that developed *in situ* was strikingly similar to a developing anterior segment, with lid-like structures connected by a periderm-like epithelial lining above the corneal surface, as described elsewhere (Findlater et al., 1993; Huang et al., 2009) (Fig. 4A). The stratified corneal surface epithelium expressed PAX6, P63α and low levels of K12; the stromal cells were VIM$^+$ and the endothelium-like cell layer was VIM$^+$, CD200$^+$ and GPC4$^+$ (Fig. 4B, Fig. S3A). Infiltrating αSMA$^+$ cells were observed within the anterior stroma (Fig. 4Biv) and the surrounding adnexal cell layers, possibly indicating the development of smooth muscle structures of limbal vasculatures and Schlemm's canal (Fig. S3B). The stromal, endothelial and lid surface epithelial cells were VIM$^+$, whereas the stratified corneal epithelial cells were VIM$^-$ (Fig. 4Ci,ii). Interestingly, a pars plicata-like ciliary process with a pigmented epithelium was observed at the periphery of MC-3, as reported previously (Kuwahara et al., 2015; Kinoshita et al., 2016). VIM$^+$ cell clusters flanked the ciliary processes, suggesting the development of trabecular meshwork and choroid-like structures (Fig. 4Ciii,iv).

The 15-week-old MC-4 was morphologically identical to an adult ocular surface (Fig. 4D), with a distinct limbus-like transition zone separating the PAX6$^+$ P63α$^+$ K3/12$^+$ K10$^-$ corneal epithelium on one side and the periodic acid-Schiff (PAS)$^+$ and Alcian Blue$^+$ goblet cell-enriched epithelium on the other (Fig. 4E, Fig. S3C). The cornea-like structure measured ∼2 mm in diameter (∼1/6th the size of an adult cornea) and expressed most of the cornea-specific markers observed in adult corneal tissues (Fig. S4). The goblet cells were PAX6$^-$ P63$^-$, which suggested their development from OSE independent of *PAX6* and *P63* regulation. Surprisingly, except for a few newly emerging cells, the majority of the goblet cells did not express the adult conjunctival goblet cell-specific mucin MUC5AC (Fig. 4Evi). Therefore, we further checked for expression of the other secretory mucin, MUC2. IHC examinations confirmed that the goblet cells were MUC2$^+$ (Fig. 4Ev). Interspersed between the goblet cells were a few brightly stained PAX6$^+$ and K19$^+$ epithelial cells (Fig. 4Ei, Fig. S5Bvii), which suggests the late emergence of conjunctival epithelium and its dependence on *PAX6* for development and maturation. Interestingly, a distinct vasculature-like structure with a central lumen and αSMA$^+$ cell lining was observed within the stroma of the transition zone. CD34 staining indicated the presence of vascular endothelium-like cells on the inner lining of the lumen, thus confirming the initiation of vascular network development along the conjunctival margin (Fig. S5Avii,viii). Another cluster of spindle-shaped CD34$^+$ cells in the peripheral stroma indicated the emergence of a mesenchymal cell wave (Fig. S5Bix).

A periderm lining in developing MC structures

The frequent detachment of an intact epithelial monolayer from the MC surface suggested that it constitutes a separate cell layer that is possibly embryonic periderm in origin. Mouse skin periderm cells are known to emerge from P63$^+$ surface epithelium during the early stratification events and are P63$^-$, K17$^+$ and K6$^+$ (Richardson et al., 2014). During development, the periderm layer plays an important role in preventing pathological cell adhesions between the epithelial linings of adjacent organs, thus ensuring normal tissue formation. Our IHC examinations confirmed that the limbal stem cell marker K15 was exclusively expressed by the basal epithelial cells and that K13 marked the surface and suprabasal epithelium, as reported previously (Ramirez-Miranda et al., 2011; Yoshida et al., 2006). Also, the entire epithelium of MC-2, including the loose surface layers, expressed K13 and the periderm markers K17 and K19 (Fig. 5A). In MC-3, the corneal surface, lid surface and the connecting periderm were lined by K17$^+$ and K19$^+$ cells (Fig. 5B). When we examined the adult tissues, we observed that the flat wing cells at the corneal epithelial surface retained K13 and K19 expression, while the entire adult ocular surface epithelium was K17$^-$ (Fig. S6).

Lid and corneal surface epithelial margins in developing organoids

The lid, forniceal and bulbar conjunctiva, limbal and corneal surfaces are lined by a contiguous sheet of epithelium and are distinguished based on minor differences in marker expression and the presence of additional cell types, such as the conjunctival goblet cells. It is well known that the basal cells of the entire epithelial lining express P63 (Fig. S7i). However, the eye-specific PAX6 is expressed only by the corneal and conjunctival epithelial cells (Fig. S7ii). To check if such higher-order cellular organization becomes established in mature corneal organoids, we examined 15-week-old MCs (MC-5) in long-term suspension cultures. As the organoids matured, the lid structures expanded simultaneously and occupied the major volume. The basally positioned corneal structure showed a remarkable cellular organization, with surface epithelium and orderly arranged, compact stromal cells, resembling

Development (2017) 144, 2338-2351 doi:10.1242/dev.143040

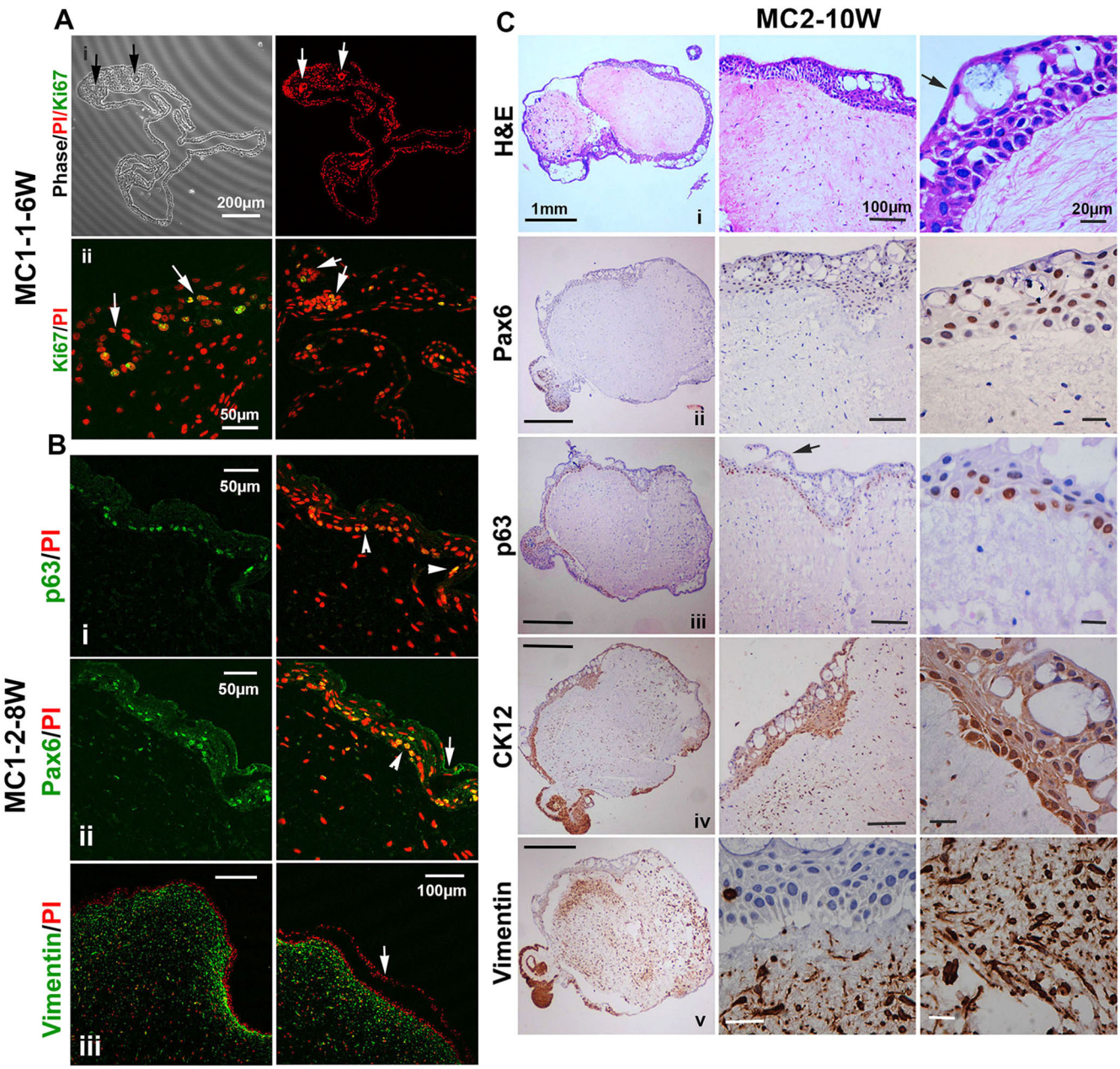

Fig. 3. IHC characterization of 6- to 10-week-old floating organoids. (A) IHC sections of 6-week-old MC1-1 showing a niche-like organizer region populated by Ki67$^+$ cells (i,ii). (B) IHC sections of 8-week-old MC1-2, immunostained for P63 (i), PAX6 (ii) and VIM (iii) (green) and counterstained with PI (red). Arrowheads point to P63$^+$ and PAX6$^+$ basal epithelium. Arrows indicate the loosely detaching surface epithelium. (C) Brightfield images of tissue sections of 10-week-old MC2 stained with H&E (i) or immunostained for PAX6 (ii), P63 (iii), K12 (iv) or VIM (v). DAB-stained sections (brown) were counterstained with Hematoxylin (blue).

that of a mature corneal tissue. Similar to MC1-1, a niche-like organizer formed the origin of P63$^+$ cells, which appeared to be migrating away from the center in an outward spiraling fashion, as a double-layered epithelium (Fig. 6i). The lid epithelium was stratified and the basal cells expressed P63. However, PAX6 expression was limited to the corneal surface epithelium, with very weak or no expression in epithelial cells along the lid margins (Fig. 6iii). Similarly, K10 expression was restricted to the lid surface epithelium, with negligible expression in the corneal epithelium (Fig. 6iv). The corneal epithelial basal cells were PAX6$^+$ P63$^+$, whereas the mature suprabasal cells were PAX6$^+$ P63$^-$ (Fig. 6v). Other adnexal structures, such as the lentoid bodies derived from OSE, could be identified as PAX6^{high} αA-crystallin$^+$ P63$^-$ cell clusters (Fig. 6ii,iii). In addition to the lens, the surface epithelial cells also expressed αA-crystallin, as observed in developing mouse eyes (Fig. S7iii).

Limbal margin establishment and delayed emergence of conjunctival epithelium

In 15-week-old adherent MC-4, P63$^+$ basal cells were restricted to the corneal side and MUC2$^+$ goblet cells were restricted to the conjunctival side, at the transition zone (Fig. 4Eii). In agreement with an earlier report (Richardson et al., 2014), upon epithelial stratification K17 expression became downregulated in the surface periderm cells, and the basal epithelial stem cells were P63$^+$ and K17$^+$ (Fig. 7Ai) and established a clear transition zone resembling that of a limbal margin. The abundance of Ki67$^+$ proliferating cells within the goblet cell-enriched epithelium indicates that the

Development (2017) 144, 2338-2351 doi:10.1242/dev.143040

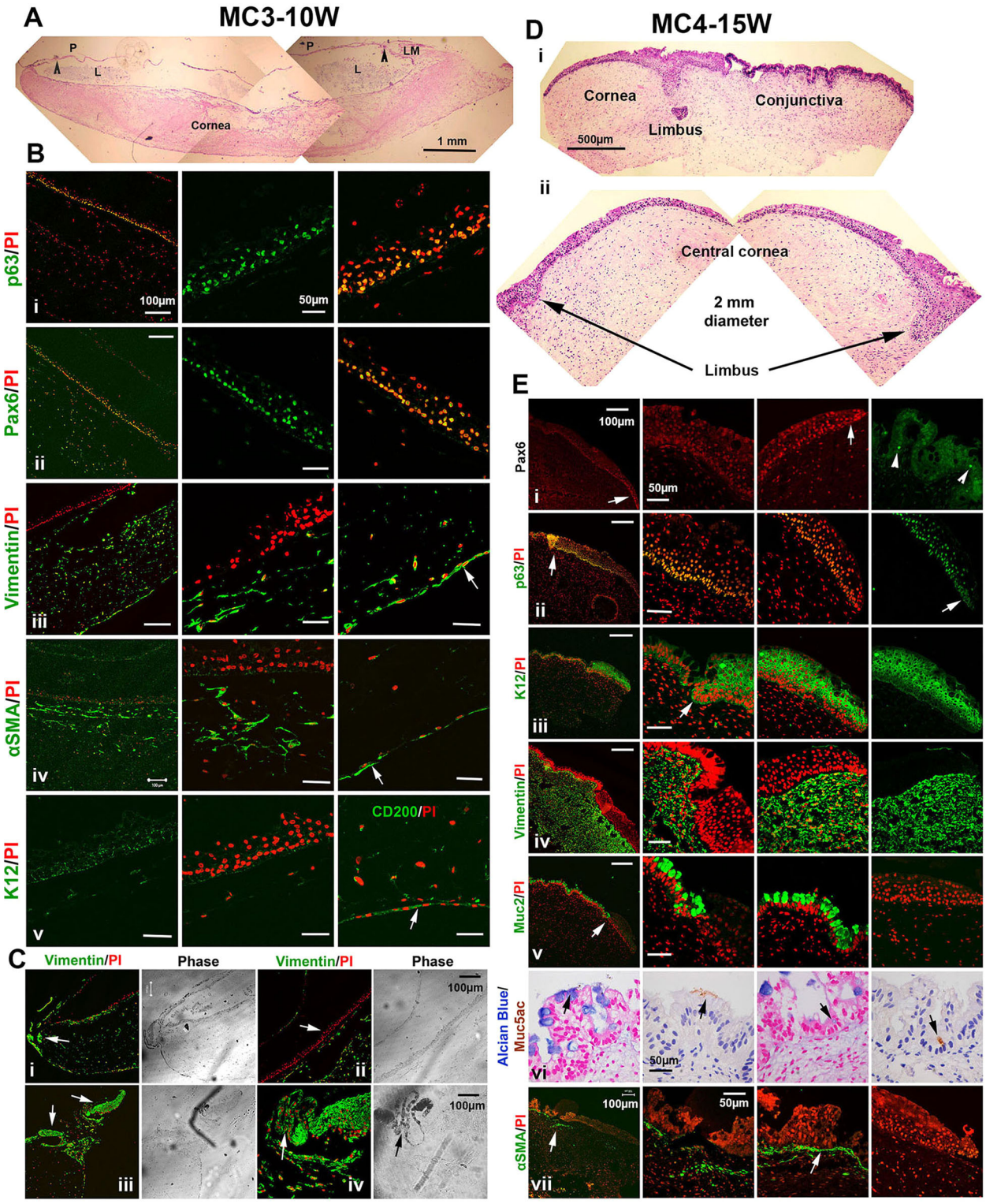

Fig. 4. IHC characterization of 10- to 15-week-old adherent MCs. (A) H&E-stained sections of 10-week-old MC3 shows a thick stroma lined by a thin monolayer of epithelium-like and endothelium-like cells on either side and a lid margin (LM) on the top (arrowhead), connected by a thin periderm-like (P) continuous epithelial lining covering the entire ocular surface, with a fluid-filled lumen (L) in between. (B) Confocal images of tissue sections of MC3, immunostained for P63 (i), PAX6 (ii), VIM (iii), αSMA (iv), K12 and CD200 (v) (green) and counterstained with PI (red). Arrows point to the endothelial cell layer. (C) The corneal surface epithelium (arrow) of MC3 is a VIM^{-} (ii), ciliary margin-like structure formed by ruffled pigmented epithelial cells (iv) and flanked by VIM^{+} ocular adnexal structures (iii). (D) H&E-stained sections of 15-week-old MC4 reveal mature cornea-like features, such as a thick stromal layer lined by a stratified squamous epithelium on the apical surface. A limbus-like structure separates the cornea-like epithelium and the goblet cell-enriched future conjunctiva. (E) Confocal images of tissue sections of MC4 immunostained with PAX6 antibody in red (i), or stained for P63 (ii), K12 (iii), VIM (iv), MUC2 (v) or αSMA (vii) in green and counterstained with PI in red. Brightfield IHC images are shown of sections stained with MUC5AC antibody (arrows) and Alcian Blue and counterstained with Hematoxylin or Nuclear Fast Red, respectively (vi).

Development (2017) 144, 2338-2351 doi:10.1242/dev.143040

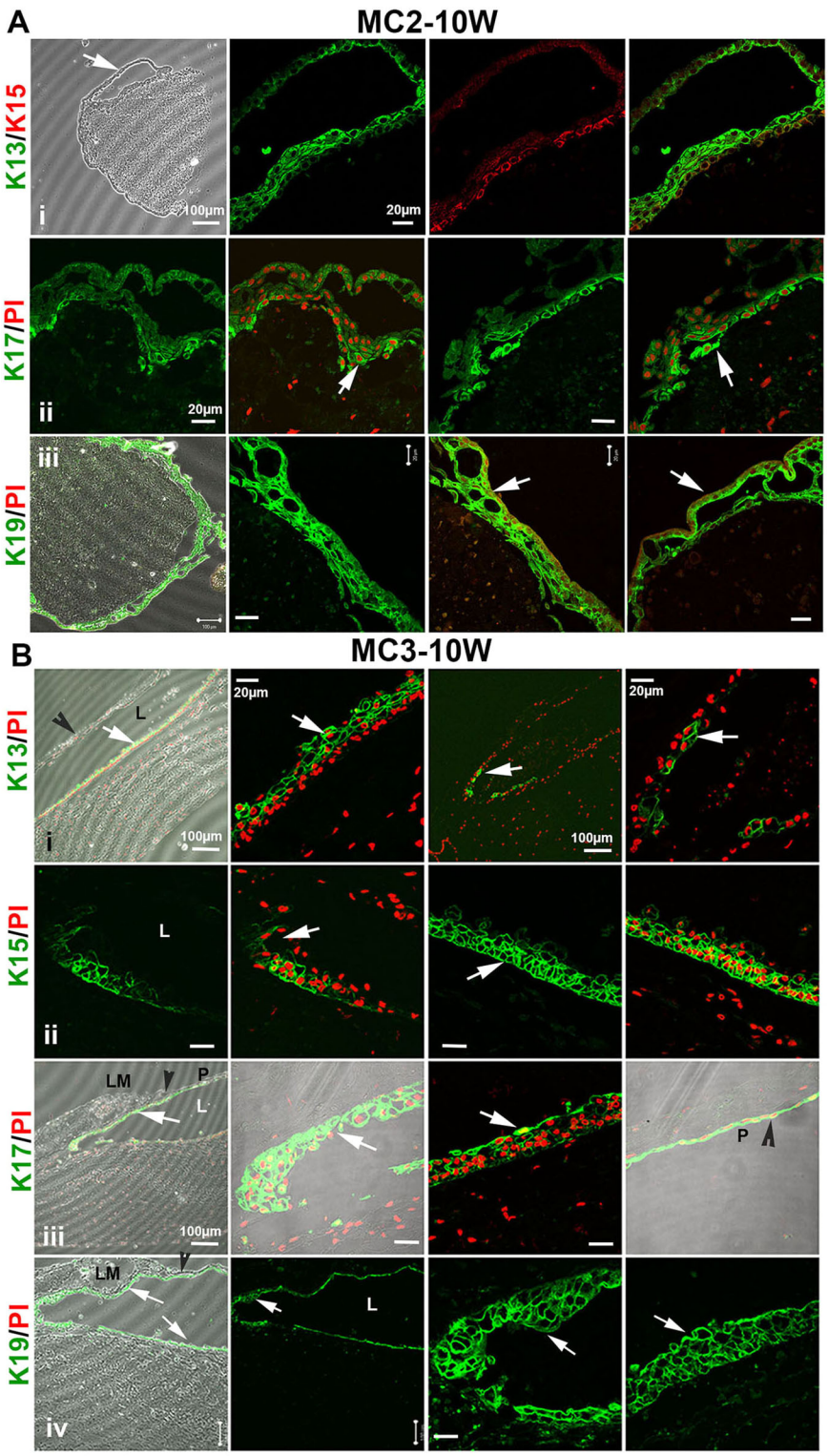

Fig. 5. Expression of periderm markers in floating and adherent MCs. (A) Confocal images of immunostained tissue sections of MC2 showing the expression of different keratins in green. The basal cells were $K15^+$, while the suprabasal cells and the apical lining were $K13^+$ (i). The basal cells also expressed K17 (arrows) (ii). However, the entire stratified epithelium and the loosely adhered, periderm-like flat surface lining cells (arrows) expressed K19 (iii). The sections were counterstained with PI to mark the nuclei in red. (B) The expression of cytokeratin markers shows a clear demarcation within the developing epithelium of a 10-week-old MC. The surface and suprabasal epithelium on the corneal surface express K13 and the expression disappears at the lid margin in the forniceal epithelium (i). K15 expression was observed in basal corneal epithelial cells and was absent at the corneal and lid surface junction (ii). The periderm, lid margin and the apical flat cell layer of the corneal epithelium showed intense K17 staining (iii). The entire epithelial lining of the developing ocular surface expressed K19 (iv). Lid margins (LM) are marked by arrowheads. The lid periderm (P) was observed as a thin continuous sheet of epithelium covering the entire corneal surface, with a fluid-filled lumen (L) in between.

progenitor cell proliferation, differentiation and tissue expansion proceed from the transition zone (Fig. 7Aii). Dual staining for MUC2 and P63 or K3/12 expression further confirmed the presence of a transition zone (Fig. 7Aiii,iv). The surface epithelium formed a collagen IV-enriched basement membrane, while the VIM^+ stromal cells laid out a well-organized collagen I-enriched extracellular matrix (Fig. 7Av,vi). When the expression patterns of other epithelial keratins were examined, we observed that $K13^+$, $K15^+$ and $K17^+$ cells were restricted to the limbal margin. Within the stratified corneal epithelium, K13 marked the surface and suprabasal cells, while K15 and K17 marked the basal and suprabasal cells (Fig. 7B). However, all of the surface epithelial cells expressed K19, with intense staining in the basal cells, surface periderm-like cells and in a few developing conjunctival epithelial cells, which suggested the late emergence of conjunctival epithelium.

Development (2017) 144, 2338-2351 doi:10.1242/dev.143040

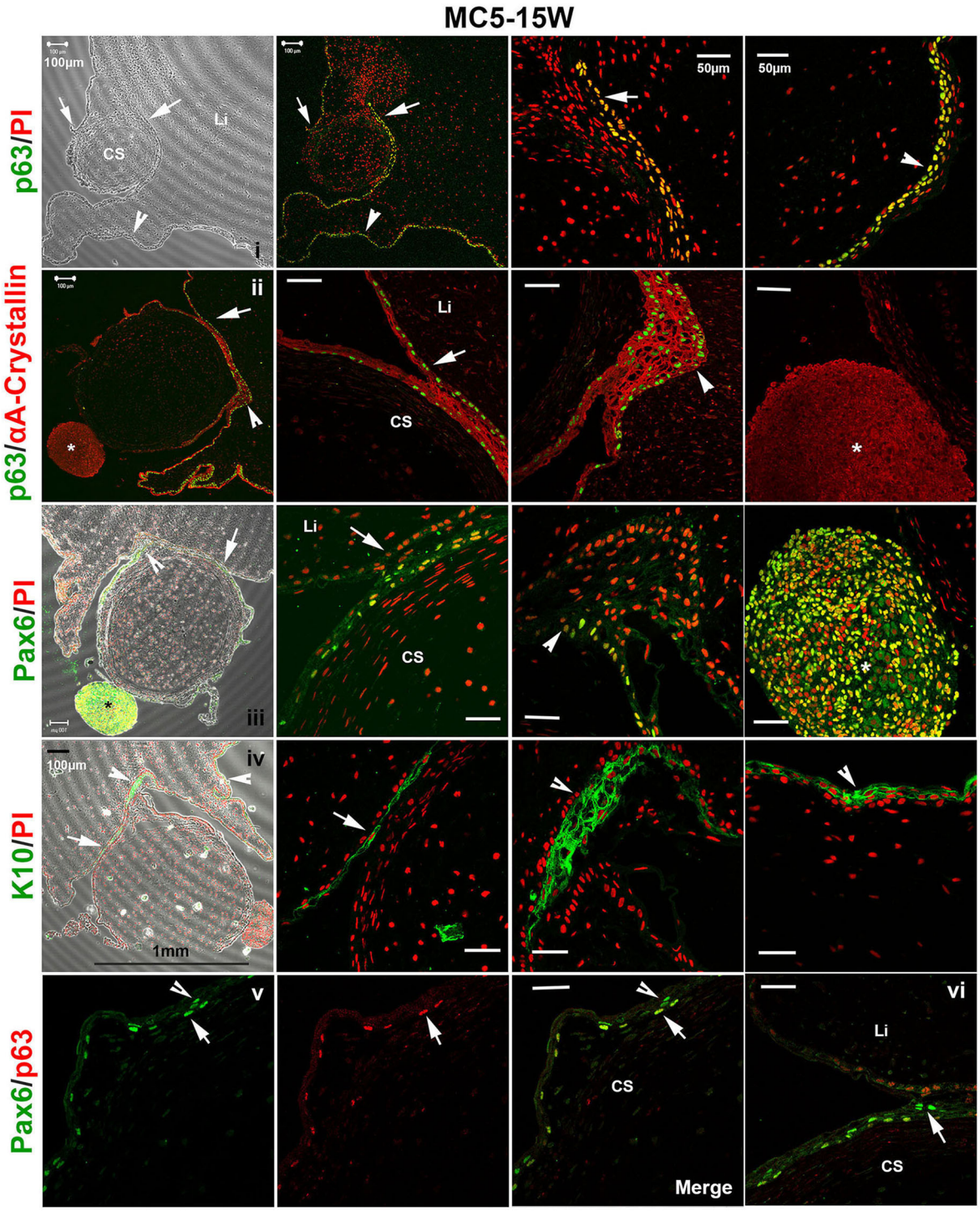

Fig. 6. IHC characterization of 15-week-old mature corneal organoid in suspension. Confocal images of tissue sections of MC5, showing a basally located MC with well-developed corneal stroma (CS) of ∼1 mm diameter. The lid-like tissue (Li) became expanded on the apical surface. The first column of all panels (i-iv) represents a lower magnification view and columns 2-4 are higher magnification views of the regions marked by arrows, arrowheads and asterisks. The $P63^{+}$ epithelial cells seem to arise from a pair of niche-like organizers within the corneal stroma and formed the corneal and lid surface epithelium (i). The basal cells of the entire epithelial lining expressed P63 and co-expressed αA-crystallin. Lentoid clusters (asterisks) are distinguished as $P63^{-}$ αA-crystallin^{+} cells (ii). Pax6 expression is limited to the corneal surface epithelium and the cells within the lentoid clusters. The anterior corneal stroma (CS) is well developed with flattened and compactly arranged stromal keratocytes, as observed in adult corneal tissues (iii). The epithelial lining on the lid surface adjoining the corneal surface showed weak PAX6 nuclear expression and was $K10^{+}$ (iv). The basal cells of the stratified corneal epithelium were $P63^{+}$ $PAX6^{+}$ (arrows), while the differentiated apical cells were $P63^{-}$ $PAX6^{+}$ (arrowhead). Columns 3 and 4 indicate two different merged images (v, vi).

Characterization of cell outgrowths from EFPs

When the cell outgrowths from EFPs were analyzed in adherent 2D cultures, we found that $SSEA4^{+}$ primordial cells tended to organize into ruffled structures resembling limbal crypts and gave rise to $P63^{+}$ and $PAX6^{+}$ ocular surface epithelial cells (Fig. 7Ci-iii, Movies 2 and 3) and waves of NES^{+}, $SOX10^{+}$ and $PAX6^{low}$ NCCs.

Development (2017) 144, 2338-2351 doi:10.1242/dev.143040

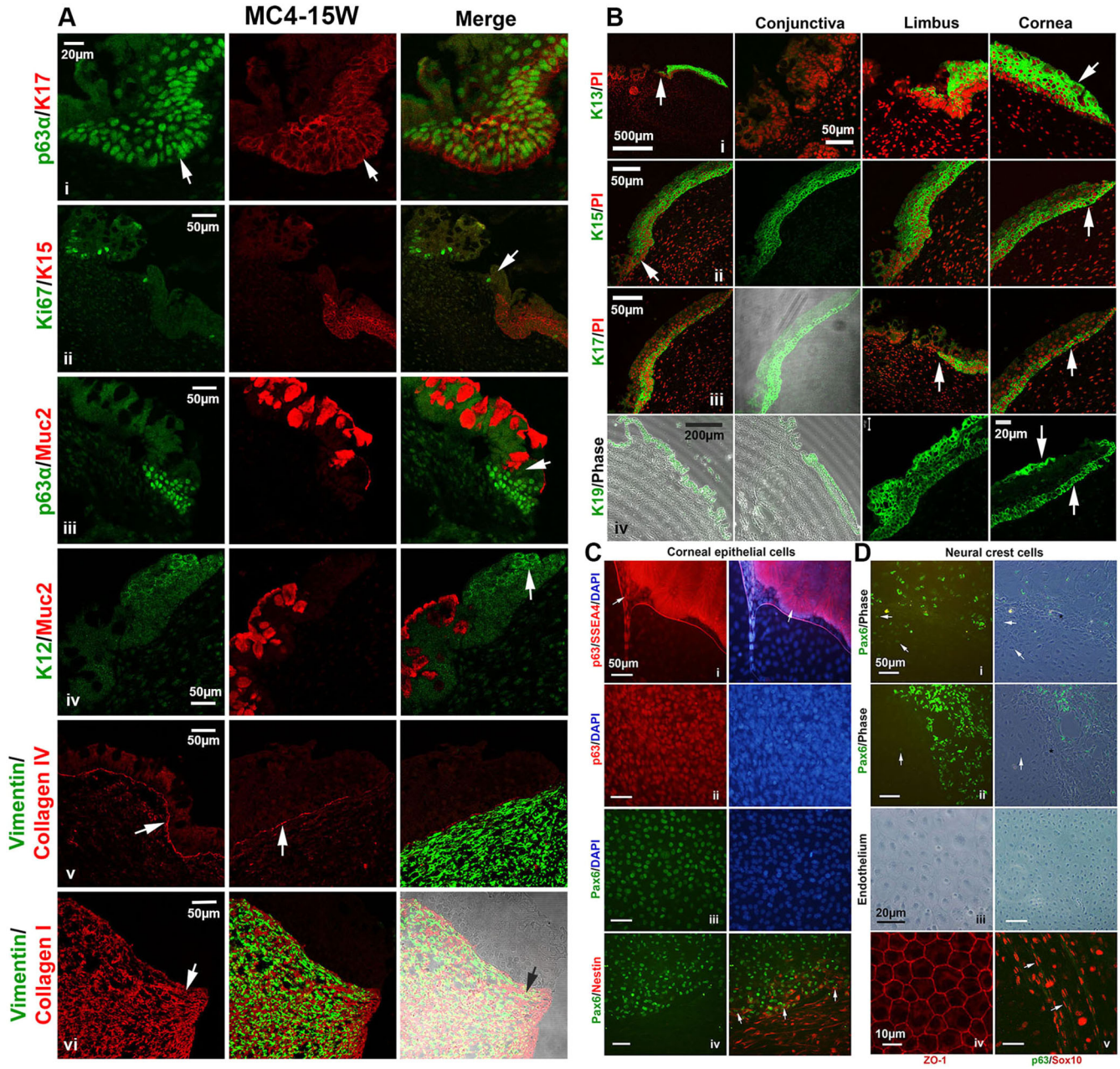

Fig. 7. Mature cornea-specific marker expression in MCs and cell outgrowths from tissue explants. (A) Confocal images of tissue sections of MC4 co-immunostained for P63α and K17 (i), KI67 and K15 (ii), P63α and MUC2 (iii), K12 and MUC2 (iv), VIM and COL4A1 (v), VIM and COL1A1 (vi). Arrows mark the limbus-like margins (i-iii), $K12^+$ corneal epithelium (iv), basement membrane (v) and the stromal matrix (vi). (B) Confocal images of tissue sections of MC4 immunostained for K13 (i), K15 (ii), K17 (iii) and K19 (iv). Note the surface epithelial expression patterns of K13 and K19, while K15 and K17 mark the basal epithelial stem cells. Apart from weak K19 expression, the conjunctival epithelium was negative for all the keratins tested. The limbus-like margins are indicated by arrows in the first column. $K13^+$ suprabasal cells (i), and $K15^+$ (ii), $K17^+$ (iii) and $K19^+$ (iv) basal cells of central corneal epithelium are indicated by arrows in the last column. (C) OSE outgrowths from EFPs formed a ruffled, limbal crypt-like arrangement of $SSEA4^+$ cells at the proximal end, giving rise to migrating $P63^+$ epithelial stem cells (arrows) (i). The outgrowths from explants result in uniform corneal epithelial sheets containing $P63^+$ (ii) and $PAX6^+$ (iii) cells. $PAX6^+$ epithelial sheets (green) are lined by NES^+ NCCs (red). Arrows indicate the double-positive cells at the boundaries (iv). (D) $PAX6^{low}$ NCC patches downregulate PAX6 expression (arrows) and morphologically differentiate into hexagonal, corneal endothelium-like cells (i,ii), with distinct $ZO\text{-}1^+$ tight junctions between the cells (iii,iv). The migratory NCCs are $SOX10^+$ $P63^-$ (arrows) (iv). DAPI (blue) and PI (red) were used as counterstains. Scale bars: 50 µm, unless otherwise specified.

NES^+ cells are a component of the native limbal niche (Fig. S4x) and we show that iPSC-derived $PAX6^+$ epithelial outgrowths are lined by NES^+ NCCs that co-express PAX6, as reported previously (Mariappan et al., 2014) (Fig. 7Civ). Patches of $PAX6^{low}$ neural crest-like cells differentiated into a corneal endothelium-like phenotype by downregulating PAX6 (Fig. 7Di,ii); they appeared as hexagonal, compactly arranged, non-pigmented flat cells with ZO-1 $(TJP1)^+$ tight junctions (Fig. 7Diii,iv). The migratory NCCs were found to be $SOX10^+$ $P63^-$ cells (Fig. 7Dv).

Characterization of corneal organoid-derived transplantable cell sheets

Explant cultures of 8- to 10-week-old MCs on glass coverslips resulted in a spiraling wave of $P63^-$ $K17^+$ OSE cells at the leading edge,

Development (2017) 144, 2338-2351 doi:10.1242/dev.143040

followed by a compactly arranged monolayer of $P63^+$ $K17^+$ corneal epithelial cells (Fig. S8). In an attempt to generate transplantable sheets of corneal epithelium, we established explant cultures on denuded human amniotic membrane (hAM) substrates, using mature cornea-like organoids at 8-10 weeks of maturation. IHC examination of 10-day-old cultures confirmed that the uniform sheets of $PAX6^+$ $K12^+$ epithelium generated using corneal organoids were comparable to those generated using adult limbal explants. The basal epithelial cells were $PAX6^+$ $P63^+$ P75 $(NGFR)^+$ and also expressed K17, K19 and VIM (Fig. 8). Interestingly, the resting corneal epithelium was found to

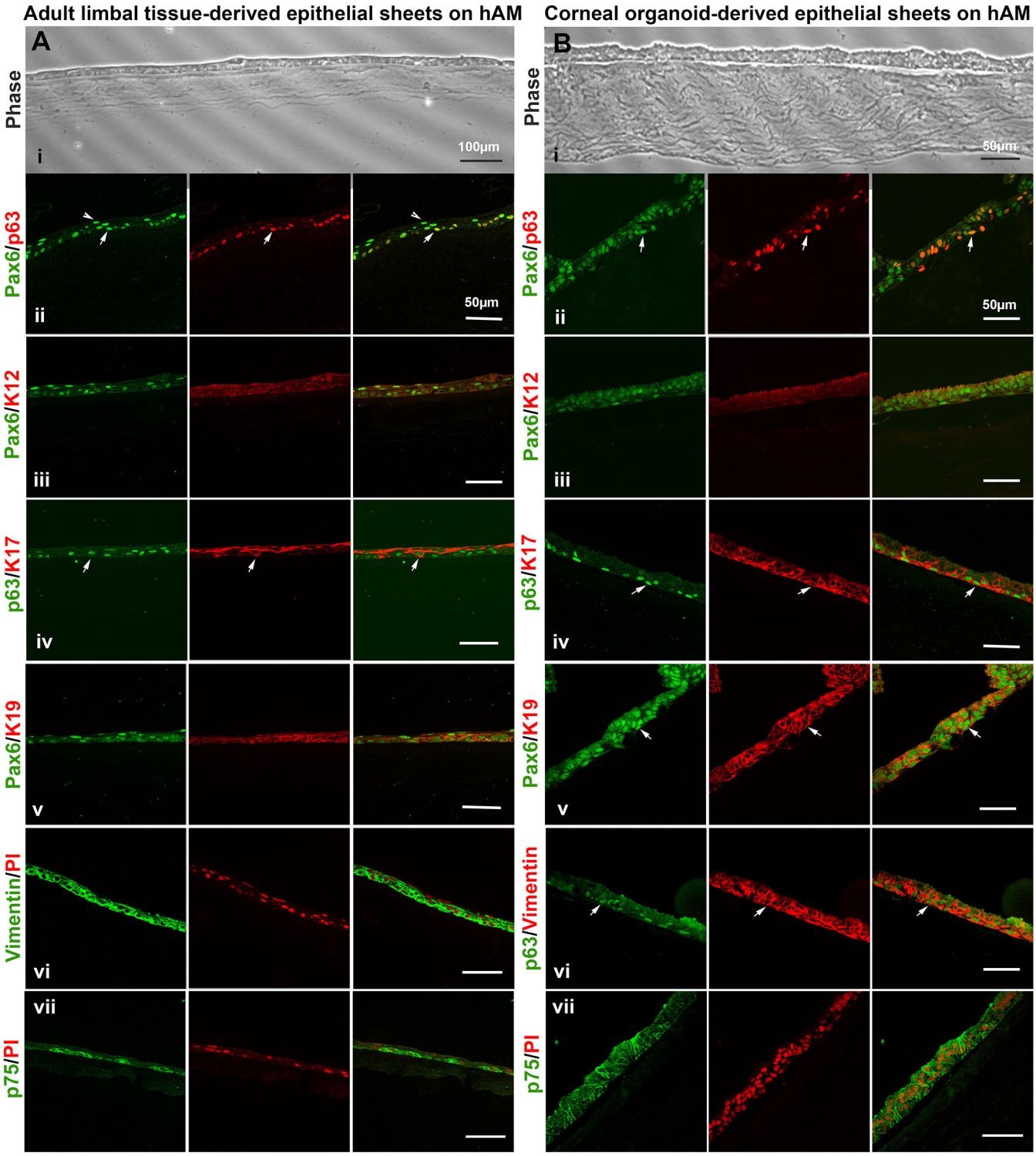

Fig. 8. Organoid-derived transplantable corneal epithelial grafts on human amniotic membrane substrate. (A) Confocal images of tissue sections of epithelial grafts generated using adult limbal tissues and (B) iPSC-derived corneal organoids on denuded hAM (i). Both the engineered grafts were comparable in terms of spatial distribution and expression patterns of corneal epithelium-specific markers such as PAX6, P63, K12 (ii-iii); cytoskeletal proteins such as K17 (iv), K19 (v) and VIM (vi); and of the basal stem cell marker P75 (vii). Arrows indicate the dual positive basal epithelial cells (ii-v). Arrowheads indicate the $PAX6^+P63^-$ suprabasal cells (ii).

Development (2017) 144, 2338-2351 doi:10.1242/dev.143040

be VIM$^-$ K17$^-$ (Figs 4 and 6). However, the actively proliferating cells in both the limbal and organoid explant cultures were VIM$^+$ K17$^+$, suggesting a possible activation of these markers during acute regeneration and wound healing responses.

DISCUSSION

An autologous iPSC-derived corneal cell source will offer a promising alternative for the treatment of patients with bilateral LSCD. A few earlier reports have demonstrated the possibility of deriving PAX6$^+$ P63$^+$ K3/12$^+$ corneal epithelial cells from PSCs in 2D cultures. Here, we report for the first time an efficient method of generating complex 3D corneal organoids using iPSCs, which circumvents the need for complicated cell enrichment procedures as are involved in establishing limbal cultures.

The adoption of a simple differentiation protocol by the direct shifting of growing cultures to retinal differentiation conditions in the absence of noggin has resulted in successful induction of EFP clusters. We also emphasize that it is crucial to excise EFPs and initiate suspension cultures at 4 weeks of differentiation, before the commencement of surface ectodermal cell and NCC migration, in order to ensure successful induction of corneal organoids in ∼40% of the EFPs by 6 weeks. We believe that the inhibition of migration of proliferating progenitor cells away from EFPs in suspension culture enables the autonomous self-assembly of various cell types, resulting in the generation of complex 3D corneal organoids.

The bilayered epithelium of the newly emerged MCs was derived from the primitive periderm-like P63$^-$ PAX6$^-$ VIM$^+$ OSE cells. The presence of internal fluid appears to help in establishing a circular and convex shape for the developing corneas. The subsequent wave of VIM$^+$ stromal cells and the deposition of collagen matrix helped to strengthen the outer scaffold of OSE cells. The developing lid-like structure in MC-3 was lined and connected by a continuous periderm-like epithelium above the corneal surface. This observation is in agreement with the fact that the developing eyelids fuse and form a continuous covering over the developing cornea. The connecting periderm disintegrates and enables lid separation and eye opening during advanced stages of embryonic development in humans and at postnatal stages in rodents (Findlater et al., 1993; Huang et al., 2009). Unlike the developing skin periderm that is shed after birth (Richardson et al., 2014), the presence of K13$^+$ K17$^+$ K19$^+$ periderm-like surface epithelium in developing MCs and in adult corneas suggests their probable role in normal ocular surface development and in adult tissue homeostasis. We hypothesize that this unique surface lining may help in preventing abnormal cell fusions between the corneal and lid surface epithelium during embryonic eye development and in wound repair processes during adult tissue regeneration.

The presence of ciliary margin zone (CMZ)-like pigmented and ruffled epithelium, flanked by VIM$^+$ structures, at the corneal periphery prompted us to speculate that CMZ development might precede or coincide with ocular surface periderm formation (∼5-6 weeks). The secretions of the CMZ cells might contribute to setting the initial corneal shape, which becomes further strengthened by the infiltration of VIM$^+$ NCCs. The NCCs also contributed to the formation of a monolayer of VIM$^+$ CD200$^+$ GPC4$^+$ endothelium-like cells beneath the thick stroma, thus resulting in the generation of a complete anterior-segment-like structure.

As the MCs matured, the lid and the limbal margins became established by the spatiotemporal pattern of expression of P63, PAX6 and keratins. The P63$^+$ cells were restricted to the corneal and limbal basal epithelial cells, thus establishing a sharp boundary between the cornea and the future conjunctiva. Whereas the entire surface epithelium expressed PAX6 at low levels, well-differentiated central corneal cells and a subset of cells within the conjunctival region were brightly PAX6$^+$, confirming its key role in corneal maturation and the emergence of conjunctival epithelium. The majority of the goblet cells on the conjunctival side were MUC2$^+$ P63$^-$ PAX6$^-$, which suggests that the goblet cells emerge from the primitive OSE cells independently of P63 and PAX6 expression. However, the adult conjunctival goblet cells expressed very low levels of MUC2 (McKenzie et al., 2000) and were predominantly MUC5AC$^+$ (Fig. S4Av). An earlier report has confirmed that goblet cell development is normal in *Muc5ac*$^{-/-}$; *Muc5b*$^{-/-}$ mice (Marko et al., 2014). Taken together, we believe that MUC2 and MUC5AC are the developing and mature conjunctival goblet cell markers, respectively. The presence of niche-like organizing structures consisting of Ki67$^+$ P63$^+$ cells suggests that the tissue growth and expansion proceeds from such transition zones. Further anatomical maturation of corneal tissue was mediated by the infiltration of CD34$^+$ mesenchymal stem cells (Sidney et al., 2014) and other neural crest-derived cell types, such as the smooth muscle cells, which contributes to the formation of limbal and episcleral vasculatures.

Earlier evidence has confirmed the roles of *PAX6* in regulating NCC migration and their differentiation into ocular cell types (Baulmann et al., 2002; Kanakubo et al., 2006) and the involvement of NCC-dependent signaling in feedback regulation on *PAX6* (Grocott et al., 2011). Our observations indicate that the PAX6^{low} NCCs differentiated into flat, non-pigmented, endothelium-like hexagonal cells by downregulating PAX6 expression. Explant cultures of 8- to 10-week-old MCs on hAM has enabled the generation of transplantable sheets of PAX6$^+$ P63$^+$ K12$^+$ corneal epithelial sheets, similar to adult limbal tissue-derived grafts intended for regenerative applications. We further plan to use these tissue grafts in xenotransplantation studies in rabbit LSCD models, to test their clinical suitability in corneal surface reconstruction procedures.

Conclusions

In summary, we show for the first time that complex 3D corneal organoids can be generated from iPSCs and that the MCs undergo maturation *in vitro* and recapitulate the steps of normal corneal development, as depicted in Fig. 9. The availability of such MCs at 10 weeks of maturation circumvents the need for complicated cell enrichment protocols and offers a simpler method of establishing enriched cultures of corneal epithelial cell sheets for basic research needs and for regenerative applications.

MATERIALS AND METHODS

Ethics

This study was approved by our Institutional Review Board (IRB) of the LV Prasad Eye Institute, Hyderabad, India. All research involving human samples followed the tenets of the Declaration of Helsinki. Experiments involving animals were conducted in adherence to the ARVO statement for use of animals and with the approval of the Institutional Animal Ethics Committee (AEC) of the National Institute of Nutrition, Hyderabad, India.

Derivation and maintenance of human iPSCs

Full-thickness punch biopsies of skin were taken from volunteers with their informed consent. The biopsies were used to establish human dermal fibroblast (HDFs) cultures. A retroviral cocktail containing individual vectors expressing the *OCT4*, *SOX2*, *KLF4* and *cMYC* (OSKM) transgenes were used to transduce passage 3 HDFs at an MOI of ∼2. The cells were then split and cultured under standard human ESC culture conditions. The reprogrammed clones that emerged after 3 weeks were manually picked

Development (2017) 144, 2338-2351 doi:10.1242/dev.143040

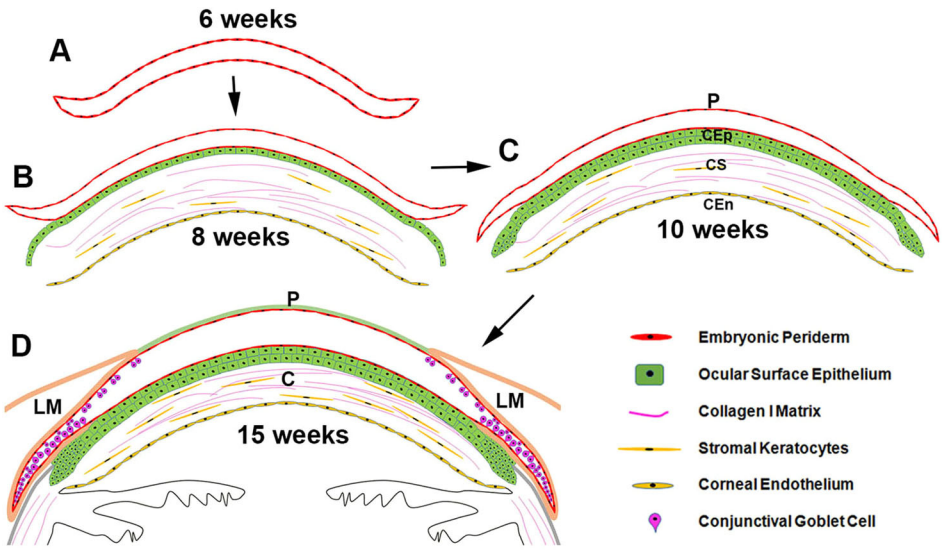

Fig. 9. Illustration of the different stages of MC development *in vitro*. (A) The transparent, bubble-like CP at 6 weeks of development consisted of a double-layered primitive embryonic periderm-like epithelium, with a fluid-filled lumen. (B) NCCs migrate into the subepithelial space at ∼8 weeks to form a thick stroma and an endothelium-like monolayer. This establishes and strengthens the corneal matrix. (C) The ocular surface epithelium (OSE) developed and stratified over the stably established stromal matrix at ∼10 weeks. The OSE remained sandwiched between the stroma and the periderm-like surface lining (P). P63α^{high} and PAX6^{low} cells appeared in the basal cell layers. The periderm lined the entire ocular surface and also formed a continuous outer covering for the developing anterior segment. (D) The lid-like structures developed on either side, connected by an intact periderm. Mature cell markers such as PAX6 and K12 became induced in the stratified OSE at ∼15 weeks. Goblet cells developed within the future conjunctival and forniceal surface epithelium, independently of PAX6 and P63 expression. C, cornea; CEp, corneal epithelium; CEn, corneal endothelium; CS, corneal stroma; LM, lid margin.

based on colony morphology and five clones were passaged for further expansion. The clones were also adapted to feeder-free culture conditions on Matrigel (Corning) coated plates using the mTeSR™1 kit, as per manufacturer's instructions (STEMCELL Technologies). The reprogramming efficiency was 0.005% and the clone hiPSC-F2-3F1 was expanded beyond 25 passages and characterized for stemness and pluripotency.

Eye field differentiation of human iPSCs and ESCs

Growing cultures of the human ESC line BJNhem20 and the normal human iPSC line hiPSC-F2-3F1 were differentiated towards eye field commitment as described below. When the cultures reached 70-80% confluence, the growth medium was replaced with differentiation medium [DM: DMEM/F12, 4% knockout serum replacement (KOSR), 4% fetal bovine serum (FBS), 1× non-essential amino acids (NEAA), 1× Glutamax, 1× Pen-Strep; Thermo Fisher Scientific] to induce spontaneous differentiation for 2 days. Subsequently, the cultures were shifted to retinal differentiation medium (RDM: DM plus 2% B27) and maintained for 1 month to induce eye field specification. Noggin was omitted from the RDM cocktail in order that uninhibited TGFβ and BMP intrinsic signals could direct OSE development. The distinct EFP clusters that emerged at 4 weeks were either continued as adherent cultures *in situ* or excised manually for suspension cultures as described below.

Corneal differentiation of eye field clusters

The EFPs were further continued *in situ* as adherent cultures in RDM for another 4 weeks to allow whole eyeball-like structure development, with transparent CP on the surface and NR cup on the basal side. These cultures were maintained in corneal differentiation medium (CDM: DM plus 1% N2, 5 µg/ml insulin, 5 ng/ml FGF, 10 ng/ml EGF; Thermo Fisher Scientific) for a further 6-8 weeks to enable maturation of the ocular surface structures. However, a majority of the EFPs gave rise to concentric cell outgrowths, as described previously (Hayashi et al., 2016). Alternatively, the EFPs were manually scooped out intact and cultured in RDM for 4 weeks in non-adherent plates. It is crucial to excise the EFPs at 4 weeks before the commencement of initial waves of surface ectodermal cell and NCC migration. Within 2 weeks of suspension culture, distinct RP and transparent, bubble-like CP structures emerged from the floating EFPs. At 6-8 weeks of differentiation, the delicate CP structures were dissected out of floating EFPs and cultured separately for a further 8-10 weeks in CDM for tissue maturation, as depicted in Fig. 1A. Alternatively, the MCs were processed directly for explant cultures or RNA isolation or fixed in 10% formalin for IHC examination.

Explant culture of MCs

MCs at different stages of maturation (6-10 weeks) were taken and the basal stalk that carries the niche-like organizer along with the adjoining epithelium was chopped out under a microscope and cut into fine pieces in a few drops of CDM. The tissue explants were picked using a needle and explanted on to the surface of de-epithelialized human amniotic membrane (hAM). Alternatively, the explants were placed on Matrigel-coated glass coverslips. The cultures were maintained in CDM and incubated at 37°C with 5% CO_2. The epithelial cells migrated out of the explants and formed growth zones that merged with each other to form uniform epithelial sheets within 10 days. The cell sheets were fixed and processed for IHC examination as described below.

Genomic PCR and semi-quantitative reverse-transcription PCR

Genomic DNA and total RNA were isolated from cell samples using standard procedures. cDNAs were prepared by reverse transcription using the SuperScript II reverse transcriptase kit (Invitrogen, Life Technologies). PCRs were performed using either genomic DNA or cDNA as the reaction template (n=3). Template concentrations were normalized based on *eEF1α* (*EEF1A1*) expression. Table S1 summarizes the primers used. The amplicons were resolved on 1% (w/v) agarose gels, stained with ethidium bromide and imaged using the Gel Doc XR+ system (Bio-Rad).

Immunohistochemistry and image analysis

The MCs were fixed in 10% formalin and paraffin embedded for further sectioning. Thin (4 µm) sections were processed for evaluation by H&E, PAS and Alcian Blue staining by standard procedures. For IHC examination, antigen retrieval was achieved by heating at 100°C with sodium citrate buffer (pH 6.2) and the slides were processed for blocking and antibody incubations. DAB staining of samples was performed as per the manufacturer's instructions (Super Sensitive One-Step Polymer-HRP

Development (2017) 144, 2338-2351 doi:10.1242/dev.143040

IHC detection system, Biogenex), with counterstaining with Hematoxylin, propidium iodide (PI) or DAPI (1 µg/ml each). Table S2 summarizes the antibodies used, including dilutions. Alkaline phosphatase staining was undertaken as per manufacturer's instruction (Chemicon, Millipore). The samples were finally mounted with DPX (SD Fine Chemicals) or glycerol and imaged using an epifluorescence (IX71, Olympus) or confocal (LSM 510, Carl Zeiss) microscope. The images were analyzed using ImagePro Express (Media Cybernetics) and LSM 510 Meta version 3.2 (Carl Zeiss) software, respectively, and the composites were prepared using Adobe Photoshop CS.

Teratoma formation assay

iPSCs at passage 25 were suspended in 20% Matrigel in DMEM/F12 and kept on ice. About 1×10^6 cells in 200 µl were aspirated into tuberculin syringes fitted with a 26 G needle and injected into the subcutaneous space above the rear right haunch of 6-week-old nude mice (n=8). Teratomas that developed at 6-8 weeks post-injection were surgically dissected after euthanizing the animals. The tissues were fixed overnight in 4% paraformaldehyde and processed for paraffin embedding. The tissue blocks were sectioned and processed for IHC examination as described above.

Karyotyping assay

The cells at passage 8 and 20 were grown under standard iPSC culture conditions. About 70-80% confluent cultures were treated with colcemid (0.1 µg/ml; Sigma-Aldrich) for 2-3 h to induce metaphase arrest and trypsinized to prepare single-cell suspensions. The cells were further treated with a hypotonic solution, fixed and then dropped onto clean glass slides (Fisher Scientific) and air dried. After a brief trypsin treatment, the chromosomes were G-banded by Giemsa staining. Well-spread metaphases were imaged and analyzed using CytoVision automated (Applied Imaging).

Transmission electron microscopy (TEM)

Tissues were fixed in 2.5% glutaraldehyde in 0.1 M phosphate buffer (pH 7.2) for 24 h at 4°C and then washed with 1× PBS thoroughly and post-fixed in 1% aqueous osmium tetroxide for 2 h. The samples were then washed, dehydrated through a graded alcohol series, embedded in Spurr's resin and incubated at 80°C for 72 h for complete polymerization. Ultra thin (60 nm) sections were prepared using an ultramicrotome (Leica Ultra Cut UCT-GA-D/E-1/00), mounted on copper grids and stained with saturated aqueous uranyl acetate and counterstained with Reynolds lead citrate. The sections were viewed using a Hitachi H-7500.

Statistics

The mean values of experimental repeats are given as ±s.d.

Acknowledgements

We thank Dr M. Lakshman of the RUSKA Lab, College of Veterinary Sciences, Prof. Jayshankar Telangana State Agricultural University (PJTSAU), Rajendranagar, Hyderabad, India, for providing TEM support; Dr Lakshmi Rao Kandukuri, Clinical Research Facility-Medical Biotechnology (CRF-MB), Centre for Cellular and Molecular Biology (CCMB), Hyderabad, India, for karyotyping; Dr Suresh Pothani, National Centre for Laboratory Animal Sciences, National Institute of Nutrition, Hyderabad, India, for providing animal facility support; and Prof. Dorairajan Balasubramanian, Dr S. Shivaji and Dr Gullapalli Nageshwara Rao for their critical review and useful suggestions in finalizing the manuscript.

Competing interests

The authors declare no competing or financial interests.

Author contributions

Conceptualization: P.J.S., S.M., I.M.; Methodology: P.J.S., S.M., V.K.P., S.R.B., R.R.N., M.N.N., G.B.R., I.M.; Software: I.M.; Validation: P.J.S., S.M., V.K.P., S.R.B., R.R.N., I.M.; Formal analysis: P.J.S., S.M., V.K.P., S.R.B., M.N.N., G.B.R., I.M.; Investigation: P.J.S., S.M., V.K.P., S.R.B., R.R.N., G.B.R., I.M.; Resources: V.K.P., S.R.B., R.R.N., M.N.N., G.B.R., V.S.S., I.M.; Data curation: P.J.S., V.K.P., I.M.; Writing - original draft: P.J.S., I.M.; Writing - review & editing: P.J.S., S.M., V.K.P., S.R.B., V.S.S., I.M.; Visualization: P.J.S., S.M., V.K.P., S.R.B., I.M.; Supervision: S.M., R.R.N., G.B.R., V.S.S., I.M.; Project administration: G.B.R., V.S.S., I.M.; Funding acquisition: V.S.S., I.M.

Funding

This study was supported by grants to I.M. and V.S.S. from the Department of Biotechnology, Ministry of Science and Technology, Government of India (BT/01/COE/06/02/10); Champalimaud Foundation; Tej Kohli Foundation; and the Hyderabad Eye Research Foundation.

Supplementary information

Supplementary information available online at
http://dev.biologists.org/lookup/doi/10.1242/dev.143040.supplemental

References

Ahmad, S., Stewart, R., Yung, S., Kolli, S., Armstrong, L., Stojkovic, M., Figueiredo, F. and Lako, M. (2007). Differentiation of human embryonic stem cells into corneal epithelial-like cells by in vitro replication of the corneal epithelial stem cell niche. *Stem Cells* **25**, 1145-1155.

Assawachananont, J., Mandai, M., Okamoto, S., Yamada, C., Eiraku, M., Yonemura, S., Sasai, Y. and Takahashi, M. (2014). Transplantation of embryonic and induced pluripotent stem cell-derived 3D retinal sheets into retinal degenerative mice. *Stem Cell Rep.* **2**, 662-674.

Basu, S., Sureka, S. P., Shanbhag, S. S., Kethiri, A. R., Singh, V. and Sangwan, V. S. (2016). Simple limbal epithelial transplantation: long-term clinical outcomes in 125 cases of unilateral chronic ocular surface burns. *Ophthalmology* **123**, 1000-1010.

Baulmann, D. C., Ohlmann, A., Flügel-Koch, C., Goswami, S., Cvekl, A. and Tamm, E. R. (2002). Pax6 heterozygous eyes show defects in chamber angle differentiation that are associated with a wide spectrum of other anterior eye segment abnormalities. *Mech. Dev.* **118**, 3-17.

Chan, A. A., Hertsenberg, A. J., Funderburgh, M. L., Mann, M. M., Du, Y., Davoli, K. A., Mich-Basso, J. D., Yang, L. and Funderburgh, J. L. (2013). Differentiation of human embryonic stem cells into cells with corneal keratocyte phenotype. *PLoS ONE* **8**, e56831.

Chen, P., Chen, J. Z., Shao, C. Y., Li, C. Y., Zhang, Y. D., Lu, W. J., Fu, Y., Gu, P. and Fan, X. (2015). Treatment with retinoic acid and lens epithelial cell-conditioned medium in vitro directed the differentiation of pluripotent stem cells towards corneal endothelial cell-like cells. *Exp. Ther. Med.* **29**, 351-360.

Cotsarelis, G., Cheng, S.-Z., Dong, G., Sun, T.-T. and Lavker, R. M. (1989). Existence of slow-cycling limbal epithelial basal cells that can be preferentially stimulated to proliferate: implications on epithelial stem cells. *Cell* **57**, 201-209.

Eiraku, M., Takata, N., Ishibashi, H., Kawada, M., Sakakura, E., Okuda, S., Sekiguchi, K., Adachi, T. and Sasai, Y. (2011). Self-organizing optic-cup morphogenesis in three-dimensional culture. *Nature* **472**, 51-56.

Findlater, G. S., McDougall, R. D. and Kaufman, M. H. (1993). Eyelid development, fusion and subsequent reopening in the mouse. *J. Anat.* **183**, 121-129.

Foster, J. W., Wahlin, K., Adams, S. M., Birk, D. E., Zack, D. J. and Chakravarti, S. (2017). Cornea organoids from human induced pluripotent stem cells. *Sci. Rep.* **7**, 41286.

Gonzalez-Cordero, A., West, E. L., Pearson, R. A., Duran, Y., Carvalho, L. S., Chu, C. J., Naeem, A., Blackford, S. J. I., Georgiadis, A., Lakowski, J. et al. (2013). Photoreceptor precursors derived from three-dimensional embryonic stem cell cultures integrate and mature within adult degenerate retina. *Nat. Biotechnol.* **31**, 741-747.

Grocott, T., Johnson, S., Bailey, A. P. and Streit, A. (2011). Neural crest cells organize the eye via TGF-β and canonical Wnt signalling. *Nat. Commun.* **2**, 265.

Hayashi, R., Ishikawa, Y., Ito, M., Kageyama, T., Takashiba, K., Fujioka, T., Tsujikawa, M., Miyoshi, H., Yamato, M., Nakamura, Y. et al. (2012). Generation of corneal epithelial cells from induced pluripotent stem cells derived from human dermal fibroblast and corneal limbal epithelium. *PLoS ONE* **7**, e45435.

Hayashi, R., Ishikawa, Y., Sasamoto, Y., Katori, R., Nomura, N., Ichikawa, T., Araki, S., Soma, T., Kawasaki, S., Sekiguchi, K. et al. (2016). Co-ordinated ocular development from human iPS cells and recovery of corneal function. *Nature* **531**, 376-380.

Hiler, D., Chen, X., Hazen, J., Kupriyanov, S., Carroll, P. A., Qu, C., Xu, B., Johnson, D., Griffiths, L., Frase, S. et al. (2015). Quantification of retinogenesis in 3D cultures reveals epigenetic memory and higher efficiency in ipscs derived from rod photoreceptors. *Cell Stem Cell* **17**, 101-115.

Huang, J., Dattilo, L. K., Rajagopal, R., Liu, Y., Kaartinen, V., Mishina, Y., Deng, C.-X., Umans, L., Zwijsen, A., Roberts, A. B. et al. (2009). FGF-regulated BMP signaling is required for eyelid closure and to specify conjunctival epithelial cell fate. *Development* **136**, 1741-1750.

Inamdar, M. S., Venu, P., Srinivas, M. S., Rao, K. and VijayRaghavan, K. (2009). Derivation and characterization of two sibling human embryonic stem cell lines from discarded grade III embryos. *Stem Cells Dev.* **18**, 423-434.

Kaewkhaw, R., Kaya, K. D., Brooks, M., Homma, K., Zou, J., Chaitankar, V., Rao, M. and Swaroop, A. (2015). Transcriptome dynamics of developing photoreceptors in three-dimensional retina cultures recapitulates temporal sequence of human cone and rod differentiation revealing cell surface markers and gene networks. *Stem Cells* **33**, 3504-3518.

Kanakubo, S., Nomura, T., Yamamura, K.-I., Miyazaki, J.-I., Tamai, M. and Osumi, N. (2006). Abnormal migration and distribution of neural crest cells in Pax6 heterozygous mutant eye, a model for human eye diseases. *Genes Cells* **11**, 919-933.

Kinoshita, H., Suzuma, K., Kaneko, J., Mandai, M., Kitaoka, T. and Takahashi, M. (2016). Induction of functional 3D ciliary epithelium-like structure from mouse induced pluripotent stem cells. *Invest. Ophthalmol. Vis. Sci.* **57**, 153-161.

Kuwahara, A., Ozone, C., Nakano, T., Saito, K., Eiraku, M. and Sasai, Y. (2015). Generation of a ciliary margin-like stem cell niche from self-organizing human retinal tissue. *Nat. Commun.* **6**, 6286.

Mariappan, I., Kacham, S., Purushotham, J., Maddileti, S., Siamwala, J. and Sangwan, V. S. (2014). Spatial distribution of niche and stem cells in ex vivo human limbal cultures. *Stem Cells Transl. Med.* **3**, 1331-1341.

Mariappan, I., Maddileti, S., Joseph, P., Siamwala, J. H. and Vauhini, V. (2015). Enriched cultures of retinal cells from BJNhem20 human embryonic stem cell line of Indian origin. *Invest. Ophthalmol. Vis. Sci.* **56**, 6714-6723.

Marko, C. K., Tisdale, A. S., Spurr-Michaud, S., Evans, C. and Gipson, I. K. (2014). The ocular surface phenotype of Muc5ac and Muc5b null mice. *Invest. Ophthalmol. Vis. Sci.* **55**, 291-300.

McCabe, K. L., Kunzevitzky, N. J., Chiswell, B. P., Xia, X., Goldberg, J. L. and Lanza, R. (2015). Efficient generation of human embryonic stem cell-derived corneal endothelial cells by directed differentiation. *PLoS ONE* **10**, e0145266.

McKenzie, R. W., Jumblatt, J. E. and Jumblatt, M. M. (2000). Quantification of MUC2 and MUC5AC transcripts in human conjunctiva. *Invest. Ophthalmol. Vis. Sci.* **41**, 703-708.

Mikhailova, A., Ilmarinen, T., Uusitalo, H. and Skottman, H. (2014). Small-molecule induction promotes corneal epithelial cell differentiation from human induced pluripotent stem cells. *Stem Cell Rep.* **2**, 219-231.

Rama, P., Matuska, S., Paganoni, G., Spinelli, A., De Luca, M. and Pellegrini, G. (2010). Limbal stem-cell therapy and long-term corneal regeneration. *N. Engl. J. Med.* **363**, 147-155.

Ramirez-Miranda, A., Nakatsu, M. N., Zarei-Ghanavati, S., Nguyen, C. V. and Deng, S. X. (2011). Keratin 13 is a more specific marker of conjunctival epithelium than keratin 19. *Mol. Vis.* **17**, 1652-1661.

Reichman, S., Terray, A., Slembrouck, A., Nanteau, C., Orieux, G., Habeler, W., Nandrot, E. F., Sahel, J.-A., Monville, C. and Goureau, O. (2014). From confluent human iPS cells to self-forming neural retina and retinal pigmented epithelium. *Proc. Natl. Acad. Sci. USA* **111**, 8518-8523.

Richardson, R. J., Hammond, N. L., Coulombe, P. A., Saloranta, C., Nousiainen, H. O., Salonen, R., Berry, A., Hanley, N., Headon, D., Karikoski, R. et al. (2014). Periderm prevents pathological epithelial adhesions during embryogenesis. *J. Clin. Invest.* **124**, 3891-3900.

Sangwan, V. S., Basu, S., Vemuganti, G. K., Sejpal, K., Subramaniam, S. V., Bandyopadhyay, S., Krishnaiah, S., Gaddipati, S., Tiwari, S. and Balasubramanian, D. (2011). Clinical outcomes of xeno-free autologous cultivated limbal epithelial transplantation: a 10-year study. *Br. J. Ophthalmol.* **95**, 1525-1529.

Sareen, D., Saghizadeh, M., Ornelas, L., Winkler, M. A., Narwani, K., Sahabian, A., Funari, V. A., Tang, J., Spurka, L., Punj, V. et al. (2014). Differentiation of human limbal-derived induced pluripotent stem cells into limbal-like epithelium. *Stem Cells Transl. Med.* **3**, 1002-1012.

Schermer, A., Galvin, S. and Sun, T. T. (1986). Differentiation-related expression of a major 64K corneal keratin in vivo and in culture suggests limbal location of corneal epithelial stem cells. *J. Cell Biol.* **103**, 49-62.

Shalom-Feuerstein, R., Serror, L., De La Forest Divonne, S., Petit, I., Aberdam, E., Camargo, L., Damour, O., Vigouroux, C., Solomon, A., Gaggioli, C. et al. (2012). Pluripotent stem cell model reveals essential roles for miR-450b-5p and miR-184 in embryonic corneal lineage specification. *Stem Cells* **30**, 898-909.

Sidney, L. E., Branch, M. J., Dunphy, S. E., Dua, H. S. and Hopkinson, A. (2014). Concise review: evidence for CD34 as a common marker for diverse progenitors. *Stem Cells* **32**, 1380-1389.

Takahashi, K., Tanabe, K., Ohnuki, M., Narita, M., Ichisaka, T., Tomoda, K. and Yamanaka, S. (2007). Induction of pluripotent stem cells from adult human fibroblasts by defined factors. *Cell* **131**, 861-872.

Völkner, M., Zschätzsch, M., Rostovskaya, M., Overall, R. W., Busskamp, V., Anastassiadis, K. and Karl, M. O. (2016). Retinal organoids from pluripotent stem cells efficiently recapitulate retinogenesis. *Stem Cell Rep.* **6**, 525-538.

Yoshida, S., Shimmura, S., Kawakita, T., Miyashita, H., Den, S., Shimazaki, J. and Tsubota, K. (2006). Cytokeratin 15 can be used to identify the limbal phenotype in normal and diseased ocular surfaces. *Invest. Ophthalmol. Vis. Sci.* **47**, 4780-4786.

Zhang, K., Pang, K. and Wu, X. (2014). Isolation and transplantation of corneal endothelial cell-like cells derived from *in-vitro*-differentiated human embryonic stem cells. *Stem Cells Dev.* **23**, 1340-1354.

Zhong, X., Gutierrez, C., Xue, T., Hampton, C., Vergara, M. N., Cao, L.-H., Peters, A., Park, T. S., Zambidis, E. T., Meyer, J. S. et al. (2014). Generation of three-dimensional retinal tissue with functional photoreceptors from human iPSCs. *Nat. Commun.* **5**, 4047.

Enriched Cultures of Retinal Cells From BJNhem20 Human Embryonic Stem Cell Line of Indian Origin

Indumathi Mariappan,[1] Savitri Maddileti,[1] Praveen Joseph,[1] Jamila H. Siamwala,[1,2] and Vasundhara Vauhini[1]

[1]Sudhakar and Sreekanth Ravi Stem Cell Biology Laboratory, Brien Holden Eye Research Centre, Champalimaud Translational Centre for Eye Research, Hyderabad Eye Research Foundation, L V Prasad Eye Institute, Hyderabad, India
[2]University of California, San Diego, California, United States

Correspondence: Indumathi Mariappan, Sudhakar and Sreekant Ravi Stem Cell Biology Laboratory, Brien Holden Eye Research Centre, Champalimaud Translational Centre for Eye Research, Hyderabad Eye Research Foundation, L V Prasad Eye Institute, Road No. 2, Banjara Hills, Hyderabad 500034, India; indumathi@lvpei.org.

Submitted: May 29, 2015
Accepted: September 20, 2015

Citation: Mariappan I, Maddileti S, Joseph P, Siamwala JH, Vauhini V. Enriched cultures of retinal cells from BJNhem20 human embryonic stem cell line of Indian origin. *Invest Ophthalmol Vis Sci*. 2015;56:6714–6723. DOI:10.1167/iovs.15-17364

Purpose. To test the retinal differentiation potential and to establish an optimized protocol for enriching retinal cells from an Indian origin, human embryonic stem cell (hESC) line, BJNhem20.

Methods. The BJNhem20 cells were cultured and expanded under feeder-free culture conditions. Differentiation was initiated by embryoid body (EB) formation and were cultured on Matrigel in neural induction medium (NIM) for 1 week and further maintained in retinal differentiation medium (RDM). After 1 month, the neuro-retinal progenitor clusters located at the center of pigmented retinal patches were picked and cultured as suspended neurospheres in RDM for 3 days and subsequently on Matrigel in neuro-retinal medium. The mildly pigmented, immature retinal pigmented epithelial (RPE) cells were picked separately and cultured on Matrigel in RPE medium (RPEM). After 1 week, the confluent neuro-retinal and RPE cultures were maintained in RDM for 2 to 3 months and characterized by immunofluorescence and RT-PCR.

Results. The BJNhem20 cells efficiently differentiated into both neuro-retinal and RPE cells. The early retinal progenitors expressed Nestin, GFAP, Pax6, Rx, MitfA, Chx10, and Otx2. Neuro-retinal cells expressed the neural markers, Map2, β-III tubulin, acetylated tubulin and photoreceptor-specific markers, Crx, rhodopsin, recoverin, calbindin, PKC, NeuroD1, RLBP1, rhodopsin kinase, PDE6A, and PDE6C. Mature RPE cells developed intense pigmentation within 3 months and showed ZO-1 and Phalloidin staining at cell–cell junctions and expressed RPE65, tyrosinase, bestrophin1, Mertk, and displayed phagocytic activity.

Conclusions. This study confirms the retinal differentiation potential of BJNhem20 cells and describes an optimized protocol to generate enriched populations of neuro-retinal and RPE cells.

Keywords: human embryonic stem cells, retinal pigmented epithelial (RPE) cells, retinal dystrophy

Retinitis pigmentosa is a progressive genetic disorder resulting in gradual degeneration of photoreceptors and RPE cells of the retina, leading to night blindness and gradual loss of vision, which later progresses to complete visual impairment and blindness. Mutations in several genes associated with the phototransduction pathway, retina-specific transporters and transcription factors, and vitamin A metabolism are linked to this disease. Therefore, gene therapy and cell replacement therapy offer great promise in the treatment of such conditions. However, the absence of stem cells in an adult retina has initiated a search for alternate sources that can generate retinal cell types suitable for regenerative applications.

Among the adult ocular stem cell sources, a minor population of the cells of the ciliary margin was shown to have retinal stem cell properties.[1] However, they have very limited potential to generate neurospheres (0.1%) and also lack the ability to differentiate to all cell types of the retina. Therefore, pluripotent cells, such as the embryonic stem cells (ESCs) and induced pluripotent stem cells (iPSCs) have become valuable stem cell sources for generating retinal cell types suitable for regenerative applications. Earlier studies have shown that it is possible to derive neuro-retinal (NR) progenitors, mature photoreceptors, and RPE cells from human ESCs.[2–11] Embryonic stem cell–derived retinal cell types also have been shown to rescue disease phenotype to some extent when transplanted in small and large animal models.[4,12–16] In an ongoing phase I/II clinical trial approved by the Food and Drug Administration (FDA), allogeneic human ESC (hESC)-derived RPE cells are being used in the treatment of patients with Stargardt's macular dystrophy and dry AMD.[17,18]

Given this interest in generating retinal cell types for clinical applications, a well-characterized hESC line with a propensity to differentiate into retinal lineages is of great value. To this end, we describe an efficient protocol to derive retinal cell types from a well-characterized Indian origin, hESC line, BJNhem20.[19–21] This line has been submitted to the UK Stem Cell Bank (UKSCB accession No. R-08-021) and listed in the European Human Pluripotent Stem Cell Registry (hPSC^{reg}) (JNCSRe002-A [BJNhem20]), International Stem Cell Registry, and the National Institutes of Health (NIH) Human Embryonic Stem Cell Registry

Table. Details of Indian-Origin hESC Lines Listed in the International Stem Cell Registry

S. No.	Name of the hESC Line	Name of the Depositor	Institute of Origin	Sex	Karyotype	Pluripotency	References	NIH Funding Eligibility and Approval No.
1	BJNhem19	Maneesha Inamdar	Jawaharlal Nehru Centre for Advanced Scientific Research (JNCASR), Bangalore	Male	Normal, 46XY	All 3 germ layers in EBs	19, 20, 21	Yes. NIHhESC-10-0083
2	BJNhem20	Maneesha Inamdar	JNCASR, Bangalore	Female	Normal, 46XX	All 3 germ layers in EBs and teratomas	19, 20, 21	Yes. NIHhESC-10-0084
3	KIND1	Deepa Bhartiya	National Institute for Research in Reproductive Health (NIRRH), Mumbai	Female	Normal, 46XX	All 3 germ layers in EBs and teratomas	23, 24	—
4	KIND2	Deepa Bhartiya	NIRRH, Mumbai	Female	Normal, 46XX	All 3 germ layers in EBs and teratomas	23, 24, 25	—
5	Relicell hES1	—	Reliance Life Sciences Pvt. Ltd., Mumbai	Female	Normal, 46XX	All 3 germ layers in EBs and teratomas	26	—
6	Relicell hES2	—	Reliance Life Sciences Pvt. Ltd., Mumbai	Female	Normal, 46XX	All 3 germ layers in EBs	27	—
7	Relicell hES3	—	Reliance Life Sciences Pvt. Ltd., Mumbai	Female	Normal, 46XX	All 3 germ layers in EBs and teratomas	27	—
8	Relicell hES4	—	Reliance Life Sciences Pvt. Ltd., Mumbai	Male	Normal, 46XY	Pluripotent both in vitro and in vivo	28	—

S. No., serial number; —, not currently approved.

(NIH Approval No. NIHhESC-10-0084). The International Stem Cell Initiative has conducted a genetic screen on ethnically diverse hESC lines and reported various genetic alterations and a common candidate on chromosome 20 that drives culture adaptation in more than 20% of the lines tested. The BJNhem20 line was part of this study and was found to be normal without any genetic abnormalities both at the early (sample code: TT-20-003-K-E-P19) and late passages (sample code: TT-20-004-K-L-P87) tested.[22] This line is also available for research use and projects involving its use are eligible for NIH funding consideration. The Table provides the details of all reported, Indian origin, hESC lines listed in the International Stem Cell Registry.

Materials and Methods

The study was reviewed and approved by the institutional review board of the LV Prasad Eye Institute, Hyderabad, India, and the research followed the tenets of the Declaration of Helsinki.

Human Embryonic Stem Cell Culture and Maintenance

The hESC line, BJNhem20 cells are cultured on irradiated or mitomycin C–treated mouse embryonic fibroblast feeders using the standard human ES medium (KnockOut Dulbecco's modified Eagle's medium (DMEM) supplemented with 10% KnockOut serum replacement [KOSR], 10% fetal bovine serum, 2 mM Glutamax, 0.1 mM nonessential amino acids [NEAA], 0.1 mM β-mercaptoethanol, 50 U/mL penicillin, 50 μg/mL streptomycin, and 10 ng/mL basic FGF [bFGF; Life Technologies, Carlsbad, CA, USA]). The cells are also adapted to feeder-free culture conditions on Matrigel (Corning, Inc., Corning, NY, USA) coated plates using mTeSR1 culture medium (STEMCELL Technologies, Vancouver, Canada). The cultures are passaged manually by cutting individual colonies using the bent tips of flame-pulled glass Pasteur pipettes, followed by gentle trituration to generate small 5- to 10-cell clusters. Alternatively, the cells are also passaged using 0.5 mM EDTA in calcium/magnesium-free PBS as described elsewhere.[29] Split ratios of approximately 1:6 to 1:10 were followed and the cultures were split after every 3 to 4 days before they reached 80% to 90% confluence.

Retinal Differentiation of hES Cells

The BJNhem20 cells were cultured under feeder-free conditions as described above. Differentiation was initiated by embryoid body (EB) formation in suspension cultures for 3 days in nonadherent dishes using differentiation medium (DM) that contains DMEM/F12, 4% KOSR, 0.1 mM NEAA, 2 mM Glutamax, 50 U/mL penicillin, and 50 μg/mL streptomycin (Life Technologies). After 3 days, the EBs are grown as adherent cultures on Matrigel-coated dishes, in neural induction medium (NIM), which contains DM supplemented with 1% N2 supplement (Life Technologies) and 100 ng/mL Noggin (R&D Systems, Minneapolis, MN, USA) for 1 week and further continued for 1 month in retinal differentiation medium (RDM), which contains DM and 2% B27 supplement (Life Technologies). Pigmented retinal progenitor cell clusters with neural progenitor rosettes and surrounding pigmented RPE patches were observed at this stage.

Subculture and Enrichment of Retinal Cells

The neural rosettes from pigmented cell clusters were isolated and further cultured as suspended neurospheres in RDM for 2

to 3 days. The resulting neurospheres containing retinal progenitors were further plated on Matrigel-coated dishes or chamber slides and maintained as adherent cultures in NR medium (NRM) containing DM supplemented with 1% N2, 5 ng/mL bFGF, and 10 ng/mL DKK1. The mildly pigmented and proliferating RPE patches surrounding the central NR islands were then manually picked using flame-pulled glass Pasteur pipettes and cultured on collagen I matrix or Matrigel-coated dishes or chamber slides (Corning, Inc.) or on Transwell cell culture inserts (Corning, Inc.) in RPE medium (RPEM) containing DM supplemented with 2% B27, 10 ng/mL ActivinA (R&D Systems), and 10 μM Y-27632 (Sigma-Aldrich Corp., St. Louis, MO, USA). Supplementary Figure S1 shows the schematic representation of the step-wise retinal differentiation protocol adapted in the study. After 1 week, the NR and RPE cultures reached confluence and were continuously maintained in RDM, with media changes on every third day for up to 2 to 3 months. The differentiation protocol was repeated several times in independent experiments, $n = 7$. The differentiated cells were characterized for NR and RPE-specific marker expression by immunofluorescence and RT-PCR analysis.

Immunocytochemistry

Growing hES cultures or the differentiated retinal cells were seeded and cultured on glass coverslips or on chamber slides. When the cells were ready for immunostaining, they were briefly washed with 1X PBS, fixed for 10 minutes using freshly prepared 3.5% formaldehyde in PBS and permeabilized for 10 minutes with 0.5% Triton X-100 in PBS, with three saline washes after each step. The cells were then blocked with 1% BSA at room temperature for 1 hour and then sequentially incubated with specific primary and fluorescent dye–conjugated secondary antibodies at appropriate dilutions for 1 hour each, with three saline washes after each incubation step. Supplementary Table S1 summarizes the details of antibodies used in the study. Propidium iodide (PI) or 4′,6-diamidino-2-phenylindole (DAPI) were used as counter stains. Intact cell sheets grown on collagen matrix were directly processed for immunohistochemistry by standard procedures and the tissue sections were examined by hematoxylin and eosin staining. Alkaline phosphatase staining was carried out using an assay kit by following the manufacturer's instruction (Merck Millipore, Darmstadt, Germany). The cells are finally washed, mounted on a glass slide, and imaged using an epifluorescence microscope (Olympus IX71; Olympus, Shinjuku, Tokyo, Japan) or a confocal microscope, LSM 510 (Carl Zeiss Microscopy GmbH, Jena, Germany). The images were analyzed using the Image-Pro Express Version 6.0 Imaging Software (Media Cybernetics, Inc., Rockville, MD, USA) and LSM 510 Meta, Version 3.2 software (Carl Zeiss Microscopy GmbH), respectively, and the composites were prepared using Adobe Photoshop CS (Adobe Systems, Inc., San Jose, CA, USA).

Florescence-Activated Cell Sorting (FACS) Quantification of Cultured Cells

Enriched passage one NR and RPE cell suspensions were prepared and processed for immune labeling as described above. The final cell suspensions were analyzed using FACS Aria I cell sorter and the data analysis was carried out using FACS Diva software (BD Biosciences, San Jose, CA, USA).

Secreted Protein Quantification by ELISA

Culture supernatants of enriched cultures of BJNhem20-derived RPE cells grown in six-well plates were collected (1.5 mL/well) and aliquots of 100 μL were used to analyze and quantify the secreted VEGF and pigmented epithelium-derived factor (PEDF) levels by sandwich ELISA method as per the manufacturer's instructions (R&D Systems). Culture supernatants of ARPE-19 and HEK 293T cells were used as controls.

Gene Expression by RT-PCR

Total RNA was isolated from cell samples by Trizol method and cDNAs were prepared by reverse transcription using SuperScript II RT kit (Life Technologies) as per the manufacturer's instruction. Polymerase chain reactions were performed for all the genes tested using the cDNAs as reaction templates. The starting template concentrations were normalized for all the samples tested based on the expression levels of the housekeeping gene, *eEF1α*. Supplementary Table S2 summarizes the primer details of various genes analyzed in the study, $n = 3$. The amplicons were resolved on 1% (wt/vol) agarose gels, stained with ethidium bromide, imaged under UV light, and documented using Gel Doc XR+ System (BioRad, Hercules, CA, USA).

Phagocytosis Assay

The BJNhem20-derived RPE cells were grown on Matrigel-coated glass chamber slides (BD Biosciences) and incubated with 1.0-μm sized green fluorescence latex beads (Sigma-Aldrich Corp.) at a concentration of 1×10^6 beads/mL for 6 hours at 37°C. The cells were then washed thoroughly with PBS for five times to remove extracellular, free-floating beads and processed for immunocytochemistry and imaging as described above.

Statistical Analysis

Test values were reported as mean values ± SD. Group means were compared using the Student's unpaired *t*-test; $P < 0.05$ was considered statistically significant (*) and $P > 0.05$ was considered statistically insignificant (#).

Results

Stemness and Pluripotent Properties of BJNhem20

The Indian origin, hESC line, BJNhem20, used in the study was originally derived, characterized, and reported by Inamdar et al.[19] Growing cultures of this hESC line maintained the typical round and flat colony morphology with distinct boundaries and the cells maintained a high nuclear to cytoplasmic ratio as shown in Figures 1A and 1B. The cells expressed the pluripotent stem cell markers, Oct4, SSEA4, Nanog, and alkaline phosphatase as shown in Figures 1D through 1G. It was also reported to express TRA 1-60, TRA 1-81, Sox2, DNMT3B, Rex1, LeftyA, and others.[19] On suspension culture, they differentiated and readily formed circular EBs within 2 to 3 days, as shown in Figure 1C, and gave rise to cell types of ectoderm, mesoderm, and endoderm lineages.[19] The cells were also shown to be capable of teratoma formation when injected subcutaneously into nude mice.[19] The karyotype of this female line was reported to be normal and was shown to have the propensity to generate beating cardiomyocytes.[19]

Here, we report the retinal differentiation potential of BJNhem20 and describe a stepwise differentiation protocol for deriving retinal progenitors and also to establish enriched cultures of RPE cells and NR cells.

Retinal Differentiation of BJNhem20

Retinal differentiation was carried out as described in the methods section. Briefly, 2- to 3-day-old EBs were grown as

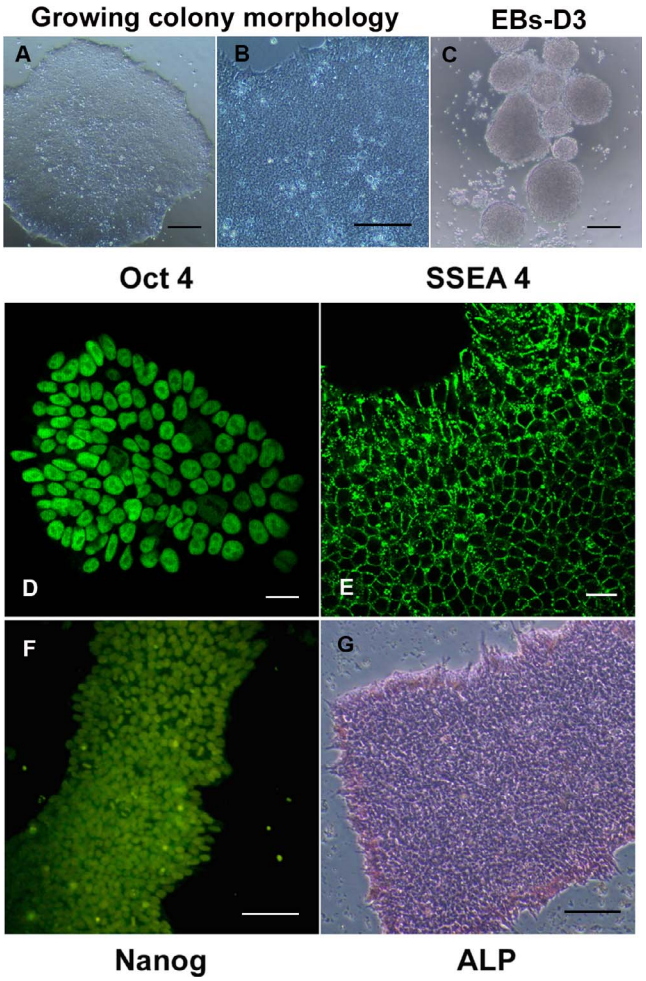

FIGURE 1. Morphology and stem cell marker expression in BJNhem20 cells. Phase images of growing cultures of BJNhem20 cells in a feeder-free culture condition on Matrigel (**A**, **B**) and floating cultures of embryoid bodies at day 3 of differentiation (**C**). *Scale bar*: 100 μM (**A**–**C**). Expression of pluripotent stem cell markers, Oct3/4 (**D**), SSEA4 (**E**), Nanog (**F**), and alkaline phosphatase (**G**) in growing cultures. *Scale bars*: 20 μM (**D**, **E**), 100 μM (**F**, **G**).

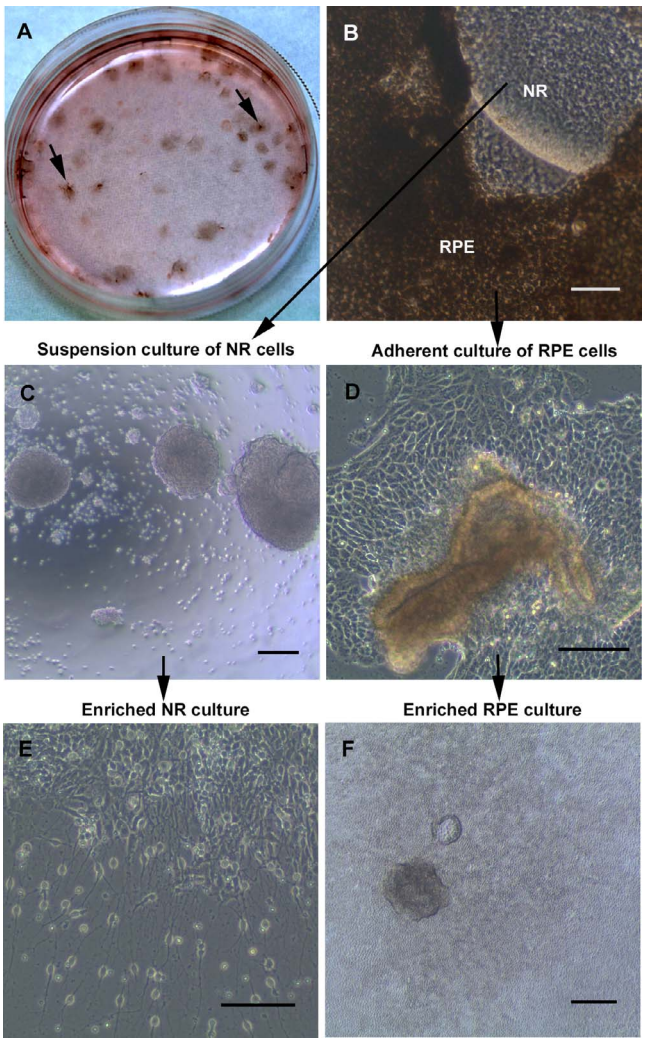

FIGURE 2. Retinal differentiation and enrichment of BJNhem20-derived retinal cells. Phase images of retinal differentiation cultures. (**A**) Full dish (60-mm diameter) view of a 1-month-old differentiation culture, wherein small clusters of retinal progenitors begin to form and appear as pigmented patches (*arrows*). (**B**) Zoomed in view of a pigmented cluster. Proliferating RPE cells are seen all around a central cluster of NR progenitors. (**C**) Suspension culture of the central island of NR progenitors to generate enriched cultures of growing neurospheres. (**D**) Adherent cultures of manually isolated patches of pigmented RPE cell clusters on matrigel. On adhesion, the RPE cells loose the pigments, become fibroblastic, and proliferate to expand in culture. (**E**) Adherent cultures of neurospheres containing NR progenitors to generate mixed populations of NR cells. (**F**) Enriched and confluent cultures resulting in sheets of mildly pigmented and uniformly hexagonal-shaped RPE cells at 2 months, which further matures and becomes intensely pigmented by 3 months. *Scale bars*: 100 μM.

adherent cultures on Matrigel-coated plates in NIM for 1 week. The addition of recombinant human noggin protein in NIM inhibits BMP signaling, and in the presence of N2 supplement, it promotes early neuro-ectodermal commitment and differentiation. The cells were further cultured under retinal differentiation-promoting conditions in RDM containing 2% B27 supplement for a further 1 month. After 1 month of retinal differentiation, visibly pigmented retinal clusters consisting of very early retinal progenitors were observed (Figs. 2A, 2B). The neural-like cell rosettes within the pigmented clusters were manually picked and grown separately as neurospheres in suspension for 3 days in RDM to enrich for NR progenitors (Fig. 2C).

It is well established that the ocular surface ectoderm-derived bFGF and the periocular mesenchyme-derived TGFβ family of proteins, such as activin A, play an important role in NR and RPE fate commitment, respectively.[30] Also, it is known that inhibition of wnt signaling is necessary to promote terminal differentiation and maturation of NR progenitors. Therefore, the neurospheres are further grown as adherent cultures in NRM containing N2 supplement (1%), bFGF (5 ng/mL), and DKK1 (10 ng/mL). Highly proliferating cells with typical neuron-like morphology are seen migrating out of the adhered neurospheres within 1 day (Fig. 2E) to generate enriched cultures of mixed populations of various NR cells within 2 months.

Both the mildly pigmented or nonpigmented immature RPE cells that proliferated and migrated out of the central pigmented retinal clusters were manually picked and maintained separately as adherent cultures in RPEM containing B27 supplement (2%), activin A (10 ng/mL), and Rho-associated protein kinase (ROCK) inhibitor, Y-27632 (10 μM),

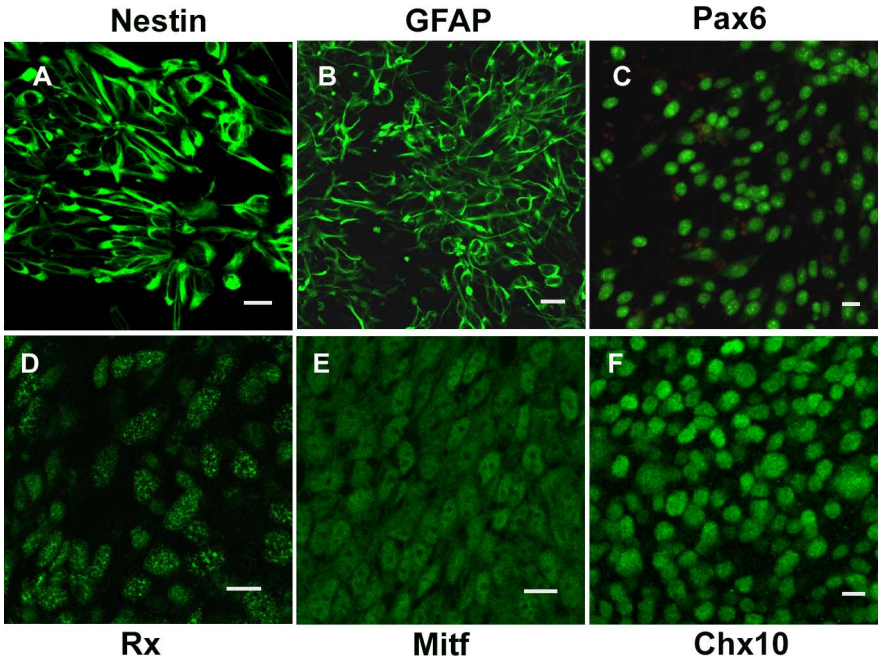

FIGURE 3. Expression of early commitment markers by BJNhem20-derived retinal progenitor cells. Early retinal progenitors present within the pigmented clusters at 1 month of differentiation expressed Nestin (**A**), GFAP (**B**), Pax6 (**C**), Rx (**D**), MitfA (**E**), and Chx10 (**F**). *Scale bars*: 20 μM.

to allow RPE cell proliferation and expansion. The proliferating and migrating RPE cells initially assumed a fibroblastic morphology (Fig. 2D). As the adherent cultures became confluent, they regained the typical cobble-stone morphology. Addition of ROCK inhibitor to RPE cultures during maintenance and passaging has been reported to promote cell proliferation, reduce cell death, prevent epithelial-mesenchymal transition (EMT),[31] and help in the establishment of a uniform monolayer of hexagonal-shaped, highly pigmented, mature RPE cells within 2 to 3 months (Fig. 2F).

Characterization of BJNhem20-Derived Retinal Cells

Retinal cells derived at different stages of differentiation were analyzed by immunocytochemistry. The pigmented retinal clusters (Fig. 2A) that emerged at 1 month after differentiation confirmed the presence of retinal progenitors that expressed the neural progenitor marker, Nestin; glial progenitor marker, glial fibrillary acidic protein (GFAP); early eye-field commitment markers, Pax6 and Rx; RPE lineage commitment marker, MitfA; and the NR lineage commitment marker, Chx10 (Fig. 3). It is important to note that the selective isolation of retinal progenitors based on pigmentation and neural rosette morphology at early stages of differentiation helps in subsequent enrichment of mature retinal cells.

Immunocytochemistry of 3-month-old NR cultures confirmed the expression of general neuron-specific, Map2, β-III Tubulin, and acetylated Tubulin; rod-cone progenitor-specific, Crx and mature photoreceptor-specific, rhodopsin and recoverin (Figs. 4A–F). Although the photoreceptor cells are not morphologically mature, they expressed rhodopsin protein in an asymmetrical pattern within the cytosol, whereas its expression is normally localized to the outer segments of mature rod photoreceptor cells. The NR cells also coexpressed some of the progenitor and mature cell markers, such as the Pax6, Crx, recoverin, and rhodopsin (Figs. 4G–I).

Enriched cultures of RPE cells resulted in the formation of uniformly pigmented sheets of matured epithelial monolayer at 3 months, as shown in Figures 5A and 5B. Immunocytochemistry of the compact epithelial sheets confirmed the expression of tight junction protein, ZO-1 (Fig. 5C), and an orderly arrangement of actin cytoskeletal bundles as shown by Phalloidin staining (Fig. 5F). The cells also expressed the mature RPE-specific marker, RPE65. This gene codes for an enzyme, isomerohydrolase that converts all-trans retinol to 11-cis retinal during phototransduction and plays an important role in the visual cycle. This enzyme exists in both the membrane-bound and cytosolic forms, as shown in Figure 5D. The RPE cells play an important role in the clearance of subretinal cellular debris, and this function is mediated by active phagocytosis. The BJNhem20-derived RPE cells also displayed phagocytosis, as shown by the internalization of fluorescently labeled latex beads (Fig. 5C). Intact monolayer sheets of RPE cells cultured on collagen I matrix appeared to be highly polarized cells with tight cell-cell junctions, basally positioned nuclei, numerous apical microvilli structures, and pigmented melanosomes in the cytosol (Figs. 5G, 5H). The BJNhem20-derived RPE cells also secreted significant levels of both VEGF and PEDF, when compared with the ARPE-19 and HEK 293T cells, respectively (Figs. 5I, 5J), and the levels were comparable with those reported for PSC-derived RPE cells in other studies.[32,33]

The FACS quantification of NR and RPE cultures confirmed cell enrichment within a single passage. Relatively lower levels of Pax6-positive cells (62%) indicated that the retinal stem cells had undergone lineage commitment and differentiation (Fig. 6B). High percentage of Chx10 (87%) and Mitf (94%) positive cells confirmed the enrichment of lineage committed progenitors (Figs. 6C, 6F). Also, the proportion of mature retinal cells expressing the markers such as Nrl and RPE65 were 31% and 34%, respectively (Figs. 6D, 6G).

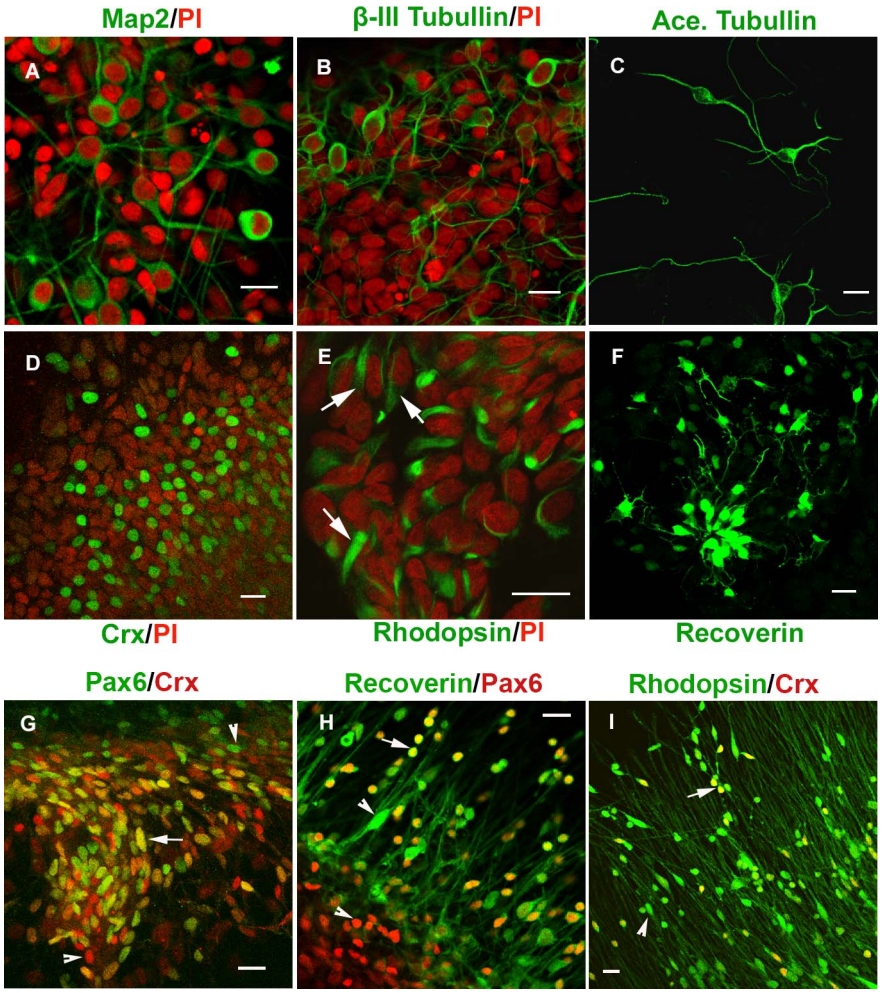

Figure 4. Expression of mature NR markers. Adherent cultures of enriched NR spheres at 2 to 3 months after differentiation consisted of mixed populations of possibly all types of retinal neurons and expressed the general neural markers, Map2 (**A**), β-III tubulin (**B**), acetylated tubulin (**C**), and the photoreceptor-specific markers Crx (**D**), rhodopsin (**E**), and recoverin (**F**) (all in *green*). *Arrows* mark the asymmetrically localized rhodopsin. The cells are counterstained with PI in (**A**, **B**, **D**, **E**) to mark the nuclei (in *red*). Retinal cells coexpressing the markers such as Pax6 (*green*) and Crx (*red*) (**G**), Recoverin (*green*) and Pax6 (*red*) (**H**), rhodopsin (*green*) and Crx (*red*) (**I**). *Arrows* indicate the dual positive cells and *arrowheads* mark the cells expressing only a single marker. *Scale bars*: 20 μM.

Further, we compared the gene expression patterns of different stem cell and retinal markers at days 0, 30, and 90 after differentiation by RT-PCR and representative gel images of various genes tested are shown in Figure 7. In brief, the pluripotent stem cell markers, Oct3/4, Nanog, and hTERT were downregulated as the cells entered into the differentiation program. This coincided with the stepwise activation of retinal progenitor markers, such as Otx2, MitfA, Chx10, and Rx at d30. Similarly, the expression of NR markers, such as NeuroD1, Crx, recoverin, calbindin, PDE6A, PDE6C, RLBP1, PKC-β, rhodopsin kinase, and Opsin-MW, and RPE markers, such as tyrosinase, RPE65, Bestrophin1, and Mertk, were upregulated at d30 and d90 (Fig. 7).

Discussion

A large body of literature evidence has confirmed that adult mammalian and primate retina are amenable for cell replacement therapy. Transplantations of human fetal retinal progenitors[34,35] or photoreceptor precursors[12] are shown to preserve or improve visual functions in animal models of retinal dystrophy. However, a reliable and renewable source of donor cells such as the hESCs and iPSCs are being intensely explored for adopting them in cell replacement therapies. As mentioned earlier, many reports have shown that retinal cells derived from hESCs are amenable for scaling up and are effective in delaying disease progression and in improving visual functions in preclinical animal studies.

The results of the present study confirm the retinal differentiation potential of the hESC line, BJNhem20. Using the protocol described here, it is possible to efficiently differentiate and enrich RPE cells and NR progenitors and expand them enough for further downstream applications. Although complex cocktails of culture components have been reported to drive retinal differentiation, our protocol involves an initial EB formation and short-term culture in the presence of Noggin and N2 supplement to drive neuro-ectodermal differentiation. Subsequent differentiation in B27-supplemented conditions promoted eye-field specification within 1 month. Manual isolation of these mildly pigmented eye-field–specified clusters ensures early enrichment of retinal progenitors. These

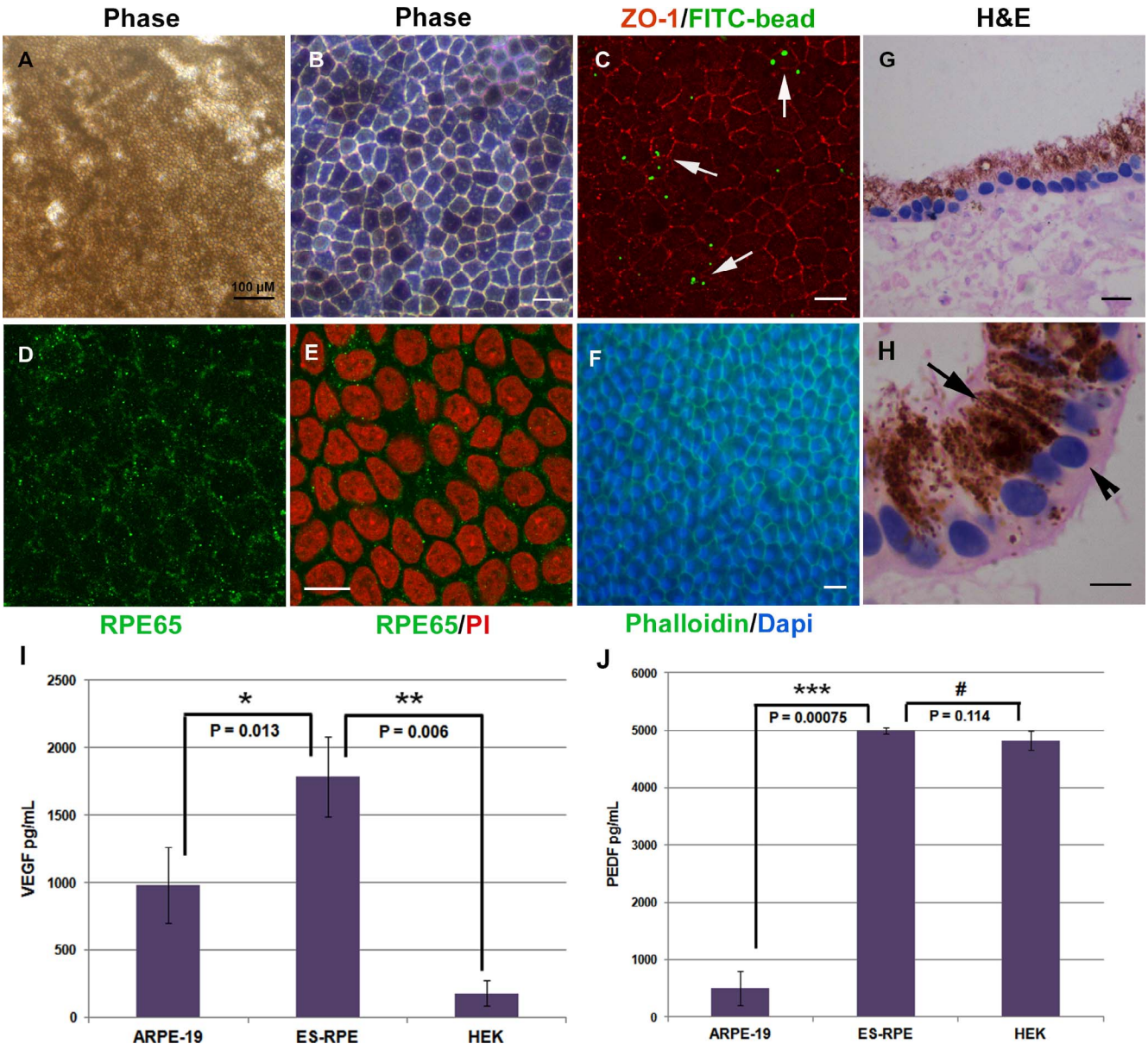

Figure 5. Expression of RPE markers. Morphology of enriched sheets of mature RPE cells at 3 months after differentiation. Note the compact arrangement of hexagonal-shaped cells with mild to intense pigmentation (**A**, **B**). Intact tight junctions are marked by ZO-1 staining in *red* (**C**). Both the cytosolic and membrane-bound forms of RPE65 protein were detected in mature, 3-month-old cultures (in *green*) with PI staining to mark the nuclei (in *red*) (**D**, **E**). The organized actin cytoskeletal bundles are marked by Phalloidin staining in *green* with DAPI staining to mark the nuclei (**F**). The green fluorescent latex beads that were phagocytosed by the cells are seen as *green dots* within the cytoplasm of intact cells (**C**). Hematoxylin and eosin–stained intact RPE cell sheets on collagen I matrix (**G**, **H**). Note the polarized epithelium with tight cell–cell junctions, basally-positioned nuclei (*arrowhead*), numerous melanosomes and apical microvilli structures (*arrow*). *Scale bars*: 100 µM (**A**), 20 µM (**B**–**H**). *Bar graphs* represent the average levels of secreted VEGF and PEDF proteins in the culture supernatants of ARPE-19, HEK 293T, and hESC-derived RPE cells, $n = 3$. *Error bars*: represent the SD.

early-stage retinal progenitors expressed Nestin, GFAP, Pax6, Chx10, Rx, and Mitf. Adherent culture of isolated retinal progenitors gave rise to both RPE and NR patches. Expansion of isolated RPE cell patches, their maturation, pigmentation, and maintenance of proper cell morphology was enabled by culturing them in the presence of ActivinA and ROCK inhibitor. The mature RPE cells were highly pigmented, polarized cells with apical microvilli and hexagonal morphology, and expressed RPE65, ZO-1, VEGF, and PEDF proteins at appropriate levels. Similarly, bFGF and DKK1 treatment enabled the expansion and maturation of NR cells that expressed Crx, recoverin, rhodopsin, cone opsin, and other NR markers.

Recent reports on the clinical outcomes of FDA-approved, phase I/II trials have established the safety and tolerability of subretinal transplantations of hESC-derived RPE cells in the treatment of patients with Stargardt's macular dystrophy and dry AMD.[17,18,36] It is well known that the eye is an immune-privileged site, being established by the barrier functions of RPE cells and the endothelial cells of retinal vasculatures. The early observations and outcomes of this trial confirm that in spite of being an allogeneic cell source, the hESC-derived RPE

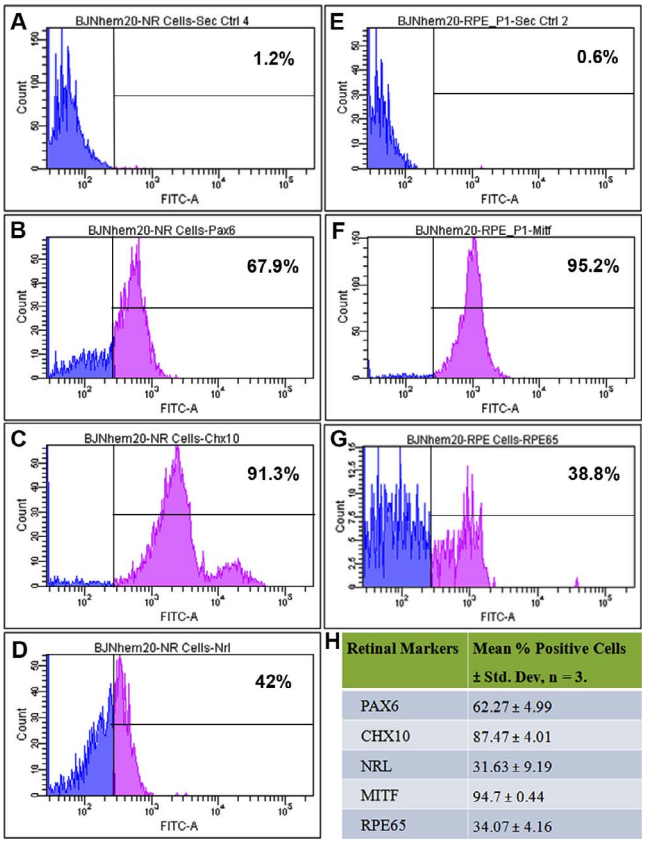

H

Retinal Markers	Mean % Positive Cells ± Std. Dev, n = 3.
PAX6	62.27 ± 4.99
CHX10	87.47 ± 4.01
NRL	31.63 ± 9.19
MITF	94.7 ± 0.44
RPE65	34.07 ± 4.16

FIGURE 6. Florescence-activated cell sorting quantification of BJNhem20 derived retinal cells. Florescence-activated cell sorting plots of passage 1 NR and RPE cells labeled with isotype control antibody (**A**, **E**), anti-Pax6 antibody (**B**), anti-Chx10 antibody (**C**), anti-Nrl antibody (**D**), anti-Mitf antibody (**F**), and anti-RPE65 antibody (**G**). Summary of the mean percent positive cells ± SD (*H*), $n = 3$.

cells transplanted in the subretinal space of the patient's eye did not elicit any significant immunologic response. The reports also revealed that there were no signs of hyperproliferation, tumorigenicity, or ectopic tissue formation. Fundus photographs and optical coherence tomography images of transplantation sites of the retina in treated eyes have confirmed that the RPE grafts survived, proliferated/expanded in vivo for up to 37 months post transplantation, and contributed to marginal improvements in visual parameters. These developments were encouraging to consider BJNhem20-derived retinal cells for possible preclinical and clinical applications.

As a next step toward clinical translation, it is important to adapt early-passage cells into feeder-free and xeno-free culture conditions under a current good manufacturing practice (cGMP) work flow. Also, the retinal differentiation steps described in the study could be easily adapted to GMP requirements using clinical grade, xeno-free reagents. To ensure the safety of hESCs and their derivatives, it is important to reconfirm their pathogen-free status (bacteria, fungi, mycoplasma, and viruses, such as human immunodeficiency virus, hepatitis B virus, hepatitis C virus, and syphilis) using appropriate GMP-compliant testing methods. It is also important to ensure that the enriched RPE cells are free of undifferentiated cell contaminants by testing them for the absence of tumor formation when transplanted in immune-compromised mice models. Finally, a preclinical safety and efficacy study in retinal dystrophic rodent models would ensure the biological activity and functional relevance of ESC-derived retinal cells.

Although these are clear and obvious requirements for future clinical considerations, this report highlights the retinal differentiation potential of the hESC line, BJNhem20. The retinal derivatives and their progenies could serve as in vitro models in basic research and in pharmacologic drug screening and testing. A cGMP-compliant cell preparation could serve as valuable allogeneic donor cells in the treatment of patients with various forms of retinal dystrophies.

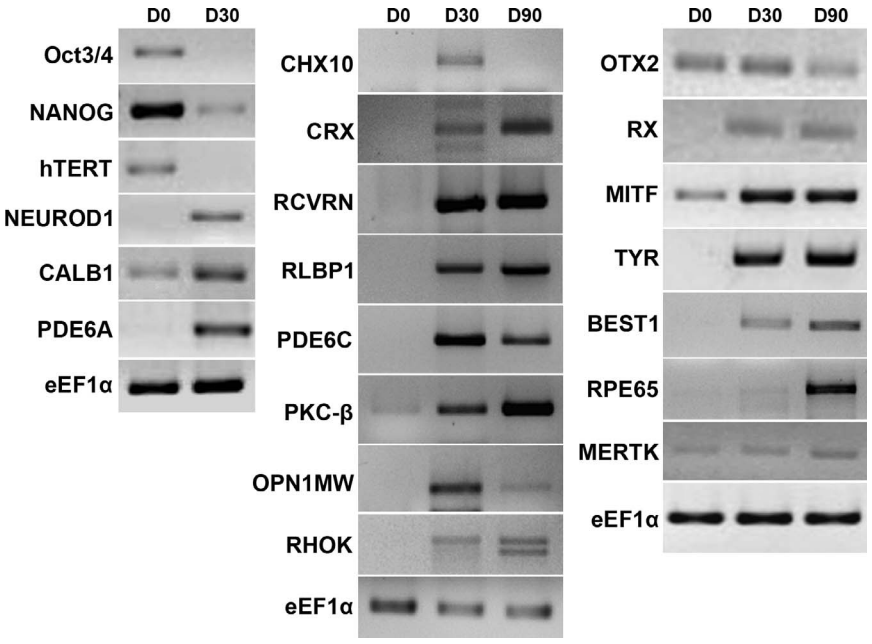

FIGURE 7. Reverse transcription PCR profiling of NR and RPE-specific genes. Agarose gel pictures of RT-PCR products of various pluripotent stem cell– and retina-specific genes expressed by the undifferentiated cells (D0) and by retinal differentiation cultures at 1 month (D30) and 3 months (D90) after differentiation. The cDNAs of different test samples were normalized using eEF1α as the loading control.

Investigative Ophthalmology & Visual Science

Acknowledgments

The authors thank Maneesha Inamdar, PhD, Jawaharlal Nehru Centre for Advanced Scientific Research, Bangalore, for providing the hESC line, BJNhem20, and also for providing technical guidance related to hESC culture; Sreedhar Rao Boyenpally, BSc, and Dilip Kumar Mishra, MD, Ophthalmic Pathology Laboratory, L V Prasad Eye Institute, for their expert guidance with immunohistochemistry experiments; and Dorairajan Balasubramanian, PhD, for his critical review and useful suggestions in finalizing the manuscript.

Supported by grants from the Department of Biotechnology, Government of India, Champalimaud Foundation, Portugal, and the Hyderabad Eye Research Foundation (IM). The authors alone are responsible for the content and writing of the paper.

Disclosure: **I. Mariappan**, None; **S. Maddileti**, None; **P. Joseph**, None; **J.H. Siamwala**, None; **V. Vauhini**, None

References

1. Coles BL, Angénieux B, Inoue T, et al. Facile isolation and the characterization of human retinal stem cells. *Proc Natl Acad Sci U S A*. 2004;101:15772–15777.
2. Ikeda H, Osakada F, Watanabe K, et al. Generation of Rx+/Pax6+ neural retinal precursors from embryonic stem cells. *Proc Natl Acad Sci U S A*. 2005;102:11331–11336.
3. Lamba DA, Karl MO, Ware CB, Reh TA. Efficient generation of retinal progenitor cells from human embryonic stem cells. *Proc Natl Acad Sci U S A*. 2006;103:12769–12774.
4. Lund RD, Wang S, Klimanskaya I, et al. Human embryonic stem cell-derived cells rescue visual function in dystrophic RCS rats. *Cloning Stem Cells*. 2006;8:189–199.
5. Osakada F, Ikeda H, Mandai M, et al. Toward the generation of rod and cone photoreceptors from mouse, monkey and human embryonic stem cells. *Nat Biotechnol*. 2008;26:215–224.
6. Osakada F, Jin ZB, Hirami Y, et al. In vitro differentiation of retinal cells from human pluripotent stem cells by small-molecule induction. *J Cell Sci*. 2009;122:3169–3179.
7. Osakada F, Ikeda H, Sasai Y, Takahashi M. Stepwise differentiation of pluripotent stem cells into retinal cells. *Nat Protoc*. 2009;4:811–824.
8. Idelson M, Alper R, Obolensky A, et al. Directed differentiation of human embryonic stem cells into functional retinal pigment epithelium cells. *Cell Stem Cell*. 2009;5:396–408.
9. Meyer JS, Shearer RL, Capowski EE, et al. Modeling early retinal development with human embryonic and induced pluripotent stem cells. *Proc Natl Acad Sci U S A*. 2009;106:16698–16703.
10. Eiraku M, Takata N, Ishibashi H, et al. Self-organizing optic-cup morphogenesis in three-dimensional culture. *Nature*. 2011;472:51–56.
11. Buchholz DE, Pennington BO, Croze RH, Hinman CR, Coffey PJ, Clegg DO. Rapid and efficient directed differentiation of human pluripotent stem cells into retinal pigmented epithelium. *Stem Cells Transl Med*. 2013;2:384–393.
12. MacLaren RE, Pearson RA, MacNeil A, et al. Retinal repair by transplantation of photoreceptor precursors. *Nature*. 2006;444:203–207.
13. Lamba DA, Gust, J, Reh TA. Transplantation of human embryonic stem cell-derived photoreceptors restores some visual function in Crx-deficient mice. *Cell Stem Cell*. 2009;4:73–79.
14. Carr AJ, Vugler AA, Hikita ST, et al. Protective effects of human iPS-derived retinal pigment epithelium cell transplantation in the retinal dystrophic rat. *PLoS One*. 2009;4:e8152.
15. Lu B, Malcuit C, Wang S, et al. Long-term safety and function of RPE from human embryonic stem cells in preclinical models of macular degeneration. *Stem Cells*. 2009;27:2126–2135.
16. Gonzalez-Cordero A, West EL, Pearson RA, et al. Photoreceptor precursors derived from three-dimensional embryonic stem cell cultures integrate and mature within adult degenerate retina. *Nat Biotechnol*. 2013;31:741–747.
17. Schwartz SD, Hubschman JP, Heilwell G, et al. Embryonic stem cell trials for macular degeneration: a preliminary report. *Lancet*. 2012;379:713–720.
18. Schwartz SD, Regillo CD, Lam BL, et al. Human embryonic stem cell-derived retinal pigment epithelium in patients with age-related macular degeneration and Stargardt's macular dystrophy: follow-up of two open-label phase 1/2 studies. *Lancet*. 2015;385:509–516.
19. Inamdar MS, Venu P, Srinivas MS, Rao K, VijayRaghavan K. Derivation and characterization of two sibling human embryonic stem cell lines from discarded grade III embryos. *Stem Cells Dev*. 2009;18:423–433.
20. Venu P, Chakraborty S, Inamdar MS. Analysis of long-term culture properties and pluripotent character of two sibling human embryonic stem cell lines derived from discarded embryos. *In Vitro Cell Dev Biol Anim*. 2010;46:200–205.
21. Shetty R, Inamdar MS. Derivation of human embryonic stem cell lines from poor quality embryos. *Methods Mol Biol*. 2012;873:151–161.
22. International Stem Cell Initiative. Screening ethnically diverse human embryonic stem cells identifies a chromosome 20 minimal amplicon conferring growth advantage. *Nat Biotechnol*. 2011;29:1132–1144.
23. Kumar N, Hinduja I, Nagvenkar P, et al. Derivation and characterization of two genetically unique human embryonic stem cell lines on in-house-derived human feeders. *Stem Cells Dev*. 2009;18:435–445.
24. Nagvenkar P, Pethe P, Pawani H, et al. Evaluating differentiation propensity of in-house derived human embryonic stem cell lines KIND-1 and KIND-2. *In Vitro Cell Dev Biol Anim*. 2011;47:406–419.
25. Pawani H, Nagvenkar P, Pethe P, Bhartiya D. Differentiation of human ES cell line KIND-2 to yield tripotent cardiovascular progenitors. *In Vitro Cell Dev Biol Anim*. 2013;49:82–93.
26. Mandal A, Tipnis S, Pal R, et al. Characterization and in vitro differentiation potential of a new human embryonic stem cell line, ReliCellhES1. *Differentiation*. 2006;74:81–90.
27. Mandal A, Bhowmik S, Patki A, Viswanathan C, Majumdar AS. Derivation, characterization, and gene expression profile of two new human ES cell lines from India. *Stem Cell Res*. 2010;5:173–187.
28. Mandal A, Mathew S, Saha D, Viswanathan C. Establishment, characterization, and differentiation of a karyotypically normal human embryonic stem cell line from a trisomy-affected embryo. *In Vitro Cell Dev Biol Anim*. 2013;49:15–26.
29. Beers J, Gulbranson DR, George N, et al. Passaging and colony expansion of human pluripotent stem cells by enzyme-free dissociation in chemically defined culture conditions. *Nat Protoc*. 2012;7:2029–2040.
30. Fuhrmann S, Levine EM, Reh TA. Extraocular mesenchyme patterns the optic vesicle during early eye development in the embryonic chick. *Development*. 2000;127:4599–4609.
31. Croze RH, Buchholz DE, Radeke MJ, et al. ROCK inhibition extends passage of pluripotent stem cell-derived retinal pigmented epithelium. *Stem Cells Transl Med*. 2014;3:1066–1078.
32. Kokkinaki M, Sahibzada N, Golestaneh N. Human induced pluripotent stem-derived retinal pigment epithelium (RPE) cells exhibit ion transport, membrane potential, polarized vascular endothelial growth factor secretion, and gene expression pattern similar to native RPE. *Stem Cells*. 2011;29:825–835.
33. Kamao H, Mandai M, Okamoto S, et al. Characterization of human induced pluripotent stem cell-derived retinal pigment

Investigative Ophthalmology & Visual Science

epithelium cell sheets aiming for clinical application. *Stem Cell Rep*. 2014;2:205–218.

34. Klassen HJ, Ng TF, Kurimoto Y, et al. Multipotent retinal progenitors express developmental markers, differentiate into retinal neurons, and preserve light-mediated behavior. *Invest Ophthalmol Vis Sci*. 2004;45:4167–4173.
35. Luo J, Baranov P, Patel S, et al. Human retinal progenitor cell transplantation preserves vision. *J Biol Chem*. 2014;289:6362–6371.
36. Song WK, Park KM, Kim HJ, et al. Treatment of macular degeneration using embryonic stem cell-derived retinal pigment epithelium: preliminary results in Asian patients. *Stem Cell Reports*. 2015;4:860–872.

Original Article

Learning curve of a trained vitreo-retinal surgeon in sub-retinal injections in a rat model: Implications for future clinical trials

Vivek Pravin Dave[1,2], Praveen Joseph Susaimanickam[2], Irfan Ahamad Mir[3], Indumathi Mariappan[2], Sayan Basu[4], Bhanuprakash G Reddy[3], Rajeev Reddy Pappuru[1], Subhadra Jalali[1], Taraprasad Das[1]

Purpose: The sub-retinal injections are not very commonly performed procedures in vitreoretina, but form a crucial step in any cell replacement therapy for retinal diseases. The purpose of this study is to describe the learning curve of a trained vitreo-retinal surgeon in sub-retinal injections in a rat model and its implications in future clinical trials. **Materials and Methods:** This is an in-vivo retrospective animal study using Wistar rats. All ARVO guidelines regarding animal handling were followed. After anesthetization, aspectic preparation and dilating the pupils with 1% tropicamide eye drops, subretinal injection of 10 µl saline was done via a limbal entry. Data recorded included time taken for the procedure, success of injection, associated complications, post-operative infections and complications. The rats were followed up for 1 month post procedure. A trend analysis was done for the above factors to look for improvement in ease of procedure, reduction in procedure time and reduction in complications for the clinician using a novel objective scale. **Results:** About 20 eyes were studied. Mean weight of the rats was 188 ± 12.82 gram. Mean time taken for the procedure was 14.1 ± 5.07 minutes. There was a significant inverse co-relation between the serial number of the eye and time taken for the procedure (r = −0.89, $P < 0.0001$). Comparative complications noted between the first ten and the last ten eyes were: conjunctival tear 30% versus 10% ($P = 0.27$), lens touch 50% versus 10% ($P = 0.05$), subretinal hemorrhage 40% versus 0% ($P = 0.13$), vitreous loss 30% versus 0% ($P = 0.06$). The successful subretinal injection without intraocular complications was achieved in 40% versus 90% ($P = 0.02$). There was a significant co-relation between the serial number of the eye and ease of the procedure (r = 0.87, $P < 0.0001$). Post operatively none of the eyes had any infection. Six eyes (12%) developed cataract and 3 eyes (6%) had non-resolving retinal detachment at the last examination visit. **Conclusions:** Subretinal injections in rats have a definite learning curve even for a trained vitreoretinal surgeon. This should be accounted for and resources allocated accordingly to achieve good technical comfort and negate confounding by the surgeon factor in the results of future clinical trials

Key words: Rat model, retinal stem cells, subretinal injections

Access this article online

Website: www.ijo.in

DOI: 10.4103/ijo.IJO_317_19

Quick Response Code:

The subretinal space is an ideal target site for drug delivery and gene therapy purposes.[1-6] This is especially true for therapies intended at regeneration of the photoreceptors (PR) and/or the retinal pigment epithelium (RPE). In comparison to an intravitreal injection, subretinal injections have a greater direct effect on the target cells in the subretinal space. Currently diseases like age related macular degeneration and retinitis pigmentosa do not have any definitive curative therapy. But, several studies have shown that there is promise in sub-retinal cellular replacement therapy in these conditions.[7-12] To test the survival, safety and functionality of the injected cells, it is imperative to perform sub-retinal injections in a rodent model and acquire technical expertise. The techniques of subretinal injection of cells are multiple and vary from trans-scleral injections,[13,14] subretinal implants[15,16] and subretinal injection following vitrectomy.[17,18] Attempting subretinal implants or a vitrectomy can be a very challenging situation and often leads to complications. A trans-scleral approach via a hypodermic needle is a relatively safer technique in small animals.

In clinical vitreoretinal practice, subretinal injections are not uncommon, for clearance of subretinal hemorrhages. While the procedure has a relatively small learning curve in human eyes due to familiar anatomy and larger size, it has a different set of challenges in a small animal eye. As attempts in translational regenerative therapy are being made around the world, it is increasingly imperative for the clinician to be able to participate in animal research to further the cause. This requires the clinician to be well versed with the technique of subretinal injections in a small animal eye and be able to do it safely

[1]Smt. Kanuri Santhamma Center for Vitreoretinal Diseases, LV Prasad Eye Institute, [2]Sudhakar and Shreekanth Ravi Stem Cell Biology Laboratory, Prof. Brien Holden Eye Research Center, LV Prasad Eye Institute, [3]National Center for Laboratory Animal Sciences, National Institute of Nutrition, [4]Center for Ocular Regeneration, LV Prasad eye Institute, Hyderabad, Telangana, India

Correspondence to: Dr. Vivek Pravin Dave, Smt. Kanuri Santhamma Center for Vitreoretinal Diseases, LV Prasad Eye Institute, Hyderabad, Telangana, India. E-mail: vivekoperates@yahoo.co.in

Manuscript received: 14.02.19; Revision accepted: 09.04.19

Cite this article as: Dave VP, Susaimanickam PJ, Mir IA, Mariappan I, Basu S, Reddy BG, *et al*. Learning curve of a trained vitreo-retinal surgeon in sub-retinal injections in a rat model: Implications for future clinical trials. Indian J Ophthalmol 2019;XX:XX-XX.

and effectively. In the current communication, we describe our experience and learning curve of a trained vitreo-retinal surgeon in sub-retinal injections in a rat model which would have implications for future clinical trials.

Materials and Methods

This was an in-vivo retrospective interventional animal study. The study was conducted at the National Institute of Nutrition and at the LV Prasad Eye Institute, Hyderabad, India with appropriate Institutional Review Board approval. All animal handling was done according to the Statement of the use of animals in ophthalmic and visual research as suggested by the Association for Research in Vision and Ophthalmology (ARVO).[19] About 20 eyes of 20 Wistar rats were included in the study. All rats were anesthetized by a trained veterinarian using 80 mg/kg ketamine and 12 mg/kg xylazine. Adequate anesthesia was confirmed after 5 minutes by observing the wince reflex by pinching the ear lobe or the tail. Post anesthesia, the pupils were dilated using 1% tropicamide eye drops.

Painting and preparation of the eye was done using 5% povidone iodine eye drops and solution. [Fig. 1]. The animal was laid under a dissecting microscope and the eyelids were retracted using a custom-made eye clamp. A glass cover slip was secured on the cornea after instilling viscoelastic to allow visualization of the fundus during the procedure. Using a micro-vitreoretinal blade, the sclera was incised to access the vitreous cavity. Through the entry, a hypodermic needle was inserted and advanced to the subretinal space. In the subretinal space, 10 µl of saline was injected to raise a small bleb using a Hamilton syringe and 27G needle. [Figs. 1 and 2] Data recorded included time taken for the procedure, success of injection, associated complications, post-operative infections and complications. The rats were followed up for 1 month post procedure. A trend analysis was done for the above factors to look for improvement in ease of procedure, reduction in procedure time and reduction in complications for the clinician using a novel objective scale [Table 1].

Statistical analysis

Statistical analysis was done using MedCalcVer 18.11 (Ostend, Belgium). Mean with standard deviation was calculated for all

Table 1: Table showing calculation of comfort score for subretinal injections in a rat eye

	Present	Absent
Conjunctival tears	0	1
Lens touch	0	1
Cataract formation on follow up	0	1
Subretinal/viteous hemorrhage	0	1
Retinal detachment	0	1
Time taken <10 min	3	-
Time taken 10<->20 min	2	-
Time taken >20 min	1	-

A score of ≥5 was assigned as good comfort

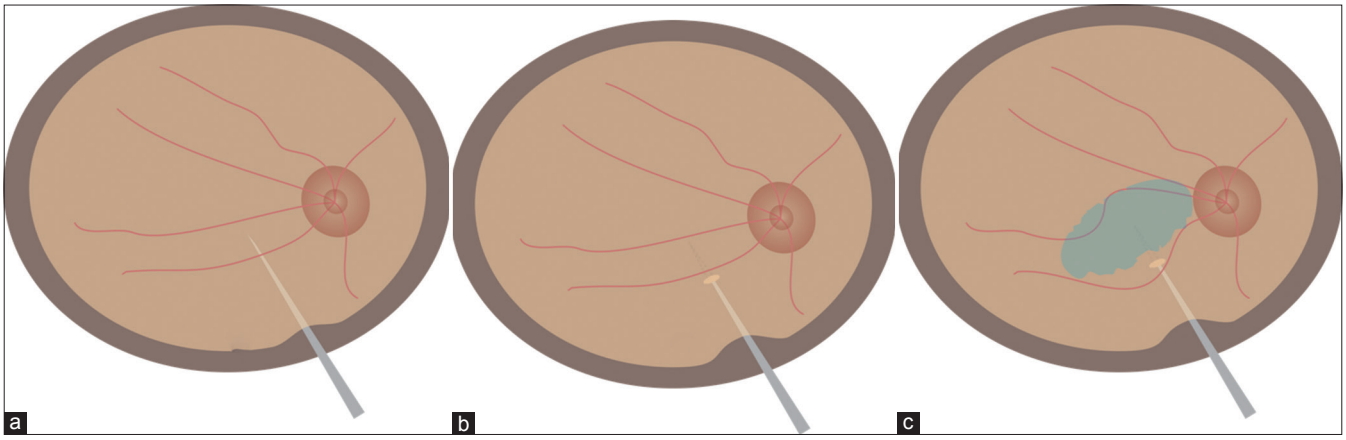

Figure 1: Cartoon showing (a) entry of a micro-vitreoretinal blade into the vitreous cavity via an incision behind the limbus. (b) A retinotomy created by the MVR blade. (c) Sub retinal injection done by 27G needle with Hamilton syringe

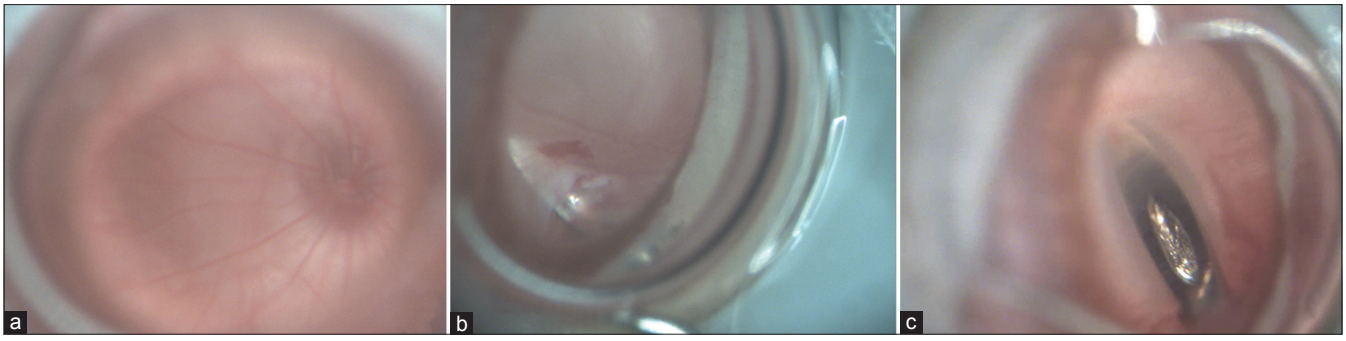

Figure 2: Panel showing (a) a normal focused rat retina. (b) A retinotomy created by the MVR blade. (c) Sub retinal injection done by 27G needle with Hamilton syringe

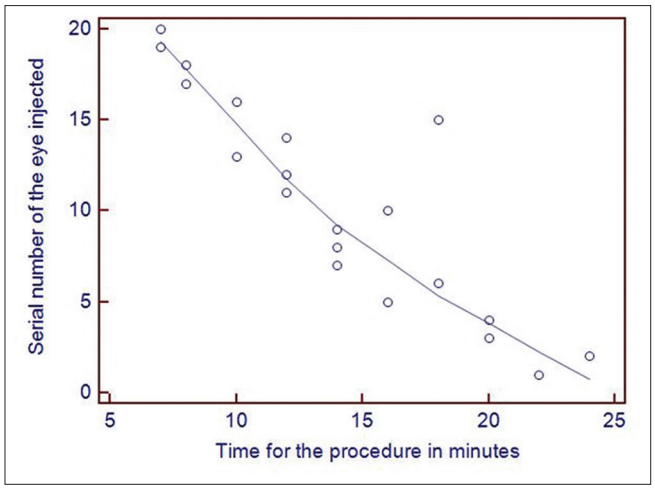

Graph 1: Graph showing serial number of eye injected plotted against the time taken for the procedure

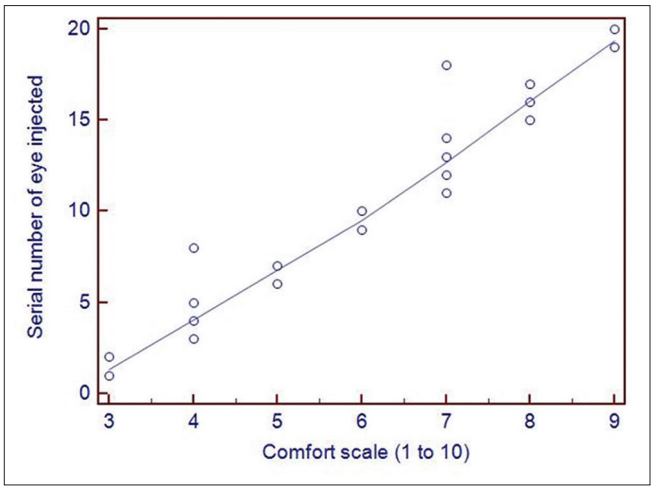

Graph 2: Graph showing serial number of the eye injected plotted against the comfort scale

continuous parametric variables whereas, median was reported for non-parametric variables. Pearson's co-relation coefficient was calculated to assess the effect of the serial number of the eye operated on the ease of the procedure and the time taken for the surgery. A *P* value of <0.05 was assigned to be statistically significant.

Results

About 20 eyes were studied. Mean weight of the rats was 188 ± 12.82 gram. Mean time taken for the procedure was 14.1 ± 5.07 minutes. There was a significant inverse co-relation between the serial number of the eye and time taken for the procedure (r = −0.89, $P < 0.0001$) [Graph 1]. Comparative complications noted between the first ten and the last ten eyes were: conjunctival tear 30% versus 10% ($P = 0.27$), lens touch 50% versus 10% ($P = 0.05$), subretinal hemorrhage 40% versus 0% ($P = 0.13$), vitreous loss 30% versus 0% ($P = 0.06$). Successful subretinal injection without intraocular complications was achieved in 40% versus 90% ($P = 0.02$) [Table 2]. There was a significant co-relation between the serial number of the eye and ease of the procedure (r = 0.87, $P < 0.0001$) [Graph 2]. Post operatively none of the eyes had any infection. Six eyes (12%) developed cataract and 3 eyes (6%) had non-resolving retinal detachment at the last examination visit.

Table 2: Comparison of complications and success between the first and the last ten rat eyes operated

Complication	First 10 eyes (%)	Last 10 eyes (%)	*P*
Conjunctival tear	30	10	0.27
Lens touch	50	10	0.05
Subretinal hemorrhage	40	0	0.13
Vitreous loss	30	0	0.06
Successful subretinal injection	40	90	0.02

Discussion

Sub-retinal injection technique in a small animal model has a definite learning curve for a clinician but can be overcome and mastered well by repetitive performance of the procedures. In the current technique, we describe approach to the subretinal space using a limbal incision with a transvitreal approach. Various workers have described techniques of subretinal injection via a transcorneal approach.[20-22] Though these techniques are simpler to perform, a relatively high rate of cataract was described in these studies (25%-40%). These cataracts resulted from damage inflicted on the lens as the cornea was punctured and/or as the blunt needle was directed toward the subretinal matrix. In our technique the risk is circumvented as the approach is via the pars plana. The cataracts noted in our study were seen mainly in the initially operated eyes. This can be attributed to the learning curve that was required to get a judgment of the relative position of the posterior lens capsule with respect to the retina. This occurs due to a peculiar anatomy of the rat eye where the lens occupies almost half of the space in the vitreous cavity.

It has been seen in previous studies that irrespective of the technique used in subretinal injections, there can be complications noted at the level of the retinal pigment epithelium and the retinal photoreceptors which can lead to progressive degeneration of the photoreceptors.[23,24] These observations indicate the importance of a correct technique to ensure minimal damage to the sensitive ocular structures during the process of injection. The clinicians trained in vitreoretinal surgeries have been performing subretinal injections over the past decade successfully for treating macular diseases especially submacular hemorrhage following trauma or an underlying choroidal neovascularization.[25,26] In spite of it being a not uncommonly performed procedure, complications like retinal detachments and choroidal hemorrhage are known with these procedures which can limit the final favorable outcome.[27,28] If we take into perspective the comparative schematic eye sizes of a rat eye and a human eye, it shows that a rat eye has an axial length which is 1/4th and the vitreous chamber depth which is 1/10th of that of a human eye.[29,30] Given such large differences in the ocular sizes, it natural that for an uninitiated clinician there would be a definite learning curve in carrying out these procedures. The current study shows how the learning curve can be overcome by repeating the procedure in a sustained manner to get a good outcome. This would avoid

the effect of technique-related confounding factors on the final procedure outcome.

In conclusion, subretinal injections in rats have a definite learning curve even for a trained vitreoretinal surgeon as clinicians are not well-versed with surgical maneuvers in a small animal eye. This should be accounted for and resources allocated accordingly to allow adequate practice of these injection techniques. This can help achieve good technical comfort and negate confounding by the surgeon factor in the results of future clinical trials.

Financial support and sponsorship

This study was supported by the Hyderabad Eye Research Foundation, Department of Biotechnology Government of India and the Cognizant Foundation.

Conflicts of interest

There are no conflicts of interest.

References

1. Peng Y, Tang L, Zhou Y. Subretinal injection: A review on the novel route of therapeutic delivery for vitreoretinal diseases. Ophthalmic Res 2017;58:217-26.
2. Yasukawa T, Ogura Y, Sakurai E, Tabata Y, Kimura H. Intraocular sustained drug delivery using implantable polymeric devices. Adv Drug Deliv Rev 2005;57:2033-4.
3. Schorderet DF, Manzi V, Canola K, Bonny C, Arsenijevic Y, Munier FL. Maurer FD-TAT transporter as an ocular peptide delivery system. Clin Exp Ophthalmol 2005;33:628-35.
4. Maia M, Kellner L, de Juan E Jr, Smith R, Farah ME, Margalit E, *et al*. Effects of indocyanine green injection on the retinal surface and into the subretinal space in rabbits. Retina 2004;24:80-91.
5. Shen WY, Rakoczy PE. Uptake dynamics and retinal tolerance of phosphorothioate oligonucleotide and its direct delivery into the site of choroidal neovascularization throughsubretinal administration in the rat. Antisense Nucleic Acid Drug Dev 2001;11:257-64.
6. Kimura H, Spee C, Sakamoto T, Hinton DR, Ogura Y, Tabata Y, *et al*. Cellular response in subretinal neovascularization induced by bFGF-impregnated microspheres. Invest Ophthalmol Vis Sci 1999;40:524-8.
7. Algvere PV, Berglin L, Gouras P, Sheng Y. Transplantation of fetal retinal pigment epithelium in age-related macular degeneration with subfoveal neovascularization. Graefes Arch Clin Exp Ophthalmol 1994;232:707-16.
8. Binder S, Krebs I, Hilgers RD, Abri A, Stolba U, Assadoulina A, *et al*. Outcome of transplantation of autologous retinal pigment epithelium in age-related macular degeneration: A prospective trial. Invest Ophthalmol Vis Sci 2004;45:4151-60.
9. Binder S, Stolba U, Krebs I, Kellner L, Jahn C, Feichtinger H, *et al*. Transplantation of autologous retinal pigment epithelium in eyes with foveal neovascularization resulting from age-related macular degeneration: A pilot study. Am J Ophthalmol 2002;133:215-25.
10. de Juan E Jr, Loewenstein A, Bressler NM, Alexander J. Translocation of the retina for management of subfovealchoroidal neovascularization II: A preliminary report in humans. Am J Ophthalmol 1998;125:635-46.
11. Falkner-Radler CI, Krebs I, Glittenberg C, Povazay B, Drexler W, Graf A, *et al*. Human retinal pigment epithelium (RPE) transplantation: Outcome after autologous RPE-choroid sheet and RPE cell-suspension in a randomised clinical study. Br J Ophthalmol 2011;95:370-5.
12. Lam TT, Fu J, Tso MO. Ahistopathologic study of retinal lesions inflicted by transscleraliontophoresis. Graefes Arch Clin Exp Ophthalmol 1991;229:389-94.
13. Ambati J, Gragoudas ES, Miller JW, You TT, Miyamoto K, Delori FC, *et al*. Transscleral delivery of bioactive protein to the choroid and retina. Invest Ophthalmol Vis Sci 2000;41:1186-91.
14. Martin DF, Parks DJ, Mellow SD, Ferris FL, Walton RC, Remaley NA, *et al*. Treatment of cytomegalovirus retinitis with an intraocular sustained-release ganciclovir implant. A randomized controlled clinical trial. Arch Ophthalmol 1994;112:1531-9.
15. Srivastava S, Taylor P, Wood LV, Lee SS, Robinson MR. Post-surgical scleritis associated with the ganciclovir implant. Ophthalmic Surg Lasers Imaging 2004;35:254-5.
16. Baba T, Bhutto IA, Merges C, Grebe R, Emmert D, McLeod DS, *et al*. A rat model for choroidal neovascularization using subretinal lipid hydroperoxide injection. Am J Pathol 2010;176:3085-97.
17. Hillenkamp J, Surguch V, Framme C, Gabel VP, Sachs HG. Management of submacular hemorrhage with intravitreal versus subretinal injection of recombinant tissue plasminogen activator. Graefes Arch ClinExp Ophthalmol 2010;248:5-11.
18. Olivier S, Chow DR, Packo KH, MacCumber MW, Awh CC. Subretinal recombinant tissue plasminogen activator injection and pneumatic displacement of thick submacular hemorrhage in Age-Related macular degeneration. Ophthalmology 2004;111:1201-8.
19. Available from: http://www.arvo.org/AboutARVO/Policies/Statement for the Use of Animals in Ophthalmic and Visual Research/. [Last accessed on 2019 Jan 02].
20. Timmers AM, Zhang H, Squitieri A, Gonzalez-Pola C. Subretinal injections in rodent eyes: Effects on electrophysiology and histology of rat retina. Mol Vis 2001;7:131-7.
21. Price J, Turner D, Cepko C. Lineage analysis in the vertebrate nervous system by retrovirus-mediated gene transfer. Proc Natl Acad Sci U S A 1987;84:156-60.
22. Turner DL, Cepko CL. A common progenitor for neurons and glia persists in rat retina late in development. Nature 1987;328:131-6.
23. Matsumoto H, Miller JW, Vavvas DG. Retinal detachment model in rodents by subretinal injection of sodium hyaluronate. J Vis Exp 2013:e50660. doi: 10.3791/50660.
24. Westenskow PD, Kurihara T, Bravo S, Feitelberg D, Sedillo ZA, Aguilar E, *et al*. Performing subretinal injections in rodents to deliver retinal pigment epithelium cells in suspension. J Vis Exp 2015;e52247. doi: 10.3791/52247.
25. Novelli FJD, Preti RC, Monteiro MLR, Nobrega MJ, Takahashi WY. A new method of subretinal injection of tissue plasminogen activator and air in patients with submacular hemorrhage. Retina 2017;37:1607-11.
26. Bell JE, Shulman JP, Swan RJ, Teske MP, Bernstein PS. Intravitreal versus subretinal tissue plasminogen activator for submacular hemorrhage. Ophthalmic Surg Lasers Imaging Retina 2017;48:26-32.
27. Haupert CL, McCuen II BW, Jaffe GJ, Steuer ER, Cox TA, Toth CA, *et al*. Pars plana vitrectomy, subretinal injection of tissue plasminogen activator and fluid-gas exchange for displacement of thick sub-macular hemorrhage in age-related macular degeneration. Am J Ophthalmol 2001;131:208-15.
28. Sharma S, Kumar JB, Kim JE, Thordsen J, Dayani P, Ober M, *et al*. Pneumatic displacement of submacular hemorrhage with subretinal air and tissue plasminogen activator. Ophthalmol Retina 2018;2:180-6.
29. Massof RW, Chang FW. A revision of the rat schematic eye. Vision Res 1972;12:793-6.
30. Vojnikovic B, Tamajo E. Gullstrand's optical schematic system of the eye - modified by Vojnikovic and Tamajo. Coll Antropol 2013;37:41-5.

Developing in vitro and in vivo models of retinal degeneration

by Praveen Joseph S

Submission date: 09-Jul-2019 04:32PM (UTC+0530)
Submission ID: 1150438901
File name: (1.66M)
Word count: 38209
Character count: 203109

Developing in vitro and in vivo models of retinal degeneration

ORIGINALITY REPORT

8%	4%	4%	6%
SIMILARITY INDEX	INTERNET SOURCES	PUBLICATIONS	STUDENT PAPERS

PRIMARY SOURCES

1	Praveen Joseph Susaimanickam, Savitri Maddileti, Vinay Kumar Pulimamidi, Sreedhar Rao Boyinpally et al. "Generating minicorneal organoids from human induced pluripotent stem cells", Development, 2017 Publication	1%
2	www.rj-robbins.com Internet Source	<1%
3	Submitted to National University of Singapore Student Paper	<1%
4	Submitted to Deakin University Student Paper	<1%
5	www.ias.ac.in Internet Source	<1%
6	Submitted to Jawaharlal Nehru University (JNU) Student Paper	<1%
7	Submitted to University of Hong Kong Student Paper	<1%

8	Submitted to University College London Student Paper	<1%
9	Submitted to University of Birmingham Student Paper	<1%
10	Submitted to University of Sheffield Student Paper	<1%
11	Hardeep Pal Singh, Subhadra Jalali, J. Fielding Hejtmancik, Chitra Kannabiran. "Homozygous Null Mutations in the ABCA4 Gene in Two Families With Autosomal Recessive Retinal Dystrophy", American Journal of Ophthalmology, 2006 Publication	<1%
12	Submitted to University of Hull Student Paper	<1%
13	d-nb.info Internet Source	<1%
14	Submitted to UC, San Diego Student Paper	<1%
15	Advances in Experimental Medicine and Biology, 2014. Publication	<1%
16	discovery.ucl.ac.uk Internet Source	<1%

17	"Stem Cells and Human Diseases", Springer Nature, 2012 Publication	<1%
18	"Transcriptional and Translational Regulation of Stem Cells", Springer Nature, 2013 Publication	<1%
19	Submitted to University of Portsmouth Student Paper	<1%
20	Philip D. Kiser, Marcin Golczak, Krzysztof Palczewski. "Chemistry of the Retinoid (Visual) Cycle", Chemical Reviews, 2013 Publication	<1%
21	repository.ubn.ru.nl Internet Source	<1%
22	www.dovepress.com Internet Source	<1%
23	Submitted to Queen Mary and Westfield College Student Paper	<1%
24	Submitted to Mahidol University Student Paper	<1%
25	Submitted to Associatie K.U.Leuven Student Paper	<1%
26	Submitted to King's College Student Paper	<1%

27	Submitted to University of Wales Institute, Cardiff Student Paper	<1%
28	www.plosone.org Internet Source	<1%
29	Submitted to Birla Institute of Technology and Science Pilani Student Paper	<1%
30	Submitted to Jawaharlal Nehru Technological University Student Paper	<1%
31	krishikosh.egranth.ac.in Internet Source	<1%
32	Giuliana Gagliardi, Karim Ben M'Barek, Olivier Goureau. "Photoreceptor cell replacement in macular degeneration and retinitis pigmentosa: A pluripotent stem cell-based approach", Progress in Retinal and Eye Research, 2019 Publication	<1%
33	d-scholarship.pitt.edu Internet Source	<1%
34	www.era.lib.ed.ac.uk Internet Source	<1%
35	Methods in Molecular Biology, 2015. Publication	<1%

36	Reichman, S., A. Terray, A. Slembrouck, C. Nanteau, G. Orieux, W. Habeler, E. F. Nandrot, J.-A. Sahel, C. Monville, and O. Goureau. "From confluent human iPS cells to self-forming neural retina and retinal pigmented epithelium", Proceedings of the National Academy of Sciences, 2014. Publication	<1%
37	dyuthi.cusat.ac.in Internet Source	<1%
38	Submitted to St George's Hospital Medical School Student Paper	<1%
39	research.lvpei.org Internet Source	<1%
40	Submitted to University of South Africa Student Paper	<1%
41	www.scribd.com Internet Source	<1%
42	Submitted to Saint George's University Student Paper	<1%
43	www.omicsonline.org Internet Source	<1%
44	Submitted to Bond University Student Paper	<1%

45	Submitted to Cranfield University Student Paper	<1%
46	Submitted to American University in Cairo Student Paper	<1%
47	Khan, Kamron N., Omar A. Mahroo, Rehna S. Khan, Moin D. Mohamed, Martin McKibbin, Alan Bird, Michel Michaelides, Adnan Tufail, and Anthony T. Moore. "Differentiating drusen: Drusen and drusen-like appearances associated with ageing, age-related macular degeneration, inherited eye disease and other pathological processes", Progress in Retinal and Eye Research, 2016. Publication	<1%
48	www.ncbi.nlm.nih.gov Internet Source	<1%
49	Submitted to University of Macau Student Paper	<1%
50	edoc.ub.uni-muenchen.de Internet Source	<1%
51	R. Parker. "Interphotoreceptor Retinoid-Binding Protein as the Physiologically Relevant Carrier of 11-cis-Retinol in the Cone Visual Cycle", Journal of Neuroscience, 03/23/2011 Publication	<1%
	www.pubmedcentral.nih.gov	

52	Internet Source	<1%
53	Submitted to CSU Northridge Student Paper	<1%
54	Submitted to Rutgers University, New Brunswick Student Paper	<1%
55	Submitted to University of Abertay Dundee Student Paper	<1%
56	theses.gla.ac.uk Internet Source	<1%
57	Submitted to Australian National University Student Paper	<1%
58	baadalsg.inflibnet.ac.in Internet Source	<1%
59	Submitted to University of Liverpool Student Paper	<1%
60	Friedman, J.S.. "Premature Truncation of a Novel Protein, RD3, Exhibiting Subnuclear Localization Is Associated with Retinal Degeneration", The American Journal of Human Genetics, 200612 Publication	<1%
61	Submitted to Imperial College of Science, Technology and Medicine	<1%

	Student Paper	
62	dspace.bracu.ac.bd:8080 Internet Source	<1%
63	Submitted to Federal University of Technology Student Paper	<1%
64	manoa.hawaii.edu Internet Source	<1%
65	Submitted to Royal Veterinary College Student Paper	<1%
66	Sehu. "Development and Malformation", Ophthalmic Pathology, 01/01/2005 Publication	<1%
67	Eker, P.. "Effects of epidermal growth factor, fibroblast growth factor, retinoic acid and serum on anchorage-dependent and anchorage-independent growth of HRRT cells", European Journal of Cancer and Clinical Oncology, 198903 Publication	<1%
68	theses.ucalgary.ca Internet Source	<1%
69	www.freepatentsonline.com Internet Source	<1%
70	www.scialert.net Internet Source	<1%

71	www.mdpi.com Internet Source	<1%
72	epdf.tips Internet Source	<1%
73	Submitted to The University of Manchester Student Paper	<1%
74	Tae-Young Choi, Kyung-Cheol Sohn, Jin-Hwa Kim, Seong-Min Kim et al. "Impact of NAD(P)H:Quinone Oxidoreductase-1 on Pigmentation", Journal of Investigative Dermatology, 2010 Publication	<1%
75	Submitted to University of Wollongong Student Paper	<1%
76	"Cellular Therapies for Retinal Disease", Springer Nature, 2017 Publication	<1%
77	Submitted to University of Warwick Student Paper	<1%
78	Malgorzata Jaremko. "MALDI-TOF MS and TaqMan® assisted SNP genotyping of DNA isolated from formalin-fixed and paraffin-embedded tissues (FFPET)", Human Mutation, 03/2005 Publication	<1%

79	orca.cf.ac.uk Internet Source	<1%
80	Submitted to City University Student Paper	<1%
81	Submitted to Dublin City University Student Paper	<1%
82	Submitted to University of Southampton Student Paper	<1%
83	"Translational Stem Cell Research", Springer Nature, 2011 Publication	<1%
84	www.hh.um.es Internet Source	<1%
85	"Stem Cells and Cancer Stem Cells, Volume 11", Springer Nature, 2014 Publication	<1%
86	Submitted to Mount St. Marys College Student Paper	<1%
87	Submitted to Royal Holloway and Bedford New College Student Paper	<1%
88	Submitted to Monash University Student Paper	<1%
89	www.3dcellculture.com	

Internet Source

<1%

Exclude quotes	On	Exclude matches	< 14 words
Exclude bibliography	On		